Cryocrystallographic and Mechanistic Studies on Glycogen Phosphorylase

Edward Peter Mitchell

Laboratory of Molecular Biophysics
and
St Catherines College, Oxford

A thesis submitted in partial fulfilment of the requirments
for the degree of Doctor of Philosophy
at the University of Oxford

Michaelmas Term 1994

ABSTRACT

Cryocrystallographic and Mechanistic Studies on Glycogen Phosphorylase
Edward Peter Mitchell
Laboratory of Molecular Biophysics and St Catherines College, Oxford
Submitted for the degree of Doctor of Philosophy
Michaelmas 1994

Glycogen phosphorylase (GPb) regulates the degradation of glycogen to glucose-1-phosphate and catalyses the first step of the reaction. Many studies have provided insights into the essentials of the catalytic mechanism. Previous time resolved crystallographic work using heptenitol has revealed a putative phosphate binding site at the active site of phosphorylase.

Using nojirimycin tetrazole, a transition state analogue, complexed with phosphate and both T and R state GPb crystals, this work has conclusively located the phosphate binding site and the concomitant active site conformational changes. This has confirmed the previous heptenitol results. Using R state crystals complexed with tetrazole and phosphate, data were collected to 2.5Å resolution, higher than for the original 2.8Å resolution native structure, and used to position water molecules in the R state model.

Further to this, direct observation of the phosphate ion orientation was made possible using flash-frozen T state crystals to collect 1.7Å resolution data at 100K. As part of this cryo-crystallographic work the relationship of cryoprotectant concentration with crystal mosaicity was established, aiding the systematic search for flash-freezing cryoprotectant conditions for all protein crystals. Collection of a new native T state data set to 1.5Å resolution was made possible using the flash-freezing technique. Refinement has produced a new higher precision native model (*R* factor currently 22.8%) containing additional N terminal residues (14-18) and 330 new water molecules. A molecule of glycerol, the cryoprotectant, was located at the active site. This study represents a considerable improvement over the 1.9Å resolution room temperature native data, and is also the first time such high resolution data have been collected from such a large enzyme.

In a further analysis of the phosphate binding properties, a link between structure, atomic charges and the ability of a ligand to bind phosphate at the phosphorylase active site was established. In order of phosphate binding ability, the nojirimycin tetrazole, nitroglucal, glucal and glucose complexes with T state GPb and phosphate were structurally analysed. As the charge difference between the pyranose ring oxygen (or equivalent atom) and anomeric atom becomes more negative (charges estimated using MOPAC) the tendency to bind phosphate decreases. The ligand must possess a half-chair conformation as this is essential to bind phosphate; glucose, having the most negative charge difference and a full chair conformation, does not bind phosphate significantly in the crystal. A novel surface binding site for nitroglucal (covalently linked to His 73) was also located during this work.

As part of an ongoing search for potential drugs for diabetes, two gluco-hydantoin inhibitors of GPb were investigated. One proved to be the best inhibitor to date, and the inhibition was rationalised using the structural results from this work. A new improved inhibitor has been proposed on the basis of these results.

ACKNOWLEDGEMENTS

I would like to thank Louise for being a superb supervisor and for starting me off in the crystallographic world. Her depth of knowledge has been invaluable over the last three years.

There are many people without whom my DPhil would have just been a non-starter. Firstly, Elspeth who not only guided inumerable data collections but then read this entire thesis for me as well; Richard and Robert who efficiently run the computer systems and helped me with starting up the Web server; Steve for preparing the many photographs for this thesis and John who helped with photographs using O. Our collaborators, Nikos and his group in Greece, Steve Withers and Bill Stirtan in Canada, George Fleet and his group in the DP and Andrea Vasella in Switzerland provided the crystals, kinetic results and compounds essential for this work. Martin, Vilmos and Elspeth gave much needed advice and help for the crystallographic theory and practice.

Thanks to everyone in LMB who has helped me during my DPhil and especially to Soichi, Liz, Kim, Martin, Marc, Dave, Elspeth and Pamela all of who have made the lab a great place to work. A poor man I would have been without the Fleeties and other inhabitants of the DP who have made the last three years fantastic and I'm sorry to be leaving. Especially Ken, thanks for the introduction to the markets, Tig, Annabel, Mark, Kirsten and Emma.

Alan is a great friend and the other half of SoundBase. Together we've prematurely damaged the hearing of a large percentage of Oxford undergraduates and Bicester school children. Valèrie has been there at all the right times, I hope she is content soon.

Finally Mum and Dad for their love and support over the last twenty-five years.

CONTENTS

1.1 GLYCOGEN PHOSPHORYLASE

Glycogen phosphorylase has been the subject of inumerable scientific studies for over fifty years. It has become the most well studied example of a regulated enzyme. Despite this, phosphorylase still guards some of its secrets.

1.1.1 Physiological Role

Glycogen phosphorylase (α-1,4-glucan-orthophosphate glycosyl transferase, EC 2.4.1.1) was first isolated from rabbit skeletal muscle in 1940 (Cori & Cori, 1940). It catalyses the first step of the catalytic pathway and regulates the intracellular degradation of glycogen to glucose-1-phosphate.

$$(\text{Glucose})_n + P_i \rightleftharpoons (\text{Glucose})_{n-1} + \text{Glucose-1-Phosphate}$$

where P_i represents intracellular phosphate

The role of phosphorylase is to supply glucose-1-phosphate from glycogen energy stores in the body. In muscle the supply of glucose-1-phosphate is utilised via glycolysis to supply ATP during muscle contraction. In contrast, liver phosphorylase functions to ensure a constant supply of glucose-1-phosphate which is converted by phosphoglucomutase and glucose-6-phosphatase to glucose (Newgard, Hwang & Fletterick, 1989). Under conditions of low levels of blood glucose, the glucose is exported from the liver for use by other organs such as the brain, which relies on glucose as its major fuel source.

1.1.2 An Allosteric Enzyme

Phosphorylase was the first example of an enzyme controlled by allostery to be discovered

(Cori, Cori & Green, 1943) and has since served as an excellent model for allosteric processes.

An allosteric enzyme contains both the active binding site and one or more additional binding sites. Two models currently exist to describe the method of allosteric regulation. Firstly the MWC model (Monod, Wyman & Changeux, 1965) defines two states, a low affinity and low activity T state (Tense) and a high affinity and high activity R state (Relaxed). This model then assumes that an allosteric enzyme exists in an equilibrium between these two states, and in the absence of activators favours the T state. In the presence of an activator or activators the equilibrium is perturbed to favour the R state. The model also assumes that the molecular symmetry between the two states is retained. The second model suggests that ligand binding causes a series of sequential structural changes giving a series of enzyme conformations (Koshland, Némethy & Filmer, 1966). In this model the molecular symmetry is no longer retained. Both models have been of vital importance for structural work but there are now known to be additional complexities in enzyme allosteric response not envisaged in these simple models.

To a first approximation, the results of the majority of kinetic work on phosphorylase supports the MWC description as a model of the enzyme (Buc, 1967; Graves & Wang, 1972) as illustrated in Figure 1.1. In the case of GPb the equilibrium constant L, expressed as [T]/[R], is approximately 3000 in the absence of ligands, but reduces to between 3 and 10 in the phosphorylated state GPa (Madsen, 1986). In resting muscle phosphorylase exists as the inactive (T state) b form which can be activated (R state) by the cooperative binding of AMP, and some analogues, and inhibited by glucose-6-phosphate, ATP and D-glucose. GP is not only regulated by noncovalent means, but also by reversible phosphorylation of a specific serine residue, Ser 14. This constitutes the main pathway to activated phosphorylase. In response to extracellular or hormonal signals Ser 14 is phosphorylated by a specific kinase, itself also regulated by similar signals, to produce the active *a* form of the enzyme. GPa is active in the

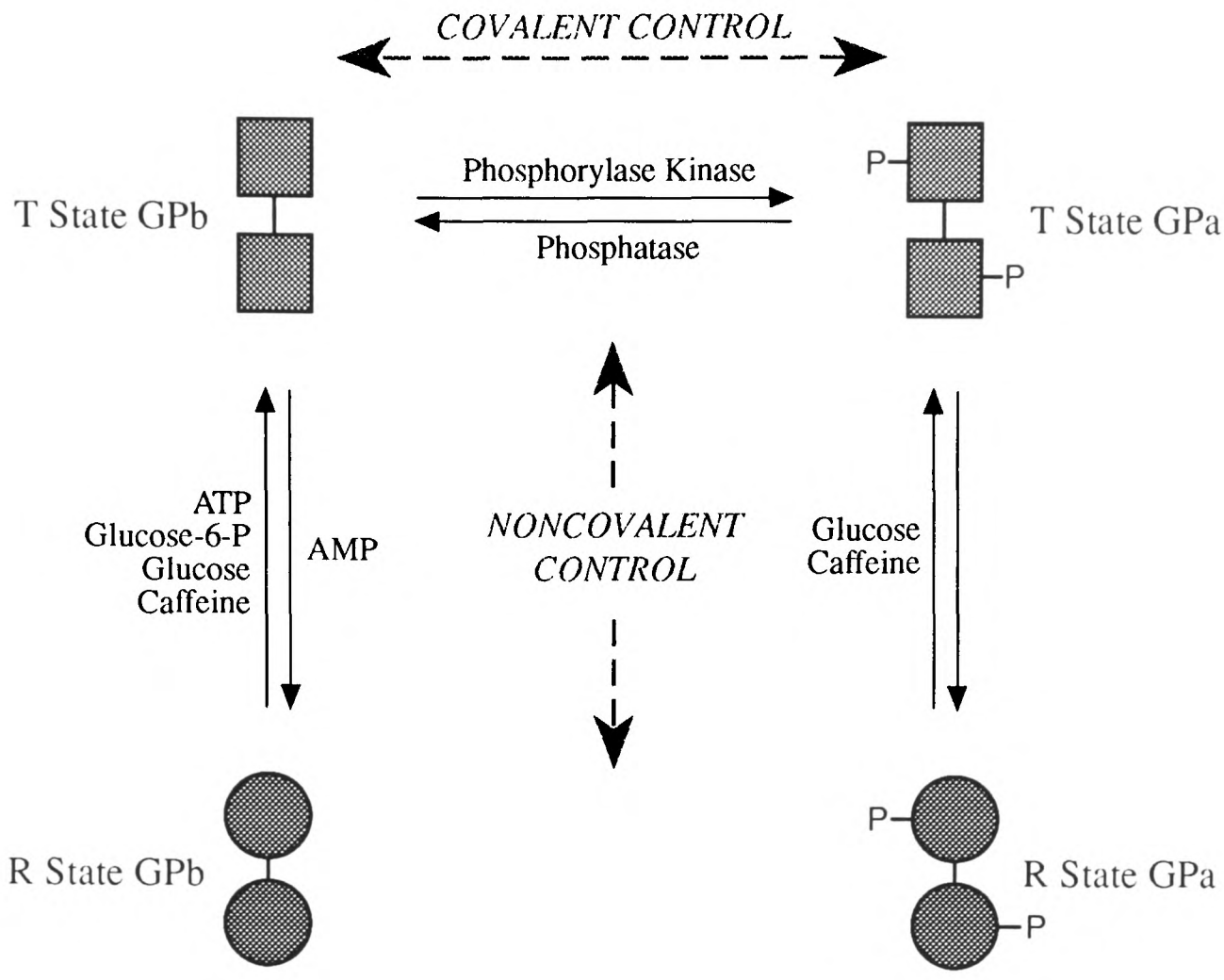

Figure 1.1. *The regulation of glycogen phosphorylase by covalent and noncovalent control.*

absence of AMP, unlike the b form, though AMP binding does increase the level of activity by approximately 10%.

1.1.3 The Overall Structure

A schematic of the subunit structure of phosphorylase is shown in Figure 1.2. The tertiary conformation of the T and R state structures are similar. The long polypeptide chain (842 amino acids and a subunit molecular weight of 97.4kDa) can be divided into two domains, domain 1 (residues 19 to 484) and domain 2 (residues 485 to 839), both of which are based on β-sheet cores flanked by α-helices. The two domains are closely interconnected with many Van der

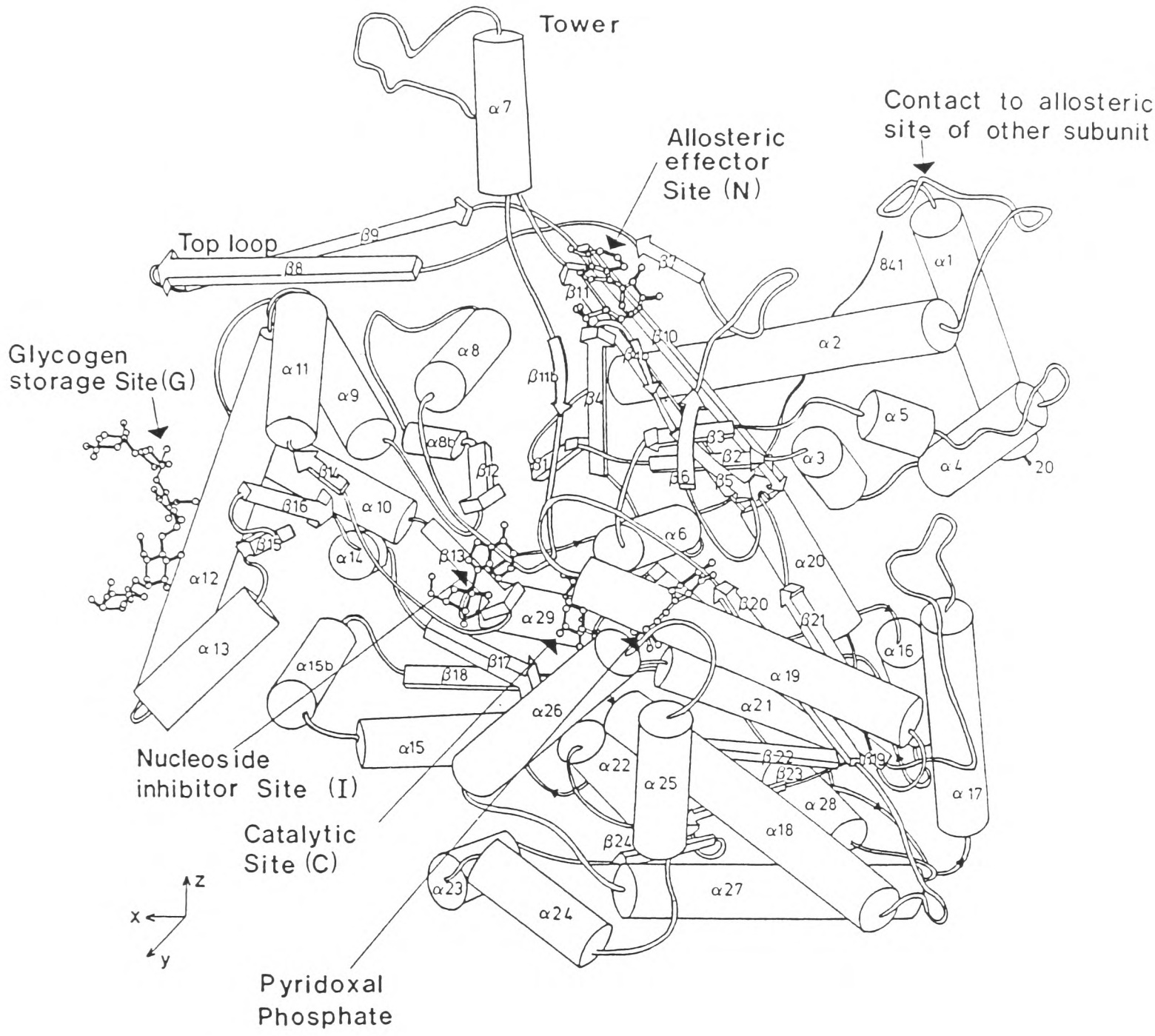

Figure 1.2. *Schematic diagram of a phosphorylase monomer showing the secondary structure elements and ligand binding sites.*

Waals and polar contacts between them.

In vitro GPb exists as a dimer and when activated by AMP binding or covalent phosphorylation the dimers associate to form tetrameric phosphorylase. Under physiological conditions, phosphorylase is associated with glycogen particles, along with many of the other enzymes involved with glycogen metabolism. Binding to glycogen dissociates tetrameric phosphorylase, which has low activity, to active dimers.

The two subunits of the active dimeric form are related by a crystallographic two-fold axis of symmetry (Figure 1.3). There are two areas of contact between the two subunits. The interface between the cap (residues 36 to 45) and residues from the other subunit form part of the AMP and glucose-6-phosphate allosteric sites (see next section). The second area of contacts is between the two tower helices (residues 262 to 274) of the subunits which stack in an anti-parallel fashion resulting in many contacts. The tower helices are connected to the loop of residues 282 to 286 (the '280s loop') which form a gate to the active site, the helices thus provide direct communication from the catalytic site to the subunit interface.

1.1.4 The Ligand Binding Sites

The structures of all four forms of phosphorylase have been solved (Acharya, Stuart, Varvill & Johnson, 1991; Barford & Johnson, 1989; Barford, Hu & Johnson, 1991; Sprang, Goldsmith & Fletterick, 1987). The results of these and many subsequent studies have led to precise

---

Figure 1.3 (Overleaf). *The dimeric structure of T state glycogen phosphorylase b viewed down the two-fold axis of symmetry. The lower subunit shows the secondary structure with the Cap (to the right) and Tower (to the left) regions highlighted in yellow. The upper subunit depicts the C-α trace which is coloured by sequence from red at the C-terminus to blue at the N-terminus. In both subunits the ligand binding sites are shown: the catalytic site (in red) with the larger coenzyme PLP and smaller glucose molecule, the caffeine site (in purple), the AMP site (in blue) and the glycogen storage site on the protein surface (in green).*

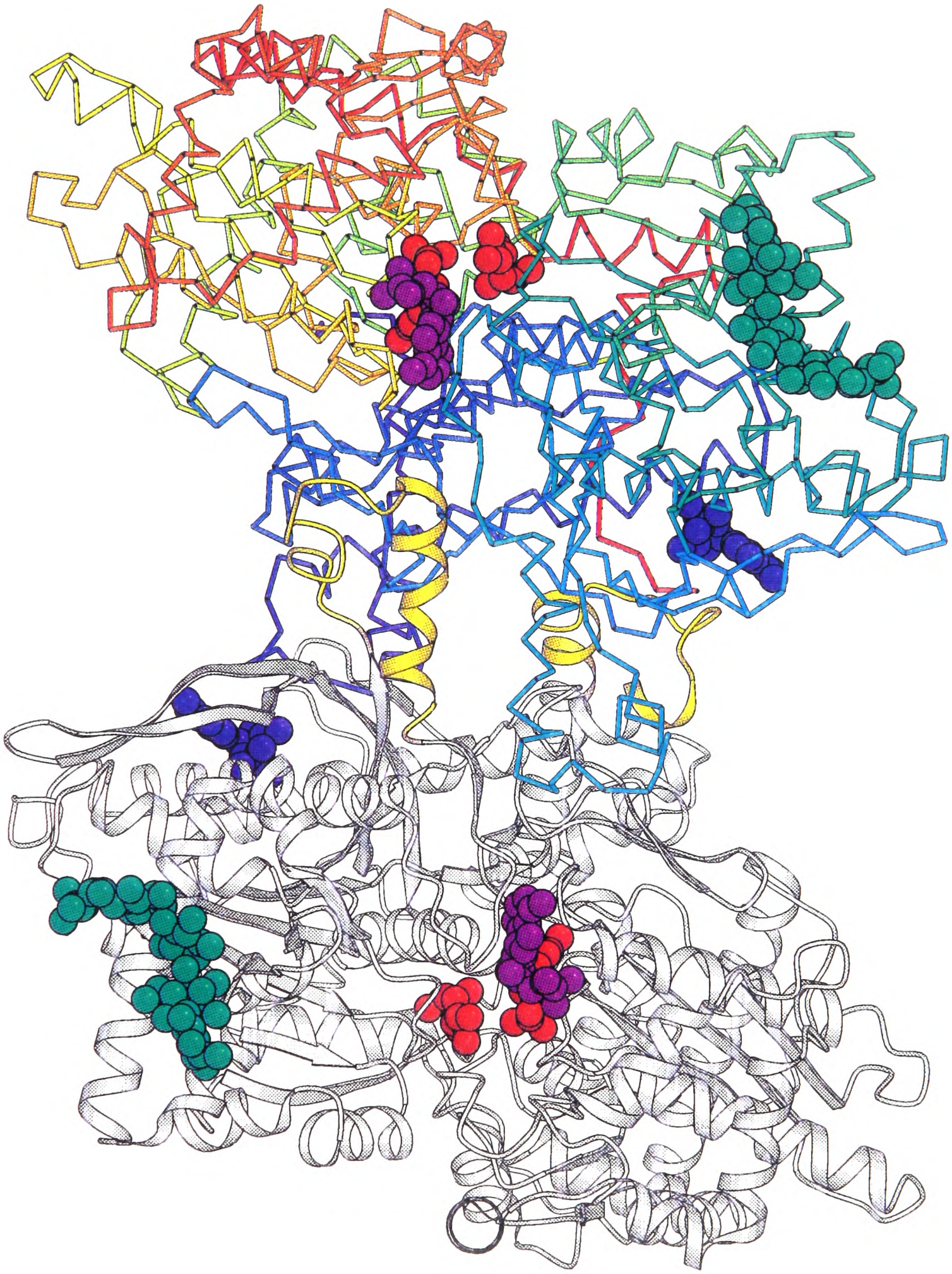

Figure 1.3. *The dimer of T state GPb. The full figure legend is on the previous page.*

structural and kinetic descriptions of the five distinct binding sites that phosphorylase possesses (Figure 1.2 and 1.3).

(i) The Serine 14 Phosphate Site. The site is located in the N-terminal tail region of phosphorylase. Upon phosphorylation the tail, containing many basic residues, becomes ordered and the resultant new contacts stabilise the active GPa dimer. The phosphate at this site in GPa makes important contacts, involving Arg 69 and Arg 43' (from the symmetry related subunit), between subunits.

R state GPb crystallises from an ammonium sulphate buffer and contains a sulphate ion at the Ser(P) site which mimics phosphorylation by the kinase enzyme.

(ii) The Allosteric Site (N). This strong AMP binding site lies close to the subunit interface and contains three subsites, the phosphate, the sugar and the base. The dianionic phosphate of AMP is essential for the activation of GPb; adenosine alone and monoanionic AMP analogues do not activate phosphorylase (Withers & Madsen, 1980). The phosphate recognition site is created by Arg 310 and Arg 309, which reposition themselves upon AMP binding. The site can also accommodate ATP, ADP, glucose-6-phosphate and UDP-glucose, all of which inhibit phosphorylase to some extent.

(iii) The Glycogen Storage Site (G). The glycogen storage site is on the protein surface and is some 30Å away from each of the other ligand binding sites. The site can bind oligosaccharides as well as glycogen. It has been suggested that this high affinity site, which has a K_m of 1mM for maltoheptaose compared with 22mM at the active site (Kasvinsky, Madsen, Fletterick & Sygusch, 1978a), needs to be filled prior to the active site in the activation process.

(iv) The Nucleoside Inhibitor Site (I). This site is close (12Å) to the catalytic (C) site and

comprises residues Phe 285 and Tyr 613. In the T state form these are stacked together allowing purines (such as caffeine and AMP) to bind between and localise the 280s loop of residues.

Ligands binding at this site act synergistically with glucose in inhibiting phosphorylase, stabilise the T state enzyme and promote dissociation of the tetrameric enzyme to dimers. No physiological role has yet been found for this site (Kasvinsky, Madsen, Sygusch & Fletterick, 1978b).

(v) The Catalytic Site (C). The active site is located in the centre of the enzyme at the base of a long 12Å channel from the protein surface. It forms a specific binding site for glucosyl molecules, with the essential coenzyme pyridoxal 5'-phopshate linked by a Schiff base to Lys 680 close by.

Glucose and many glucose analogues (such as glucose-1-phosphate, heptenitol and the fluorodeoxy analogues) have been observed to bind at the active site (Sections 1.2.6 to 1.2.8), but oligosaccharide has never been located here. In the T state access to the catalytic site is blocked by the 280s loop of residues. In the R state, these residues become mobile, suggesting access to the site may be less hindered and Arg 569 swings out into the active site from a buried position.

1.2 THE CATALYTIC MECHANISM

Over the years extensive structural and biochemical studies of phosphorylase have provided insights into the essentials of the catalytic mechanism and the role of the coenzyme pyridoxal 5'-phosphate. However there are still some details that require experimental verification.

1.2.1 The Reaction Kinetics

The kinetic mechanism of phosphorylase action is a rapid equilibrium random bi bi (Engers, Bridger & Madsen, 1969; Gold, Johnson & Tseng, 1970; Engers, Shechosky & Madsen, 1970). This states that the substrates bind in a non-compulsory order to the enzyme and the interconversions of the ternary complexes are the rate limiting steps (Figure 1.4).

1.2.2 The Reaction Intermediate

An early isotope exchange study carried out by Mildred Cohn (Cohn, 1949) on muscle phosphorylase found that the glycosidic α-C1-O1 bond was broken and that the α-configuration at C-1 was retained during the reaction. A reaction mechanism of double displacement

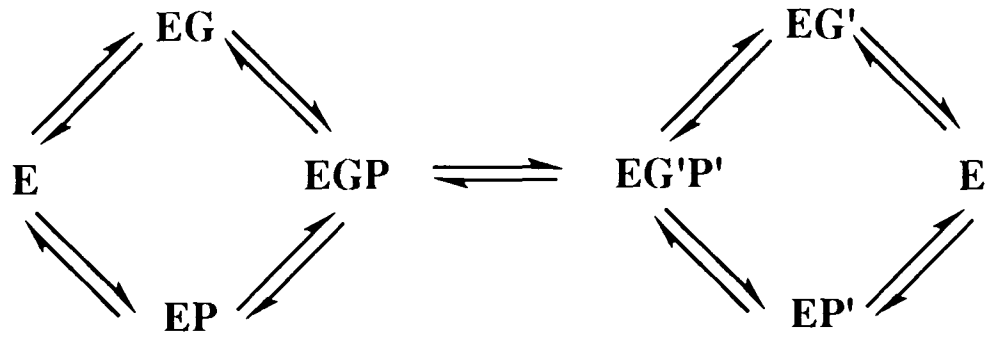

Figure 1.4. *The rapid equilibrium bi bi mechanism. E, G and P are respectively, enzyme-AMP complex, glycogen and P_i. G' is glycogen with one less terminal glucose unit and P' is glucose-1-phosphate.*

with formation of a β-glucosyl enzyme covalent intermediate or an oxocarbonium ion has been invoked to account for the retention of configuration. There is no conclusive evidence for an oxocarbonium ion intermediate but there is some support from a secondary isotope effect with k_i/k_d=1.1 (Tu, Jacobson & Graves, 1971) though a later study found a ratio of 1.0 (Firsov, Bogacheva & Bressler, 1974), which is more consistent with a covalent intermediate. If the intermediate is the chemically plausible oxocarbonium ion, then compounds modelling the half-chair conformation and charge distribution may act as transition state analogues (see the introduction to Chapter 2).

1.2.2 The Role of Pyridoxal 5'-Phosphate

The precise role of the coenzyme, pyridoxal 5'-phosphate (PLP, Figure 1.5), in the phosphorylase reaction has been the major challenge in elucidating the catalytic mechanism. The presence of pyridoxal phosphate in GP was discovered in 1957 (Baranowski, Illingworth, Brown & Cori, 1957) and it was later found to be essential for the catalytic activity of phosphorylase (Illingworth, Janz, Brown & Cori, 1958). The apo form of the enzyme can be reconstituted with pyridoxal phosphate, leading to full reactivation (Hedrick, Shaltiel & Fischer, 1966).

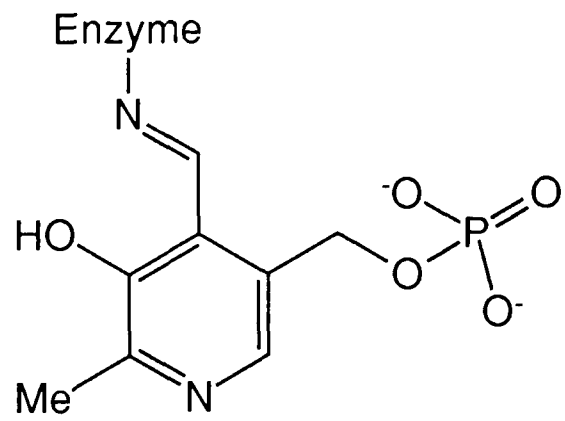

Figure 1.5. *The chemical structure of pyridoxal 5'-phosphate.*

A number of studies using a plethora of PLP analogues (Chang & Graves, 1985; Chang, Scott & Graves, 1987; Parrish, Uhing & Graves, 1977; Pfeuffer, Ehrlich & Helmreich, 1972; Shaltiel, Hedrick, Pocker & Fischer, 1969; Takagi, Fukui & Shimomura, 1982) have probed the catalytic role of PLP and shown that it is only the 5'-phosphate that plays an important part in the GP mechanism. In addition, analogues that were investigated containing 5' groups which were neither dianionic nor protonable in nature did not lead to reactivation of the enzyme. The 5'-phosphate group is of prime importance in the mechanism but it has been shown that it is not transferred during catalysis (Illingworth, Janz, Brown & Cori, 1958).

The ionic state of the 5'-phosphate group has been probed using ^{31}P n.m.r. (Feldmann & Hull, 1977; Klein, Im, Palm & Helmreich, 1984) and these investigations have concluded that the T state contains monoanionic and the R state contains dianionic 5'-phosphate. Upon formation of the ternary complex the ^{31}P n.m.r. studies suggest that the coenzyme phosphate may exist in two states, neither of which can be said to conclusively exist, either as a partially protonated monoanion (Klein & Helmreich, 1985) or as a tightly coordinated dianion (Withers, Madsen & Sykes, 1981b). The n.m.r. signal was consistent with both cases and the uncertainty lies in the interpretation of the ^{31}P n.m.r. spectra. From the results of this work and other studies, two roles for PLP in the phosphorylase catalytic mechanism have been proposed. It could be, firstly a proton donor-acceptor shuttle in a general acid-base mechanism, or secondly an electrophilic dianion constrained and distorted by its environment.

1.2.3 The Acid-Base Catalytic Mechanism

This mechanism, first considered by Kastenschmidt, Kastenschmidt and Helmreich (1968) and furthered by the work of Jenkins *et al.* (1981), has the 5'-phosphate in a catalytic proton donor and acceptor role. The mechanism originally invoked a basic or nucleophilic residue above C-1 (Klein, Palm & Helmreich, 1982) to stabilise the carbocation intermediate.

Structural work has, however, not indicated any obvious candidate lying within reach of C-1. Crystallographic and kinetic analyses of the reaction of heptenitol with phosphate in phosphorylase to form heptulose-2-phosphate, have led to the proposal of the current theory of the acid-base mechanism, as illustrated in Figure 1.6 (McLaughlin, Stuart, Klein, Oikonomakos & Johnson, 1984; Klein, Im & Palm, 1986; Johnson, Acharya, Jordan & McLaughlin, 1990).

In the direction of glycogen breakdown, upon formation of the ternary complex, the 5'-phosphate becomes protonated and functions through direct interaction as an acid to promote general acid attack of the substrate phosphate on the α-C1-O1 glycosidic bond. This leads to a carbonium ion intermediate which is stabilised by the substrate phosphate itself. The reaction is completed by nucleophilic attack of the substrate phosphate to C-1 of the carbonium ion to form the product, glucose-1-phosphate. In the reverse direction of oligosaccharide synthesis, the 5'-phosphate operates to protonate the phosphate of glucose-1-phosphate and cleavage of the α-C1-O1 bond follows. Attack of the oligosaccharide O4, promoted by acid-base action of the 5'-phosphate and substrate phosphate, then completes the synthesis.

This proposal necessitates the close interaction of the substrate and the 5'-phosphate moeties. A crystallographic study of the T state GPb-heptulose-2-phosphate complex supports the existence of this interaction with a phosphorus-phosphorus distance of 4.5Å (McLaughlin, Stuart, Klein, Oikonomakos & Johnson, 1984). The main evidence against this acid-base mechanism is that the phosphate analogues fluorophosphate (pKa 4.8) and phosphite (pKa 6.6) have been shown to be as effective as each other in activating pyridoxal reconstituted phosphorylase (Parrish, Uhing & Graves, 1977). At the physiological pH of 6.8, fluorophosphate cannot become protonated and thus the activation observed is surprising if the 5'-phosphate is operating as a proton transfer group. Structural studies of the phosphate analogues bound to T state GPb crystals (Oikonomakos *et al.*, 1987) have shown them not to bind in the same

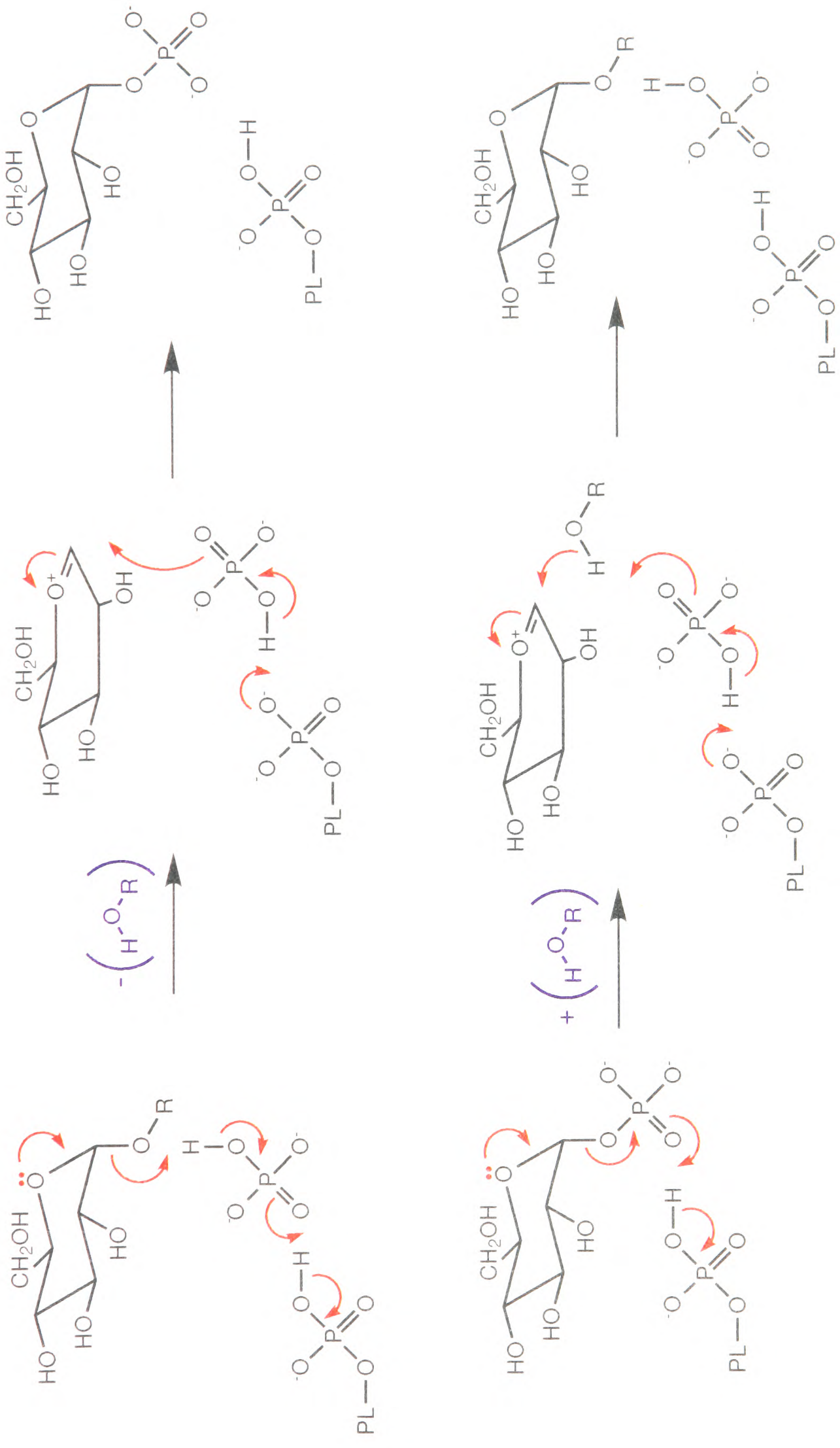

Figure 1.6. *The acid-base mechanism. The top scheme shows phosphorylysis of oligosaccharide and the lower scheme oligosaccharide synthesis.*

position as when these analogues are covalently linked to pyridoxal. It is possible that these analogues are not a good model for the native enzyme and that therefore the non-covalently bound phosphates may be operating by a different mechanism.

The general acid-base model of the mechanism explains the reversibility of the phosphorylase reaction and does not require the presence of a nucleophilic or basic residue above C-1 to stabilise the carbonium ion intermediate.

1.2.5 The Electrophilic Catalytic Mechanism

In contrast to the general acid-base mechanism, the electrophilic mechanism (Withers *et al.*, 1981a; Takagi, Fukui & Shimomura, 1982; Madsen & Withers, 1986) requires a pyrophosphate like interaction between the neighbouring 5'-phosphate and substrate phosphate.

Upon forming the ternary complex, the 5'-phosphate remains dianionic and is tightly coordinated by basic groups and in this process is constrained towards a trigonal bipyramidal configuration, with the empty apical position pointing towards the substrate phosphate. The empty apical position would be electrophilic in nature, and could withdraw electrons from the substrate phosphate, thereby labilising the glycosidic bond (Figure 1.7).

Such a proposal would require an even closer association of phosphates than the general acid-base mechanism, though there are basic groups in the vicinity which would be able to stabilise an intimate interaction.

An attempt to verify the electrophilic mechanism has been made using ^{31}P n.m.r. (Withers, Madsen & Sykes, 1981b). The results did suggest that the 5'-phosphate was tightly coordinated, but were not conclusive. Molybdate is a trigonal bipyramidal oxyanion and it has been

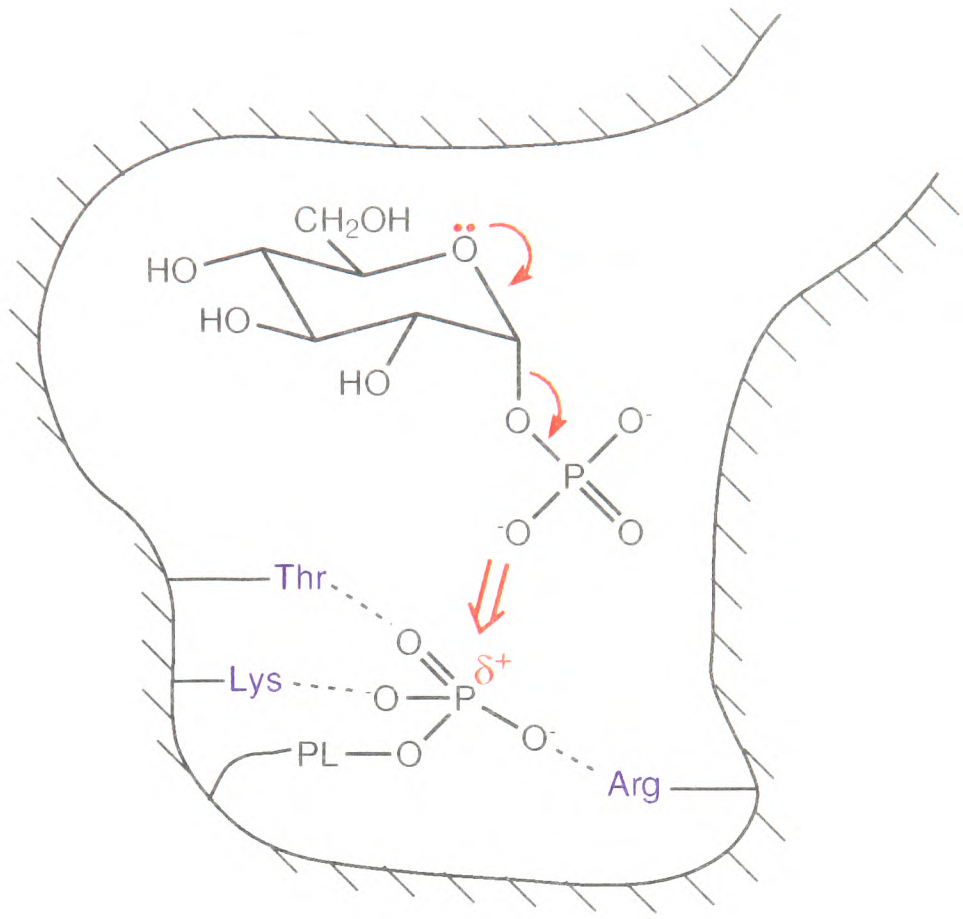

Figure 1.7. *The electrophilic mechanism. Possible candidate groups located in the active site to coordinate the 5'-phosphate include Lys 568 and 574, Arg 569 and Thr 677.*

tested for its inhibitory property with pyridoxal phosphorylase (Chang, McAlmont & Graves, 1983). If the phosphorylase reaction were to proceed through a trigonal bipyramidal like structure, the molybdate should act as an inactive transition state analogue and inhibit the enzyme. The inhibition found, K_i ~0.1mM, was consistent with the electrophilic mechanism but the oxyanion was not as inhibitive as had been anticipated for a transition state analogue and thus the study was not conclusive.

1.2.6 Mechanistic Evidence from Glycosylic Substrates

Both of the mechanisms, the general acid-base and the electrophilic, which have been proposed for phosphorylase require the direct interaction of the 5'-phosphate of PLP with substrate

phosphate and invoke a carbonium ion intermediate.

There have been many crystallographic, kinetic and n.m.r. studues carried out with the aim of providing evidence for the interaction and for the carbonium ion transition state but none, as yet, have unambiguously observed such an interaction.

In the past, glycosylic substrates have often been utilised as transition state analogues and used to probe the enzyme mechanism. Glycosylic substrates are compounds of non-glycosidic structure with the pseudo anomeric carbon linked to an electron rich bond. Though none studied have been kinetically proven to be a true transition state analogue, useful insights into the phosphorylase mechanism have been obtained.

1.2.7 The Heptenitol Reaction

To date the most mechanistically informative study has been the work on the reaction of heptenitol with phosphate in phosphorylase (McLaughlin, Stuart, Klein, Oikonomakos & Johnson, 1984; Hajdu *et al.*, 1987; Johnson, Acharya, Jordan & McLaughlin, 1990; Duke, Wakatsuki, Hadfield & Johnson, 1994). Heptenitol contains a methylene group at C-1 providing an electron rich pseudo anomeric carbon and this compound will react with phosphate to form heptulose-2-phosphate (H2P) as product (Figure 1.8).

Heptulose-2-phosphate is an extremely tightly binding dead end product, with a K_i of 14μM (Klein, Im & Palm, 1986), and may model the transition state of the native reaction. In its preferred conformation, H2P makes a direct contact with the PLP 5'-phosphate and Arg 569 moves into the active site from a buried position to coordinate the H2P phosphate. It is thought that the C-1 methyl group forces the phosphate into a conformation where it is below the pyranose ring, making an internal hydrogen bond contact between O-2 and the phosphate. This

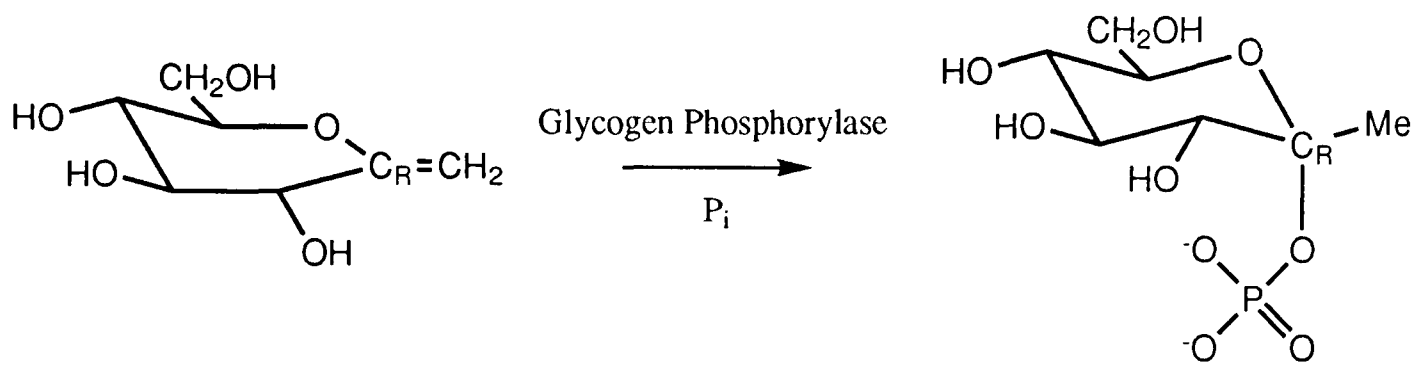

Figure 1.8. *The reaction of heptenitol with phopshate to give heptulose-2-phosphate as product. C_R represents the electron rich pseudo-anomeric carbon*

is unlike the complex of GPb with glucose-1-phosphate where no direct contact is made between the ligand phosphate and the PLP 5'-phosphate (see later).

A time-resolved study on the heptenitol reaction (Hajdu *et al.*, 1987) revealed the formation of heptulose-2-phosphate at the catalytic site and a putative attacking site for substrate phosphate. The 2.8Å resolution data precluded a definitive conclusion and the peak may have represented phosphate from a small amount of product. This result was further substantiated by the Laue work of Duke, Wakatsuki, Hadfield and Johnson (1994) on the heptenitol reaction. A study on the complex of dead end product (heptulose-2-phosphate) with GPb, a direct interaction between the 5'-phosphate and product phosphate was observed. The crystal structure of the T state GPb-heptulose-2-phosphate complex with oligosaccharide and AMP has been refined (McLaughlin, Stuart, Klein, Oikonomakos & Johnson, 1984; Johnson, Acharya, Jordan, McLaughlin, 1990) and the refined coordinates confirmed that there was a direct hydrogen bond interaction between the 5'-phosphate and phosphate of H2P (a closest contact of 2.3Å). Protein conformational changes were observed at the catalytic site,with the 280s loop residues moving to partially open a channel to the surface of the protein (Barford *et al.*, 1988). Moreover, Arg 569 was seen to move more than 7Å into the catalytic site, taking the place of Asp 283, and contributing to the stabilisation of the close proximity of the two

phosphate groups.

1.2.8 Other Structural and Kinetic Studies

Other structural and kinetic studies of GPb-complexes which have provided insight into the catalytic mechanism have included: glucose-1-phosphate and several derivatives; glucose-1,2-cyclicphosphate; PLPPGlc; D-1,5-gluconolactone; D-gluconohydroximo-1,5-lactone *N*-phenylurethane (PUG) and D-gluconohydroximo-1,5-lactone.

(i) α-D-Glucose-1-phosphate and derivatives. The studies upon α-D-glucose-1-phosphate and two derivatives (2-deoxy-2-fluoro-α-D-glucose, α-D-glucose-1-methylenephosphonate), stabilising the R state conformation, showed there to be a movement of the 280s loop at the catalytic site (Martin, Johnson & Withers, 1990).

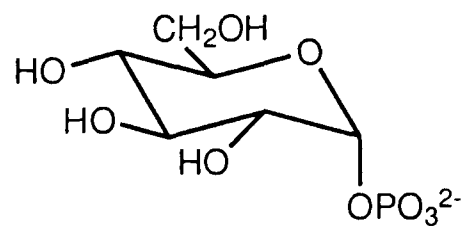

α-D-Glucose-1-Phosphate

Upon binding the phosphorylated ligands the 280s shifted out of the catalytic site towards the protein surface. Interestingly, the conformations of the phosphate groups at the active site were different from the H2P structure pointing away from the PLP phosphate. Also in contrast to the H2P structure, Arg 569 remained buried and did not interact with the two phosphates.

(ii) Glucose-1,2-cyclicphosphate. This cyclic ester acts as an R state inhibitor, mimicking the action of glucose-1-phosphate (Hu & Gold, 1978; Withers, Madsen, Sprang & Fletterick,

1982).

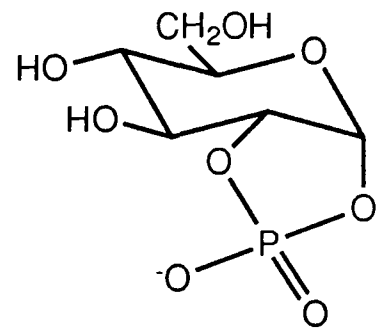

Glucose-1,2-Cyclicphosphate

However, analysis of the ester complexed with cross-linked GPb-AMP crystals showed the conformationally constrained ester phosphate to interact with the cofactor phosphate unlike G1P (Jenkins *et al.*, 1981). An important ^{31}P n.m.r. study has shown that on binding glucose-1,2-cyclicphosphate to the GPb-AMPS-maltopentaose complex, the PLP 5'-phosphate signal is broadened (Withers, Madsen & Sykes, 1981b). This can be interpreted as either acting by a change in protonation state (supportive of the acid-base mechanism), or by a change to a more tightly constrained dianion (supportive of the electrophilic mechanism). The interpretation of this n.m.r. remains unresolved.

(iii) Pyridoxal-(5')-diphospho-(1)-α-D-glucose (PLPPGlc). Radio-labelled PLPPGlc has been used to reconstitute apophosphorylase (Takagi, Fukui & Shimomura, 1982).

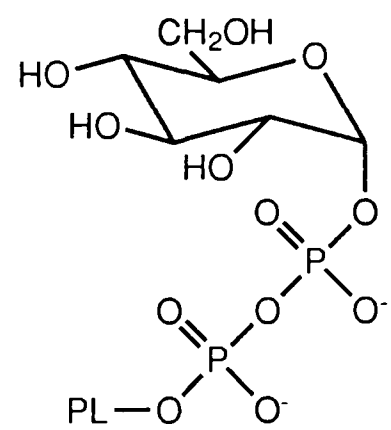

Pyridoxal-(5')-Diphospho-(1)-α-D-Glucose

Upon incubation with maltopentaose of glycogen, the cofactor decomposed to pyridoxal 5'-

diphosphate and the radiolabelled glucose was incorporated into the glycogen chain. The reaction had a $t_{0.5}$ of about 13 minutes, $t_{0.5}$ for the native reaction being 4 minutes (Klein, Im, Palm & Helmreich, 1984). These results suggest that this reaction mimics, to a certain extent, the normal catalysis and supports a catalytic mechanism where the coenzyme interacts directly with the substrate phosphate, possibly by an intimate pyrophosphate like action.

(iv) D-1,5-Gluconolactone. This half-chair compound has been shown to be a potent inhibitor of GPa in the presence of saturating AMP and phosphate (Gold, Legrand & Sánchez, 1971).

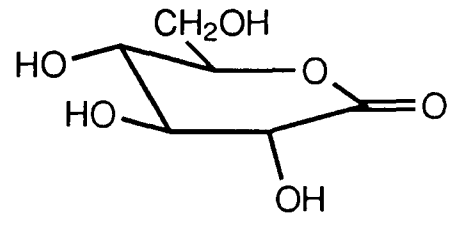

D-1,5-Gluconolactone

A kinetic analysis led to the finding that gluconolactone binding increased by 28 fold from a K_i of 0.69mM for gluconolactone alone to 0.025mM in the presence of AMP and phosphate. This suggested that in the presence of phosphate, phosphorylase undergoes a change to confer a preference for half-chair compounds. Phosphorylase shows no increase in affinity for glucose in the presence of phosphate. Therefore 1,5-gluconolactone may be an analogue of the substrate part of the transition state. A structural analysis of the complex with GPb has, however, been precluded by the hydrolytic instability of this compound.

(v) PUG and D-gluconohydroximo-1,5-lactone. These compounds were designed to stabilise the half-chair conformation of 1,5-gluconolactone by resisting hydrolysis. It was also hoped that PUG, with its bulky phenylurethane substituent, would mimic the phosphorylase oligosaccharide transition sate, and indicate the channel from protein surface to active site.

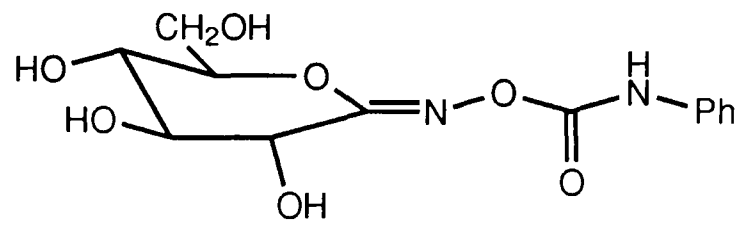

PUG

Kinetic studies with PUG and the unsubstituted compound, gluconohydroximo-1,5-lactone, showed them to inhibit GPb with K_i values of 0.4mM and 0.9mM respectively and also showed them to have different kinetic properties from each other (Papageorgiou, Oikonomakos & Leonidas, 1989; Papageorgiou *et al.*, 1991). Despite the trigonal stereochemistry both compounds possess at C-1, structural analysis found that they bound in different manners. PUG was found to bind in a half-chair conformation and be an R state stabilising inhibitor (Barford *et al.*, 1988), whilst the unsubstituted compound bound as a full chair and stabilised the T state (Papageorgiou *et al.*, 1991).

These results from analysis of the T state GPb-complexes, concluded that the binding of PUG was not analogous to oligosaccharide, the phenylurethane binding channel to the surface being blocked by the 279-293 loop. Crystallographic analysis also concluded that the catalytic site offered no dominating steric factors to promote distortion of the glucopyranose ring towards a half-chair conformation, but that it is stabilisation by substrate phosphate of the oxocarbonium ion intermediate that is important.

1.2.9 The Binding of Phosphate and Oligosaccharide

The binding of a phosphate ion (P_i) at the active site of GPb has not been observed, even in experiments with crystals soaked in 0.5M phosphate. It does however bind at the allosteric site, and also at the active site of GPa crystals (Goldsmith, Sprang, Hamlin, Xuong & Fletterick, 1989), but not within direct contact of the PLP 5'-phosphate.

Oligosaccharide has never been observed to bind at the active site of GPb even at concentration up to 1M, though the enzyme is active in the crystal (Kasvinsky & Madsen, 1976). It is assumed that the channel to the active site can open to allow access by substrate oligosaccharide but not for a sufficient length of time to be observed crystallographically. Oligosaccharide has been seen to bind at the glycogen storage site (Kasvinsky, Madsen, Sygusch & Fletterick, 1978b; Johnson, Stura, Sansom & Babu, 1983; Johnson *et al.*, 1988).

1.2.10 Summary

Both the acid-base and electrophilic mechanisms are, in general, consistent with the current level of phosphorylase mechanistic knowledge. Both proceed via a carbonium intermediate, retain configuration and involve the close association of the 5'-phosphate and substrate phosphate. They differ on the role of pyridoxal phosphate and as yet neither mechanism can be ruled out. Neither oligosaccharide nor phosphate have been crystallographically seen to bind at the active site of GPb and observation of this is crucial for the resolution of the debate on the phosphorylase catalytic mechanism.

2.1 INTRODUCTION

2.1.1 Overview

Many crystallographic studies on T state phosphorylase crystals have attempted to verify the direct interaction between substrate phosphate and the PLP 5'-phosphate proposed in the general acid-base (Johnson, Acharya, Jordan & McLaughlin, 1990) and electrophilic (Madsen & Withers, 1986) mechanisms. The results of work on the reaction of heptenitol with phosphate in phosphorylase have provided good evidence for such an interaction, with the phosphate of the reaction product, heptulose-2-phosphate, forming a hydrogen bond with the 5'-phosphate. Time resolved studies, also on heptenitol, have provided a putative attacking site for phosphate (Hajdu *et al.*, 1987). Further studies on the early stages of the heptenitol reaction using Laue diffraction located a phosphate peak consistent with the position expected for phosphate in the attacking position (Duke, Wakatsuki, Hadfield & Johnson, 1994). However, the study also pointed out the difficulties in distinguishing between a Fourier peak due to unreacted phosphate and a peak due to phosphate from a small amount of product, heptulose-2-phosphate. Such a situation is exacerbated when no other diagnostic information is available.

A binding study with a transition state analogue could allow the creation of a phosphate recognition site at the active site of phosphorylase. Enzyme kinetic studies have shown that the rate limiting step is turnover of the ternary enzyme substrate complex and that binding of one substrate increases affinity for the other.

2.1.2 A Good Transition State Analogue

A good transition state analogue should mimic the proposed oxocarbonium ion intermediate of the native reaction by adopting a half chair conformation and possessing an electron rich

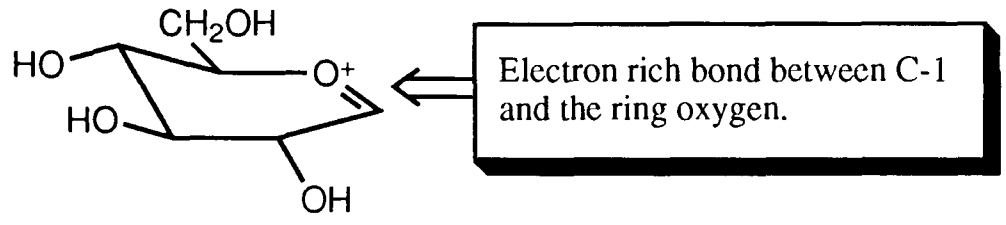

Figure 2.1. An idealised glycogen phosphorylase transition state analogue.

bond between C-1 and the oxygen position (Figure 2.1).

2.1.3 Nojirimycin Tetrazole

Recently a new tight binding inhibitor (e.g. K_i for β-glucosidase from *Agrobacter* 1.4μM; Ermert, Vasella, Weber, Rupitz & Withers, 1993) of glycosidases, nojirimycin tetrazole, was reported (Ermert & Vasella, 1991). A single crystal X-ray crystallographic analysis of the inhibitor revealed that the fused tetrazole ring forced the sugar ring to adopt a half chair conformation (Figure 2.2). The half-chair conformation and electro positive nature of the ring nitrogen mimic the transition state, thus explaining the high affinity binding observed. The glucose tetrazole and its mannose equivalent have subsequently been subjected to detailed kinetic analysis as inhibitors of a range of β-glycosidases and β-mannosidases (Ermert, Vasella, Weber, Rupitz & Withers, 1993). A linear correlation was established between log K_i for each inhibitor/enzyme pair and log k_{cat}/K_m for the corresponding substrate/enzyme pair. This is required if the tetrazole compound functions as a transition state analogue. The measure of k_{cat}/K_m is an apparent second order rate constant that refers to the properties and reactivities of free enzyme and free substrate and determines specificity for competing substrates (Fersht, 1985).

In common to phosphorylase and glycosidases is the presumption that their mechanisms both proceed through a carbonium ion transition state, although they do exhibit differences in the

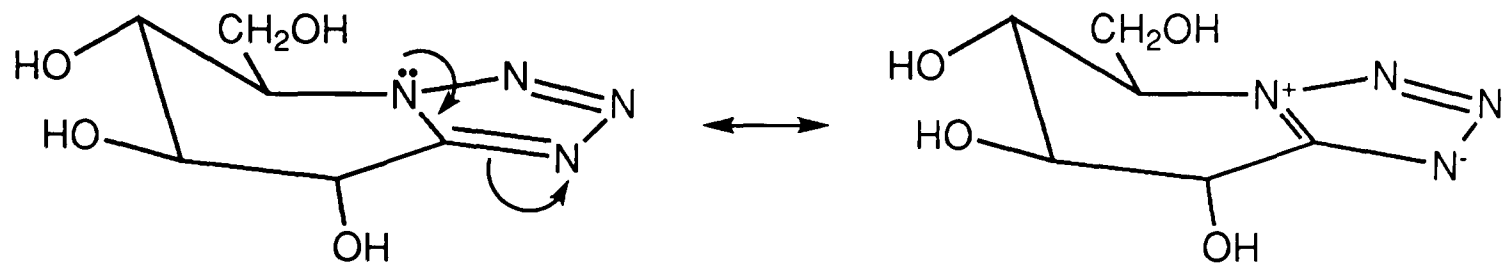

Figure 2.2. *Nojirimycin tetrazole and one of its possible canonical forms illustrating the similarity to an oxocarbonium ion intermediate.*

way that this transition state is promoted. Hence it was considered possible that nojirimycin tetrazole would also function as a transition state analogue inhibitor of phosphorylase. On the other hand it is known that deoxynojirimycin itself is a poor inhibitor of phosphorylase (K_i of 55mM, Ariki & Fukui, 1977) whereas it is a potent inhibitor of many glucosidases (eg K_i of 0.032μM for rabbit intestinal sucrase, Hanozet, Pircher, Vanni, Oesch & Semenza, 1981). The weak inhibition of phosphorylase can be attributed to a bad contact from the pyranose ring nitrogen to the main chain of Leu 136 (L N Johnson, unpublished results). This stresses the differences between the active sites of phosphorylase and of the glycosidases.

This chapter describes the kinetic analysis (in collaboration with Stephen Withers, University of British Columbia, Canada) and a detailed X-ray crystallographic analysis of the binding of nojirimycin tetrazole to the T state of GPb. These studies for the first time unambiguously show phosphate to bind at the active site of T state GPb and confirm the putative phosphate attacking site proposed by Hajdu *et al.* (1987) and recently furthered by Duke, Wakatsuki, Hadfield & Johnson (1994). The importance of the glucosidic oxygen O-2 is emphasised and its role in the catalytic mechanism discussed.

2.2 EXPERIMENTAL METHODS

2.2.1 Kinetic Studies

The kinetic studies were carried out by Professor Steven Withers and his group at the University of British Columbia in Canada.

Rabbit muscle phosphorylase b was prepared by the method of Fischer & Krebs (1962) using DTT instead of cysteine and recrystallised at least three times before use. Protein concentration was determined from absorbance measurements at 280 nm by using the absorbance index $\varepsilon^{1cm\ 1\%}$ of 13.2 (Buc & Buc, 1968). Rabbit liver glycogen (type III) purchased from Sigma Chemical Co. was purified on a Dowex 1-Cl column and assayed by the method of Dishe (Ashwell, 1957).

Initial reaction rates in the direction of saccharide synthesis were determined at 30°C by the Fiske-Subbarow phosphate analysis as described by Engers (1970). Reaction mixture volumes were 0.25mL and contained 1mM AMP and 0.5% glycogen in pH 6.8 buffer containing 20mM sodium glycero-phosphate, 1.5mM EDTA and 5mM DTT. Initial reaction rates in the direction of glycogen breakdown were determined in the same buffer system using the coupled assay described previously (Engers, 1970) in which the product glucose-1-P is converted to glucose-6-phosphate by phospho-glucomutase and then to 6-phospho-gluconic acid with conversion of NAD to NADH, the reaction being monitored by changes in absorbance at 340 nm. Values for inhibition constants (K_i) were determined by measuring initial reaction rates at a constant concentration of AMP (1mM) and either glycogen (0.5%) or phosphate (20mM) with different amounts of the varied substrate and inhibitor as shown in the appropriate figure legends. Data were analysed by use of the non-linear regression programme GraFit (Leatherbarrow, 1990).

2.2.2 Crystallographic Binding Studies

Chemicals were purchased from Sigma Chemical Company with the exception of nojirimycin tetrazole which was prepared by Philipp Ermert and Andrea Vasella (1991).

For the present work models of the ligands were generated using the program SYBYL (Tripos Associates) and a Powell method minimisation. A comparison of the final model of the tetrazole with the published single X-ray crystal structure (Ermert & Vasella, 1991) revealed no significant differences. The AM1 method (Dewar, Zoebisch, Healy & Stewart, 1985) was used to calculate partial charges on indiviual atoms in each model.

Crystallisation of T state GPb was carried out by Dr Nikos Oikonomakos and his group at the National Hellenic Foundation in Greece. Purified rabbit skeletal muscle glycogen phosphorylase was prepared by the method of Fischer and Krebs (1962) with minor modification. T state enzyme was crystallised from solutions containing 20-40 mg/ml glycogen phosphorylase b, 1mM IMP, 1mM spermine, 10mM BES, 0.1mM EDTA and 0.02% sodium azide (pH 6.7). These conditions gave tetragonal crystals, space group $P4_32_12$ with unit cell a = b = 128.5Å and c = 116.3Å.

Binding studies using these crystals were carried out by diffusion of ligands into the enzyme crystal. Prior to data collection crystals of T state GPb, approximately 1.5mm x 0.5mm x 0.5mm in size, were prepared by soaking native GPb crystals in a buffered solution (10mM BES, 0.5mM EDTA, 0.02% sodium azide) containing the appropriate ligand (e.g. tetrazole, sodium dihydrogen phosphate or 4-fluoro-4-deoxyglucose) at selected concentrations for 72 hours (Table 2.1). For data collection the crystals were mounted in thin glass capillaries 2mm in diameter.

	Ligand concentration in soak solution (mM)			Binding sites occupied in the complexes			
				Catalytic		Allosteric	Other
	Tetrazole	Phosphate	Other	Tetrazole	Phosphate	Phosphate	
(1)	100	0	0	Yes	No	No	No
(2)	1	1	0	Yes	No	Yes	No
(3)	100	1	0	Yes	No	Yes	No
(4)	1	10	0	Yes	Yes	Yes	No
(5)	0.1	50	0	Yes	Yes	Yes	No
(6)	1	50	0	Yes	Yes	Yes	No
(7)	1	50	300[a]	Yes	Yes	Yes	Yes (G Site)
(8)	100	50	0	Yes	Yes	Yes	No
(9)	0	50	0	No	No	Yes	No
(10)	0	50	100[b]	No	No	Yes	Yes (C Site)

[a]Maltoheptaose [b]4-Fluoro-4-deoxy-glucose (organic synthesis procedure in Appendix C)

Table 2.1. *Table of the ten complexes studied and the composition of the soak solutions with the binding sites subsequently shown to be occupied.*

Data to 2.4Å resolution were collected on a Siemens IPC multiwire detector (Howard *et al.*, 1987) using a Rigaku RU-200H rotating anode X-ray source with a graphite monochromator, producing CuKα X-radiation of wavelength 1.54Å, operating at 50kV, 60mA and an effective source size 0.3mm x 0.3mm. The detector was placed 16cm away from the crystal and at a 2θ angle of 22° to give a maximum resolution of 2.3Å. Data frames of 0.2° oscillation were collected with exposure times of between 100 and 120 seconds for a total angular range of 90°. Each experiment was performed with a single crystal of glycogen phosphorylase b. The data were subsequently processed with either the XENGEN (Howard *et al.*, 1987) package or with the XDS (Kabsch, 1993) package to produce scaled sets of indices and intensities.

2.3 RESULTS

2.3.1 Kinetic Studies

Inhibition in the direction of glycogen synthesis is seen to be competitive with respect to glucose-1-P and a K_i value of 0.70mM (phosphorylase-AMP-glycogen complex) was determined. The Lineweaver-Burke plot of the kinetic results is shown in Figure 2.3. When assayed in the reverse direction (glycogen breakdown) in the presence of varying phosphate concentrations, different kinetic behaviour was observed (Figure 2.4). In this case uncompetitive inhibition was seen and a K_i value of 53μM (phosphorylase-AMP-glycogen-P_i complex) determined. Finally, assays performed in the direction of glycogen breakdown at a constant concentration of phosphate but varying the glycogen concentrations revealed non-competitive inhibition behaviour, with a K_i value of 59μM (data not shown).

The inhibition constant for nojirimycin tetrazole does not indicate the high affinity of phosphorylase for tetrazole which might be anticipated if the tetrazole alone were a transition state analogue. However the thirteen fold decrease in K_i for the tetrazole in the presence of phosphate is significant and indicates P_i tightens tetrazole binding. This may indicate that the tetrazole and phosphate complex is closer to the transition state for phosphorylase than tetrazole alone. Although the tetrazole and phosphate are not an ideal transition state analogue, for which a lower K_i would be expected, they are a reasonable model.

2.3.2 Structural Studies: Difference Fourier Maps

The statistics for data collection and processing are shown in Table 2.2. The data sets were all at least 70% complete to 2.4Å and 79% complete to 3.2Å resolution which produces clear difference maps for phosphorylase. The merging R factor, R_m, values were between 4.5 and

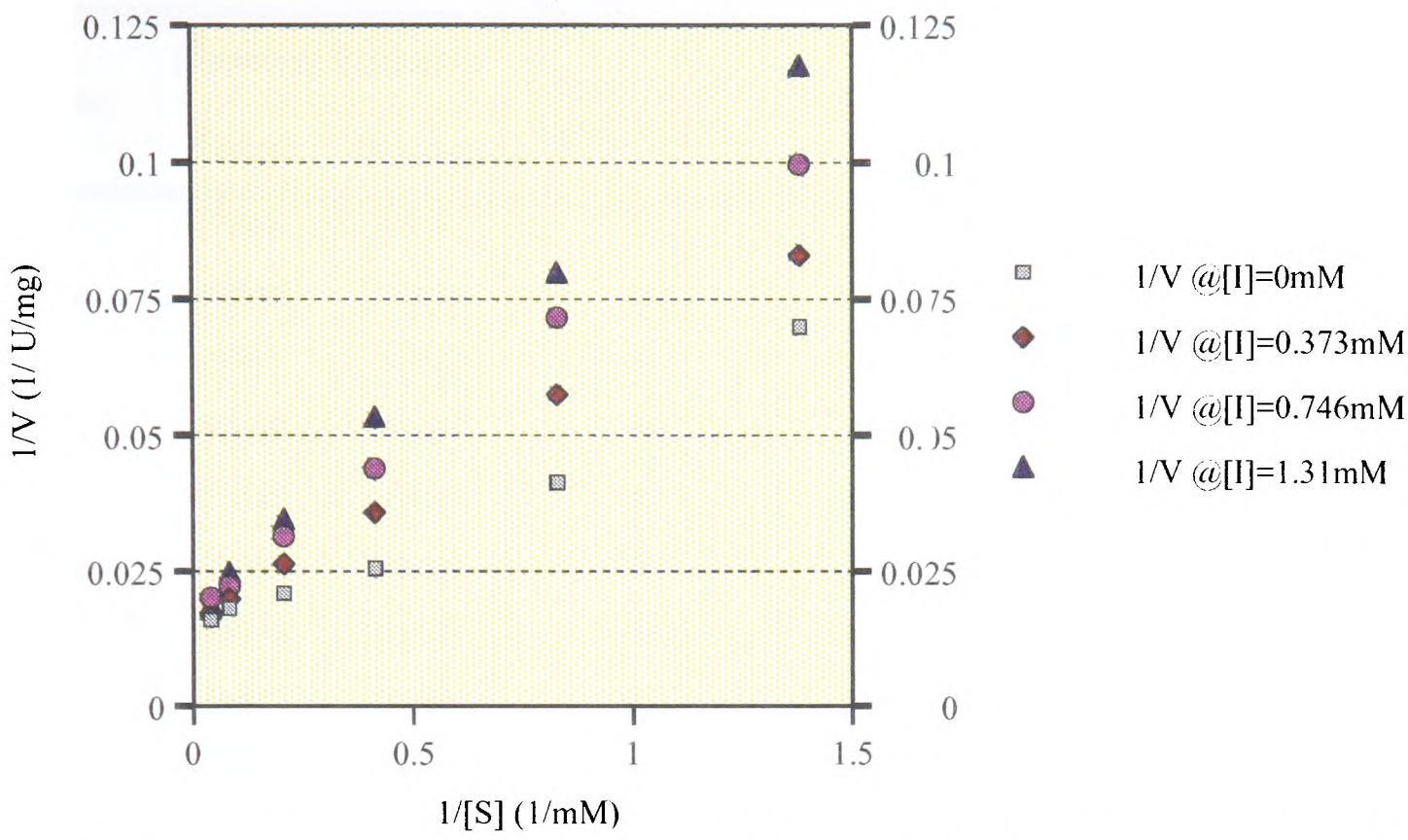

Figure 2.3. *Graph showing the competitive inhibition of phosphorylase assayed in the direction of glycogen synthesis. Concentration of tetrazole,[I] 0-3.7mM (for clarity not all data shown); α-glucose-1-phosphate,[S] 0.7-40mM; GPb 4.40μg/ml.*

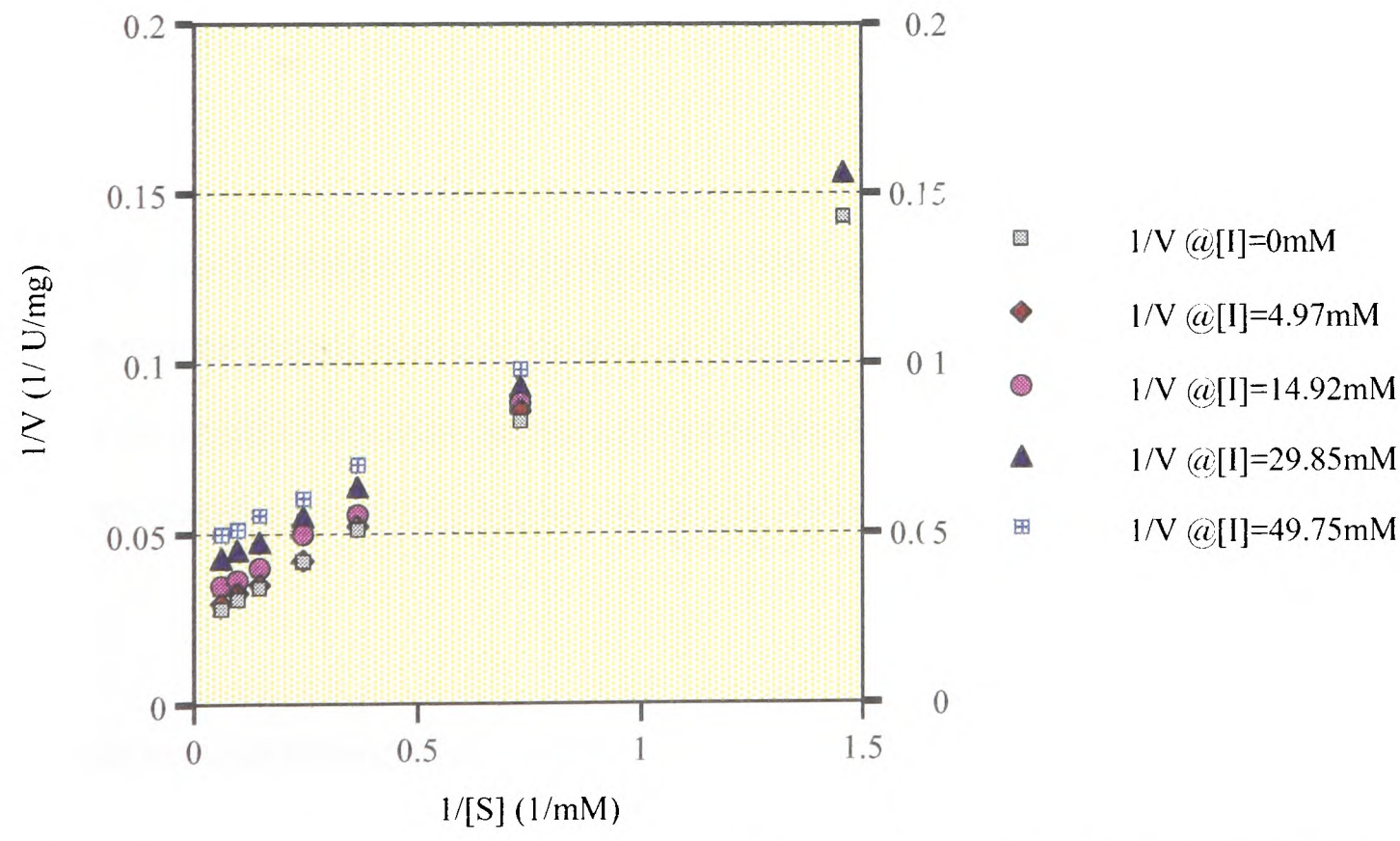

Figure 2.4. *Graph showing the uncompetitive inhibition of phosphorylase assayed in the direction of glycogen breakdown. Concentration of tetrazole,[I] 0-50μM; P_i, [S] 0.7-17mM; 0.5% glycogen; 1mM AMP.*

Complex	Number of Reflections		Completeness of Data(2.4Å) (%)[a]	$R_m(I)$ (%)	Number of Reflections I/σ > 3	R_{iso}[b] (%)
	Unique	Observed				
(1)	37024	82739	95	6.8	21273	11.7
(2)	30555	74446	78	5.8	22059	9.5
(3)	28951	60160	74	4.5	21337	10.6
(4)	30778	73497	79	6.0	20235	9.7
(5)	36447	79847	93	6.4	21876	14.4
(6)	27392	72437	70	6.1	19203	13.6
(7)	31642	73117	81	5.5	22239	12.7
(8)	31917	75889	82	5.9	19283	15.3
(9)	30393	74509	78	5.9	20650	12.4
(10)	30608	74644	78	5.1	22357	12.4

[a]In some cases data completness is not optimal due to availability of instrument time. The data does, however, give clear experimental results. [b]Mean fractional isomorphous difference calculated with respect to native T state data (Acharya, Stuart, Varvill & Johnson, 1990)

Table 2.2. *Crystallographic data collection and processing statistics for the T state GPb complexes.*

6.8%.

The observed structure factors were scaled together with native T state phosphorylase structure factors and refined phases from a 1.9Å data set (Acharya, Stuart, Varvill & Johnson, 1991). These were then used to calculate difference Fourier electron density maps. A summary of the binding sites occupied in each complex, as deduced from the difference maps, is shown in Table 2.1.

(i) Tetrazole Alone at 100mM Concentration - Complex [1]. In the difference map of the GPb-tetrazole complex (tetrazole 100mM) the highest peak in the Fourier difference map occurred at the catalytic site, corresponding to binding of a tetrazole molecule (Figure 2.5a). Several alterations of the enzyme structure were evident. Ligand binding at the catalytic site caused

movement of His 377 away from O6 of the tetrazole. A similar adjustment in the enzyme conformation is observed upon ligation of other glucose like compounds (Oikonomakos *et al.*, 1988; Martin *et al.*, 1991; Watson *et al.*, 1994). Positive density close to Leu 136 indicated that the tetrazole ring of nojirimycin tetrazole was forcing Leu 136 away from the catalytic site to accommodate the additional bulk. At the caffeine site poorly resolved density between Phe 285 and Tyr 613 showed partial occupancy by a tetrazole molecule.

(ii) Phosphate 1mM/Tetrazole 1mM and 100mM Concentration - Complexes [2] and [3]. Both experiments with phosphate at 1mM concentration (tetrazole 1mM and 100mM) gave Fourier difference maps containing peaks at the allosteric site corresponding to phosphate binding and movement of Arg 309 to coordinate and complete the phosphate recognition site. Positive density surrounding the side chain of Arg 310 indicated these atoms to be less mobile in the phosphate complexes than in the native structure. At the active site a bound tetrazole molecule was evident from the density maps. At 100mM concentration of tetrazole (complex [3]), density at the caffeine site indicated partial occupancy by tetrazole between the aromatic rings of Phe 285 and Tyr 613, which at 1mM was no longer present. Similar changes at the active site to those seen for the GPb-tetrazole complex were also evident in both 1mM phosphate experiments. No significant density attributable to a phosphate ion was observed in either case at the active site. A small amount of density, though, was present in both Fourier maps to the side of the expected phosphate position. This may have been due to a weakly bound water molecule or to a small amount of bound phosphate.

(iii) Phosphate 10mM/Tetrazole 1mM Concentration - Complex [4]. Including phosphate at a concentration of 10mM (tetrazole 1mM) in the soak solution gave similar results to those described below for the 50mM phosphate/1mM tetrazole experiment but with poorer density for the phosphate ion, indicating lower occupancy of the phosphate site (Figure 2.5b). Movement of Arg 569 and the 280s loop was evident, but the density was not well defined.

(iv) Phosphate 50mM/Tetrazole 0.1mM, 1mM and 100mM Concentration - Complexes [5], [6], [7] and [8]. The increased concentration of phosphate resulted in strong spherical density at the active site corresponding to a phosphate ion. The density was located between the PLP 5'-phosphate and tetrazole molecule and distinct from both. There was a small deterioration in the tetrazole density between complex [6] (tetrazole 1mM) and complex [5] (tetrazole 0.1mM).

In all of these difference maps negative density surrounded Asp 283 and the side chain of Arg 569. Positive density close to the phosphate site indicated a possible new position for Arg 569 coordinating the phosphate ion, but no new position for Asp 283 could be interpreted from the maps. In all three cases this density was superior to that observed in the 10mM phosphate/1mM tetrazole experiment. Figures 2.5a to 2.5d compare the Fourier difference maps at the active site for the series of complexes: 100mM tetrazole with no phosphate [1], 1mM tetrazole with 10mM [4] and 50mM [6] phosphate and 100mM tetrazole with 50mM phosphate [8].

Some differences were apparent between the 50mM phosphate difference maps. At a tetrazole concentration of 100mM, density indicating movement of Arg 569 and Asp 283 was not as clearly defined as at tetrazole concentrations of 1mM and 0.1mM, being more continuous at the lower concentrations.

As previously observed with complexes [2] and [3], the higher tetrazole concentration (100mM) of complex [8] led to some density between Phe 285 and Tyr 613 of the caffeine site. At the lower tetrazole concentrations (1mM and 0.1mM) of complexes [5], [6] and [7], no such density was apparent at a map contour level of 3 sigma.

In all of these experiments density at the allosteric site indicated binding of a phosphate ion there, with movement of Arg 309 to coordinate it. Where maltoheptaose (300mM) had been

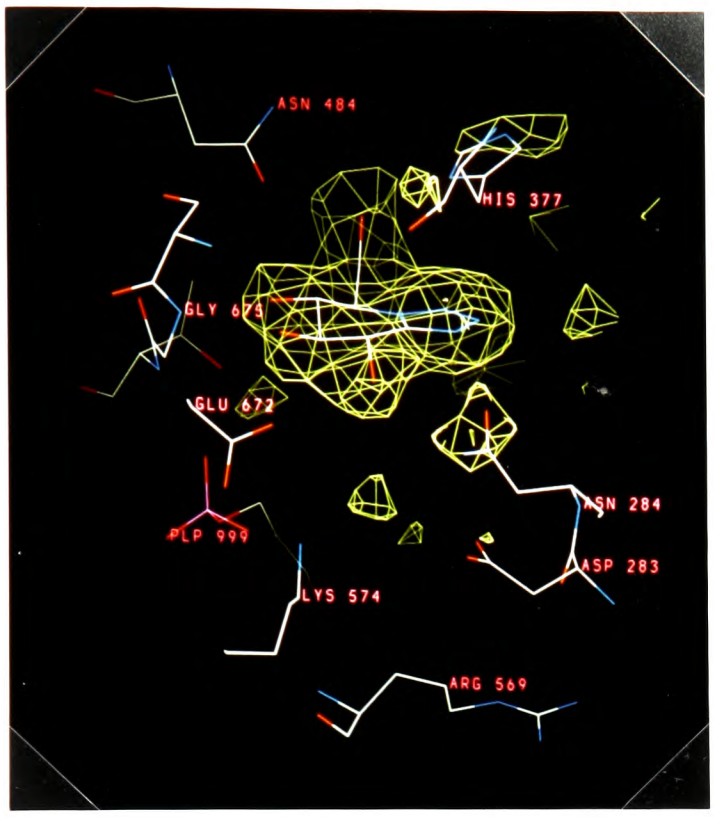

(a)

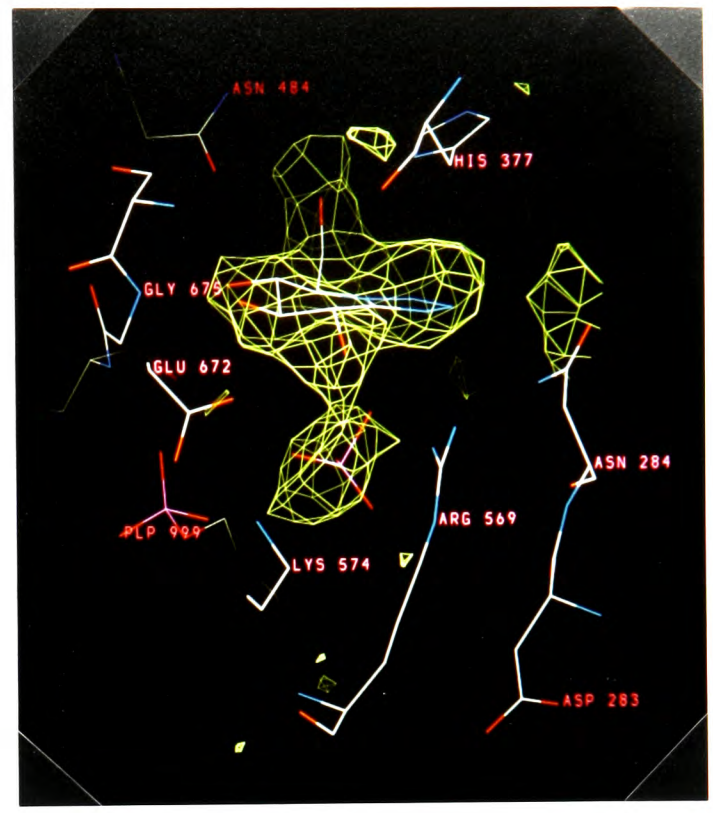

(b)

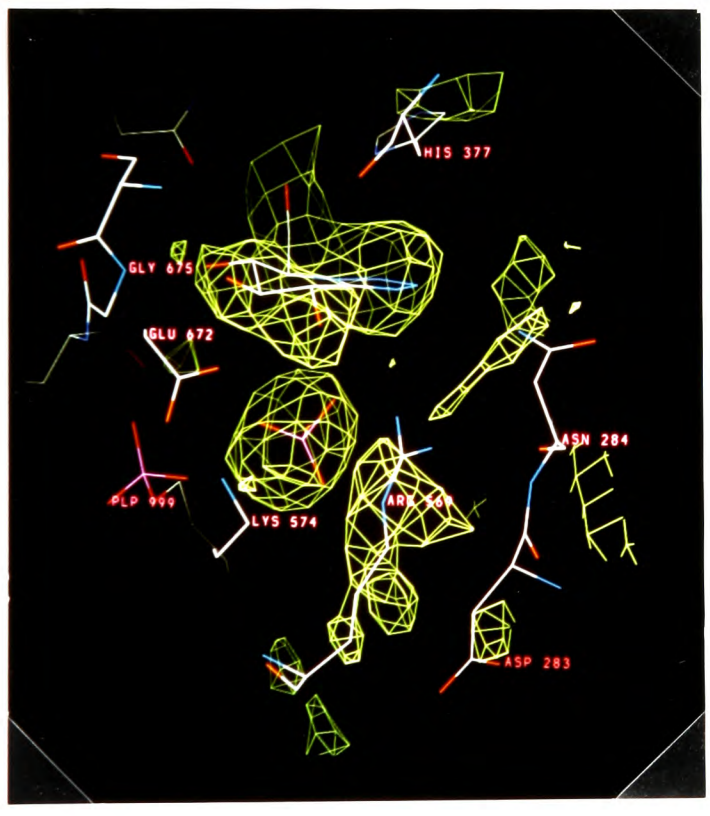

(c)

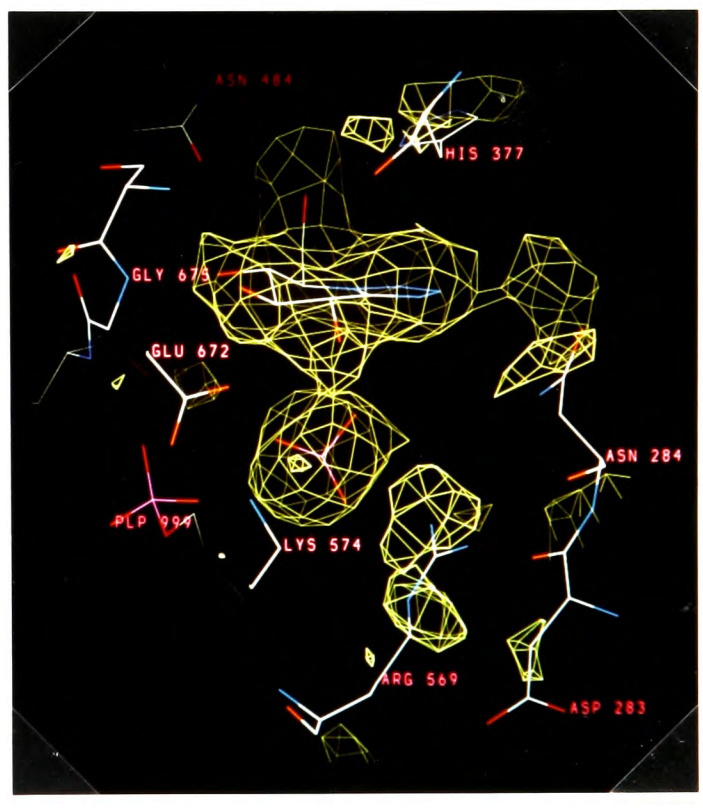

(d)

Figures 2.5a to 2.5d. *Comparison of the (F_o-F_c) Fourier maps at the active sites for the complexes: (a) 100mM tetrazole alone (b) 1mM tetrazole/10mM phosphate - the phosphate peak is not well defined (c) 1mM tetrazole/50mM phosphate - the phosphate peak is well defined and the density for the Arg 569 side chain is the best observed out of all the tetrazole-phosphate complexes (d) 100mM tetrazole/50mM phosphate - the Arg 569 side chain atoms are less well observed in the difference map compared to (c). The structures shown are the refined models for each complex.*

included in the soak solution (1mM tetrazole, 50mM phosphate, 2.5mM AMP), the difference Fourier map contained similar features to the other 50mM phosphate experiments. Disappointingly, no features were more pronounced in the Fourier map of this complex compared to the other GPb-tetrazole-phosphate complexes and there was no indication of oligosaccharide binding at the active site, though it was present at the glycogen storage site.

(v) Other Binding Experiments - Complexes [9] and [10]. Two experiments were carried out to test if the tetrazole molecule was essential for creation of the phosphate binding site. Firstly, a soak with just phosphate (50mM) gave very weak density at the phosphate site, which could be interpreted as either a poorly located water molecule or a small amount of bound phosphate. Secondly, a soak with phosphate (50mM) and 4-fluoro-4-deoxyglucose (100mM), as an inactive glucose analogue, also gave a similar negative result but with well resolved density associated with an analogue molecule bound to the site. In both cases density in the difference maps showed a phosphate ion to bind at the allosteric site with accompanied movement of Arg 309. It is apparent from these experiments that the tetrazole molecule is necessary for phosphate to bind.

The graph in Figure 2.6 summarises the apparent occupancy of phosphate at the active site for the GPb-tetrazole-phosphate complexes. The occupancy was estimated by the sigma level at which the phosphate peak could be no longer observed. The occupancy increases with increasing phosphate concentration and shows a small variation with tetrazole concentration, decreasing as the tetrazole concentration drops.

2.3.3 Structural Studies: X-PLOR Refinement

To refine all the complexes from which data had been collected would have taken much computing time and been unnecessary. Consequently only those showing novel features in

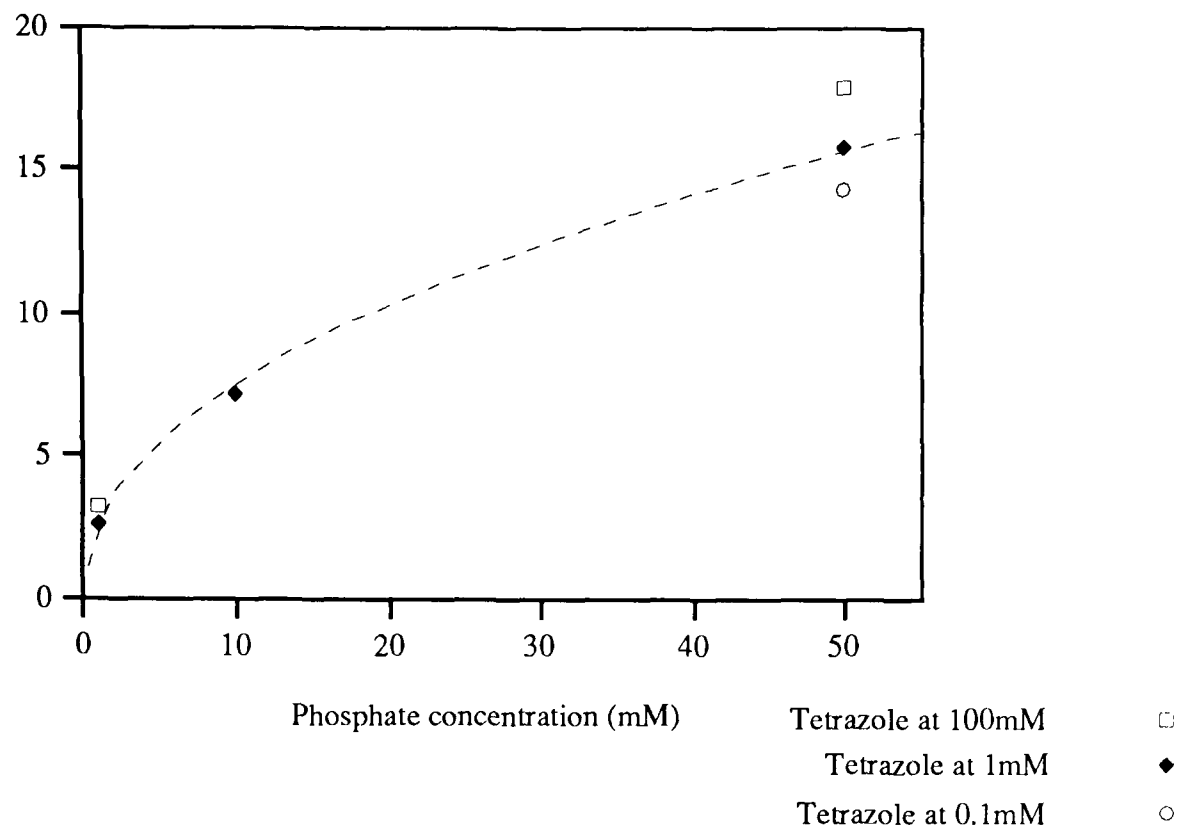

Note added post viva: With hindsight perhaps a superior method to estimate the phosphate occupancy would have been the use of *B* factors and occupancy during refinement: e.g. by comparison of the *B* factors of the pyridoxal 5'-phosphate (occupancy 1) with those of the inorganic phosphate ion (occupancy 1).

Figure 2.6. *The graph shows apparent occupancy of the phosphate site, estimated from the Fourier difference maps, against phosphate concentration. The dotted line is intended as a guide only.*

their Fourier difference maps were pursued.

A refinement protocol making use of the simulated annealing technique was used in those complexes where movement of the 280s loop was indicated (complexes [4], [6] and [8]). The remaining interesting complexes ([1] and [10]) were refined using a conventional route. The starting protein model for refinement was the refined structure of the GPb-glucose complex comprising residues 12 to 841 (Martin, Johnson & Withers, 1990) with the torsion angles of several residues adjusted manually (see refinement protocols for details). Water molecules and ligand models (nojirimycin tetrazole, phosphate and 4-fluro-4-deoxy-glucose) were fitted as appropriate to density at the catalytic and allosteric sites. Tetrazole molecules were not included at the caffeine binding site for complexes [1], [3] and [8], the density in the Fourier difference maps being too poor to allow placement and indicating only partial occupancy.

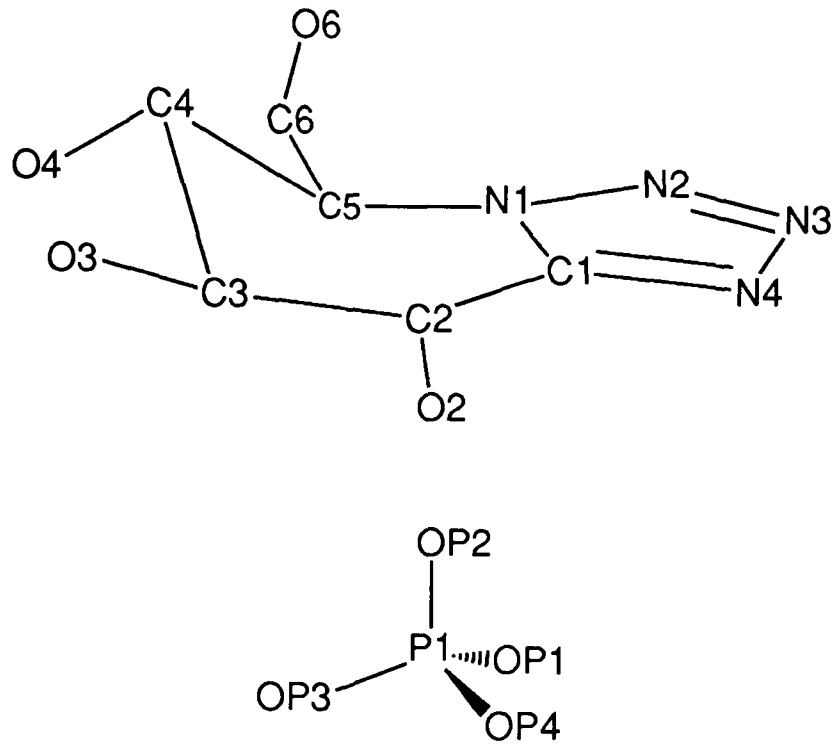

Figure 2.7. *The atom numbering scheme used for nojirimycin tetrazole and the phosphate ion. The OP-3 of phosphate was modelled as being protonated.*

Several waters at the active and allosteric site were removed from protein coordinate files where they had been displaced by ligands.

The topology and parameter files for X-PLOR were obtained as follows. Pyridoxal phosphate was input as described by Johnson, Acharya, Jordan & McLaughlin (1990); briefly, the files were based upon the pyridoxamine structure already present in X-PLOR (Brünger, 1988) with the phosphate charge altered to the monoanion form. For this work an AM1 calculation using MOPAC was used to estimate the partial charges on the phosphate ion and tetrazole molecule. The glucopyranose ring charges were similar to those used by W Weiss in X-PLOR. From the calculations the charges on the tetrazole ring nitrogen atoms were deduced as follows: N-1 0.08; N-2 -0.07; N-3 -0.20; N-4 -0.13. For the phosphate ion the total charge was set at -2.0 with a charge of 2.51 on the phosphorus atom (P-1), -0.84 on the protonated oxygen (OP-1), 0.15 on the proton and -1.28 on the three remaining oxygen atoms (OP-2, OP-3 and OP-4). Refinement was performed using X-PLOR (Brünger, 1988; Brünger, 1989; Brünger, Karplus

& Petsko, 1989)

(i) Simulated Annealing Refinement. At the active site the torsion angles of residue Arg 569 were manually adjusted to bring the side chain from its buried position into the active site, as indicated by the Fourier difference maps. The 280s loop of residues were also adjusted using the difference maps and the refined coordinates for the T state GPb-heptenitol-2-phosphate (Johnson, Acharya, Jordan & McLaughlin, 1990) as a guide. The side chain of Asp 283 was moved out of the active site to partially occupy the site vacated by Arg 569 and the side chain of Asn 284 was moved into free space towards His 341 and also away from the active site. The main chain of atoms for these residues was adjusted, using the Fourier maps as a guide, to maintain continuity with the side chains. A negative electron density peak, corresponding to the side chain of Arg 309 at the allosteric site, and associated positive peak in all the GPb-phosphate complex difference maps indicated a new position for this side chain coordinating the phosphate. The torsion angles were adjusted accordingly.

The simulated annealing refinement protocol commenced with least squares conjugate gradient refinement (100 cycles, tolerance 0.05Å) in preparation for the annealing stage. During S.A. the structure was heated to 3000K and gradually cooled to 300K with a timestep of 5fs. Following this further least squares refinement (120 cycles) and individual atomic *B* factor refinement (60 cycles, with target standard deviations of 1.5 and 2.0Å^2 for bonded atoms and atoms bound to the same atom respectively) completed the series.

(ii) Conventional Refinement. This established refinement procedure for GPb T state complexes (Watson *et al.*, 1994) comprised least squares conjugate gradient refinement (200 cycles, tolerance 0.05Å) followed by individual atomic *B* factor refinement (60 cycles, with target standard deviations of 1.5 and 2.0Å^2 for bonded atoms and atoms bound to the same atom respectively) to give the final refined model.

		Complex				
		[1]	[4]	[6]	[8]	[10]
Number of Atoms	Protein	6780	6780	6780	6780	6780
	Ligands	14	24	24	24	12
Number of Waters		569	568	568	568	569
Number of Reflections (8.0-2.4Å, I>0)		36005	29931	26563	30844	30608
R Factor (%)	Starting	23.7	23.4	23.8	24.8	22.9
	Final	19.3	16.3	15.6	16.9	19.3
RMS Deviation	Bond Lengths (Å)	0.017	0.016	0.016	0.016	0.017
	Bond Angles (°)	3.2	3.1	3.1	3.2	3.4

Table 2.3. *Statistics of refinement of the five complexes.*

The X-PLOR refined coordinate sets were used to generate Fourier difference maps with ($2F_o$-F_c) coefficients. The maps were then inspected for a satisfactory fit of the atoms to the electron density.

2.3.4 Structural Studies: X-PLOR Refined Structures

Examination of the final refined structures showed them to generally agree well with the ($2F_o$-F_c) electron density maps. An example of the ($2F_o$-F_c) Fourier map density at the active site is shown in Figure 2.8. The statistics of refinement are shown in Table 2.3. The actual standard deviations of *B* factors for the complexes were approximately 3.3Å^2 and 5.1Å^2 for bonded atoms and atoms bound to the same atom respectively. Both the GPb-4-fluoro-4-deoxy-glucose and GPb-tetrazole complexes had essentially the same enzyme conformation as the

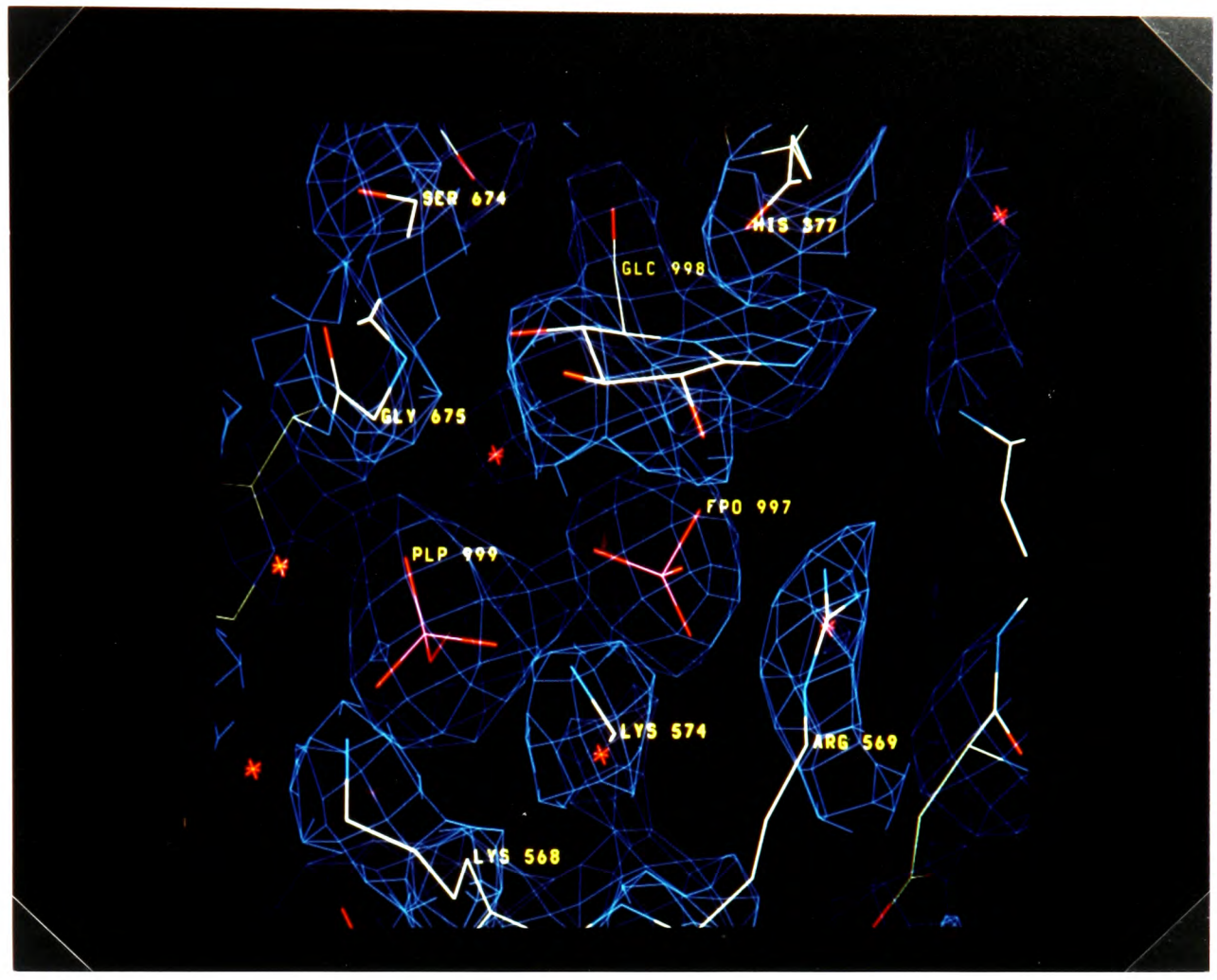

Figure 2.8. *The* ($2F_o$-F_c) Fou*rier map at the active site of T state phosphorylase soaked in 1mM tetrazole and 50mM phosphate [6].*

GPb-glucose model used as a starting point for refinement. The most significant changes in the enzyme structure were observed in the refined structures of the GPb-tetrazole-phosphate complexes.

(i) Interactions Between Nojirimycin Tetrazole and Catalytic Site Residues. The tetrazole binds in an identical position whether phosphate is present or not. The rms deviation between the coordinates for nojirimycin tetrazole in complexes [1] and [6] is just 0.22Å, the estimated error in coordinates being 0.20-0.30Å (Acharya, Stuart, Varvill & Johnson, 1991). The tetrazole ring of nojirimycin tetrazole makes one hydrogen bond contact to the enzyme, N Leu 136, and binding of the ligand is dominated by contacts from O-2, O-3, O-4 and O-6 to active site residues (Table 2.4). These are essentially identical to those made by glucose (Martin,

Ligand Atom	Protein Atom	Hydrogen Bond Contact (Å)			
		[1]	[4]	[6]	[8]
Tetrazole					
O-2	O2 Phosphate	-	2.9	3.0	2.9
	ND2 Asn 284	3.2	-	-	-
	OH Tyr 573	3.2	2.9	3.0	3.1
	OE1 Glu 672	3.1	3.2	3.2	3.3
	Wat 890	2.9	2.9	3.0	3.2
O-3	OE1 Glu 672	2.8	2.7	2.8	2.9
	N Ala 673	-	3.3	3.3	3.2
	N Ser 674	3.1	3.0	3.1	3.1
	N Gly 675	3.1	2.9	3.2	3.2
O-4	N Gly 675	2.8	2.7	2.8	2.8
	Wat 897	2.7	2.7	2.7	2.9
O-6	ND1 His 377	2.7	2.6	2.6	2.8
	OD1 Asn 484	2.9	2.9	2.8	2.9
N-1	OP1 Phopshate[a]	-	2.8	3.1	3.1
N-2	N Leu 136	3.3	3.0	(3.4)	3.3
Phosphate					
OP-1	N1 Tetrazole[a]	-	2.8	3.1	3.1
	Wat 887	-	-	-	2.7
OP-2	O2 Tetrazole	-	2.9	3.0	2.9
	NH1 Arg 569	-	-	(3.4)	(3.5)
	NH2 Arg 569	-	2.5	(3.5)	-
	OH Tyr 573	-	3.1	3.3	(3.5)
	NZ Lys 574	-	3.0	3.3	3.0
OP-3	OP2 PLP 999	-	2.8	2.7	2.7
	Wat 897	-	2.5	2.7	2.5
OP-4	N Gly 135	-	3.0	3.1	3.0
	Wat 879	-	2.9	2.8	3.0
	Wat 887	-	2.6	2.7	2.7

[a]Contact represents an electrostatic interaction.

Table 2.4. *Hydrogen bond contacts between nojirimycin tetrazole, phosphate and T state GPb active site residues for complexes [1], [4], [6] and [8]. Complex [1] is the GPb-tetrazole complex which included no phosphate. Distances in brackets indicate a weak contact, a dash indicates no contact.*

Johnson & Withers, 1990) varying slightly in the length of the hydrogen bonds. The active site of phosphorylase forms a specific binding site for glucose and the pyranose ring of the tetrazole binds in a position very close to that of glucose.

Where inclusion of phosphate had caused movement of the 280s loop (Figure 2.9), the hydrogen bond between O-2 of the glucosyl ring and ND2 Asn 284, found in the GPb-tetrazole complex, is no longer formed. Van der Waals interactions, apart from hydrogen bonding contacts, are made to Gly 135, Leu 136, Leu 139, Val 455 and Ala 673. The main chain and side chain of Leu 136 is forced away from the tetrazole molecule by the bulk of the nitrogen ring and adopts a new conformation approximately 0.5Å away, slightly lengthening hydrogen bond contacts between the main chain oxygen of Leu 136 and the main chain nitrogen atoms of Leu 139 and Ala 140.

(ii) Interactions Between Phosphate and Catalytic Site Residues. The phosphate binds in a site between the pyridoxal 5'-phosphate and the tetrazole in a position very close to the postulated attacking site (Hajdu *et al.*, 1987; Duke, Wakatsuki, Hadfield & Johnson, 1994) and the refined position of the phosphate of heptulose-2-phosphate (Johnson, Acharya, Jordan & McLaughlin, 1990).

The phosphate is contained within a tightly binding pocket (Figure 2.10). In complex [6] the phosphate makes a total of 8 hydrogen bonds and 47 Van der Waals interactions, of which 29 are to polar atoms. The phosphate and 5'-phosphate of PLP have a closest contact of 2.7Å and an inter phosphorus-phosphorus distance of 4.7Å. Such an intimate interaction of negatively charged groups requires compensating neighbouring residues. This is provided by several basic side chains (Lys 568, Lys 574 and Arg 569), nojirimycin tetrazole and two water molecules bridging between the phosphates. Lys 574 lies equidistant between the two phosphates and hydrogen bonds to OP-2 of the free phosphate and the PLP 5'-phosphate. The

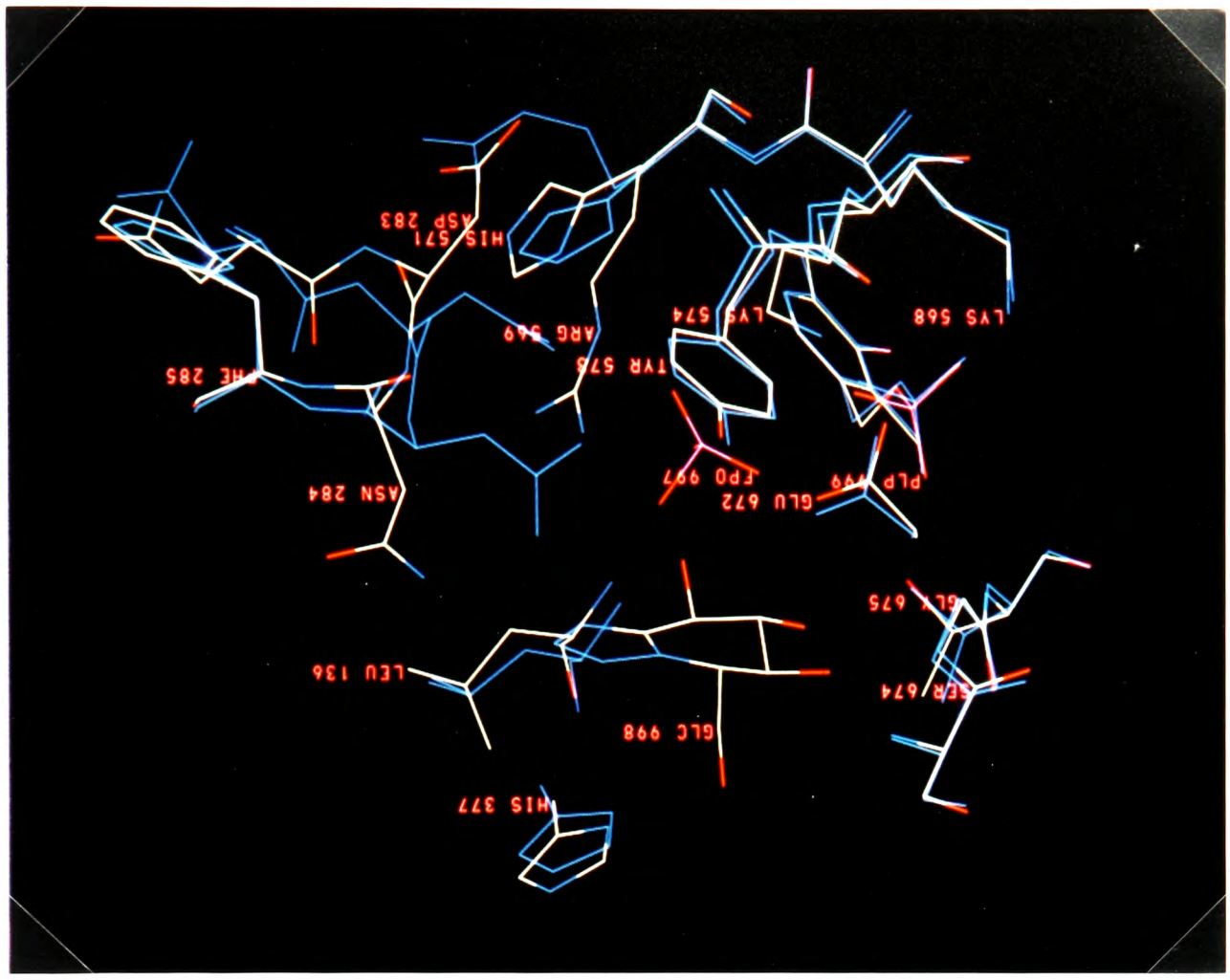

Figure 2.9. *Comparison between the refined structure of complex [6], 1mM tetrazole and 50mM phosphate, and the native structure of T state phosphorylase (in blue).*

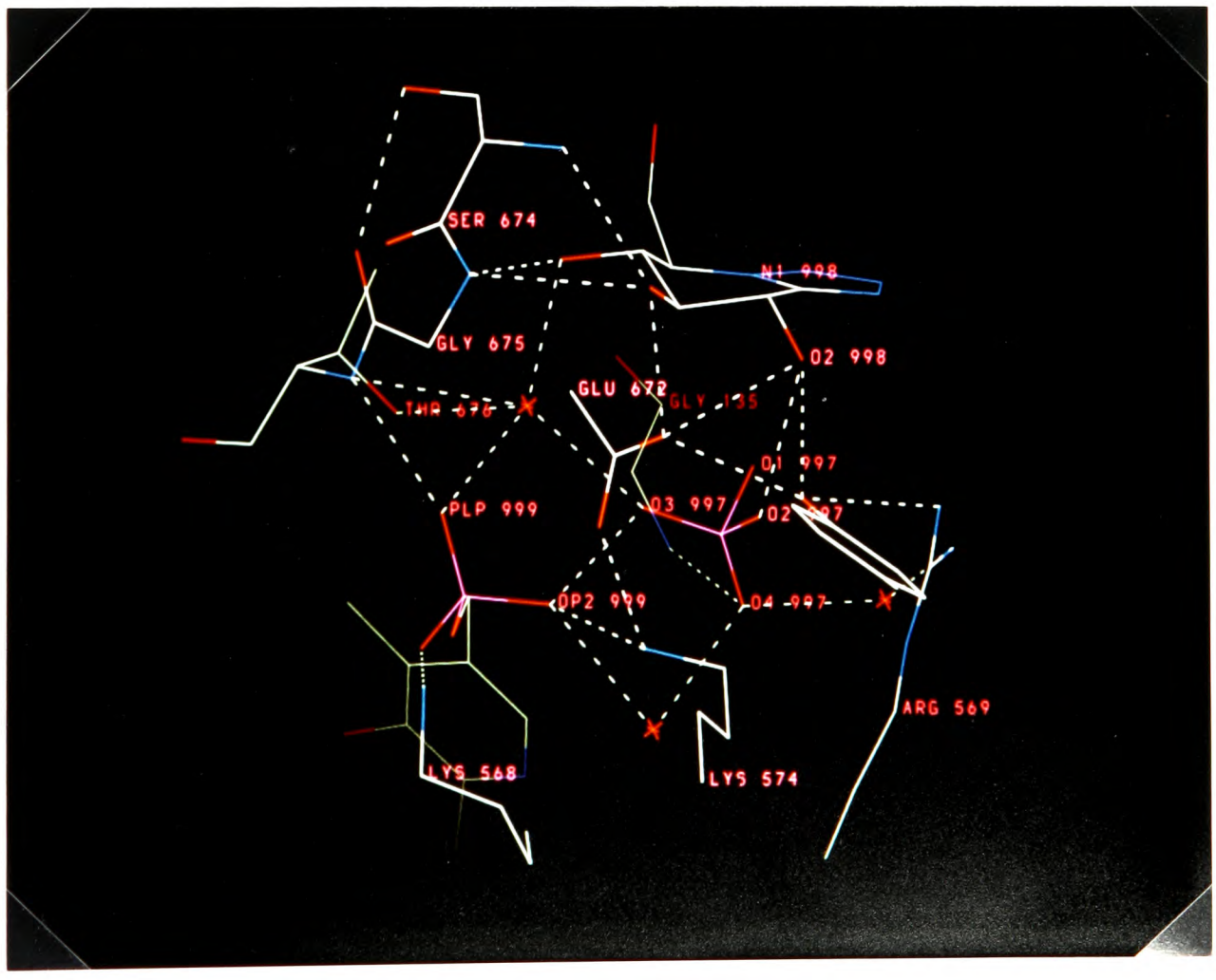

Figure 2.10. *Hydrogen bond contacts between tetrazole, phosphate and phosphorylase. The structure is the refined model of complex [6], 1mM tetrazole and 50mM phosphate.*

two well ordered water molecules, WAT 879 and WAT 897, also form a bridge between the phosphates. The side chain of Arg 569, swinging into the active site, lies close to the substrate phosphate, but the precise location of the Arg 569 side chain is ambiguous. The $(2F_o\text{-}F_c)$ density is not continuous between main chain and side chain atoms. The position of the side chain varies between the three refined complexes, with the guanadinium group rotating and resulting in some changes in hydrogen bond contacts with the phosphate.

Glycogen phophorylase contains a nucleoside inhibitor site at the entrance to the catalytic site channel which is located some 12Å from the active site. In addition to nucleosides the site is known to bind a number of aromatic compounds. These intercalate between the aromatic rings of Phe 285 and Tyr 613 and help to locate the 280s loop in its inactive T state conformation. At high concentrations, nojirimycin tetrazole was observed to bind weakly at this site, eg complex [8], and in this complex Arg 569 moves into the active site. However the arginine interacts less strongly with phosphate than in complex [6], which was soaked in a lower tetrazole concentration and in which there was no tetrazole bound at the inhibitor site. In complex [6] the arginine head lies flat against the substrate phosphate oxygens with both amine groups interacting with the phosphate. Thus when tetrazole binds at the inhibitor site, Arg 569 appears to be partially restricted, but if the tetrazole concentration is reduced the arginine can move to fully create the phosphate recognition site.

With the exception of complex [8] where WAT 887 is contacted, OP-1 of the phosphate makes no contacts with the enzyme. The contact to the water is caused by the incomplete transition of Arg 569 mentioned above, which displaces the water towards OP-1.

(iii) Interactions between Phosphate and Nojirimycin Tetrazole. The phosphate interacts with the tetrazole in two ways. A hydrogen bond, of 2.9Å in length, is formed between OP-2 of the phosphate and the O-2 hydroxyl of the tetrazole. The second contact is a favourable

	Average Side Chain *B* Factors (Å²)			
	[1]	[4]	[6]	[8]
Phe 285	21	36	48	40
Tyr 613	19	26	28	25

Table 2.5. *Average B factors for the side chains of Phe 285 and Tyr 613.*

electrostatic interaction between OP-1 and N-1. The separation of these atoms is 3.1Å in the refined structure and OP-1 is located directly under the C-1 to N-1 bond. It is assumed that there is a charge-charge interaction without the possibility of a hydrogen bond.

(iv) The Caffeine Site. A comparison of the final ($2F_o$-F_c) Fourier difference maps at the caffeine site shows density lying directly between and parallel to the aromatic rings of Phe 285 and Tyr 613 which disappears as the tetrazole concentration in the soak buffer is reduced. Complexes [4] and [6] (1mM tetrazole/10mM phosphate and 1mM tetrazole/50mM phosphate respectively) contained no density but complexes [1] and [8] (100mM tetrazole and 100mM tetrazole/50mM phosphate respectively) contained some density between the rings. These refined results are consistent with the initial Fourier difference maps.

The ($2F_o$-F_c) Fourier maps of complexes [1] and [8] both had superior density for the sidechains of residues 285 and 613 compared to the significantly weaker density of the low tetrazole concentration experiments, [4] and [6]. This is consistent with the idea of tetrazole binding at this site and localising the aromatic rings. A comparison of the side chain *B* factors for residues 285 and 613 highlights the differences (Table 2.5). Complex [1], with only tetrazole binding, has low *B* factors and there is no need for the 280s loop to move and allow the creation of the phosphate recognition site. The remaining three complexes, [4], [6] and [8] all contain phosphate and this promotes the R state. The conformational changes occuring at the catalytic

		Complex of T state GPb				
		Native	[1]	[4]	[6]	[8]
Average *B* Factor (Å²)	All CA	28	23	27	27	29
	Active Site	27	16	23	24	26
	281-286	26	18	34	39	41
	569	19	18	30	26	32
	Tetrazole	-	16	33	25	35
	Phosphate	-	-	58	38	19
RMS Deviation[a] (Å)	Active Site	-	0.63	1.34	1.36	1.20
	All CA	-	0.55	0.66	0.55	0.62

[a]RMS deviation with respect to the native structure, including all atoms of residues 88, 132-137, 281-286, 376-384, 568-574, 613, 671-676 and PLP.

Table 2.6. *Comparison of the active site average B factors and RMS deviations of native and ligand bound GPb.*

site in these phosphate containing complexes, predominantly residues Asp 283, Asn 284 and Arg 569, are echoed in the significantly increased mobility of Phe 285. This represents part of the transition from T to R state phosphorylase where the 280s loop becomes mobile and the caffeine site is broken. Interestingly, complex [4] where only 10mM phosphate was used, shows lower *B* factors in the caffeine site side chains compared to the 50mM phosphate soaks. The lower phosphate concentration leads to only partial occupancy and therefore not so great an activation of the structure towards the R state enzyme.

(v) Conformational Changes at the Active Site. The structure of the GPb-tetrazole complex approximates to the native enzyme, but with the small changes expected on binding a glucosyl ligand, namely movement of the histidine ring of His 377 away from O-6 of the tetrazole. In addition, Leu 136 is forced away from the bulk of the tetrazole ring.

The greatest conformational changes at the active site compared to the native structure are observed in the GPb-tetrazole-phosphate complexes (Figure 2.9). Table 2.6 compares the average *B* factors of active site residues in complexed GPb to native phosphorylase. In the complexes where both tetrazole and phosphate are bound, the active site undergoes several large conformational shifts. In particular the side chain of Arg 569 rotates by 154° about the Cα-Cβ angle to move 7Å into the active site. In moving from its native buried location, Arg 569 breaks four hydrogen bonds and in its new position makes up to three new hydrogen bonds to active site residues, as well as making an ionic contact of the guanadinium group to substrate phosphate. A variation of this is observed for the 100mM tetrazole/50mM phosphate complex [8], where Arg 569 does not undergo a full conformational shift and extends by 2Å less into the active site than in the other complexes.

The new position of Arg 569 is partly that vacated by Asp 283, which moves out of the active site and forms part of an extensive reorganisation of the 280s loop. There is some variation between the GPb-tetrazole-phosphate complexes in the exact location of the 280s loop residues, particularly Asp 283 and Asn 284, and this reflects the greater disorder of the loop in the complexed enzyme. This disorder is shown in the increased *B* factors observed for the 280s loop compared to the active site as a whole (Table 2.6). The same general conformational changes do however occur in all of the complexes. The side chains of basic Arg 569 and acidic Asp 283 neatly interchange and Asn 284 moves out of the catalytic site by some 4Å, in the process displacing a water molecule. In their new positions OD1 and OD2 of Asp 283 make similar contacts to those of Arg 569 in the native structure: namely hydrogen bonds to the main chain oxygens of Lys 608 and Pro 281 and the side chain of Asn 133. Asn 284 makes a new hydrogen bond to WAT 891, which in turn contacts His 341.

The histidine ring of His 571 makes a small conformational change and rotates by 60° in order to make a hydrogen bond to the new position of the main chain oxygen of Asp 283.

In order to optimise the contacts of the amine group of Lys 574 to the substrate phosphate and PLP 5'-phosphate, the side chain moves towards the PLP phosphate and is directly between the two phosphates in its new position. The PLP phosphate does not move from its native position in any of the complexes studied.

(vi) Conformational Changes at the Allosteric Site. All of the phosphate complexes make similar changes. In order to create the phosphate binding site, Arg 310 moves by 3.5Å and Arg 309 slightly adjusts its conformation to contact the phosphate.

(vii) Conformational Changes at the Tower and Cap Regions. These regions form the subunit-subunit interactions and are thus important for transmission of conformational changes from the active site. The tower helix is directly connected to the catalytic site residues and there are changes in the conformation of the tower and cap regions upon activation of the T state enzyme to the R state enzyme. Thus upon binding nojirimycin tetrazole and phosphate, which together form a transition state analogue, it might be expected that the tower and cap residues would undergo a conformational change. However a comparison of the complexed T state GPb with native GPb shows there to be little change in the cap region (residues 36 to 41) and also in the residues comprising the tower helix (residues 262 to 278). The residues forming a loop from the top of the tower helix back to the enzyme, residues 262 to 249, do show mobility and the conformation varies between all the complexes individually and with the native T state structure. This region does have a high thermal mobility in the native structure and this is not decreased in the complexed protein, all showing high *B* factors in the tower loop.

The subunit-subunit contacts also form part of the lattice contacts. No cracks were observed in the crystals during and after soaking, though they did become noticably more fragile and cleaved easily if not handled delicately. Though the lattice may be under strain in the

complexed crystals, the lattice contacts seem to dominate and prevent crystal cracking and also prevent a change in the conformation of the tower and cap loops.

2.4 DISCUSSION

2.4.1 Kinetic Studies

Nojirimycin tetrazole shows the kinetic behaviour for a competitive inhibitor with a K_i value of 0.7mM for binding to the phosphorylase-glycogen-AMP complex. However, when phosphate is present, the binding improves by over an order of magnitude, a K_i value of 53μM being determined for binding to the phosphorylase-glycogen-AMP-phosphate complex. The presence or absence of glycogen has no significant effect on the inhibitor's affinity, as indicated by the non-competitive kinetics seen on competition with glycogen in the presence of a fixed phosphate concentration. The competitive inhibition seen with respect to glucose-1-P is consistent with the two sugar moieties competing for the active site, while the observation of uncompetitive inhibition when phosphate was the varied substrate implies that nojirimycin tetrazole does not bind significantly to the enzyme unless phosphate is present.

These findings are similar to those of Gold, Legrand and Sanchez (1971) on the binding of D-gluconolactone to phosphorylase a, where phosphate was found to improve the affinity of the enzyme-glycogen complex for this inhibitor by 28 times. On this basis they proposed that D-gluconolactone is an analogue of the substrate part of the transition state. A similar conclusion would appear to be warranted for the binding of nojirimycin tetrazole. In support of this notion that nojirimycin tetrazole is a good transition state analogue for phosphorylase, is the recent demonstration that inhibitors of this type can be classified as transition state analogues for β-glycosidases (Ermert, Vasella, Weber, Rupitz & Withers, 1993).

2.4.2 Creation of the Phosphate Recognition Site

In native T state crystals the phosphate recognition site is not fully developed; even at high

(0.5M) concentrations of P_i, phosphate still does not bind at the active site. The kinetic study on nojirimycin tetrazole binding to GPb has shown that the K_i decreases from 0.7mM to 53μM in the presence of phosphate. The phosphate tightens the binding of the tetrazole. The X-ray experiments suggest that by binding at the active site the half-chair tetrazole creates a phosphate recognition site: there is synergy between the two ligands. The experiment with 4-fluoro-4-deoxy-glucose shows there to be no such synergy and no appreciable phosphate binding in the presence of a glucosyl compound in the chair conformation.

The two contacts between tetrazole and phosphate, the O-2/OP-1 hydrogen bond and N-1/OP-1 electrostatic contact, are essential in establishing the synergy between ligand and phosphate. The importance of the O-2 of glucosyl substrates has been pointed out by Street, Rupitz and Withers (1989) in their kinetic analysis on fluoro-deoxy-glucose analogues and also discussed by Duke, Wakatsuki, Hadfield and Johnson (1994). The contact of O-2 to the active site residues Tyr 573 and Glu 672 is important in locating the glucosyl ligand and the contact from O-2 to phosphate in locating the phosphate in the correct orientation for catalysis. This is discussed further in section 2.4.6.

In the GPb-tetrazole-phosphate complex the free phosphate and PLP 5'-phosphate closely interact, a requirement of both the acid-base and the electrophilic mechanisms. This high negative charge density is counteracted by the surrounding constellation of atoms, made up of the basic residues Lys 568, Lys 574 and Arg 569 (Figure 2.10). Lys 568 maintains its native T state conformation, whilst Lys 574 and Arg 569 adopt new conformations. In its new conformation, the face of the guanidinium group is in ionic contact with the phosphate and has moved over 7Å from its native location. The importance of Arg 569 in the phosphorylase catalytic mechanism and T to R state transition was recognised by work on the reactivity of the group to arginine specific reagents (Dreyfus, Vandenburger & Buc, 1980; Vandenburger & Buc, 1983). It was shown that Arg 569 was unreactive to reagents in the T state, where it is

buried, whereas in the R state Arg 569 moves into the active site and is reactive. The experiment resulted in inactivation of GPb and GPa, though it was also demonstrated that this inactivation could be partially protected by glucose-1-phosphate.

2.4.3 The Transition From T to R State Enzyme

Transition from T to R state phosphorylase results in both an increase in affinity for substrate and also an increase in activity. These allosteric kinetic results were partially explained by comparison of the T and R state structures which showed that one component of the transition was movement of Arg 569 into the active site (Barford, Hu & Johnson, 1991). The arginine created a phosphate recognition pocket at the active site and displaced Asp 283 to remove a negatively charged group from the catalytic site. These results did not explain explicitly why there should be enhanced activity in the R state, although clearly structural changes that localise substrate phosphate are important.

The results of the kinetic study on nojirimycin tetrazole in phosphorylase show that phosphate tightens nojirimycin tetrazole binding and the crystallographic results show that the tetrazole tightens phosphate binding. Nojirimycin tetrazole and the phosphate ion are both mutually interdependent. On Arg 569 undergoing a large conformational change, the 280s loop becomes disordered with the acidic residue Asp 283 moving out of the site where basic Arg 569 is newly positioned. The final density for the loop is disjointed and the *B* factors are high, suggesting that the loop has become more mobile in the GPb-tetrazole-phosphate complexes relative to the ground state. The 280s loop cannot be located in the R state enzyme.

Though the active site does become more R state like, these changes are not complemented by alterations at the tower helix, one of the regions where subunit-subunit communication occurs. The helix remains in the T state conformation, and this is likely to be caused by the lattice

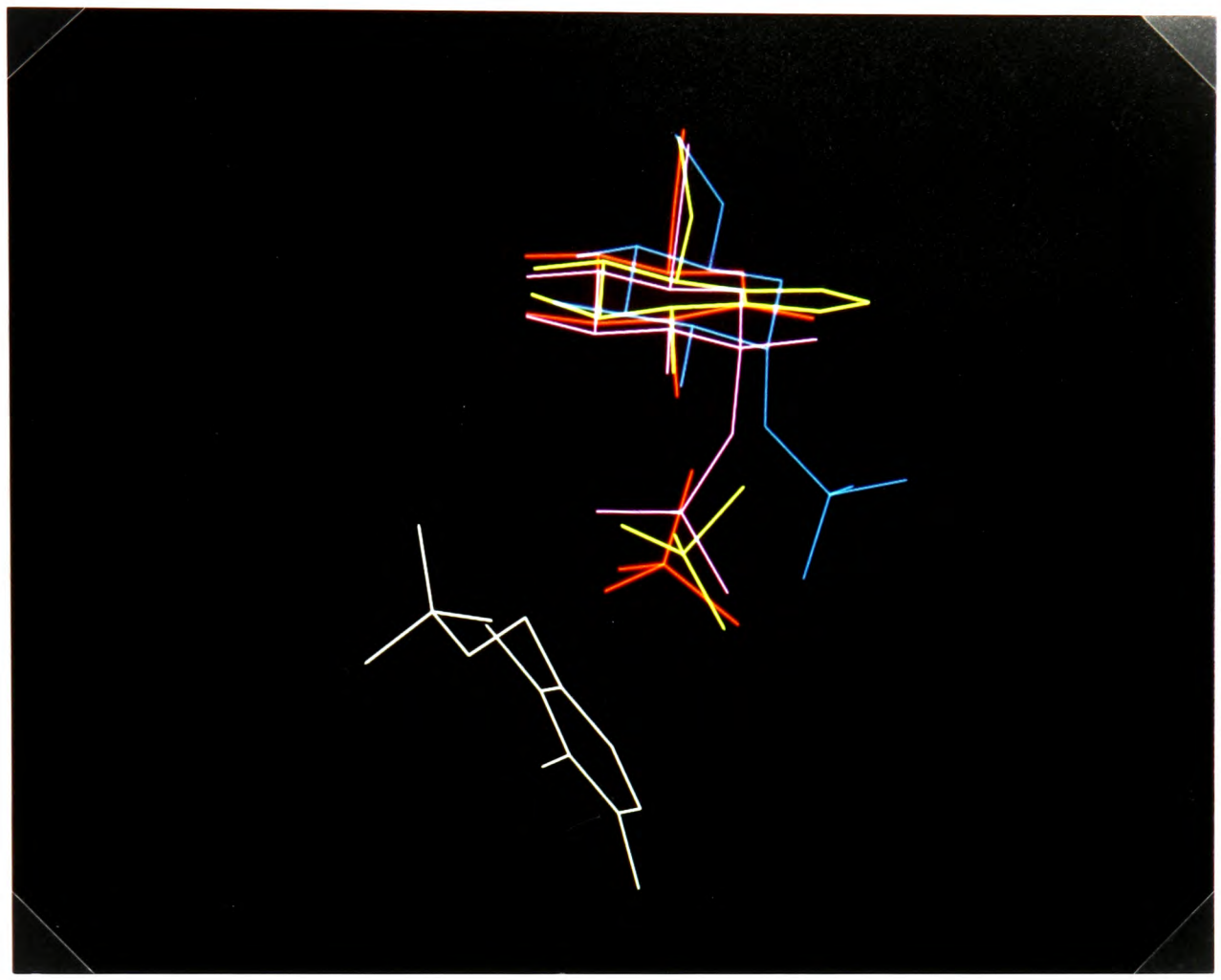

Figure 2.11. *Comparison of the binding of nojirimycin tetrazole and phosphate (in yellow) at the active site with heptenitol and the putative phosphate site (in orange), heptulose-2-phosphate (in purple) and glucose-1-phosphate (in blue). Pyridoxal 5'-phosphate is shown in white for reference.*

constraints placed upon the T state crystals at the subunit-subunit interface. There is only one phosphorylase monomer per asymmetric unit and the subunit-subunit interface represents a lattice contact of the crystal.

2.4.4 Comparison with the T State GPb-H2P Complex

The global conformation of the active site is similar in both the GPb-tetrazole-phosphate and GPb-heptulose-2-phosphate complexes. In both cases a mutual interchange of Asp 283 and Arg 569 is observed and also a shift of the 280s loop. The one significant difference lies in the conformation of His 571, which in the H2P complex allows the catalytic channel to be more open than in the GPb-tetrazole-phosphate structure.

The two complexes do differ in the ligand binding locations (Figure 2.11). The glucosyl ring of H2P binds approximately 0.5Å lower and the phosphate of H2P 0.5Å higher than their tetrazole-phosphate counterparts. This is a result of a compromise between maintaining the hydrogen bonds of the glucosyl ring whilst allowing the phosphate to fit into the phosphate recognition site. The covalent link between the pyransose ring of H2P and its phosphate is not long enough to allow ideal positioning of the pyranose and phosphate moeties into their respective binding sites. For tetrazole and phosphate, which are not covalently linked, the pyranose ring and phosphate can optimise the hydrogen bonds between themselves with those to the surrounding enzyme.

The putative phosphate attacking site, deduced from the work of Hajdu *et al.* (1987) and Duke, Wakatsuki, Hadfield and Johnson (1994), is just 0.2Å (this is within the estimated experimental error of 0.20-0.30Å) away from the location of the GPb-tetrazole-phosphate phosphate, thereby strengthening their hypothesis that the low intensity phosphate peaks observed do indeed represent phosphate.

2.4.5 Catalytic Mechanism

The structural studies on the T state GPb-tetrazole-phosphate complex have provided conclusive evidence for the location of the substrate phosphate binding site. They also confirm that there is direct interaction between the PLP 5'-phosphate and the substrate phosphate which is a requirement for both the proposed acid-base and electrophilic mechanisms.

Previous studies on the reaction of heptenitol with phosphate in T state GPb crystals have emphasised the importance of the hydrogen bond between O-2 of the glycosidic pyranose ring and phosphate. In the product, heptulose-2-phosphate, this is an internal contact but in recent

Laue diffraction experiments a similar interaction was observed in the partially catalysed GPb-heptenitol-phosphate complex (Duke, Wakatsuki, Hadfield & Johnson, 1994). In the present work, the observation of a free phosphate ion bound at the active site of T state phosphorylase, where the phosphate peak is a prominent feature of the difference map and significantly more resolved than in the H2P studies, confirms these findings.

In this study of the GPb-tetrazole-phosphate complex at 2.4Å resolution the orientation of the phosphate with respect to the active site residues is not conclusively established. However, density in the ($2F_o$-F_c) Fourier difference maps does indicate hydrogen bonding from OP-2 of the 5'-phosphate and O-2 of the tetrazole to the substrate phosphate. This effectively defines the phosphate orientation. Simple modelling of the active site, with the terminal glucose of an oligosaccharide placed over the tetrazole position, shows OP-1 of the phosphate to be in an ideal position to donate a proton to the glycosidic bond (Figure 2.12). This is suggestive that the phosphate is in an orientation indicative of the true catalytically active position. This is not unreasonable given the transition state nature of nojirimycin tetrazole.

The pattern of hydrogen bonding between the phosphate groups and the active site residues of phosphorylase can be established using the refined model of the T state GPb-tetrazole-phosphate complex. With reference to Figures 2.10 and 2.12 it can be seen that there is a hydrogen bond between OE1 Glu 672 and O-2 of the tetrazole. This must be donated by the tetrazole oxygen. Therefore OP-2 of the inorganic phosphate ion has to be protonated since it too contacts O-2 of the tetrazole. The phosphate oxygen, OP-4, is likely to be unprotonated since it is surrounded by a favourable positive electrostatic environment (Arg 569 and Lys 574). OP-1 of the phosphate does not make any hydrogen bond contacts to the enyme, and thus has no enzyme residues to compensate if it were unprotonated. The atom also appears to be the active oxygen, being in a position suitable to donate a proton to the substrate glycosidic bond. It is thus likely to be protonated. The two oxygens contacting between inorganic phosphate and

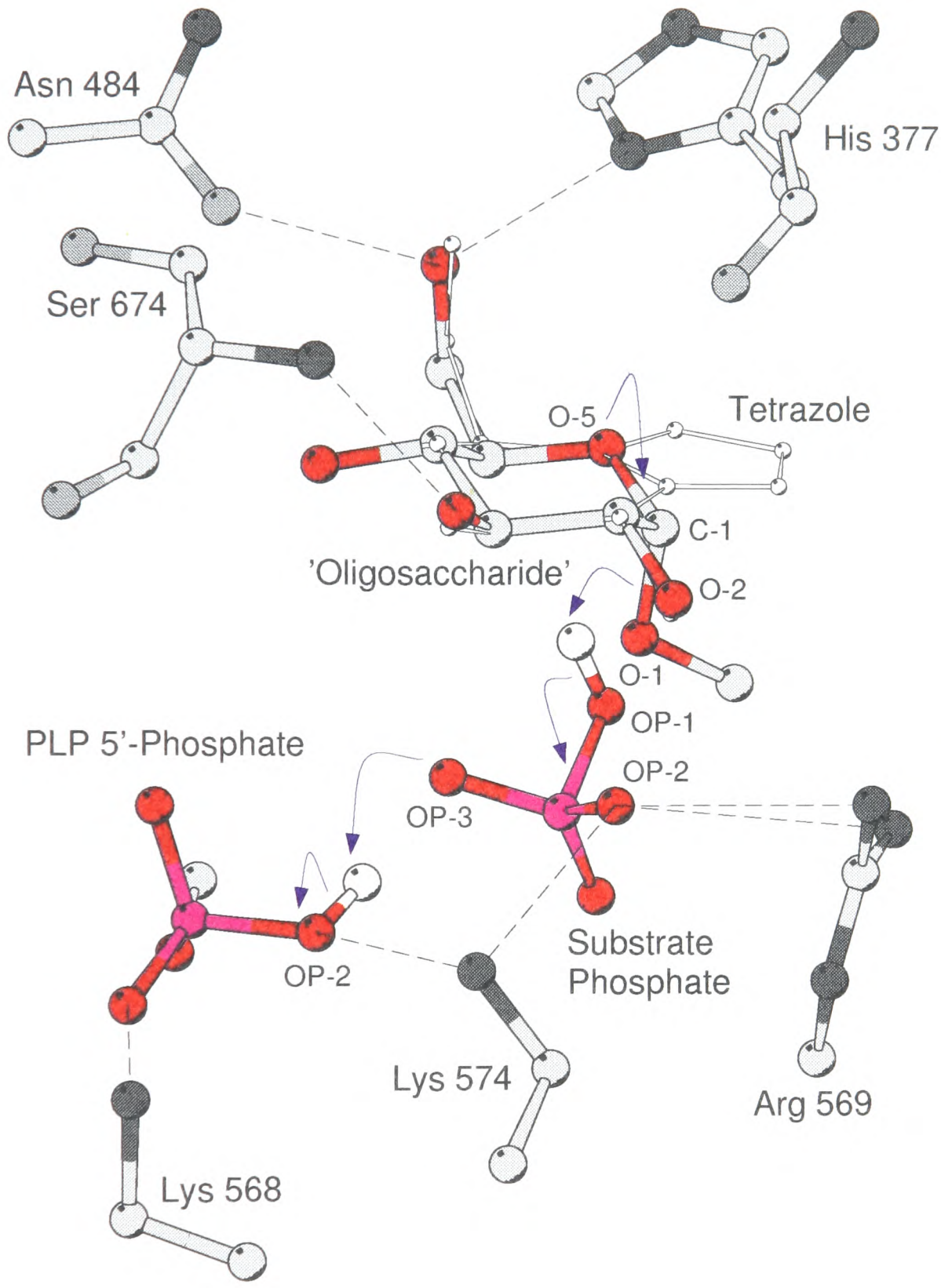

Figure 2.12. *Model of the phosphorylase active site demonstrating the relative orientations of substrates (oligosaccharide and phosphate) and PLP 5'-phosphate as interpreted from the GPb-tetrazole-phosphate complex. The arrows indicate movement of electrons in the acid-base mechanism. For clarity hydrogen atoms are only depicted for the active oxygens on phosphate groups. Nojirimycin tetrazole is shown in the background for reference.*

the PLP 5'-phosphate require a hydrogen to be present on one of the oxygen atoms. If it is on the inorganic phosphate, the ion would thus be monoanionic. However an n.m.r. study (Klein & Helmreich, 1985) suggested the phosphate ion to be dianionic. If this is the case (P^{31} n.m.r. studies are notoriously difficult to interpret) then the hydrogen atom would be positioned on the PLP 5'-phosphate (atom OP-2). The remaining available 5'-phosphate oxygens are OP-1 and OP-3 which are likely to be both unprotonated giving a dianionic group. OP-1 contacts Lys 568 and OP-3 is in a positive electrostatic environment contacting two main chain nitrogen atoms. This would lead to the situation shown in Figure 2.12 with the active site in readiness to donate a proton through the proton shuttle system of 5'- and inorganic phosphates to the oligosaccharide glycosidic bond. The pK_a values of the protons on inorganic phosphate are 2.1, 7.4 and 12.3. Thus at the physiological pH of 6.8 there would be a significant population of monoanionic and dianionic ions. The argument above appears to suggest the active form is the dianionic species of both the 5'- and inorganic phosphate ions. However, the environment of the ion in the enzyme active site may affect the pK_a values. The environment of the phosphate ions will change during the course of the reaction. Such a flexibility of the protonation state of the phosphate groups may be necessary for the proton shuttle to work effectively, allowing the exchange of protons in an efficient catalytic mechanism and subsequent release of products.

2.5 SUMMARY

This work has achieved several important objectives. Firstly it has provided conclusive evidence for the location of the substrate binding site. Secondly, it has confirmed both the results of previous time resolved studies on phosphorylase (Hajdu *et al.*, 1987; Duke, Wakatsuki, Hadfield & Johnson, 1994) and the direct phosphate-phosphate interaction necessary for the electrophilic and acid-base catalytic mechanisms.

In the presence of phosphate, nojirimycin tetrazole has proved to be a good transition state analogue provoking conformational changes in the T state enzyme. Work on R state crystals of phosphorylase in the next chapter takes this further.

3.1 INTRODUCTION

Crystallographic studies on T or R state phosphorylase have never found oligosaccharide to bind at the catalytic site. Observation of an oligosaccharide bound at the phosphorylase active site is crucial to resolution of the GP catalytic mechanism.

3.1.1 Some R State Kinetics

Kinetic studies on crystals of phosphorylase with an oligosaccharide substrate have shown the crystals to be active (Kasvinsky & Madsen, 1976). The work was carried out on cross-linked T state crystals of phosphorylase b and showed the crystals to weakly bind oligosaccharide (K_m of 175mM for maltoheptaose) and have a V_{max} approximately 10% of the V_{max} in solution. Crystallographic studies on T state crystals of phosphorylase have suggested that in the crystal the oligosaccharide visits the active site transiently, presumably because the active site is blocked in the T state (Hajdu *et al.*, 1987). Later kinetic work on crystals of R state phosphorylase with oligosaccharide also showed them to be active but with activity similar to that determined in solution for the enzyme tetramer (Leonidas, Oikonomakos, Papageorgiou & Sotiroudis, 1992). The K_m for maltohexaose was 85mM in the R state crystals.

The T state results, of a low V_{max} and high K_m for oligosaccharide, can be explained if the conformational changes required for catalysis are prevented by cross-linking or by lattice forces. The R state is the active form of the enzyme and the 280s loop of residues, which in the T state are thought to block access to the active site, are mobile in the R state and may therefore allow oligosaccharide to bind there. Oligosaccharide can thus enter the active site more easily and be turned over, as suggested by the V_{max} values. Perhaps in order to break the glycosidic link in the phosphorylase reaction it is preferable for the α-1,4-oligosaccharides to distort away from their preferred conformation which has a narrow energy well. Such a situation could

explain the relatively high K_m observed for oligosaccharides in both R and T state phosphorylase. Oligosaccharides would therefore be difficult to observe at the active site of either enzyme and indeed a crystallographic study by Hu on the R state GPb-maltose complex (Hu, 1991) showed maltose to bind at the glycogen storage site of phosphorylase but not at the catalytic site.

3.1.2 Binding Studies in R State GPb Crystals

Compared to the T state form of GPb, very little structural analysis has been carried out on the R state form of the enzyme since the structure was solved in 1989 (Barford & Johnson, 1989). Complexes of R state phosphorylase with AMP (Barford, Hu & Johnson, 1991), α-D-glucose-1-phosphate (Hu, 1991) and maltose (Hu, 1991) have been completed and also a study on R state GPb reconstituted with the modified cofactor pyridoxal 5'-diphosphate (Leonidas, Oikonomakos, Papageorgiou & Sotiroudis, 1992). The results of the study on the GPb-AMP complex led to the proposal of a structural explanation for allosteric control of phosphorylase by the binding of AMP and by phosphorylation. Though the study on the complex of GPb with glucose-1-phosphate did find the ligand to bind at the active site, it bound in a similar manner to that in the T state (Martin, Johnson & Withers, 1990) with no direct contact between the ligand phosphate and the 5'-phosphate of PLP.

There has been no observation of direct interaction between the 5'-phosphate of PLP and a phosphate of a bound ligand or a bound phosphate ion in R state GPb. The R state crystallises in the presence of 1.0-1.2M ammonium sulphate and a sulphate ion binds at the active site of the native crystals making a contact to the 5'-phosphate of PLP. The S-P distance between the active site sulphate of crystallisation and cofactor PLP 5'-phosphate is 5Å. A comparison between the T state coordinates of Hajdu *et al.* (1987) superimposed onto the native R state structure shows that the R state active site sulphate binds in a similar, but distinct, position to the putative phosphate recognition site proposed by Hajdu *et al.* (1987).

Sulphate binding sites are not necessarily identical to phosphate sites and replacing one anion with the other in a structure may lead to conformational changes at the binding site (Verlinde *et al.*, 1991; Johnson & Barford, 1993). Indeed, in the study on phosphorylase reconstituted with pyridoxal 5'-diphosphate (Leonidas, Oikonomakos, Papageorgiou & Sotiroudis, 1992) the second phosphate of the modified cofactor was found to displace the active site sulphate of R state GPb. Subsequently several conformational changes of residues in order to coordinate the phosphate, for instance Arg 569, were observed. The higher *B* factor of the second phosphate compared to the first phosphate indicated that the second phosphate was more mobile in the structure.

3.1.3 Nojirimycin Tetrazole

Since the R state is the active form of the enzyme, it was hoped that a binding study of the transition state analogue nojirimycin tetrazole would further elucidate the interactions that stabilised the complex and allow comparison with the binding studies with T state crystals. Since the active site channel is open in the R state it was also hoped that the tetrazole-phosphate transition state analogue would encourage oligosaccharide to bind at the active site, producing an analogue of the ternary complex.

This chapter describes the crystallographic analysis of two R state complexes, GPb-nojirimycin tetrazole-phosphate and GPb-nojirimycin tetrazole-phosphate-maltopentaose (G5). Data from the first complex were collected to 2.5Å resolution and water molecules were placed in the structure. R state data had been previously collected to a maximum resolution of 2.8Å and no waters had been positioned. Data for the second complex were obtained to 2.8Å resolution. The R state enzyme did bind tetrazole and phosphate in a similar environment to that of the T state complexes. However no oligosaccharide was bound at the active site.

3.2 EXPERIMENTAL METHODS

3.2.1 General

Chemicals were purchased from Sigma Chemical Company with the exception of nojirimycin tetrazole which was prepared by Philipp Ermert and Andrea Vasella (1991).

Models of the ligands were generated using the program SYBYL (Tripos Associates) and a Powell method minimisation. A comparison of the final model of the tetrazole with the published single X-ray crystal structure (Ermert & Vasella, 1991) revealed no significant differences. The AM1 method (Dewar *et al.*, 1985) was used to calculate partial charges on individual atoms in each model. The model of maltopentaose was based upon the amylose helix.

3.2.2 Data Collection

R state phosphorylase was crystallised by Dr Nikos Oikonomakos and his group at the National Hellenic Research Foundation in Greece. Purified rabbit skeletal muscle glycogen phosphorylase was prepared by the method of Fischer and Krebs (1962) with minor modification. R state enzyme crystals were obtained from solutions containing 1.2-1.4M ammonium sulphate and 6mM IMP at pH 7.5 (Leonidas, Oikonomakos, Papageorgiou & Sotiroudis, 1992) giving monoclinic crystals of space group $P2_1$ and with cell parameters a=119.0Å, b=190.0Å, c=88.2Å and β=109.35°.

For data collection from the complexes of R state GPb, the crystals were prepared by soaking in a buffered solution containing 1.2M sodium tartrate, 10mM β-glycerophosphate, 0.5mM EDTA, 3mM DTT, 0.02% sodium azide (pH 7.0) for 30 minutes. The enzyme, which is

crystallised in the presence of 1.0-1.2M ammonium sulphate, has a sulphate ion bound at the catalytic site that prevents substrate binding. Crystals were transferred to 1.2M sodium tartrate in order to circumvent this problem.This was followed by 3 hours in the same buffer but with the addition of 25mM tetrazole, 25mM sodium hydrogen phosphate and plus/minus 300mM G5 (pH 7.0). No preparation was necessary for the native R state crystals.

Data were collected from the R state GPb-tetrazole-phosphate and GPb-tetrazole-phosphate-G5 complexes and native crystals on an 18cm diameter MAR Research image plate system mounted on the wiggler beam line PX9.5 at the SRS Daresbury. The silicon monochromator was aligned for a wavelength of 0.90Å and a 0.4mm aperture collimator was positioned in the beam line. The detector was placed 21cm away from the crystal to give a maximum resolution of 2.5Å at the edge of the detector. Data frames of 1.0° oscillation were collected with exposure times of 120s over a total angular range of at least 100°. During data collection the synchrotron was operated at an energy of 2.0GeV and the beam current varied between 201mA and 128mA. Each experiment used a single crystal of R state glycogen phosphorylase b. The original data set from native R state phosphorylase had used a total of 10 crystals in collecting a 2.8Å native data set. The surprising resilience of the R state crystals used in this work may be due to the presence of nojirimycin tetrazole and phosphate or superior crystals.

Crystal orientations were determined using the autoindexing algorithm in DENZO (Otwinowski, 1993) and then the data integated also using DENZO (Otwinowski, 1993). Inter-frame scaling, partial reflection summation, data reduction and post-refinement were performed by SCALEPACK (Otwinowski, 1993) to give unique sets of reflections.

3.3 RESULTS AND DISCUSSION

3.3.1 Data Collection

The statistics for collection of data from the two R state complexes and native R state phosphorylase are shown in Table 3.1. Data from the GPb-tetrazole-phosphate (TETPO) complex were collected to 2.5Å, an increase in resolution compared to the native R state structure for which data were collected to 2.8Å resolution (Barford & Johnson, 1989), and from the GPb-tetrazole-phosphate-G5 (TETG5) complex to 2.8Å. Additionally, new data from the native crystal were collected to 2.6Å resolution. After soaking, the unit cell of the complexed crystal GPb-tetrazole-phosphate was found to have decreased by 1.0Å on c. The GPb-tetrazole-phosphate-G5 complex, though, maintained the native cell constant on c of 88.0Å. There were small changes in the unit cell a and b dimensions for both complexes and the native crystal relative to the original native crystals (Table 3.1). Since the original R state native data were collected sometime ago on film, systematic errors in calculating the mean fractional isomorphous difference were minimised by using the new native data set. However, the new native data set was not refined since the gain of information did not warrant the computing time required.

3.3.2 Fourier Difference Maps

In each case a difference Fourier electron density map using SIGMAA weighted (F_o-F_c) coefficients (Read, 1986), where F_o are the observed amplitudes from the complex and F_c are amplitudes calculated from the refined model of R state GPb (Barford & Johnson, 1989) was calculated. Phases were also calculated from the refined model. The maps were averaged over the four copies of the sub-unit in the asymmetric unit according to their geometric relation-

		R State Data Set		
		TETPO	TETG5	Native
Soak Conditions		25mM nojirimycin tetrazole, 25mM sodium hydrogen phosphate (pH 7.0).	25mM nojirimycin tetrazole, 25mM sodium hydrogen phosphate, 300mM G5 (pH 7.0).	None
Number of Reflections	Unique	107826	80201	86695
	Observed	263189	149343	176708
Maximum Resolution (Å)		2.5	2.8[a]	2.6[a]
Completeness of Data (%)		88	90	78
Unit Cell After Denzo Post-Refinement (Å)		a=118.8 b=189.8 c=87.0 β=109.4°	a=118.8 b=190.5 c=88.0 β=109.9°	[b]
R_m (*I*) (%)		7.0	8.4	6.3
Average ($I / \sigma I$)		13.6	10.8	7.9
R_{iso}[c] (%)		36.1	31.4	-

[a]For higher resolution shells R_m>25%. [b]Unit cell a=119.5 b=189.4 c=88.1 β=109.1°. [c]Mean fractional isomorphous difference calculated with respect to the native R state data collected to 2.6Å resolution on identical X-ray optics.

Table 3.1. *Crystallographic data collection and processing statistics for the two R state GPb-nojirimycin tetrazole complexes.*

ships. These averaged maps gave sufficiently well resolved density at the catalytic site to indicate that a tetrazole molecule and phosphate ion were bound. In both cases the phosphate peak was the highest feature in the Fourier difference map and movement of the side chain of Arg 569 towards the phosphate ion could also be identified. No continuous density for the 280s loop of residues, which are not located in the R state structure and are omitted from the model, was observed. Some density was present at low map contouring levels but was close to the noise level.

(i) R State GPb-Tetrazole-Phosphate Complex. Surprisingly no negative density surrounded

the catalytic site sulphate ion in this difference map. The position of the new phosphate ion was close to but distinct from the sulphate site and it was clear that the sulphate ion had diffused out of the crystal during the 30 minute sodium tartrate soak. Negative density did indicate a repositioning of Arg 569 to coordinate the phosphate. In order to do this the side chain of Arg 569 has to move to approximately cover the catalytic sulphate position, therefore cancelling the negative density that would otherwise have been present due to removal of the sulphate.

Several other alterations in structure around the catalytic site were evident from negative density, though no positive density showing new conformations was apparent at a map contour level of 3 sigma. A change in position of Tyr 573 coordinated with movement of Arg 569, to which it is hydrogen bonded in the native structure, was implied by negative density over the phenol ring. Negative density over the phosphate of pyridoxal phosphate suggested movement of the group away from the bulk and charge of the newly located free phosphate ion. The (F_o-F_c) Fourier map did indicate the locations of many ordered water molecules, with many strong peaks at the active site.

(ii) R State GPb-Tetrazole-Phosphate-G5 Complex. At the active site the (F_o-F_c) Fourier map of the TETG5 complex shares many common features with that of the TETPO complex. Tetrazole, phosphate and movement of Arg 569 could all be identified, but no density due to oligosaccharide binding was observed. Even though data were collected to a highest resolution of only 2.8Å, several ordered waters could be observed at the active site. These corresponded to the two bridging waters between the phosphate ion and the PLP 5'-phosphate, previously observed in the T state complexes.

Maltopentaose does, however, bind at the major glycogen storage site on the protein surface. There is well defined density for oligosaccharide sugars occupying the subsites labelled S4, S5 and S6 (McLaughlin, 1985; Johnson, Acharya, Jordan & McLaughlin, 1990) at a map

contour level of 3 sigma (Figure 3.1). At lower contour levels some density was observed for glucose units in S3 but none for S7. The contour level had to be dramatically reduced before any sign of a sugar occupying S7 became apparent. Density suggesting low occupancy of oligosaccharide at the minor site, close to the major site, was also observed.

3.3.3 X-PLOR Refinement

The program X-PLOR (Brünger, 1988; Brünger, 1989; Brünger, Karplus & Petsko, 1989) was used to refine the models of each complex. In both cases the initial model for refinement was based upon the refined R state GPb model, which contains no water molecules and consists of 4 monomers each with residues 10 to 837 (Barford & Johnson, 1989). The final *R* factor for the refined native structure is 17.7% and rms deviations of bond lengths and angles from ideality of 0.018Å and 4.0° respectively. The coordinates for the sulphates of crystallisation from the catalytic and allosteric sites were removed from the coordinate file. Refinement progress of the TETPO complex was monitored using both the *R* and R_{free} factors and for the TETG5 complex using the *R* factor only. The *R* factors for each model before refinement were 34.5% (R_{free} 33.6%) and 35.9% for the tetrazole-phosphate and tetrazole-phosphate-G5 complexes respectively.

Initially the refinement for each R state complex followed a common route and proceeded with treatment of the tetramer as 4 rigid bodies (50 cycles) followed by similar treatment of the domains of each subunit (50 cycles). Subsequent refinement constrained the subunits with non-crystallographic symmetry (ncs) restraints of 200 kcal mol^{-1} (300 cycles) on residues selected to differ by a positional rms deviation of less than 1.0Å between the four subunits of the tetramer. Ncs restraints were loosened to 100 kcal mol^{-1} (140 cycles) to give *R* factors, after individual *B* factor refinement (60 cycles), of 22.9% (R_{free} value of 29.8%) for the tetrazole-phosphate complex and 23.7% for the tetrazole-phosphate-G5 complex.

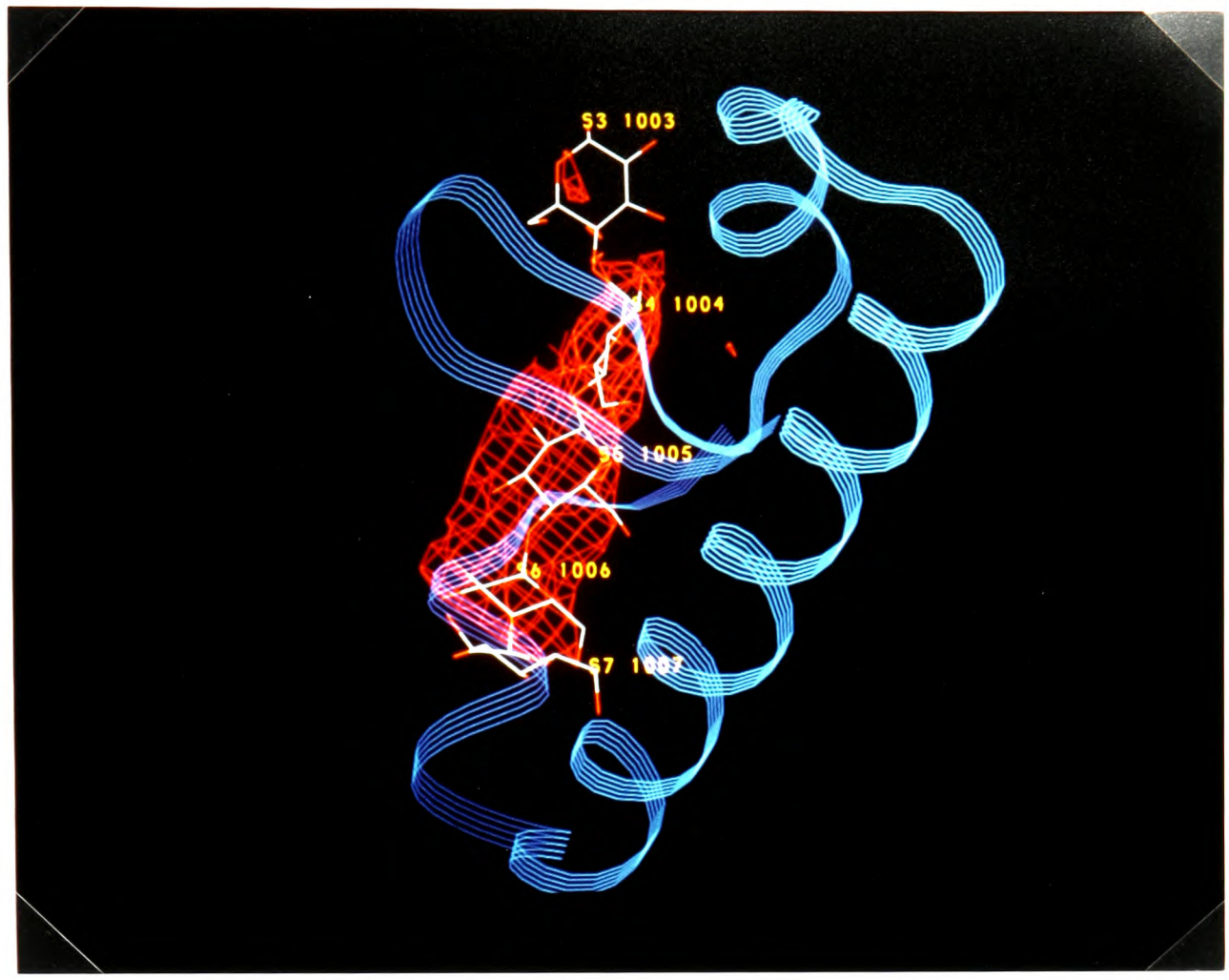

Figure 3.1. *The difference Fourier map of TETG5 at the glycogen storage site with the sugar subsites labelled.*

These coordinates were used to generate new unaveraged difference Fourier electron density maps using SIGMAA (F_o-F_c) coefficients, where F_c and the phases were calculated from the refined models above. The significantly improved density in the new maps was used to place phosphate ions and tetrazole molecules at the catalytic sites and include sulphate at the allosteric site in the models. For the G5 complex, models of maltopentaose were positioned at the glycogen storage sites for each monomer. The refinement then continued with a different protocol for each complex.

(i) R State GPb-Tetrazole-Phosphate Complex. Further least squares, using ncs restraints of 200kcal mol^{-1} (150 cycles) and 100 kcal mol^{-1} (40 cycles), and individual *B* factor refinement (80 cycles) reduced the *R* factor to 22.1% (R_{free} value 28.6%). At this stage water molecules

were added to the model. For the purpose of adding water molecules, each subunit of the tetramer was treated as identical. Using the CCP4 program PEAKMAX (CCP4, 1979) a new averaged difference Fourier map was automatically searched for peaks greater than 2.5 times the rms density of the map. Water molecules were assigned to these peaks using the program WATPEAK (CCP4, 1979) and manually screened for sensible positioning, density shape and hydrogen bonding. The water molecules were independently assigned in the structure with no reference to waters in the T state enzyme. In total 252 waters were added to each subunit. Further least squares refinement with ncs restraints of 200 kcal mol-1 (200 cycles) and 100 kcal mol-1 (110 cycles) followed by individual *B* factor (70 cycles) refinement of the tetramer with all ligands and waters in place proceeded. The last stages of least squares refinement with no ncs restraints (90 cycles) and individual *B* factor refinement (50 cycles) gave a final *R* factor of 17.1% (R_{free} factor 27.3%). Such a discrepency between the crystallographic *R* factor and free *R* factor at 2.5Å resolution is not untypical (Brünger, 1992).

(ii) R State GPb-Tetrazole-Phosphate-G5 Complex. Refinement of this complex proceeded with least squares refinement, using ncs restraints of 200 kcal mol^{-1} (220 cycles), of which the first 20 cycles used the X-PLOR repel energy function. Further refinement continued using ncs restraints of 100 kcal mol^{-1} (130 cycles) followed by individual *B* factor refinement (80 cycles) giving a reduced *R* factor of 22.6%. Finally, least squares refinement with no ncs restraints (50 cycles) and individual *B* factor refinement (40 cycles) gave an *R* factor of 19.8%.

3.3.4 X-PLOR Refined Structures

The refined models fitted the final ($2F_o$-F_c) Fourier maps well (Figure 3.2), with the exception of residues known to be mobile; for instance Ile 380 and the loop 250 to 260. There was no density for the 280s loop of residues. The statistics for each refinement is shown in Table 3.2.

		Complex	
		TETPO	TETG5
Number of atoms in final refinement cycle		27952	27148
Number of waters in final refinement cycle		1008	0
Number of reflections used in refinement (I>0)		104617	76578
Resolution range		8.0 - 2.5	8.0 - 2.8
R factor (R_{free})	Initial (%)	34.5 (33.6)	35.9
	Final (%)	17.1 (27.3)	19.8
RMS deviation from ideality of	Bond lengths (Å)	0.018	0.023
	Bond angles (°)	3.4	4.1

Table 3.2. *Refinement statistics for the TETPO and TETG5 complexes.*

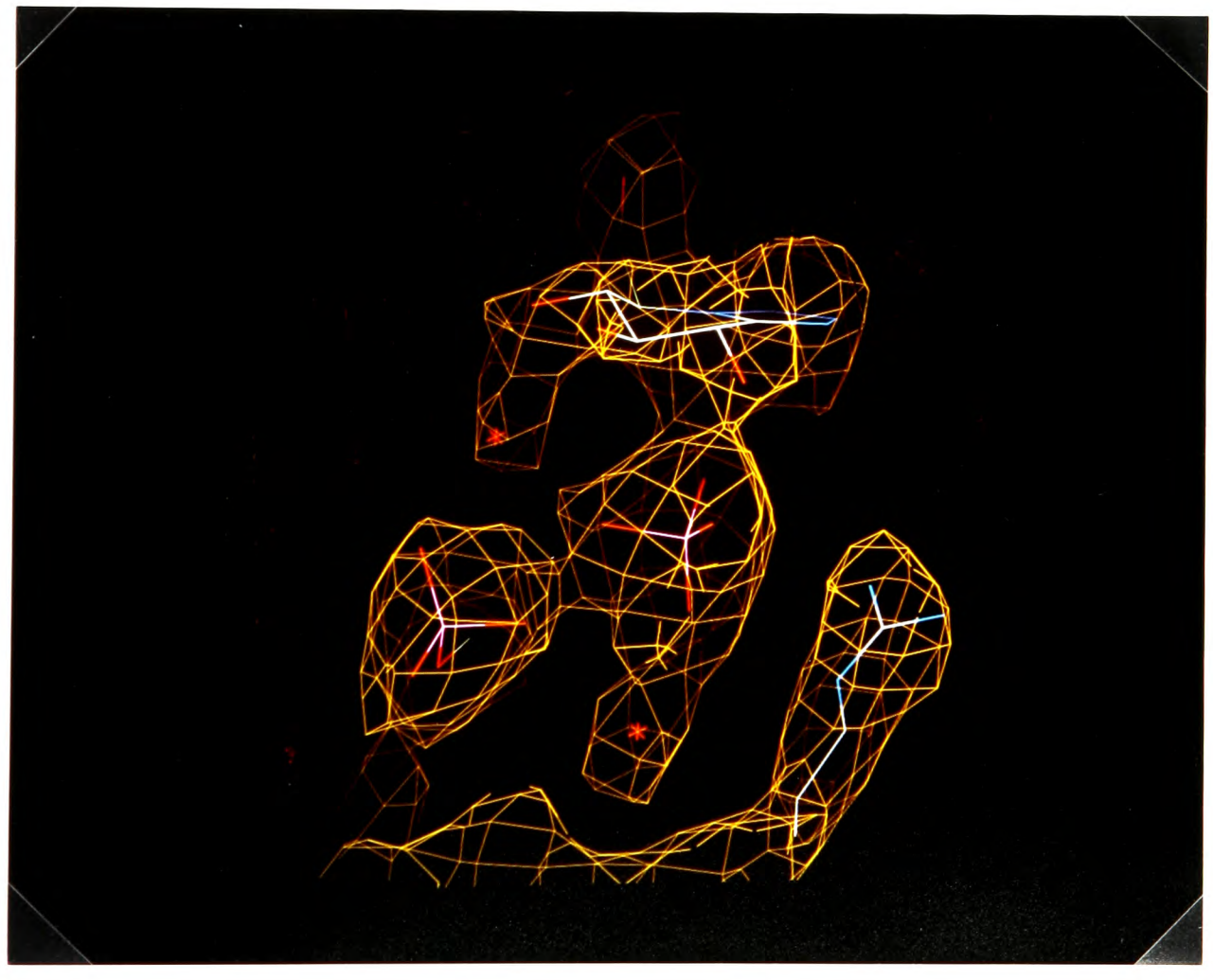

Figure 3.2. *The ($2F_o$-F_c) Fourier map of the TETPO complex at the active site.*

The global and quaternary structure remains conserved between the native R state and the two R state complexes. The individual subunits of each tetramer of the complexes are all similar within the resolution of experimental data. The estimated atomic positional error is 0.30-0.35Å (Luzatti plot). Table 3.3 compares the rms deviations between C-α positions of the complexes and also with the native R state structure.

(i) Comparison of the TETPO and TETG5 complexes to the native R state structure. The graphs in Figure 3.3 show the superimposition of the complexed R state C-α positions onto native R state phosphorylase and also the average main chain *B* factors for the complexes. The average *B* factor of all C-α atoms is 32Å^2 for TETPO and 38Å^2 for TETG5. The largest positional deviations are seen for those residues poorly located in density and those exhibiting high *B* factors: the N terminus, 211-212, 250-263, 313-320 and 378-384. In previous R state studies these regions have also been poorly located (Hu, 1991; Barford, Hu & Johnson, 1991).

In R state phosphorylase, an anionic binding site already exists at the active site. This is unlike the T state which requires a suitable glucosyl ligand, for instance nojirimycin tetrazole, to create the recognition site. In native R state crystals this site contains no glucosyl ligand but has a sulphate of crystallisation which is coordinated by Arg 569 and Lys 574. The sulphate makes a hydrogen bond contact with the PLP 5'-phosphate, the centres being separated by 5Å. In both of the complexes studied, TETPO and TETG5, phosphate binds at the site but is separated from the original sulphate ion location by over 2Å (Figure 3.4).

The glucosyl recognition pocket at the active site is retained from the T state with no significant structural changes. The R state complexes studied, TETPO and TETG5, bind nojirimycin tetrazole at this site and the phosphate binds close by to make the important synergistic contacts to O-2 and N-1 of the tetrazole already observed in this work in the T state complexes. To complete the shift and construction of the phosphate recognition site, Arg 569 moves from its

	RMS deviation of C-α (Å)	Number of excluded atoms from the C-α comparison[a]
A. Complexes onto native R state GPb		
TETPO	0.70	-
	0.61	81
	1.48[b]	-
TETG5	0.67	-
	0.59	71
	1.43[b]	-
B. For each complex, subunits 2,3 and 4 onto subunit 1		
TETPO (subunits)	0.59 (1-2), 0.55 (1-3), 0.61 (1-4)	-
	0.40 (1-2), 0.33 (1-3), 0.39 (1-4)	22 (1-2), 24 (1-3), 27 (1-4)
TETG5 (subunits)	0.57 (1-2), 0.57 (1-3), 0.60 (1-4)	-
	0.33 (1-2), 0.33 (1-3), 0.33 (1-4)	26 (1-2), 27 (1-3), 31 (1-4)
C. TETPO onto TETG5		
	0.43	-
	0.36	39

[a]Criteria for omission C-α deviation>1.5Å. [b]Based upon all atoms within 10Å of the phosphate in the R state complexes (TETPO/TETG5).

Table 3.3. *Superimposition of the refined coordinates of TETPO, TETG5 and the native R state structure.*

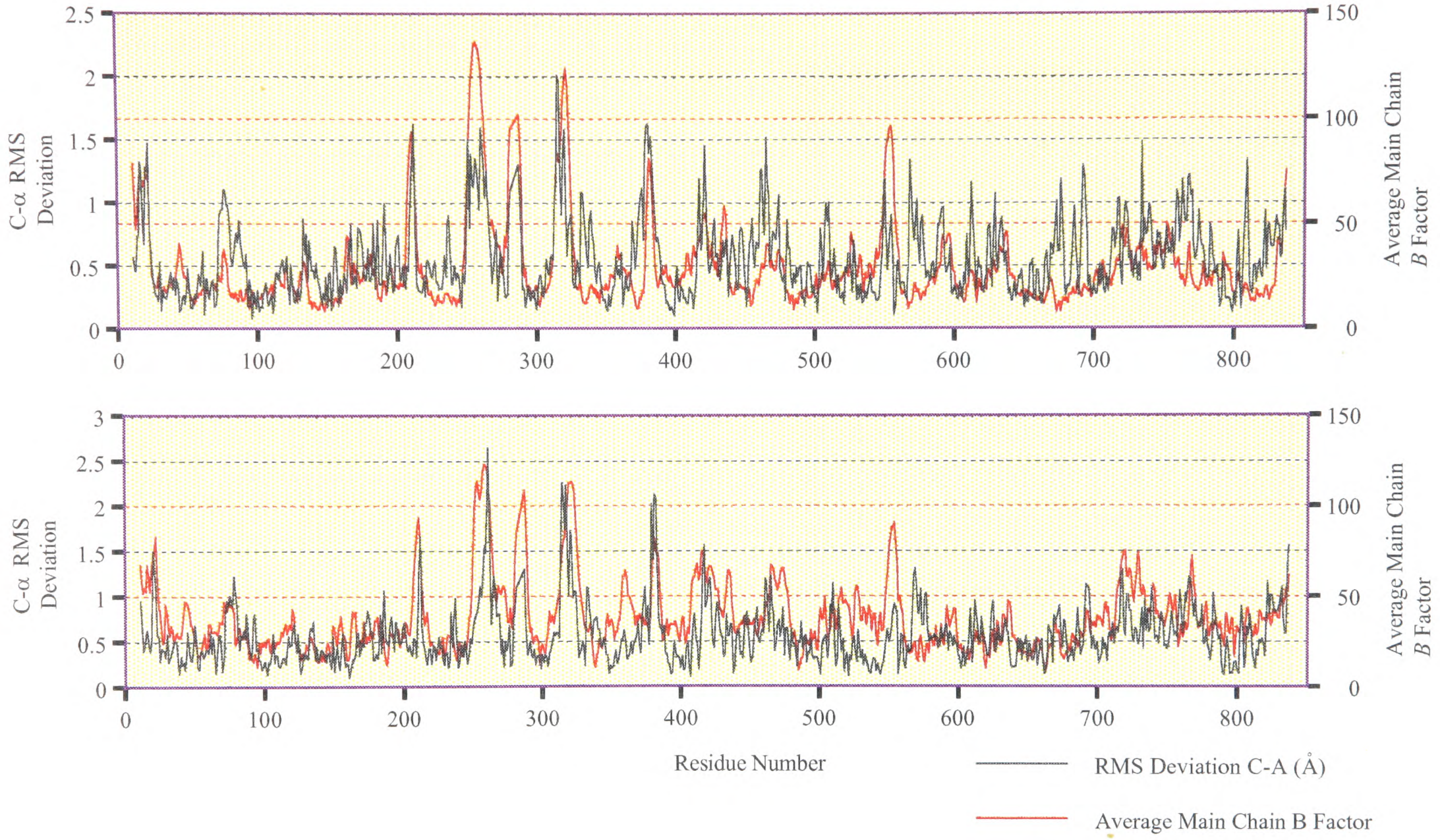

Figure 3.3. *Superimposition by residue of the C-α atoms from the TETPO (top) and TETG5 (lower) complexes onto the native R state structure. In red the average main chain B factors for the complexes are also shown.*

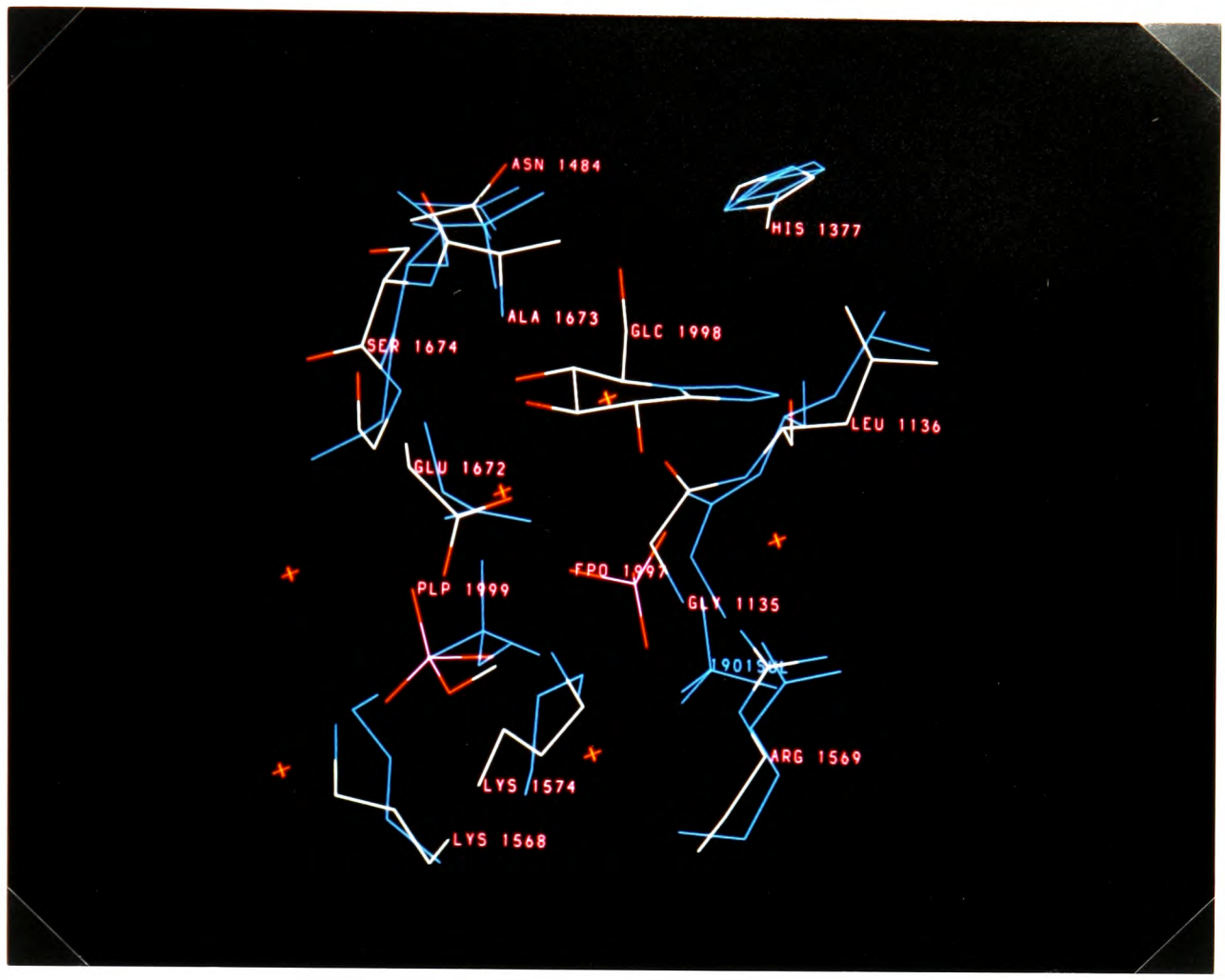

Figure 3.4. *The refined model of TETPO at the active site with the native R state structure superimposed in blue. The native sulphate is labelled as residue 1901.*

native conformation further into the active site to coordinate the phosphate. The guanadinium group of Arg 569 is in contact with the phosphate ion and makes two hydrogen bonds from NE and NH1. Moreover the PLP 5'-phosphate is forced some 1.5Å away from its native position by the newly located free phosphate, but remains in direct contact with this phosphate. Table 3.4 compares the hydrogen bond contacts between the native R state structure, containing a sulphate ion, and the R state and T state GPb-tetrazole-phosphate complexes. The T and R state complexes have very similar contacts, even down to the conserved shell of waters surrounding the 5'-phosphate. The movement of the PLP group between native and complexed R state GPb, accompanied with binding of the tetrazole, drags Thr 676 and Gly 677 closer into contact with the 5'-phosphate tightening the hydrogen bonds with these residues.

These essential conformational changes are supported by smaller movements around the

PLP Atom	Protein or Ligand Atom	Hydrogen Bond Contact (Å)		
		Native[a]	R State Complex[b]	T State Complex[c]
OP-1	NZ Lys 574	2.4	2.7	2.9
	WAT 895	-	2.7	2.8
OP-2	NZ Lys 574	(3.7)	(3.4)	2.9
	OP3 Phosphate	-	2.5	2.7
	O3 Sulphate	3.2	-	-
	WAT 879	-	2.9	2.9
OP-3	N Thr 676	(3.5)	2.9	2.7
	N Gly 677	(3.4)	3.0	2.9
	WAT 885	-	3.0	3.5
	WAT 897	-	3.0	2.7
OP-4	WAT 895	-	3.0	2.8

[a]Native R state structure (Barford & Johnson, 1989). [b]R state GPb-tetrazole-phosphate. [c]T state GPb-tetrazole-phosphate, complex [6] of Chapter 2.

Table 3.4. *Comparison between the hydrogen bond contacts of the PLP 5'-phosphate in three GPb structures. For convenience the water molecules are labelled with the T state assignment; the waters concerned are conserved between the T and R state. There are no waters placed in the native structure.*

active site of other side chains and main chain atoms. The side chains of Lys 568 and Lys 574 retain their positions coordinating the 5'-phosphate. The phenyl ring of Tyr 573 is dragged towards the free phosphate and the OH makes a hydrogen bond to OP-2 of the phosphate. The torsion angles of Glu 672 are adjusted and the carboxyl oxygens successfully make two hydrogen bonds to O-2 and O-3 of the tetrazole and also one to the OH of Tyr 573 at its new location. Table 3.5 summarises the hydrogen bond contacts made between phosphate, tetrazole and enzyme which are depicted in Figure 3.5.

The completed phosphate binding site appears to be tighter than the native sulphate site. No

Ligand Atom	Protein Atom	Hydrogen Bond Contact (Å)	
		TETPO	TETG5
Tetrazole			
O-2	OH Tyr 573	2.9	3.1
	OE1 Glu 672	3.2	(3.4)
	OP2 Phosphate	2.9	3.0
	WAT 890	2.8	-
O-3	OE1 Glu 672	2.7	2.9
	N Ser 674	3.3	(3.6)
	N Gly 675	3.1	(3.4)
O-4	N Gly 675	2.9	3.2
	WAT 897	2.7	-
O-6	ND1 His 377	2.8	2.6
	ND2 Asn 484	3.0	3.1
N-1	OP1 Phosphate	3.1[a]	3.0[a]
N-2	N Leu 136	3.1	3.1
Phosphate			
OP-1	N1 Tetrazole	3.1[a]	3.0[a]
	N Gly 135	3.1	3.2
	WAT (no equiv)	2.5	-
OP-2	O2 Tetrazole	2.9	3.0
	NH1 Arg 569	2.9	3.0
	OH Tyr 573	3.2	3.1
	NZ Lys 574	2.9	2.9
OP-3	OP2 PLP 999	2.6	2.7
	WAT 897	3.1	3.2
OP-4	N Gly 135	2.9	3.2
	NE Arg 569	(3.4)	2.8
	WAT 879	2.7	-

[a]Contact represents an electrostatic interaction.

Table 3.5. *Hydrogen bond contacts between nojirimycin tetrazole, phosphate and R state GPb catalytic site residues averaged over the R state tetramer. Distances in brackets indicate a weak contact and a dash indicates no contact. Waters were not included in the TETG5 structure. For ease of comparison to the T state the waters are labelled with the T state assignment.*

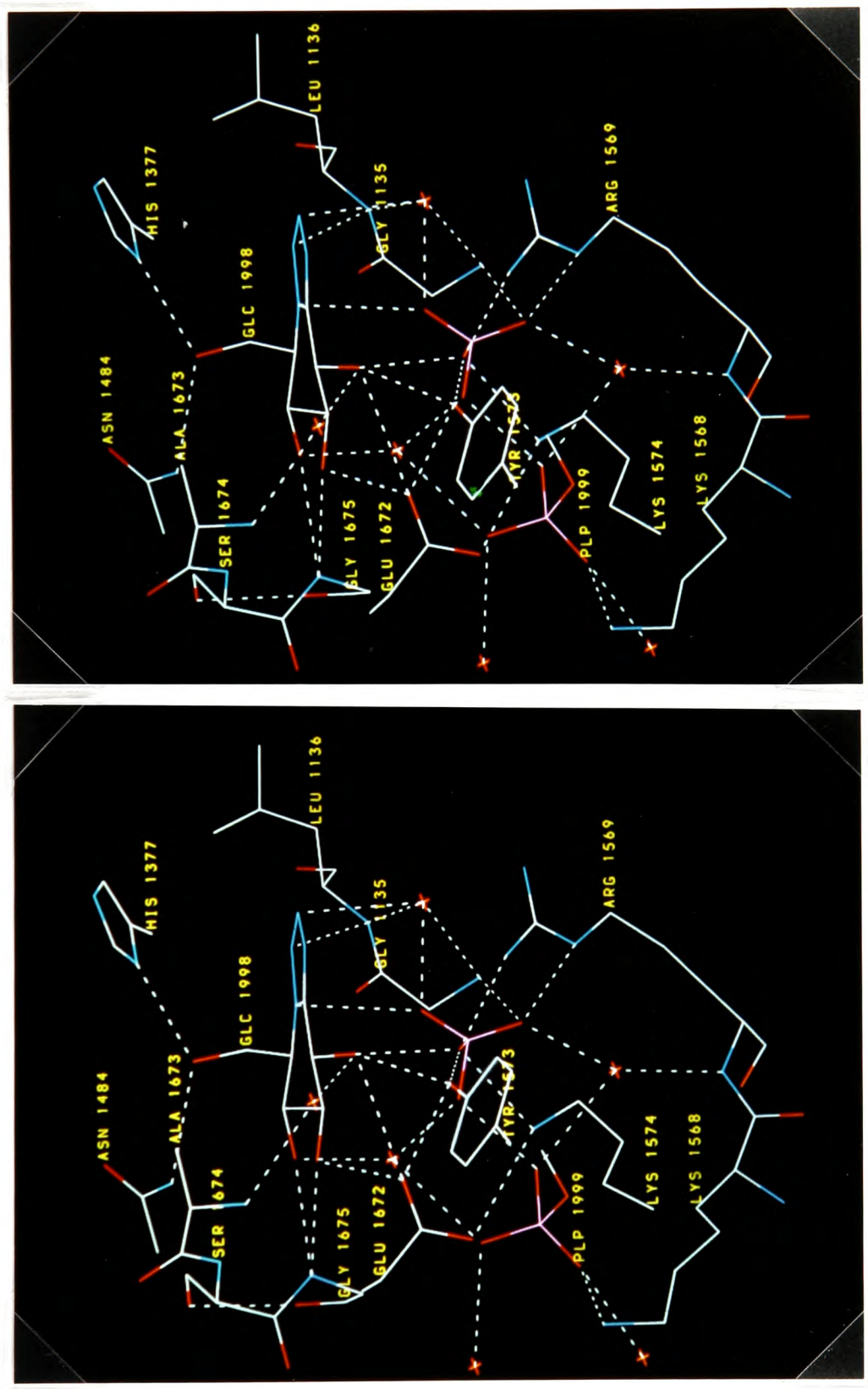

Figure 3.5. *A stereo diagram of the active site hydrogen bonds between R state protein, phopshate and nojirimycin tetrazole. The structure is from the refined model of the TETPO complex.*

K_m values are available, but the average *B* factors for the phosphate in the TETPO and TETG5 complexes are 21Å^2 (2.5Å resolution) and 29Å^2 (2.8Å resolution) respectively compared to 61Å^2 (2.8Å resolution) for the native sulphate ion. The phosphate does make a total of 7 hydrogen bond contacts to the protein, 3 more than the sulphate (contacting N Gly 135, NE Arg 569, NZ Lys 574 and OP2 PLP 999), and has the additional benefit of the presence of nojirimycin tetrazole to further tighten the binding pocket. A recent review of phosphate and sulphate binding sites (Copley & Barton, 1994) revealed an average of 3.5 contacts from protein residues to each phosphate ion, with 2 contacts being most common, over the 38 proteins studied. This suggests the R state phosphate site, with 7 contacts and a further 4 to waters and tetrazole, is particularly tightly coordinated. This perhaps reflects the importance of the phosphate orientation and thus the structure of the binding site in the phosphorylase catalytic mechanism.

The majority of the structural changes observed at the active site are associated with the creation of a phosphate recognition pocket distinct from the native R state sulphate site. Some may be due in part also to the higher resolution data collected from the complexes compared to the native data set.

(ii) The Glycogen Storage Site. The most detailed structural study of the glycogen storage site to date has come from work on the binding of maltoheptaose to T state GPb (Johnson *et al.*, 1988; Johnson, Acharya, Jordan & McLaughlin, 1990). The glycogen storage site is located on the protein surface, away from other ligand binding sites and the subunit-subunit interface. The previous studies have found that the storage sites consists of two α-1,4-oligosaccharide binding sites, known as the major and minor sites.

The major site is formed by the α12 helix (residues 410 to 418) and by β15-β16 (residues 430 to 441). Up to five glucosyl residues have been observed to bind at the major site and the

subsites are labelled as S3, at the reducing end, to S7. A binding study by Hu (Hu, 1991) of the maltose disaccharide in R state phosphorylase revealed the sugar to occupy subsites S4, S5 and S6. The subsite S5 appeared to be the most strongly binding site, as also observed in the maltoheptaose binding studies. The minor site consists of just two glucosyl residues and is close to the end of the α12 helix at the non-reducing end of the major site.

In the refined model of TETG5 maltopentaose arches over the α12 helix, making hydrogen bond contacts to hydrophilic residues such as Asn 407 and Gln 433 (Figure 3.6). The hydrogen bond contacts are listed in Table 3.6. Van der Waals interactions are made to Val 422 (S3), Leu 411 (S4) and Val 431 (S5). The sugar in subsite S5 is the most strongly bound and is the best defined sugar in the Fourier map. A total of six hydrogen bond contacts are made from all of the oxygen atoms to the protein. Additionally extensive Van der Waals contacts are made from S5, and partly S6, to Tyr 404 which stacks against the S5 pyranose ring approximately 4.5Å away. The positions of the three central sugars (S4, S5 and S6) are well supported by the final ($2F_o$-F_c) Fourier map. The map contains density for the α-1,4-glycosidic link of the two terminal glucose units, but little for the pyranose ring or hydroxy groups. The geometry of the amylose helix model is approximately retained in the refined complex. There are intramolecular hydrogen bonds between O2 of S6 and S7 to O3 of S5 and S6 respectively. There is no direct contact between S4 and S5, but OE1 of Gln 433 mediates a hydrogen bond and contacts both glucose residues.

A comparison of the R state maltopentaose complex with the transformed coordinates of T state GPb complexed with heptulose-2-phosphate and maltoheptaose (Johnson, Acharya, Jordan & McLaughlin, 1990) shows the oligosaccharide binding site to be similar. Only five of the seven glucose units of maltoheptaose could be observed in the T state complex, and the refined positions of these are very close to those of the R state complex. The hydrogen bonding pattern is similar with small differences (Table 3.6). In particular the contacts to S5 are very

Ligand Atom	Protein or Ligand Atom	Hydrogen Bond Contact (Å)	
		TETG5	Reference[a]
O2 (S3)	O Val 422	3.1	2.7
O3 (S3)	O Val 422	3.3	-
	N Arg 426	2.7	-
	O Lys ' 753	2.9	-
O3 (S4)	OG Ser 429	2.9	-
	O Val 431	3.3	-
	OE1 Glu 433	3.1	3.3
O2 (S5)	OE1 Glu 433	2.6	2.3
	NZ Lys 437	2.8	2.5
O3 (S5)	NZ Lys 437	3.2	3.3
	O2 (S6)	3.2	3.3
O5 (S5)	ND2 Asn 407	2.6	2.8
O6 (S5)	O Tyr 404	2.8	2.9
	ND2 Asn 407	2.9	2.8
O2 (S6)	O3 (S5)	3.2	3.3
O3 (S6)	O2 (S7)	3.0	2.6
O2 (S7)	O3 (S6)	3.0	2.6
O3 (S7)	O Asp #78	2.7	-
O4 (S7)	O Lys #77	2.5	-
O6 (S7)	OE1 Glu 405	3.2	-

[a]The reference hydrogen bonds are taken from the T state coordinates of GPb complexed with heptulose-2-phosphate, AMP and maltoheptaose fitted, using C-α atoms, to the R state structure (Johnson, Acharya, Jordan & McLaughlin, 1990).

Table 3.6. *Hydrogen bond contacts, averaged over the tetramer, between maltopentaose and R state phosphorylase. A dash indicates no contact. Lys 753 is from subunit 4 of the tetramer. Lys 77 and Asp 78 both belong to the crystallographically related subunit 2.*

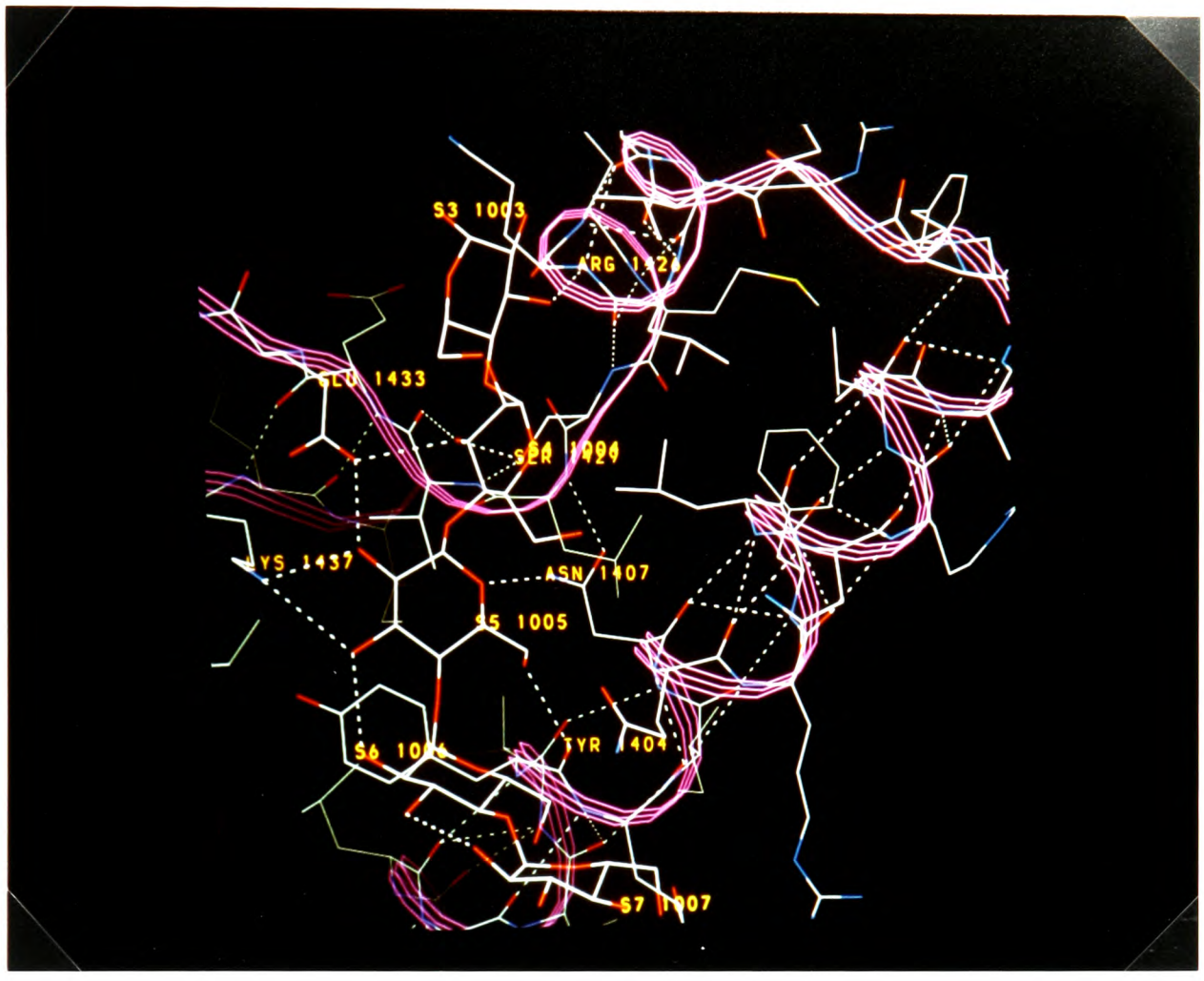

Figure 3.6. *The refined structure of the TETG5 complex with maltopentaose at the glyccogen storage site.*

much the same in both complexes, reflecting the greater ordering of this glucose unit.

(iii) Water Molecules in the R State. The model of native R state GPb contains no water molecules. Data to 2.5Å were collected from the GPb-tetrazole-phosphate complex (TETPO) and at this resolution water molecules could be located in the structure. A total of 252 waters per subunit were added to the model, with some of the highest peaks in the Fourier map used to place them corresponding to waters at the active site. Of these 252 waters, 130 are open to solvent to some degree and 127 are buried within the protein structure.

A comparison of the water structure of the T state and R state GPb-tetrazole-phosphate complexes reveals there to be 86 (34%) conserved water molecules, allowing a fit of within 1.0Å. This falls to 46 (18%) waters when allowing just 0.5Å positional variation. Of the 86

conserved waters 65 (76%) of them are buried within the protein structure with no solvent access. This observation is in agreement with other studies on proteins adopting different crystal systems (Blake, Pulford & Artymiuk, 1983; Finer-Moore, Kossiakoff, Hurley, Earnest & Stroud, 1992; Zhang & Mathews, 1994) where it was found that waters internal to the protein tended to be conserved more often than surface solvent as one would expect.

(iv) Comparison of the R State and T State GPb-Tetrazole-Phosphate Complexes. Superimposing the GPb-tetrazole-phosphate T state coordinates onto the R state equivalent reveals there to be little difference between them. Figure 3.7 compares the locations of PLP, anion (phosphate or sulphate) and tetrazole in the T and R state GPb-tetrazole-phosphate complexes, the native R state and the R state GPb-glucose-1-phosphate complex (Hu, 1991).

Most of the active site residues and particularly those forming the glucosyl and phosphate recognition sites have, within experimental error, identical conformations in both the T and R state complexes. The obvious exception is the 280s loop of residues, which in the native and in the complexed R state cannot be located. The positive electrostatic pocket formed by Lys 568, Arg 569, Lys 574 and the tetrazole to compensate for the close proximity of substrate phosphate and PLP 5'-phosphate is conserved between the T and R state complexes. The side chain of Arg 569 does however adopt a different conformation and engages the substrate phosphate with two hydrogen bond contacts from NH1 and NE of the guanadinium group. Unlike in the T state complex, where the side chain appears to be more mobile, the side chain of Arg 569 is well located in both of the R state ($2F_o$-F_c) Fourier maps. In the R state complexes, the inhibitor site consisting of Phe 285 and Tyr 613 is broken and the 280s loop of residues is flexible. This may allow Arg 569 more freedom to adopt a full R state conformation with phosphate and tetrazole, whereas in the T state interactions with the localised 280s loop bias the side chain conformation. The histidine ring of residue 571 maintains its native R state conformation, which opens the active site channel and contributes to the T to R state transition

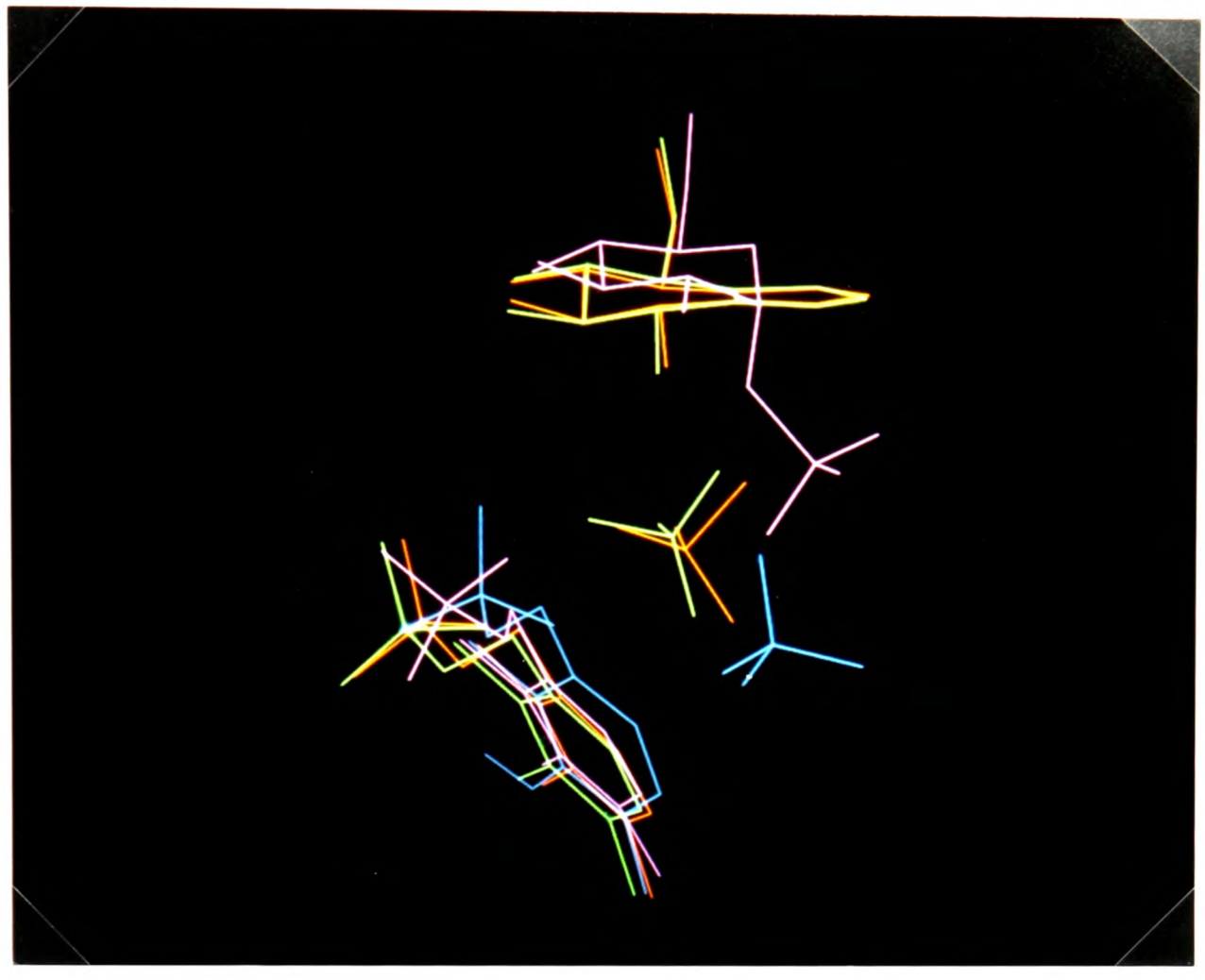

Figure 3.7. *Comparison of PLP, tetrazole and anion at the active sites of T and R state GPb complexes: T (orange) and R (green) state GPb-tetrazole-phosphate, native R state (blue) and GPb-glucose-1-phosphate (pink.*

of phosphorylase. In the T state GPb complexes with phosphate and tetrazole, His 571 was observed to move slightly but remained close to the T state conformation. In Chapter 2 of this thesis it was suggested that lattice forces in the tetragonal T state crystals prevented full transition towards the R state.

The orientation of substrate phosphate deduced from Fourier maps of the T state complexes is vindicated in the R state complexes. The $(2F_o\text{-}F_c)$ maps of the refined R state models allows clear identification of hydrogen bonds between the phosphate and surrounding residues and support the T state phosphate orientation. In the R state continuous density, suggesting hydrogen bonds, is observed between the phosphate and O-2 and N-1 of the tetrazole, OP-2 of the pyridoxal 5'-phosphate, NZ Lys 574, OH Tyr 573 and WAT 879 (T state assignment)

which bridges between substrate phosphate, PLP 5'-phosphate and N Arg 569.

The great majority of water molecules located at the T state active site are also observed in the R state structures. The exceptions to this all occur in the region that would be occupied by the 280s residues if they were localised. The R state active site waters are well ordered with strong peaks in the difference maps and an average *B* factor of 18Å^2 compared to the active site C-α average of 14Å^2. Two waters are located between the substrate phosphate and PLP 5'-phosphate making identical contacts to protein and ligands as the equivalent waters in the T state. These waters contribute, together with the surrounding protein, to stabilisation of the phosphate-phosphate interaction (Figure 3.4). Other active site waters mediate contacts between nojirimycin tetrazole, pyridoxal phosphate and the protein. The shell of five waters surrounding the 5'-phosphate make contacts to all the phosphate oxygens and bridge to the surrounding protein residues Val 567, Arg 569, Tyr 648, Glu 665 and Asn 678. The conservation of waters at the active site suggests that they play an important role in maintaining the active site structure and in promoting the positioning and orientation of substrates.

In general the R state structure is remarkably similar to the T state nojirimycin complexes, especially so at the active site and even extending to the locations of conserved water molecules. This similarity supports the notion that the changes observed in the T state phosphorylase structure when complexed with tetrazole and phosphate are those that would occur upon binding natural substrates to form the ternary complex and reaction intermediates.

3.5 SUMMARY

The observation of a direct phosphate-phosphate interaction in R state GPb and the similarity of the R state complexes to the T state has confirmed the results from the binding study of nojirimycin tetrazole and phosphate to the T state enzyme. It strongly suggests that the interactions and conformational changes observed in the T state complexes are indicative of the allosteric response and the interactions of the transition state.

It was disappointing that despite the transition state nature of the R state GPb-tetrazole-phosphate complex, oligosaccharide did not bind at the active site. Work currently being undertaken on E. coli maltodextrin phosphorylase (M O'Reilly & K Watson, work in progress), which has a lower K_m for oligosaccharide than rabbit muscle phosphorylase, is aiming to solve the enigma of oligosaccharide binding at the active site.

4.1 INTRODUCTION

4.1.1 Overview

Crystals of macromolecules are damaged by X-ray radiation and the increasingly bright sources of X-rays from synchrotrons make this problem ever more acute. As a result flash frozen crystals are now often being used to collect X-ray diffraction data. This technique prolongs the useful crystal lifetime in the X-ray beam (Henderson, 1990). This means that a full data set may be recorded from a single crystal; giving more accurate data. Production of free radicals within a crystal lattice, by ionising radiation, is likely to be responsible for initiating crystal damage. At room temperature these radicals are free to move and produce a disruptive domino effect through the lattice. At low, liquid nitrogen, temperatures the radicals are locked into a solid matrix and though still created by the X-rays are not mobile and unable to damage the crystal. High resolution data are the first to be affected by radiation damage. Flash freezing allows more high resolution data to be collected before damage to the crystal destroys lattice ordering, resulting in the loss of these reflections. Another important potential benefit of cryocrystallography is the possibility of direct observation of unstable enzyme-substrate complexes and intermediate states during the course of enzyme reactions (Douzou & Petsko, 1984).

4.1.2 A Brief History

Cooling of protein crystals to temperatures below -150°C was first attempted by Low *et al* in 1966. The studies used orthorhombic insulin crystals wiped clean of mother liquor and frozen over the course of less than one minute to below -150°C. However, after cooling the mosaic spread of the crystal had increased dramatically. Low concluded that the difference in volume of water in the protein lattice between room temperature and -150°C had caused the increase

of mosaicity. Attempts by Low and co-workers to improve the mosaic spread, by introducing alcohols and glycols to the crystals or by using glutaraldehyde as a cross-linking agent to stabilise the crystal (Quiocho & Richards, 1964), failed. The work was eventually abandoned in favour of a higher temperature range of -13°C to 0°C.

Subsequent attempts to collect data from crystals at low temperature have included: cross-linking lysozyme crystals followed by transfer to 50% glycerol (Haas, 1968), equilibration of lactate dehydrogenase crystals in 3M sucrose (Haas & Rossmann, 1970) and freezing sperm whale myoglobin crystals at a pressure of 2500atm to form an ice phase which has a volume smaller than water (Thomanek *et al.*, 1973).

However, each of these methods was a special case for a particular crystal system and it was not until the approach of Petsko (1975) that a general method to stabilise protein crystals at cryo-temperatures was proposed. Petsko suggested using a salt-free aqueous-organic cryoprotectant mixture to replace the crystal mother liquor. This gave lower mosaicity and small unit cell dimension changes on freezing, and simplified access to temperatures below -100°C.

Six years ago, Hope (Hope, 1988) published a technique that enabled easy crystal mounting and data collection at temperatures close to that of liquid nitrogen (80K). Hope had originally developed over a number of years this procedure for small molecule crystallography, but then suggested it could also be used for macromolecules. Crystals were first transferred into an inert oil, mounted onto a thin glass spatula and finally flash frozen in a cold nitrogen stream. This method was more straight forward than previous techniques, but still lent itself to crystal deformation, and thus increase in mosaicity, due to lack of flatness of the glass spatulas. However, it did represent an improvement over traditional capilliary crystal mounting.

Today, the most widely used technique is the thin-film method devised by Teng (1990) and this new method is proving more widely applicable to macromolecular crystallography than any proposed so far.

4.1.3 The Thin-Film Method

The procedure developed by Teng for flash freezing protein crystals involves the transfer of the crystal to, or cocrystallising the protein, with a cryoprotectant. The crystal is then suspended in a small (less than 1mm diameter) loop of fibre, where it is supported by a liquid film of cryoprotected buffer, and flash frozen in a stream of cold (80-100K) nitrogen gas (Figure 4.1). The cryoprotectant freezes as an amorphous glass with no ordered water present. Strain upon the crystals from contact with mechanical mounting supports, such as Hope's glass spatulas, is eliminated by this technique, and consequently frozen crystals tend to have lower mosaic spreads than those mounted by other methods.

The choice of cryoprotectant is dependent on the protein and its crystallisation conditions. In fortunate cases the mother liquor itself contains a suitable cryoprotectant and no additive is required. Typical agents used, where a cryoprotectant is needed, are glycerol, ethylene glycol and PEG (Petsko, 1975; Hope *et al.*, 1989; Gamblin & Rodgers, 1993). In a brief survey of recently published structures, where cryoprotectants were added, glycerol (Guo *et al.*, 1992; Lee *et al.*, 1994) and ethylene glycol (Freymann *et al.*, 1990; Rini, Schuize-Gahmen & Wilson, 1992) were both used twice, one used PEG (Ellenberger, Brandi, Struhl & Harrison, 1992) and one a glycerol/PEG mixture (Nikolov *et al.*, 1992).

This chapter describes the search for suitable flash freezing conditions for T state GPb crystals and lays the groundwork for studying flash frozen GPb-ligand complexes. The

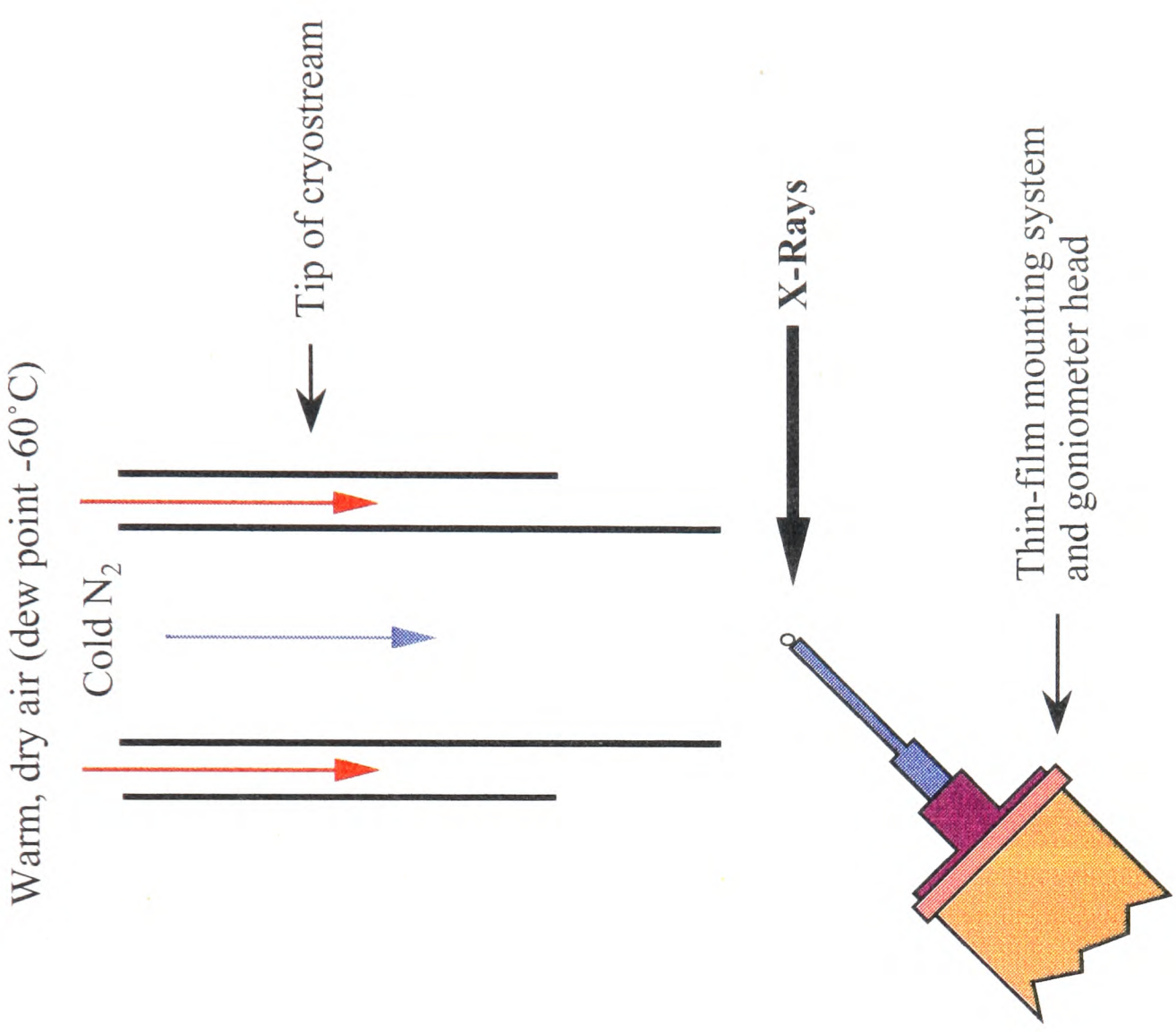

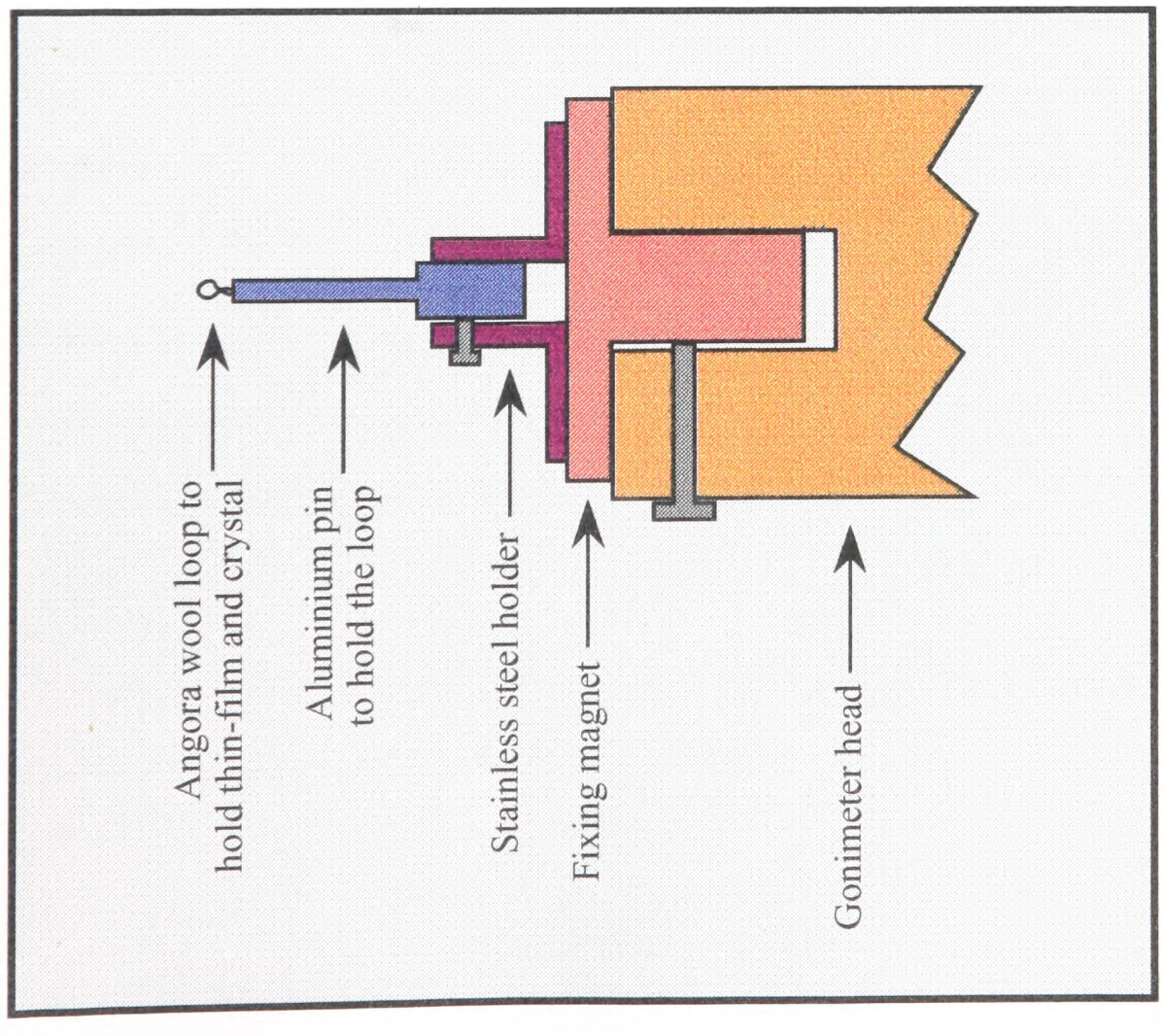

Figure 4.1. *Diagrams showing the flash freezing arrangement and thin-film crystal mounting method.*

ultimate aims are to collect high resolution data from native GPb crystals and also a complex of T state GPb with nojirimycin tetrazole and phosphate ions (Chapter 5). It also examines the effect of cryoprotectant (in this case glycerol) concentration upon the mosaicity and diffraction limit of the crystals. The results of this investigation (Mitchell & Garman, 1994) show that there is a well defined optimum in glycerol concentration giving lowest mosaicity, maximum resolution and no ice formation. The results also demonstrate how flash freezing conditions can be systematically determined in-house using a minimum number of crystals.

4.2 EXPERIMENTAL METHODS

4.2.1 Data Collection

T state GPb crystals ($P4_32_12$, a=b=128.5Å, c=116.3Å) were grown as described previously (Oikonomakos, Melpidou and Johnson, 1985; Johnson, Madsen, Mosley and Wilson, 1974) from a buffer solution of 1.1mM IMP, 1.1mM spermine, 10mM BES, 2.9mM dithiothreitol and 0.1mM EDTA at pH 6.7. Prior to data collection, crystals (between 0.2 and 0.3mm in the largest dimension) were soaked for 5 minutes in a BES buffer solution containing glycerol concentrations from 0 - 70% *v/v* (10mM BES, 0.1mM EDTA, 0.02% sodium azide, pH 6.7). Previous tests with other possible cryoprotectants had shown glycerol to be the most suitable candidate. At glycerol concentrations of 60% and 70% the cryoprotected buffer was gently stirred after placing the crystal in to soak. For comparison, the following additional soaks were also carried out: 20 minutes and 2.5 hours in 50% glycerol, sequential soaking for a total of 5 minutes in 10%, 30% and 50% glycerol, 60% glycerol with no stirring, and 60% glycerol for 20 minutes.

After soaking, an Oxford Cryostream cooling device (Cosier & Glazer, 1986) operating with nitrogen gas at 100K was used to flash freeze the crystals and maintain this state during data collection. Transfer time from cryoprotected buffer to flash freezing was as short as possible and always less than 2 seconds. In order to allow freezing over as short a time period as possible, the cold nitrogen stream was temporarily diverted away from the goniometer using a piece of card, whilst the crystal and loop were positioned. As soon as the loop with the crystal were in place the card was quickly removed to allow freezing. Two people are essential for this procedure.

Precentering of the cryostream, before mounting the crystals, was vital to ensure the crystal was positioned in the coldest region of the nitrogen stream and not inadvertantly moved into

a warmer part when it was already frozen and being centered at the beam position. Since the whole technique can fail if the stream is inaccurately centered, a special attachment, shown in Figure 4.2, was designed to ensure foolproof centering (E. Garman, private communication). Centering of the Cryostream was aided by mounting the coldhead on a system of screw adjusters allowing fine movements. It is also important to minimise air turbulence around the loop mounting system. The turbulence was reduced by designing the pin holding the loop to be thin and long, and also by enclosing the whole experiment in a plastic sheeting tent. The Oxford cryostream cooling device provides a dry (dew point -60°C) room temperature air stream coaxially with the cold nitrogen stream. The flow rate of dry air is matched to that of the cold nitrogen gas. This cuts down turbulence between them, thus preventing the ingress of warm moist air which could cause ice build up around the crystal. The thin-film loop method of mounting crystals developed by Teng (1990) was used. The loop, also precentered, was made out of a single strand of angora wool, used for its very high strength/weight ratio. It was mounted in a metal pin fixed to a steel button, held by a magnet on to the goniometer head. The metal pin provides a thermally conducting path across the cold nitrogen/warm dry air boundary, and this significantly reduces frost build up as compared to using a non-conducting pin material.

Data were collected on a Siemens area detector mounted on a monochromated Rigaku RU-200H rotating anode X-ray source, operating between powers of 50kV, 50mA and 60kV, 70mA. The detector was placed 16cm away from the crystal and at a swing angle of either 0° (maximum resolution of 4.9Å) or 22° (maximum resolution of 2.3Å). For each crystal at least 15 data frames each of 0.2° oscillation width each were collected, with exposure times of between 120 and 240 seconds. At the optimum cryoprotectant conditions (a glycerol concentration of 50%) data sets from two crystals were collected and subsequently processed (using the XDS package, Kabsch 1993) in order to check the unit cell size and data quality.

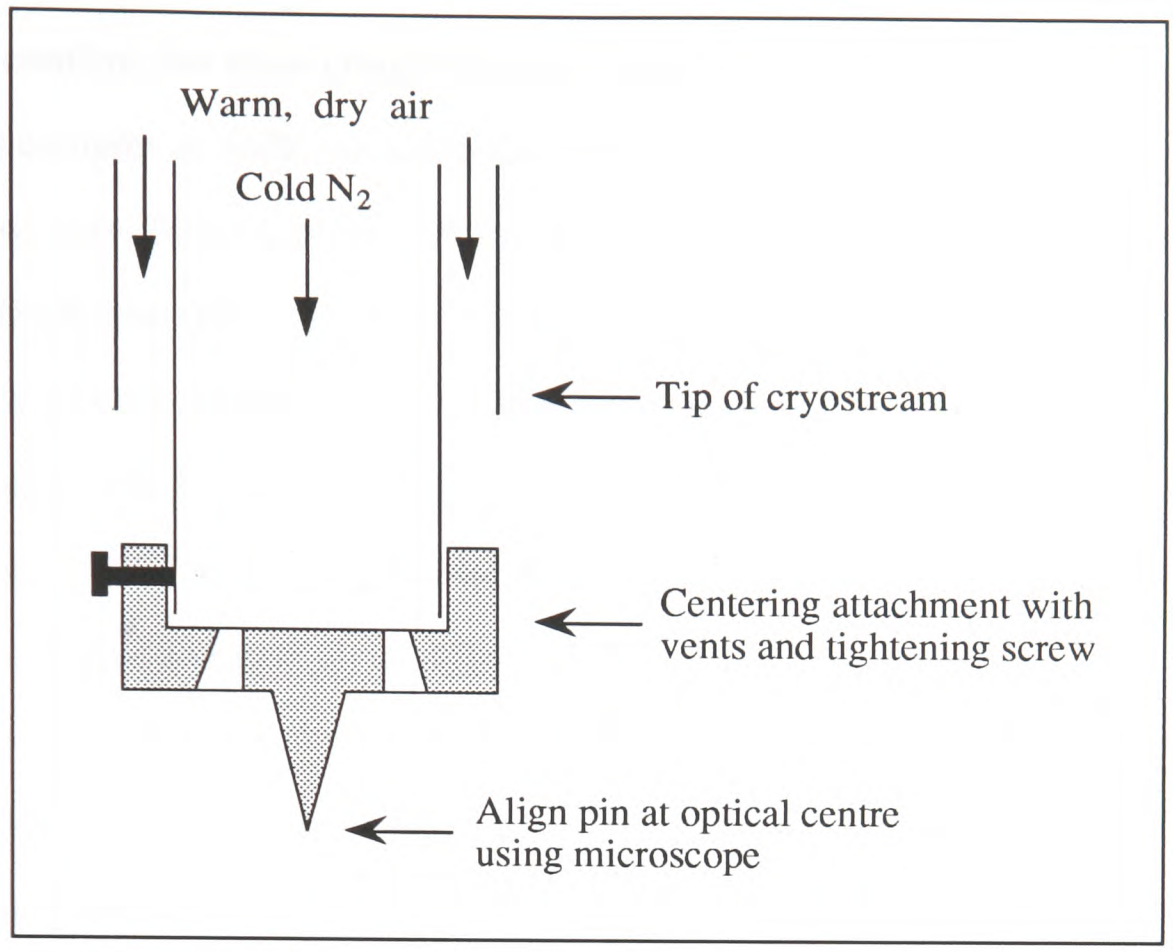

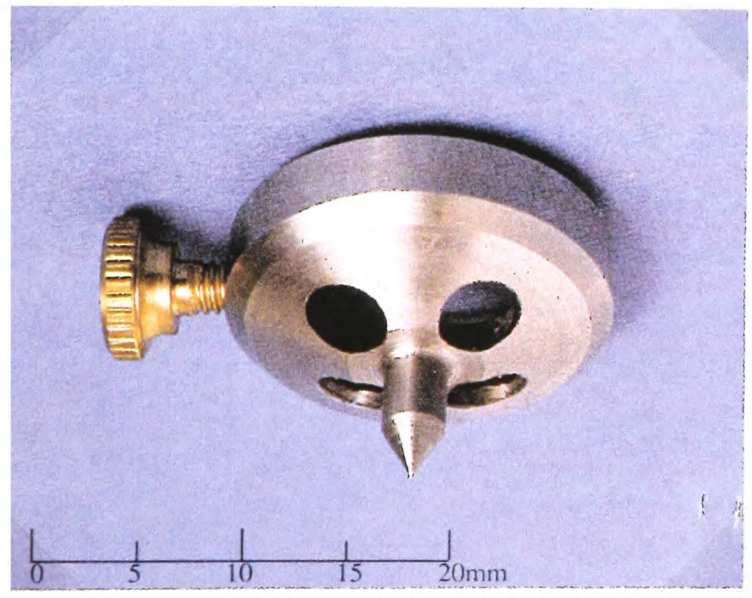

Figure 4.2. *The centering attachment consists of a collar which is held onto the cold nitrogen nozzle by a tightening screw. A pin below the centre of the collar allows centering, before mounting crystals, of the cryostream with the X-ray beam position using a microscope. Slots were drilled around the pin to enable cold nitrogen gas to escape and avoid back pressure on the cold stream during alignment. A stainless steel metal with a low thermal expansion coefficient was chosen, since the prototype, made of brass, contracted too much when on the nozzle.*

In order to confirm that these cryoprotectant conditions allowed data to be collected from a GPb-ligand complex at 100K, an additional data set was taken from a GPb crystal treated in the following way. Firstly, the crystal was soaked for 40 minutes in BES buffer containing 200mM α-D-glucose (pH 6.7) and then transfered to BES buffer containing 50% glycerol and 200mM α-D-glucose (pH 6.7) for 5 minutes. The crystal was flash frozen as described above and data frames of 0.2° oscillation width and 100 seconds exposure were collected for a total angular range of 90°. These were processed and merged using the XDS (Kabsch 1993) package of programs to give a unique set of reflections.

Data statistics for collection from the frozen native crystal and frozen GPb-glucose complex are shown in Table 4.1.

4.2.2 Mosaic Spread of the Crystals

In order to examine the effect of glycerol upon the mosaicity of the T state GPb crystals, full width half-maxima of the reflection rocking curves as a function of oscillation angle were extracted using the program OSCIL (W. Minor, private communication). Reflections for these measurements were chosen so that the entire profile was contained within the total angular range over which data had been collected.

			Native GPb	GPb-Glucose
Number of Reflections		Unique	19306	19737
		Observed	49668	50731
Maximum Resolution (Å)			2.8	2.8
Completeness of Data (%)	Signal:Noise >= 0.0	∞ - 2.8Å	81	83
		3.2 - 2.8Å	75	77
	Signal:Noise >= 2.0	∞ - 2.8Å	65	62
		3.2 - 2.8Å	46	43
$R_m(I)$ (%)		∞ - 2.8Å	13	9.1
		3.2 - 2.8Å	29	21
R_{iso} [a] (%)			41	27

[a]Mean fractional isomorphous difference of the structure factor amplitudes of the frozen protein crystal (F_F), calculated with respect to the structure factor amplitudes of the native enzyme (F_P): $\Sigma_h[||F_F| - |F_P||] / \Sigma_h|F_P|$.

Table 4.1. *Crystallographic data collection and processing statistics for native GPb and GPb-glucose crystals at 100K.*

4.3 RESULTS AND DISCUSSION

4.3.1 Effect of Glycerol Concentration upon Crystal Mosaicity and Diffraction Limit

Using the above experimental technique, the mosaicity of 3 different crystals was measured for each glycerol concentration investigated. The results are summarised in Figure 4.3.

There are two parameters to consider in optimising X-ray data quality from flash frozen crystals: the diffraction limit of the crystals and their mosaic spread. In the present work, the maximum resolution obtained improved as the glycerol concentration was increased to 50%, and then unexpectedly worsened at 60 and 70%. At 50% glycerol, the resolution of 2.9Å was lower than the 2.3Å normally observed in room temperature data collection from large GPb crystals. This difference was due to the smaller crystals and low counting times used for the comparative freezing experiments, shown in Figure 4.3. With a longer exposure 2.3Å diffraction was observed at 50% glycerol concentration. Small crystals are necessary to ensure successful flash freezing. A large crystal takes significantly longer to freeze than a small (less than 0.3mm in the longest dimension) crystal and freezes anisotropically through the crystal. A dramatic increase of mosaicity and lower diffraction limit are the consequences.

The mosaicity followed the same general trend as the resolution, dropping as the percentage glycerol was increased, reaching a minimum at 50% glycerol, and then rising as the glycerol concentration in the soak buffer was raised further (Figure 4.3). The lowest mosaicity attained was 0.25°, which compares well with the 0.25-0.30° observed for T state GPb crystals at room temperature (measured using the same X-ray optics). At 60% and 70% glycerol the cryo-protected buffer became viscous and consequently was gently stirred to ensure good mixing of the crystal with cryoprotectant. However, a trial with 60% glycerol where the crystal was

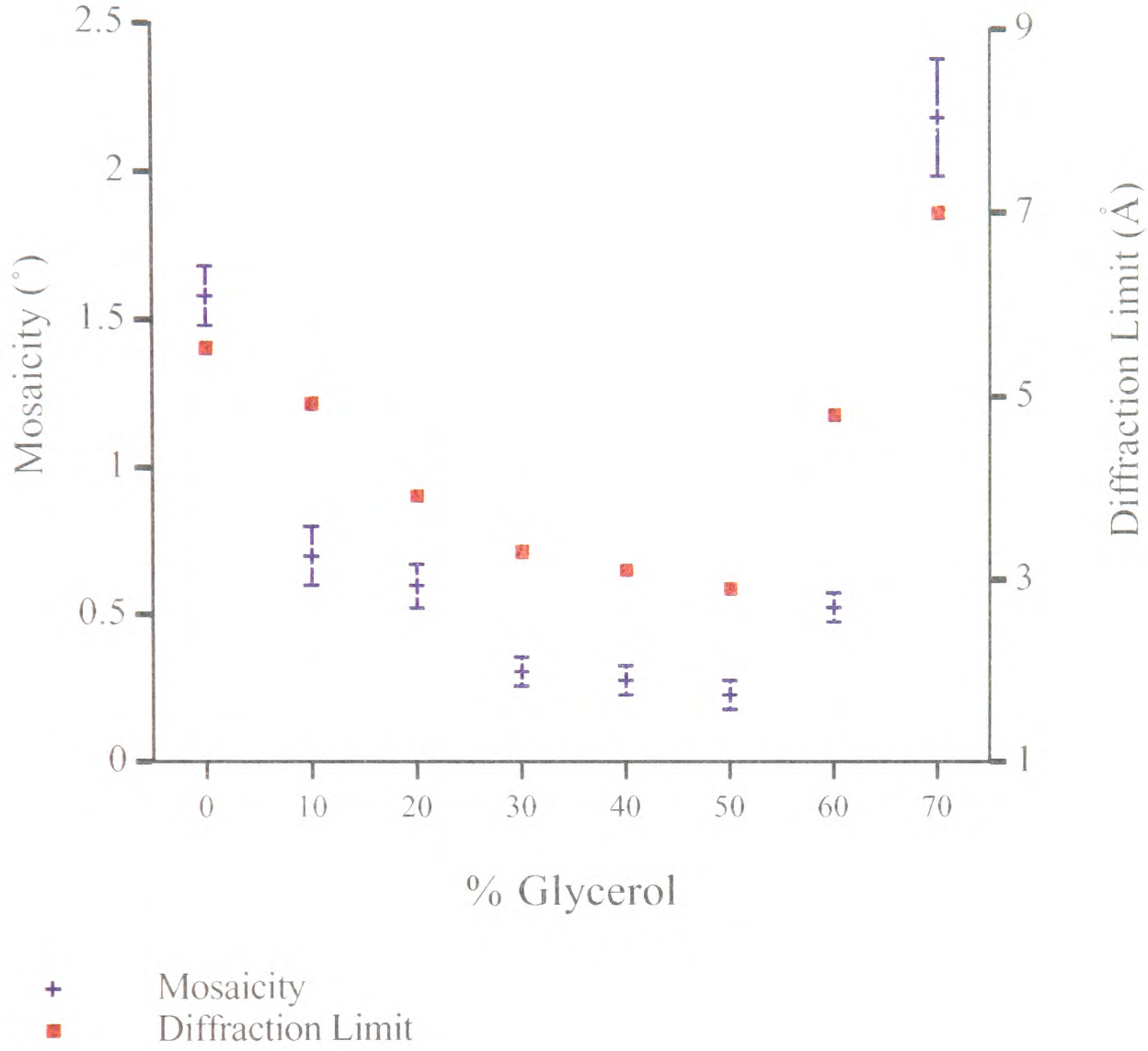

Figure 4.3. *Variation of mosaicity and diffraction limit of GPb crystals with percentage glycerol in the buffer.*

soaked in buffer without stirring showed the mosaicity to be similar to that with the stirred buffer. Another trial of a 20 minute soak in 60% glycerol with stirring showed no improvement over the 60% glycerol 5 minute soak. As the concentration of glycerol is increased bulk mother liquor is replaced by cryoprotectant which better tolerates the flash freezing. Perhaps as the concentration is raised above 50%, the viscosity of the buffer becomes so high that glycerol cannot diffuse into the crystal within a reasonable time, and upon flash freezing unreplaced water freezes as crystals thus causing high mosaicity. Sequential soaks for an overall time of 5 minutes in 10%, 30% and 50% glycerol gave indistinguishable results to the 50% alone soak,

but since it involved more crystal handling, was not pursued. A soak of 20 minutes in 50% glycerol gave results indistinguishable from the 5 minute soak, whereas a 2.5 hour soak made both the resolution and mosaicity worse. These tests showed that longer soaking times would not be beneficial.

The series of Figures 4.4a to 4.4d depict the progressive improvement in mosaicity and diffraction limit as the percentage glycerol in the cryoprotected buffer was increased from 0% to 50%. For comparison Figure 4.4e shows diffraction from a GPb crystal at room temperature. With the exception of a few elongated spots, Figure 4.4a (glycerol 0%, 2θ of 0°) shows virtually no diffraction from the protein. Both Figure 4.4b (10% glycerol, 2θ of 22°) and 4.4c (30% glycerol, 2θ of 22°) contain strong powder diffraction rings, showing as white at approximately 4.2Å and 3.3Å resolution, caused by ice formation in the buffer. However, at 30% glycerol there has been a significant improvement in the diffraction limit to around 3Å. Figure 4.4d (the optimum conditions of 50% glycerol with 2θ of 22°) shows superior diffraction from the GPb crystal and diffuse scattering from disordered water molecules in the cryoprotected buffer but none from ice.

At low glycerol concentrations (0% and 10%) the buffer solution did not freeze as a glass but instead produced an opaque solid containing ice (Figure 4.5a). Strong ice diffraction rings were observed on the images (Figure 4.4b). At 30% glycerol the ice diffraction became less apparent and was not detectable at all at 40% glycerol and above (Figure 4.4d). At these concentrations the buffer froze as a clear glass (Figure 4.5b). In order to ensure efficient data collection from a flash frozen crystal at a synchrotron source, it is vital to determine the conditions as well as possible beforehand. Using in-house resources, a suitable starting cryoprotectant for a particular protein buffer can be found without wasting any crystals. A poor cryoprotectant mixture will freeze to an opaque solid and give strong ice diffraction, whereas a potential cryoprotectant mixture will freeze to a clear glass and give no ice diffraction. However,

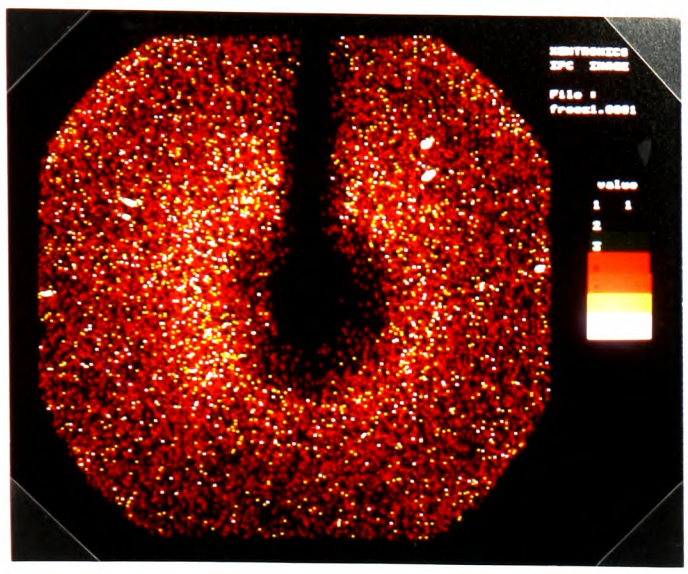

(a)

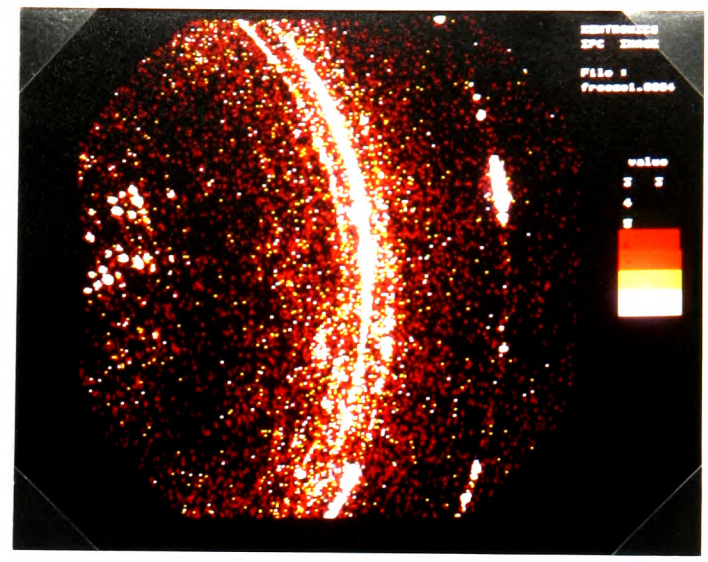

(b)

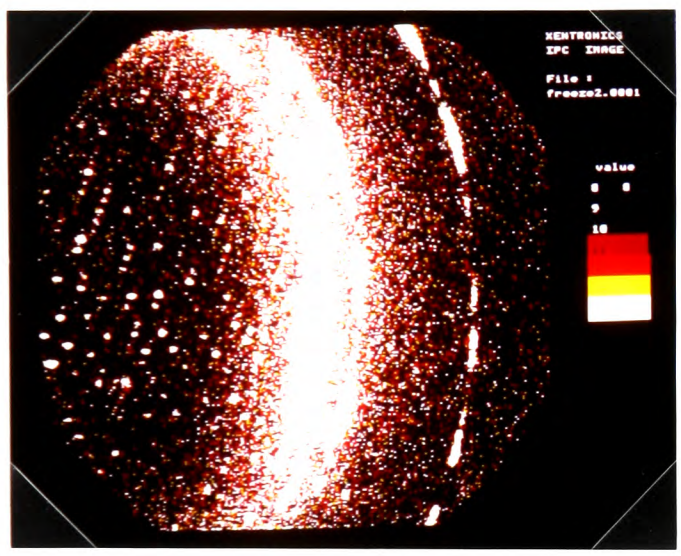

(c)

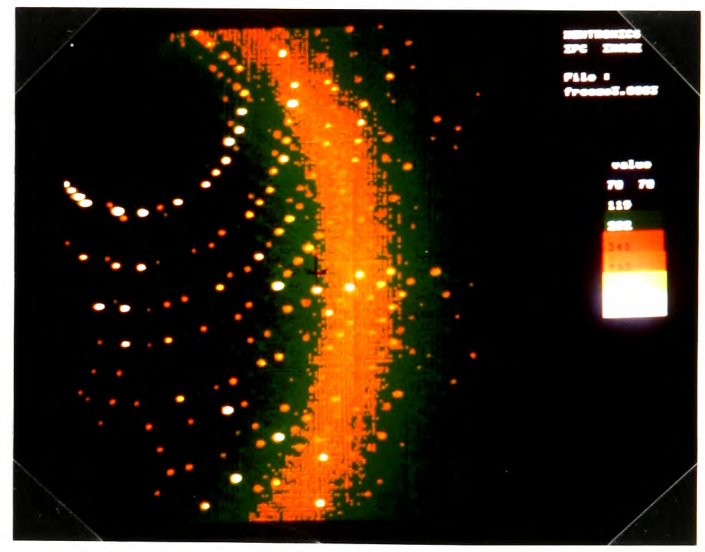

(d)

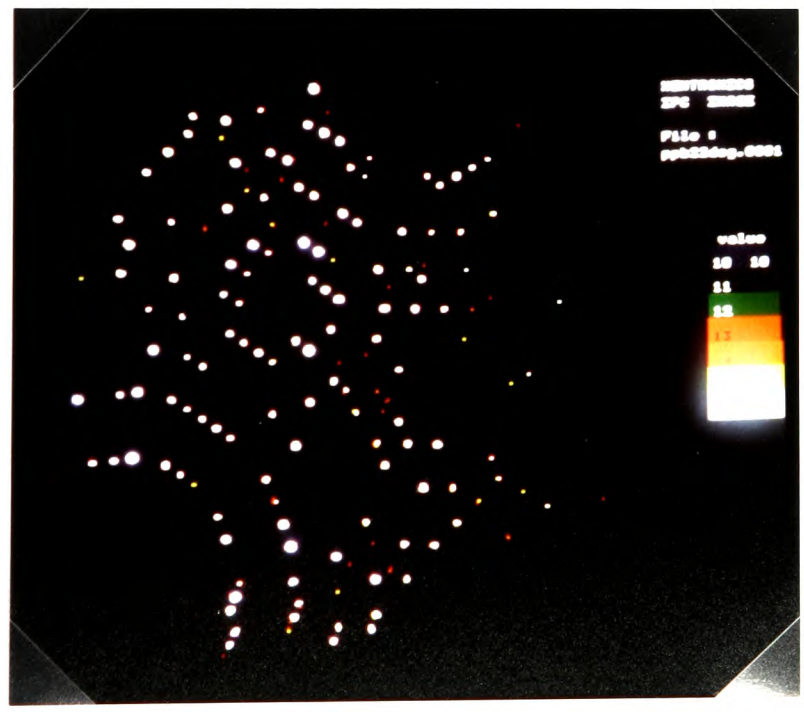

(e)

Figures 4.4a to 4.4e. *Comparison of X-ray diffraction from GPb crystals soaked in 0% (a), 10% (b), 30% (c) and 50% (d) glycerol cryoprotectant mixtures. For comparison Figure (e) is of diffraction from T state GPb at room temperature.*

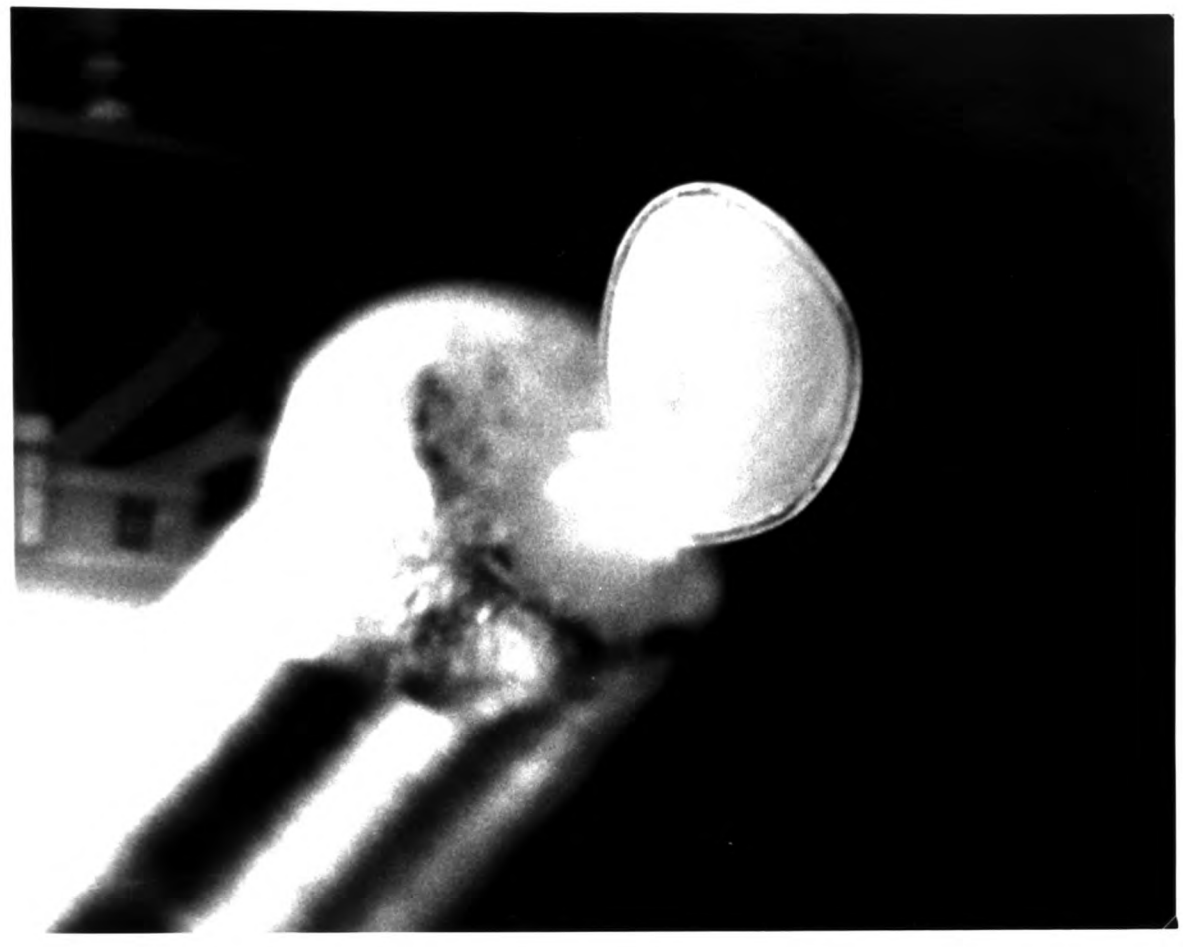

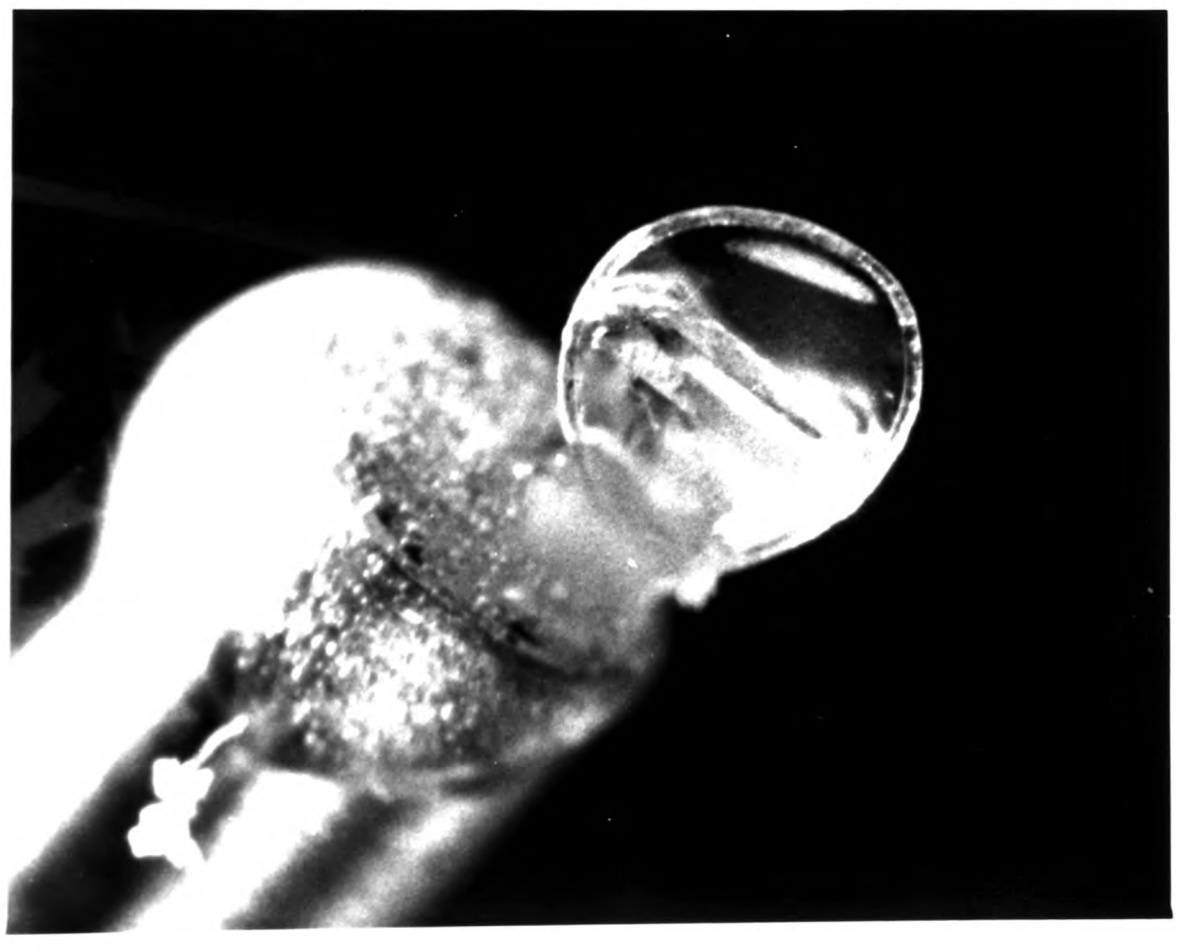

Figures 4.5a and 4.5b. *Photographs showing the visible differences between frozen cryoprotected buffer likely (top) and unlikely (bottom) to give rise to ice diffraction. The thin film of buffer is opaque in the top picture and is clear in the lower, except for a reflection obscuring the lower right portion of the loop.*

satisfying this condition will not necessarily give an ideal cryoprotectant: experiments using crystals are required to fine tune the concentration of cryoprotectant and soaking times to give the lowest mosaicity and highest resolution.

From these results, a 5 minute soak in 50% glycerol was the obvious choice for the cryoprotectant conditions, since both mosaicity and diffraction limit were optimised. The unit cell of frozen GPb crystals, soaked in 50% glycerol, was found to be a=b=126.7Å and c=115.6Å. This corresponds to an approximate 1.4% shrinkage on a and b and 0.6% on c, and an overall volume decrease of 3.4% compared to native crystals from which data were collected at room temperature.

4.3.2 Comparison of the Structure of GPb-glucose Complex at 100K and 293K

Table 4.1 shows the data collection and processing statistics for a frozen native crystal and the GPb-glucose complex crystal. As before, the data from the frozen crystals were weaker than that usual for data collected from T state GPb crystals at room temperature using in-house resources due to the smaller volume of the crystal used. The value of R_m, by resolution shells, increased rapidly beyond 2.8Å.

(i) Difference Fourier Map. The structure factor amplitudes for the glucose bound enzyme were anisotropically scaled to the native structure factors using the CCP4 program SCALEIT (CCP4, 1979). The native structure factors were taken from the final refinement of glycogen phosphorylase (Acharya, Stuart, Varvill & Johnson, 1991). A difference Fourier map, based upon (F_o-F_c) coefficients, was calculated and examined for features.

This initial Fourier map was noisy and contained poorly defined density for a glucose molecule

at the catalytic site. The map was difficult to interpret and for this reason, glucose was not included in the first stages of refinement. The small decrease in unit cell lengths upon flash freezing leads in turn to a much larger change in the structure factor amplitudes and phases. This would manifest itself as a 'noisy' Fourier difference map.

(ii) X-PLOR Refinement. The starting model for X-PLOR refinement of the frozen GPb-glucose complex was the refined room temperature GPb-glucose coordinates (Martin, Johnson & Withers, 1990). Refinement proceeded, using reflections between 8.0 and 2.8Å resolution, with 200 positional least-square cycles followed by 60 cycles of individual *B* factor refinement, reducing the *R* factor from 35.5% to 17.1%. At this stage a new Fourier difference map, using structure factor amplitudes calculated from the partially refined coordinates by the CCP4 program SFALL (CCP4, 1979), was examined. This map showed superior density for a glucose molecule and confirmed that glucose was indeed bound (Figure 4.6). On the basis of the map, a model of α-D-glucose was placed at the active site. The glucose model was generated using the program SYBYL (Tripos Associates). Further positional least-squares (90 cycles) and *B* factor (30 cycles) refinement gave a final *R* factor of 16.4%. New calculated structure factor amplitudes (F_c), from the refined structure, were scaled to the observed data (F_o). A Fourier difference map using ($2F_o$-F_c) coefficients was calculated and used with the refined GPb-glucose coordinates to examine the GPb-glucose complex structure.

The ($2F_o$-F_c) map, contained good density for the glucose molecule and, in general, the refined structure agreed very well with the map. Several loop regions of the protein chain known to be flexible (Sprang *et al.*, 1988; Acharya, Stuart, Varvill & Johnson, 1991) had high *B* factors and little density associated with them: residues 250 to 261, 314 to 325, the C-terminus tail 832 to 842 and the N-teminus tail 12 to 15.

There were two purposes to this experiment. One was to ensure the 100K and room temperature

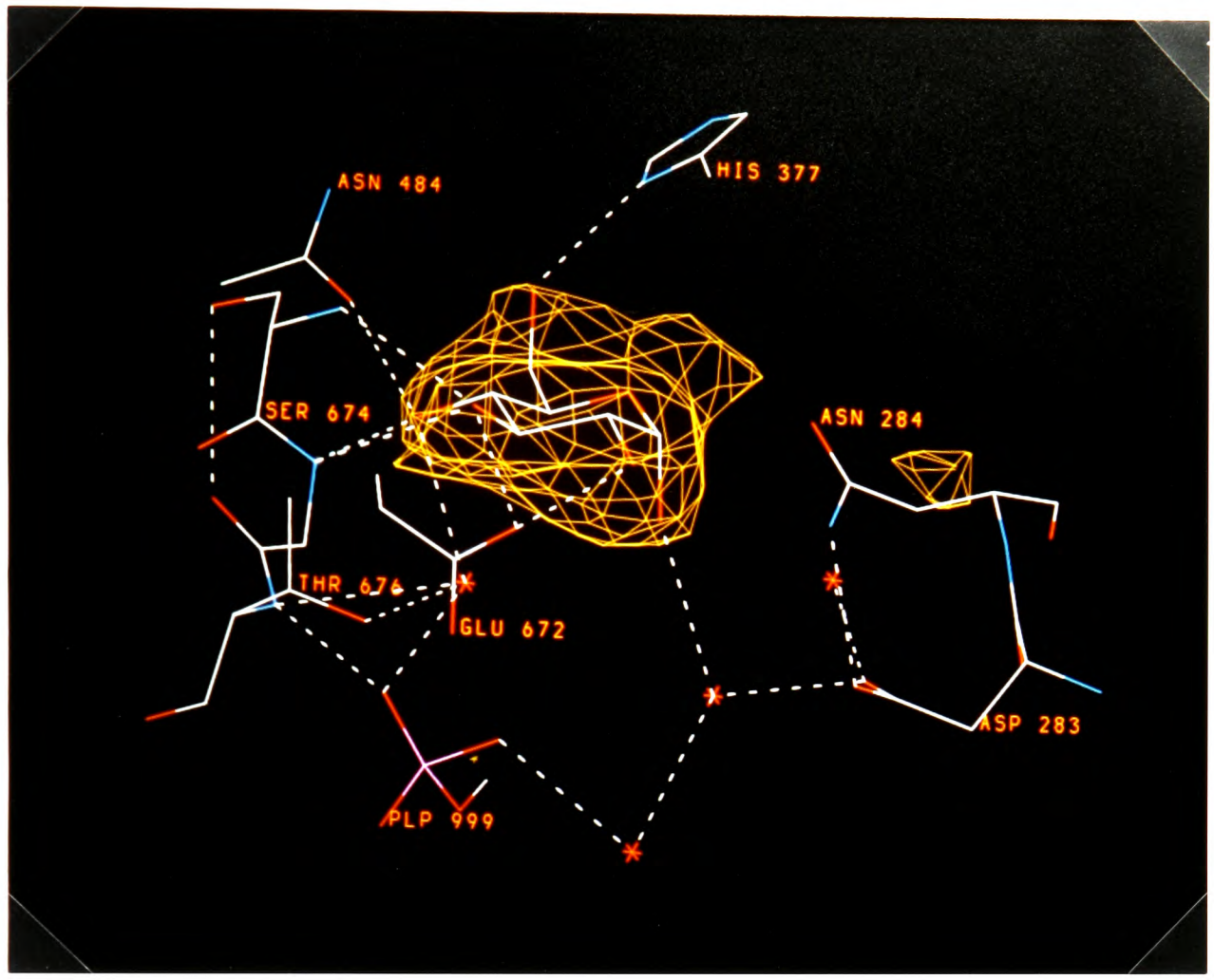

Figure 4.6. *The (F_o-F_c) Fourier map density at the active site for the partly refined frozen GPb-glucose model.*

structures were consistent with each other and that the shortening of unit cell lengths, on flash freezing, did not result from a significant change in secondary and tertiary structure. The second was to check that the conditions used to prepare T state GPb crystals for flash freezing allowed a ligand to bind at the catalytic site, since there was a possibility of competitive binding between glycerol and a ligand of interest. In both aspects, that of structural similarity and ligand binding, the experiment was successful. The protein structure changed little, with an overall r.m.s. deviation in coordinates of 0.54Å between the room temperature and frozen GPb-glucose complexes reflecting the entire structure compacting rather than any modifications in the protein topology. The r.m.s. deviation within 10Å of the catalytic site was 0.46Å and between the glucose molecules themselves, 0.64Å. The estimated error in coordinates (from a Luzatti plot) was 0.20-0.25Å. The structure had good stereochemistry as indicated by the

Ligand Atom	Protein Atom	Hydrogen Bond Contact (Å)	
		100K	Room Temperature[a]
O1	WAT OH8 872	3.0	3.0
O2	ND2 Asn 284	(3.6)	3.2
	OH Tyr 573	3.2	(3.4)
	OE1 Glu 672	2.8	2.9
	WAT OH7 890	(3.5)	3.0
O3	OE1 Glu 672	2.9	2.9
	N Ala 673	(3.4)	(3.4)
	N Ser 674	2.9	3.0
	N Gly 675	3.0	3.0
O4	OD1 Asn 484	3.3	3.1
	N Gly 675	3.0	2.8
	WAT OH1 897	2.9	2.6
O6	ND1 His 377	2.6	2.7
	OD1 Asn 484	3.2	3.0

[a]Martin, Johnson & Withers, 1990.

Table 4.2. *Hydrogen bond contacts between glucose and the catalytic site residues of T state glycogen phosphorylase b. Distances in brackets indicate a weak contact. In general the hydrogen bond network is consistent between the 100K and room temperature structures, with some variation in the length of the contact.*

r.m.s. deviation in bonds and angles of 0.018Å and 3.49° respectively. Within the accuaracy of the experimental data, the pattern of hydrogen bonding at the active site between protein and glucose was also maintained (Table 4.2).

4.4 CONCLUSIONS

4.4.1 Effect of Glycerol Concentration upon Crystal Mosaicity and Diffraction Limit

The freezing experiments with glycerol cryoprotectant on GPb crystals show that as the glycerol concentration is increased there is a well defined minimum in the mosaic spread and maximum in the diffraction limit. Beyond this concentration, both the mosaicity and the diffraction limit worsen again. These results are relevant to the search for cryoprotectant conditions for freezing any protein crystals, in that they show the importance of a systematic approach to ensure the best possible data quality. The results demonstrate that by observing how a buffer with cryoprotectant freezes, opaque or clear, a starting point for cryoprotectant conditions can be determined before using crystals.

4.4.2 GPb-Glucose Complex Structure at 100K

The GPb-glucose binding experiment has shown that it is possible to bind glucose at the active site under the flash freezing conditions and maintain structural consistency between room temperature and 100K. The work has confirmed the viability of using flash freezing as a technique to study GPb complexes, and is extended to a GPb-nojirimycin tetrazole-phosphate complex in Chapter 5.

5.1 INTRODUCTION

5.1.1 Overview

At a resolution of 2.4Å the electron density of the phosphate peak is almost spherical with just slight lobes to indicate the positions of the oxygens. Hence assumptions drawn about the phosphate orientation in the T state GPb-tetrazole-phosphate complex are not certain (Chapter 2). The only additional guide is the interpretation of the X-PLOR refined structure in terms of the possible hydrogen bonds. The resultant orientation, though, can be interpreted favourably and is consistent with kinetic evidence (which indicates the importance of O-2 of the pyranose ring which forms a hydrogen bond to the phosphate and the direct interaction of the phosphate with the PLP 5'-phosphate).

A high, better than 1.8Å, resolution structure would provide direct evidence for the relative orientation of the active site residues and the phosphate. The electrophilic mechanism (Madsen & Withers, 1986) suggests that at the transition state the PLP 5'-phosphate becomes distorted and is electrophilic. At high resolution this distortion could possibly be observed in the presence of nojirimycin tetrazole and phosphate, and lend support to the electrophilic mechanism. Such a conformation of the PLP phosphate would, however, be high in energy and unlikely to be crystallographically observed.

The work reported in this Chapter combines the study of nojirimycin tetrazole with the flash freezing of T state phosphorylase to provide a detailed picture of the active site in the presence of a transition state analogue. Two high resolution data sets were collected; one from the GPb-tetrazole-phosphate complex to 1.7Å and one from native T state crystals to 1.5Å resolution. This represents a considerable advance over the original room temperature native data set which contained data to only 1.9Å resolution.

5.2 EXPERIMENTAL METHODS

5.2.1 Data Collection

T state crystals of glycogen phosphorylase (space group $P4_32_12$ and unit cell parameters a=b=128.5Å and c=116.3Å) were grown as described previously (Chapter 2, Section 2.2.2) by Dr Nikos Oikonomakos at the National Hellenic Foundation in Greece.

Prior to data collection, crystals (with a maximum size of 0.3mm on the longest dimension) were soaked for 30 minutes in a BES buffer containing 100mM nojirimycin tetrazole and 50mM sodium dihydrogen phosphate (10mM BES, 0.1mM EDTA, 0.02% sodium azide at pH 6.7). After the preliminary soak, crystals were trnasferred to a BES buffer containing 50% *v/v* glycerol (with an overall concentration of 10mM BES, 0.1mM EDTA and 0.02% sodium azide, pH 6.7) for a further 5 minutes. Crystals for collection of the high resolution native data set were only subjected to the second 5 minute soak in 50% glycerol.

After the soak in the glycerol buffer was completed, crystals were flash frozen using the technique described in Chapter 4 Section 4.2.1. For the GPb-tetrazole-phosphate complex data were collected from a single frozen crystal of T state GPb. Due to time restrictions at the synchrotron, two separate data collections were necessary for the native data set and thus two crystals were used. Data were collected using a 30cm diameter MAR Research image plate system which was mounted on the wiggler beam line PX9.6 at the SRS Daresbury. The station slits were all set at 0.2mm and the X-ray wavelength used was 0.895Å. The data collection parameters are shown in Table 5.1. Since the detector was set close to the crystal the oscillation angles (0.50° and 0.65°) were small to avoid spots overlapping at the edge of the detector. During data collection, the synchrotron storage ring was operated at an energy of 2.0GeV and at a current of between 280mA and 162mA.

	Native T State		GPb-Tetrazole-Phosphate Complex
	Crystal 1	Crystal 2	
Crystal-Detector Distance (cm)	20.0	25.0	25.0
Maximum Resolution (Å)	1.4	1.7	1.7
Oscillation Angle (°)	0.50	0.65	0.65
Exposure Time (s)	180	100	100
Angular Range Collected (°)	22.5	51.1	88.05
Sigma Cutoff Applied During Scaling	0	1	0

Table 5.1. *Data collection parameters for the two high resolution data sets.*

The data processing program DENZO (Otwinowski, 1993) was used to determine the crystal orientation. Integration was performed also using DENZO and inter-frame scaling, partial reflection summation, data reduction and post-refinement were all completed using SCALEPACK (Otwinowski, 1993) to give a unique set of reflections.

5.3 RESULTS AND DISCUSSION

5.3.1 Data Collection

The statistics for the two data collections are shown in Table 5.2. Since little time was available at the synchrotron the exposure times for the GPb-tetrazole-phosphate complex were shorter than was desirable for measuring weak data with reasonable statistical accuracy. The unit cells of all of the frozen crystals were consistent with that found earlier using in-house resources (a=b=126.7Å and c=115.6Å).

5.3.2 Fourier Difference Maps

Fourier difference maps were calculated using SIGMAA weighted (F_o-F_c) coefficients (Read, 1986) where the phases and F_c were calculated from the native room temperature T state structure (Acharya, Stuart, Varvill & Johnson, 1991). The maps were both noisy and the GPb-tetrazole-phosphate map contained no density suggesting tetrazole or phosphate to be bound at the active site. However, bearing in mind the unit cell change between room temperature and frozen GPb crystals (volume change of 3.4%), the phases for the map calculation could have had significant errors. These could be enough to result in the noise in the initial difference maps and the apparent lack of bound tetrazole and phosphate. The lack of isomorphism was indicated by inadequate scaling of the data from the frozen crystals to the native room temperature data, which resulted in high mean fractional isomorphous differences.

5.3.3 X-PLOR Refinement

Both structures were refined making use of the Engh and Huber parameters for X-PLOR (Engh & Huber, 1991). The parameter and topology files for the phosphate and tetrazole were used

		Native T State GPb	GPb-Tetrazole-Phosphate
Number of Reflections	Unique	125898	88768
	Measured	466518	304397
Maximum Resolution (Å)		1.50	1.70
Completeness of Data (%)		84 (15-1.5Å) 71 (1.55-1.50Å)	86 (20-1.7Å) 67 (1.76-1.70Å)
Unit Cell After Denzo Post-Refinement (Å)		a=b=126.5 c=115.5	a=b=126.5 c=115.6
R_m (I) (%)		7.9 (15-1.50Å) 22.2 (1.55-1.50Å)	4.9(20-1.7Å) 22.5 (1.70-1.76Å)
Average I / σI		16.4	18.8

Table 5.2. *The statistics of data collection for the two high resolution data sets.*

as described in Chapter 2, Section 2.3.3. In both refinement protocols the X-PLOR electrostatic energy term was switched off.

(i) Native T State GPb. The initial model for this refinement was the native room temperature T state GPb coordinates (Acharya, Stuart, Varvill & Johnson, 1991) comprising residues 19 to 842 and including 633 water molecules. The refinement protocol led with least squares conjugate gradient refinement (225 cycles) and restrained individual B factor refinement (40 cycles, target standard deviations of 1.5Å^2 for 1-2 atom pairs and 2.0Å^2 for angle atom pairs). A simulated annealing (SA) procedure followed by further positional and unrestrained individual B factor refinement completed the first stage. This gave a large drop in the R factor from a starting value of 46.2% (R_{free} 46.2%) to 24.9% (R_{free} 32.7%). For SA the structure was heated to 3000K and gradually cooled to 300K with a timestep of 5fs. At this stage new Fourier difference maps were calculated with (F_o-F_c) and ($2F_o$-F_c) SIGMAA weighted coefficients. Using PEAKMAX (CCP4, 1979) the (F_o-F_c) Fourier map was searched for peaks over 3 sigma

in height. Water molecules were assigned to these peaks using WATPEAK (CCP4, 1979) and the waters manually screened for sensible positioning, hydrogen bonds and difference density shape. A total of 232 new water molecules were added, giving 865 waters overall in the structure. Numerous small manual adjustments were made to the enyzme model using FRODO (Jones, 1978, 1985). Notable changes include a peptide flip at Leu 117 and a flip of the tryptophan ring at Trp 797. Some multiple conformations of amino acid side chains were apparent in the electron density maps, for instance, Ile 486, Val 565 and Ile 710. Virtually no density to indicate residue positions for the N-terminus before residue 13 and for the C-terminus after residue 835 existed in the Fourier difference maps.

The refinement continued with positional (100 cycles) and unrestrained individual *B* factor (60 cycles) refinement. New Fourier difference maps were calculated and another 111 water molecules positioned with 13 original waters deleted (final total of 963 water molecules). A further check of the enzyme against the Fourier maps was carried out and indicated many small changes to side chain conformations but also revealed Ile 380 to be a leucine (Figure 5.1). This change is consistent with the original sequence (Titani *et al.*, 1977). For the original 1991 structure, residue 380 was built as an isoleucine since that residue was more consistent with the Fourier difference maps at that time. At the active site of the native enzyme structure at 100K binding of a molecule of glycerol, the cryoprotectant, was evident. Earlier in the refinement water molecules had been fitted at the glycerol site, but it was clear from the Fourier maps that glycerol was in fact bound. Glycerol was fitted to the density and included in the remainder of the protocol. Also at this point, a refinement stage was included to aid in rebuilding the N-terminus. Atoms within a 5Å radius of CA Ser 14 were deleted and those between 5Å and 7Å radius were fixed during refinement (simulated annealing, where the structure was heated to 800K, followed by 50 cycles of positional refinement). Subsequently an omit Fourier map was calculated and used to substantially rebuild the N-terminus residues (13 to 16). Residues 10 to 12 were deleted from the model since they had high *B* factors and

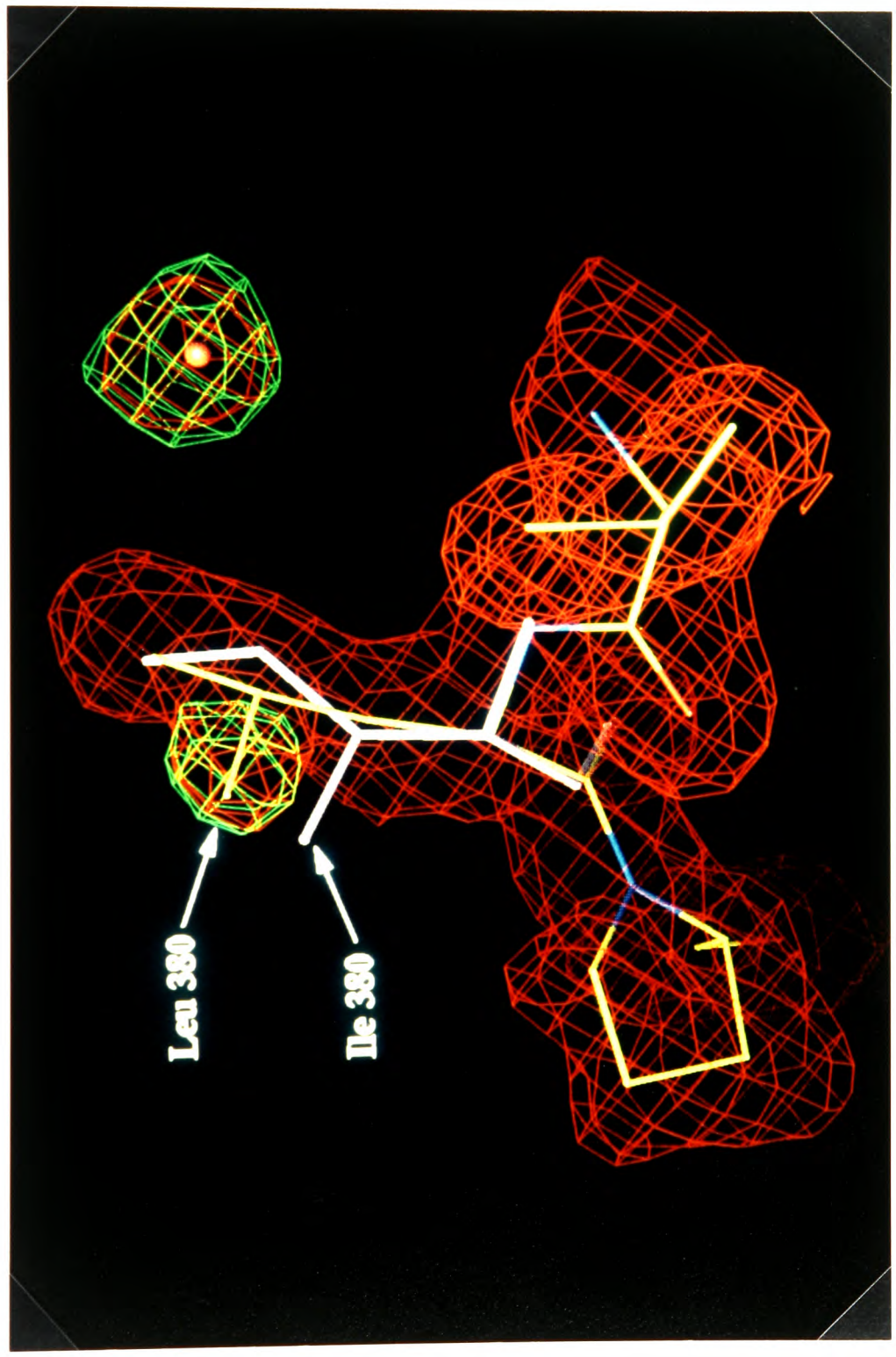

Figure 5.1. *The intermediate (F_o-F_c) Fourier difference map (green) used to remodel Ile 380 to Leu 380 with the final ($2F_o$-F_c) map in red.*

no supportive electron density.

The refinement concluded with positional (270 cycles) and unrestrained individual *B* factor (60 cycles) refinement to give an *R* factor of 22.8% (R_{free} 29.6%). The *R* factor over all reflections from 5.0Å to 1.94Å was 20.0% (R_{free} 28.0%). Due to time restrictions the refinement was left at this stage but future work will hopefully produce a final model of native T state GPb at a resolution of 1.5Å. The multiple conformations of some residues that could be observed in the later Fourier maps will be included in this further refinement.

(ii) T State GPb-Tetrazole-Phosphate Complex. The starting model for refinement was the 2.4Å resolution GPb-glucose complex structure of Martin, Johnson and Withers (1990) comprising residues 12 to 841. This model (without glucose) was used, rather than the refined GPb-tetrazole-phosphate model from Chapter 2, in order not to bias the refinement. Initially no models of phosphate or nojirimycin tetrazole were positioned in the structure since the density of the initial map was so poor. However, 633 water molecules from the glucose structure were included.

The refinement of this complex commenced with least squares conjugate gradient refinement (225 cycles, tolerance 0.05Å) followed by individual *B* factor refinement (40 cycles) with target standard deviations of 1.5 and 2.0Å^2 for bonded atoms and atoms bound to the same atom respectively. Over these stages the *R* factor dropped from an initial value of 42.1% (R_{free} 42.6%) to 27.9% (R_{free} 32.3%). Simulated annealing, heating the structure to 3000K and cooling to 300K with a timestep of 5fs, and positional refinement (200 cycles) saw the *R* factor further reduced to 24.0% (R_{free} 30.5%). At this stage new Fourier difference maps were calculated with (F_o-F_c) and ($2F_o$-F_c) SIGMAA weighted coefficients. The Fourier maps were searched for peaks and waters assigned to the peaks using the technique described above. In total 144 new waters were added to the model giving an overall total of 777 water molecules. Several side

chains of the enzyme model were adjusted and, without reference to the 2.4Å resolution room temperature structure, models of phosphate and nojirimycin tetrazole added. The difference density was sufficiently well resolved to indicate at least partial occupancy by the two ligands at the active site. The Fourier maps contained very little density to suggest the side chain of Arg 569 to be coordinating the phosphate, consistent with less than 100% occupancy by the phosphate ion. The 280s loop of residues was, however, not well supported in the Fourier map suggesting that the loop had moved or become more mobile. Little density was present to indicate a new location for the 280s loop. Consequently Arg 569 and the 280s loop were not conformationally adjusted. Similar features were seen in the Fourier maps of the room temperature T state GPb-tetrazole-phosphate complex where phosphate was at a concentration of 10mM in the soak buffer (Chapter 2).

The refinement continued with a round of positional (70 cycles), individual *B* factor refinement (this time with no target standard deviations) and another simulated annealing calculation. This gave a final *R* factor of 21.0% (R_{free} 31.0%).

5.3.4 X-PLOR Refined Structures

The statistics for refinement of the two structures are shown in Table 5.3. Both refined models fit the Fourier maps well (for example Figure 5.2), with the exception of regions known to be flexible (see later for details).

(i) GPb-Tetrazole-Phosphate Complex. Though the ($2F_o$-F_c) density of the Fourier map suggests partial occupancy of the active site by nojirimycin tetrazole and phosphate, the density is sufficiently well resolved to indicate the phosphate ion orientation (Figure 5.3). A comparison with the equivalent room temperature complex, with data to 2.4Å resolution, shows the phosphate to be in the same orientation in this higher resolution structure (1.7Å).

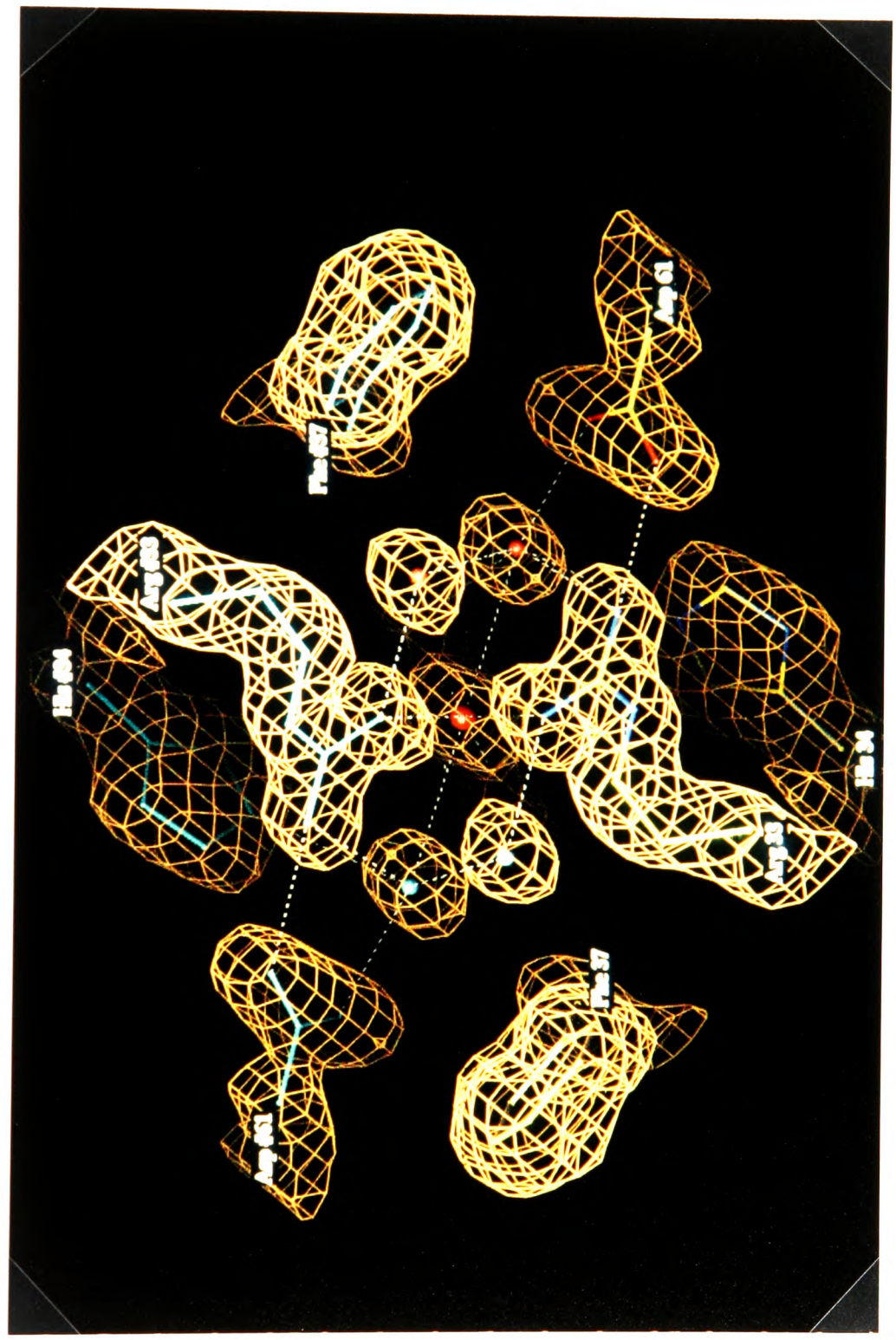

Figure 5.2. *The ($2F_o$-F_c) Fourier map for the native T state phosphorylase structure at the crystallographic subunit-subunit contact.*

		Native T State GPb	GPb-Tetrazole-Phosphate
Total Number of	Protein Atoms	6755	6755
	Ligand Atoms	6	19
	Water Molecules	963	777
No of Reflections used in Refinement (I>0)		119711	84349
Resolution Range		5.0-1.5	5.0-1.7
R Factor	Initial (%) (R_{free})	46.2 (46.2)	42.1 (42.6)
	Final (%) (R_{free})	22.8 (29.6)	21.0 (31.0)
RMS Deviation	Bonds (Å)	0.011	0.008
	Angles (°)	1.6	1.4
	Dihedrals (°)	23	23
	Impropers (°)	1.5	1.3

Table 5.3. *The refinement statistics and parameters of the two high resolution structures of T state GPb.*

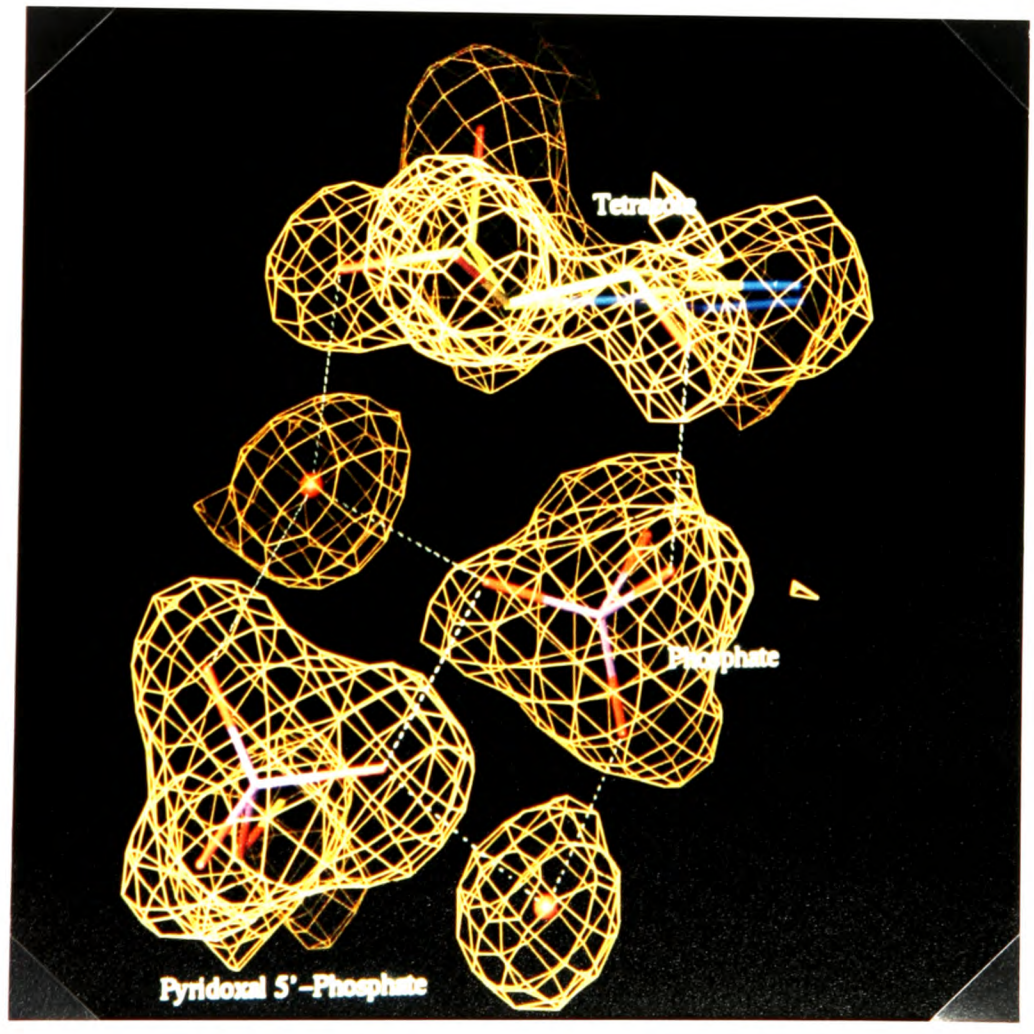

Figure 5.3. *The final ($2F_o$-F_c) Fourier difference map at the active site for the low temperature GPb-tetrazole-phosphate complex showing the lobes for the phosphate electron density.*

Disregarding the positions of Arg 569 and the 280s loop, which were not remodelled from their native positions in the higher resolution structure, the phosphate ion makes similar contacts in both the room temperature and flash-frozen models. The hydrogen bond contacts are shown in Figure 5.4 and listed in Table 5.4. The length of the comtacts do vary slightly but within the coordinate experimental error of the 2.4Å structure (0.20-0.30Å). The estimated error of the 1.7Å structure is 0.13Å (SIGMAA plot). The results from this structure at 1.7Å resolution confirm the orientation of the phosphate deduced from the earlier results and refinement (Chapter 2 and 3).

(ii) Native T State GPb. The native structure, with a glycerol molecule bound at the active site, perhaps offers an explanation for the partial occupancy by tetrazole and phosphate observed in the structure discussed above. Given that 50% of the cryoprotectant buffer is glycerol and thus glycerol is in high concentration, it is possible that some glycerol may bind in a competitive manner at the active site, even though tetrazole has a low K_i in the presence of phosphate. The glycerol molecule does bind in such a way that its three oxygen atoms are located in the same postions as O-3, O-4 and O-6 of the tetrazole pyranose ring (Figure 5.5). The glycerol oxygens make similar contacts to the protein as the equivalent tetrazole atoms (Table 5.6).

At such a high resolution (1.5Å), the *B* factors associated with atoms become meaningful. Residues with high *B* factors reflect the relatively greater mobility of those residues with respect to the remainder of the enzyme. In this structure several regions of the protein have main chain B factors of over 50Å^2, a total of 55 residues, and are not well ordered (Figure 5.6): 14, 15, 18, 21, 23, 209-212, 250-260, 284, 314-325, 423, 432-435, 529, 547, 549-552, 554, 556, 834, 836-842. These are similar to those reported as being flexible (66 residues) in the original 1991 structure (Acharya, Stuart, Varvill & Johnson, 1991) and suggest that the disorder of these residues is static rather than dynamic. The residues adopt many different conformations

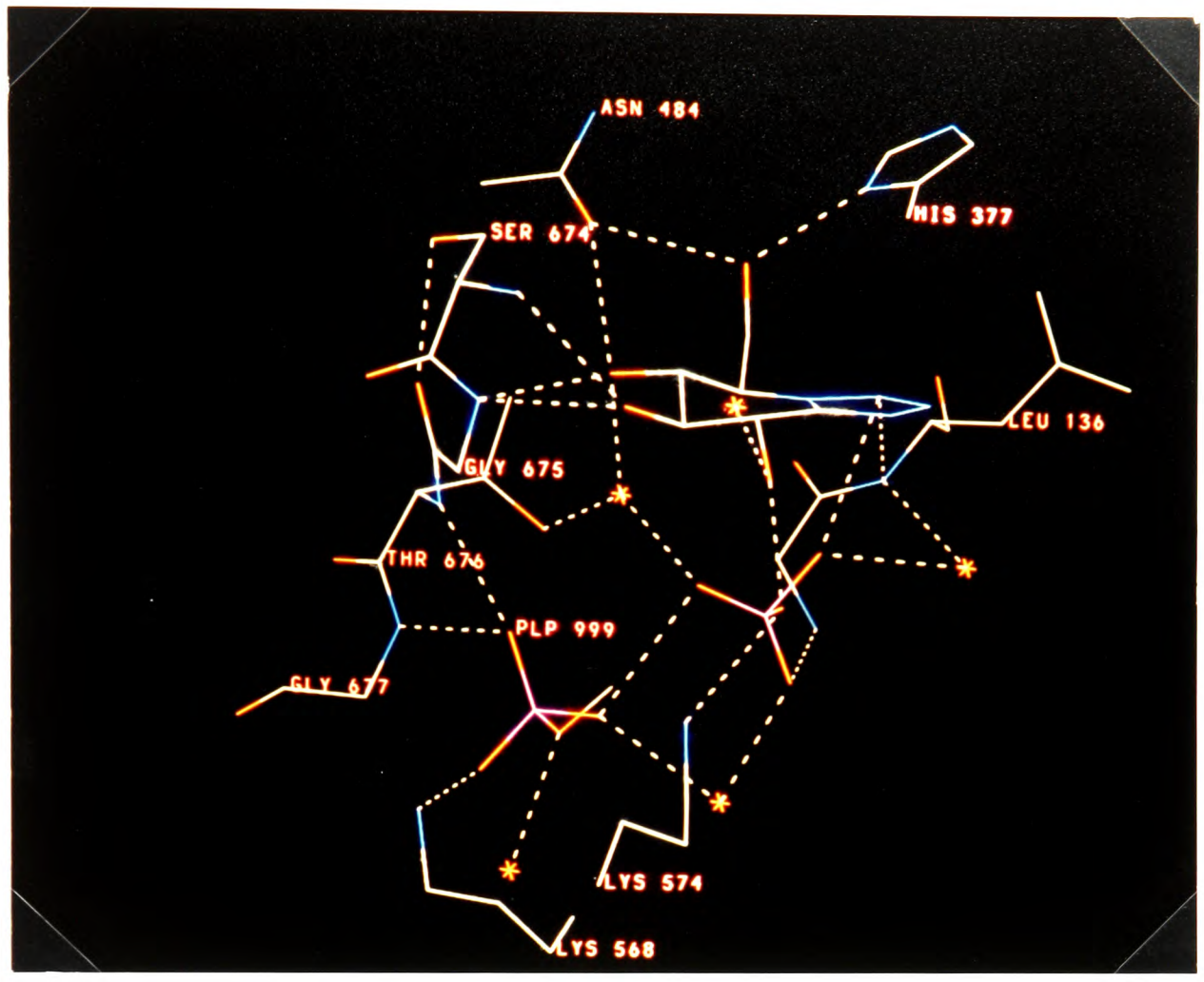

Figure 5.4. *The hydrogen bond contacts between phosphate, tetrazole and enzyme at the active site of phosphorylase (1.7Å low temperature structure).*

Phosphate Atom	Protein Atom	Length of Contact (Å)
OP-1	N-1 Tetrazole[a]	2.8
	WAT 885	2.8
OP-2	NZ Lys 574	3.2
	O-2 Tetrazole	2.7
OP-3	OP2 PLP 999	3.0
	WAT 895	2.7
OP-4	N Gly 135	2.7
	WAT 877	2.5

[a]Contact represents an electrostatic contact.

Table 5.4. *Hydrogen bond contacts from the phosphate to tetrazole and protein (ignoring contacts to the 280s loop).*

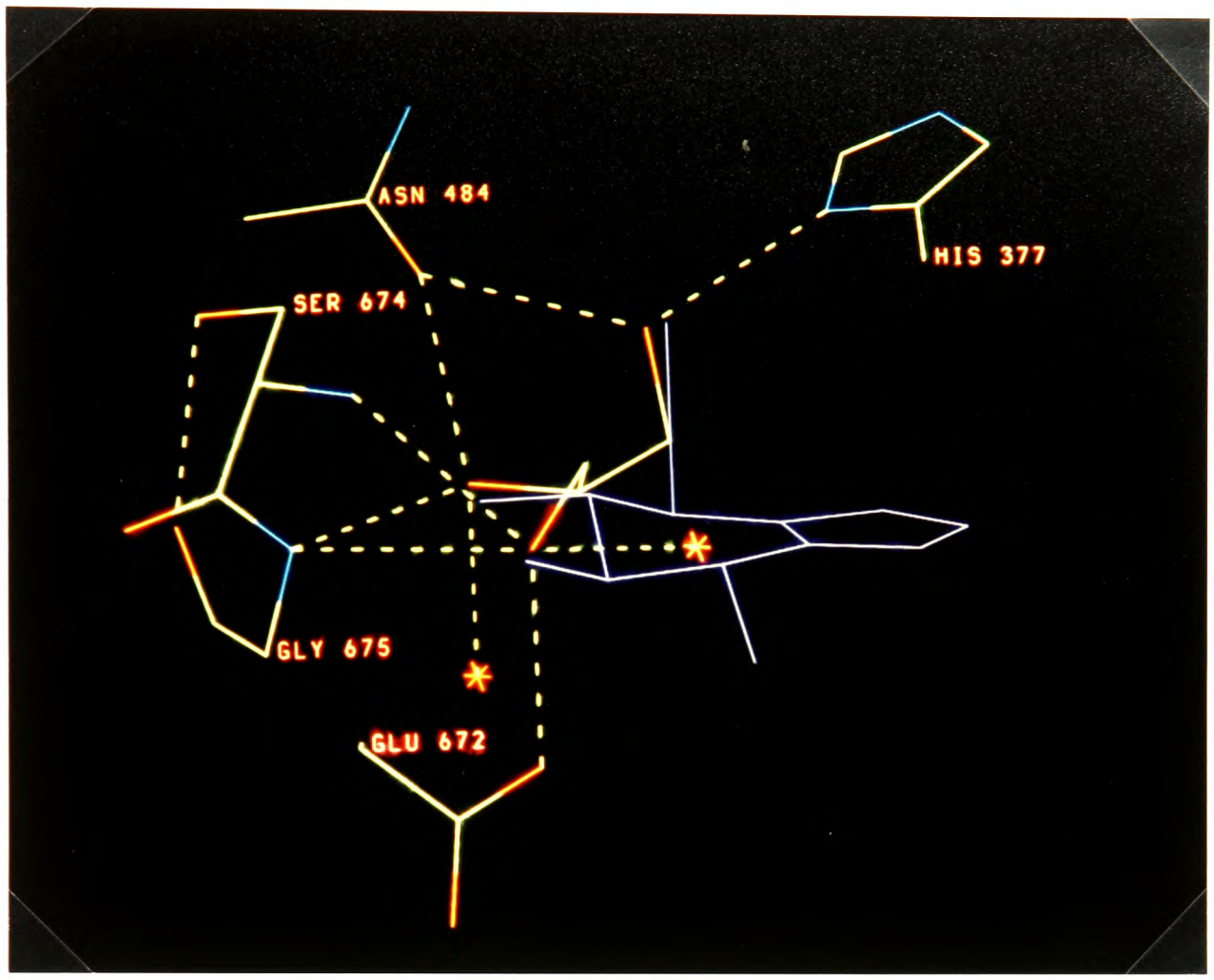

Figure 5.5. *Comparison between the glycerol site (1.5Å low temperature native structure) and that of tetrazole (1.7Å low temperature GPb-tetrazole-phosphate complex, blue)*

Glycerol (Tetrazole) Atom	Protein Atom	Length of Contact (Å)	
		Glycerol	Nojirimycin Tetrazole
O-1 (O-3)	OE1 Glu 672	2.9	2.9
	N Ser 674	3.1	2.9
	N Gly 675	3.1	3.1
	WAT 906	2.9	-
O-2 (O-4)	OD1 Asn 484	2.9	3.3
	N Gly 675	2.9	2.7
	WAT 895	2.7	2.7
O-3 (O-6)	ND1 His 377	2.7	2.6
	OD1 Asn 484	2.9	3.1

Table 5.5. Comparison of the hydrogen bond contacts made by glycerol (from the native 1.5Å structure) with those made by equivalent atoms of nojirimycin tetrazole (from the 1.7Å complex structure). A dash indicates no contact. The estimated error in coordinates for the 1.5Å data is 0.13Å (SIGMAA plot).

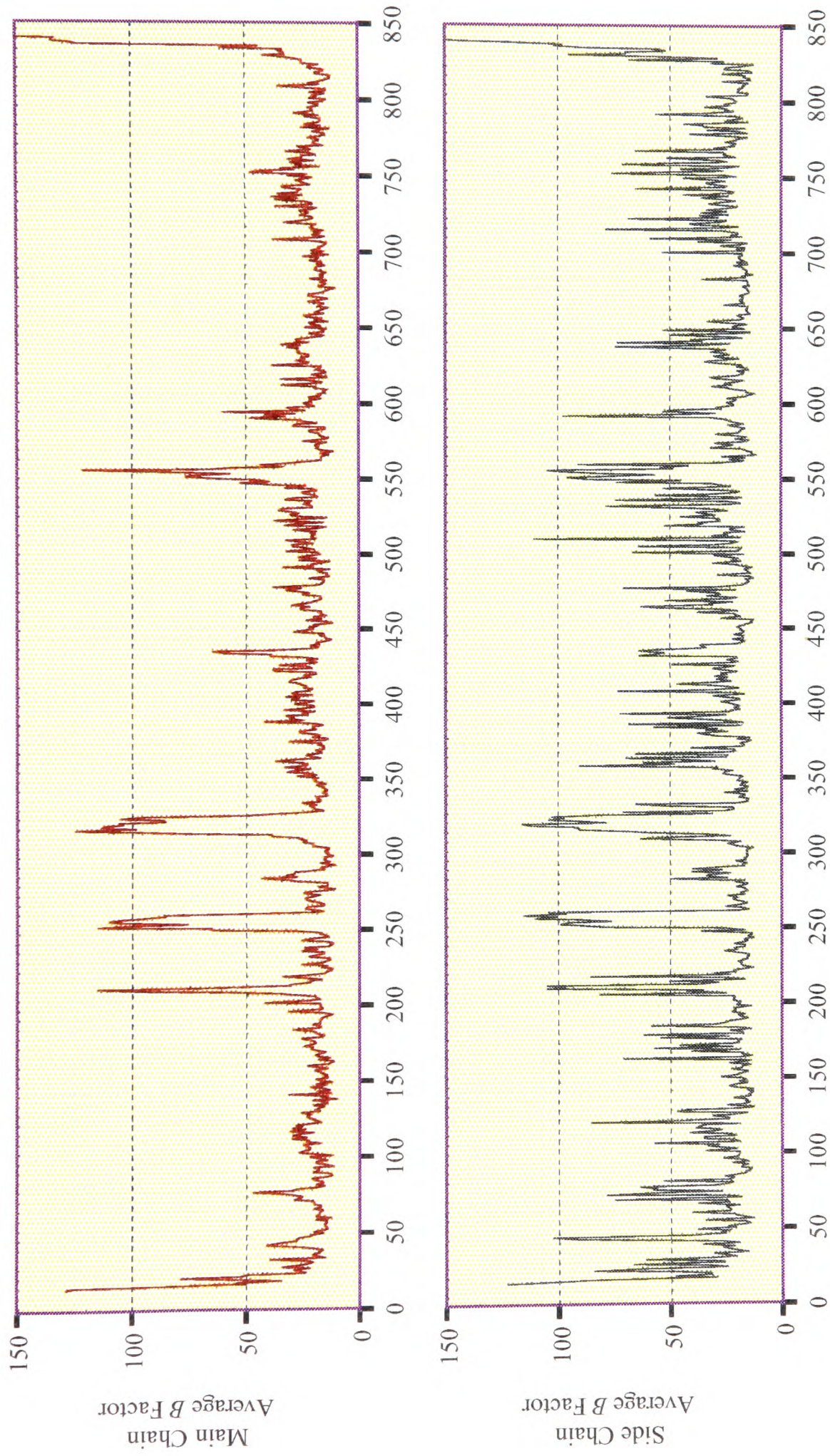

Figure 5.6. *Graphs showing the average B factors by residue number for the main chain atoms (top) and side chain atoms (lower) for the 1.5Å native T state structure.*

rather than, say, two or three, which may appear as multiple conformations in the Fourier maps. The average *B* factor for all CA is 25Å^2, for all main chain atoms is 26Å^2 and for all atoms (excluding water molecules) is 29Å^2.

Additional density was observed in the Fourier difference maps for the N-terminus residues. In the original native structure the final model consisted of residues 19 to 842. For this work residues 13 to 18 were added, using as a model the N-terminus residues of the GPb-glucose coordinates of Martin, Johnson and Withers (1990). Residues 13 to 16 were rebuilt, resulting in a substantial movement of Ser 14, the phosphorylation site for activation of GPb to GPa, away from its original location. The side chain atom OG moved by over 6Å and the main chain CA atom by 4Å from the location observed for the room temperature GPb-glucose complex of Martin, Johnson and Withers (1990). The new locations of residues 13 to 16 are supported by electron density, though the *B* factors are high. The side chain oxygen of Ser 14 makes a contact to WAT 860 (2.8Å) and is on the enzyme surface. The helix containing Glu 501 and Glu 505 is not far away, suggesting that Ser 14 may move on phosphorylation away from these acidic side chains.

Figure 5.7 shows a Ramachandran plot of the 1.5Å GPb model. Nearly 90% of non-glycine and non-proline residues are placed in the most favoured regions. Of the remaining 10 residues, 4 are supported by electron density (Tyr 203, Asp 339, Thr 466 and Ser 674) and the rest are contained in flexible loop regions of the chain.

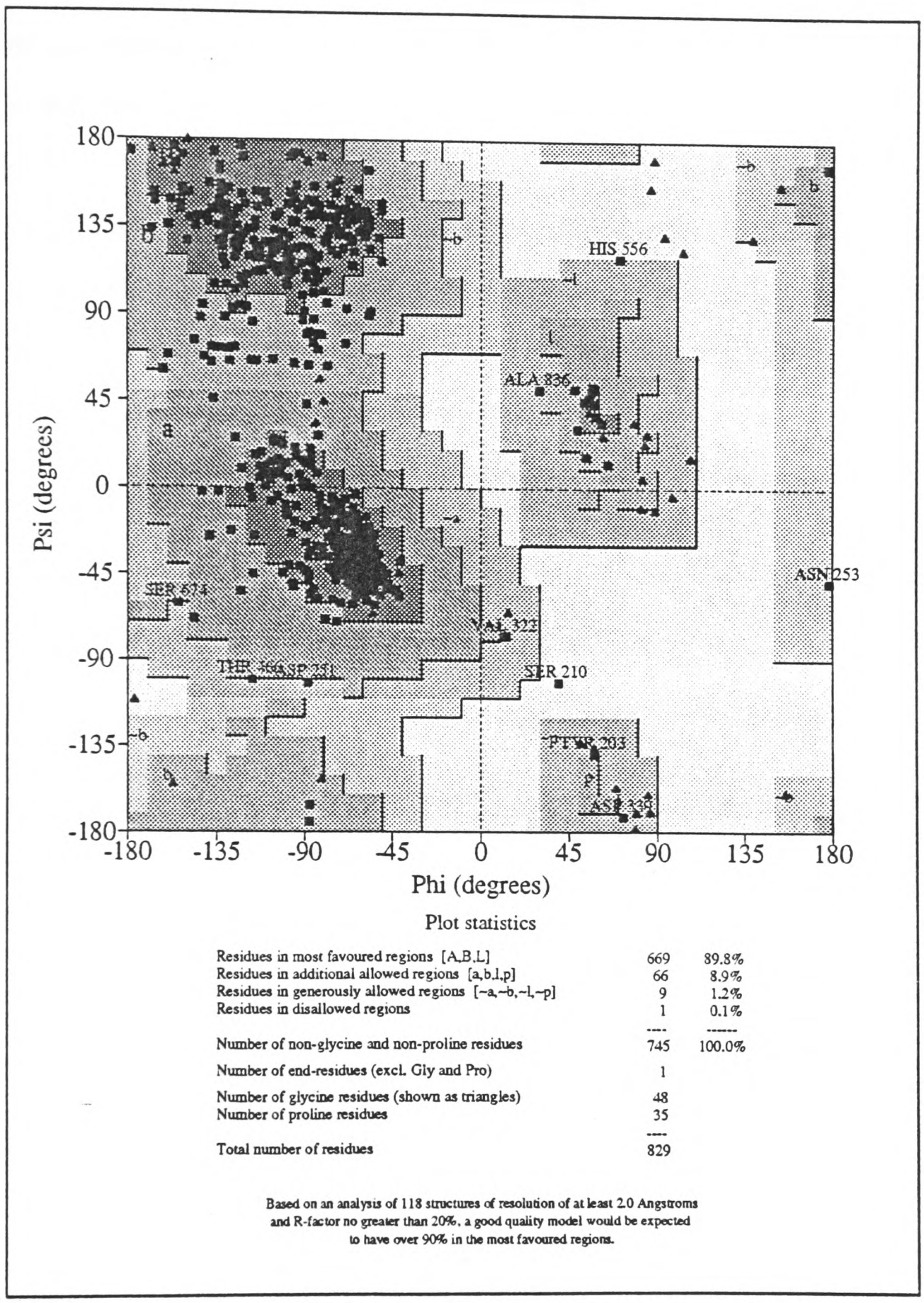

Plot generated using PROCHECK (Laskowski, MacArthur, Moss & Thornton, 1993).

Figure 5.7. *Ramachandran plot for the GPb native T state structure refined to an R factor of 22.8% (1.5Å resolution).*

5.4 SUMMARY

This work has confirmed the results of the earlier experiments of Chapters 2 and 3. High resolution data from native T state glycogen phosphorylase crystals has been collected and refinement from the 1.9Å structure of Acharya *et al.* (1991) has thus far given a model with an *R* factor of 22.8%. Further work is required on the model to give a final accurate structure. There is scope for additional data to even higher resolution to be collected. Reflections to 1.2Å resolution were observed at station 9.6 at the SRS Daresbury, possibly allowing atomic resolution data to be collected using the ESRF X-ray source.

6.1 INTRODUCTION

6.1.1 Overview

The precise catalytic mechanism of glycogen phosphorylase, despite much investigation, is not known. The results of many crystallographic and kinetic studies have led to several hypotheses concerning the mechanism, but to no definitive answer (Takagi, Fukui & Shimomura, 1982; McLaughlin, Stuart, Klein, Oikonomakos & Johnson, 1984; Klein, Im & Palm, 1986; Madsen & Withers, 1986; Johnson, Acharya, Jordan & McLaughlin, 1990). An approach to elucidating enzyme mechanism, which is complementary to X-ray crystallography, is the chemical modification of amino acids. By using chemical modification of residues and observing the results by kinetic and/or crystallographic methods, amino acids essential to enzyme processes such as allosteric activation or catalytic activity can be identified. Several such modifiers exist; for instance carbodiimide (Gray, 1962) and 2,3-butanedione (Ray & Koshland, 1962). However, these labels tend to be general in their action, targeting residue types (i.e. arginine for 2,3-butanedione and carboxy groups for carbodiimide) rather than specific binding sites.

Despite the non-specificity of these reagents, work upon glycogen phosphorylase using them has provided useful information. A study, using 2,3-butanedione, has investigated the mechanism of allosteric activation using the reactivity of arginyl residues with 2,3-butanedione as a probe (Dreyfus, Vandenburger & Buc, 1980). This work, on both GPa and GPb, identified the reactive residue as Arg 569 and suggested that this amino acid might have an essential role in the activation mechanism. Another study using carbodiimide has suggested there to be an essential carboxyl group at the catalytic site but this early work did not identify the group involved (Avramovic-Zikic, Breidenbach & Madsen, 1974).

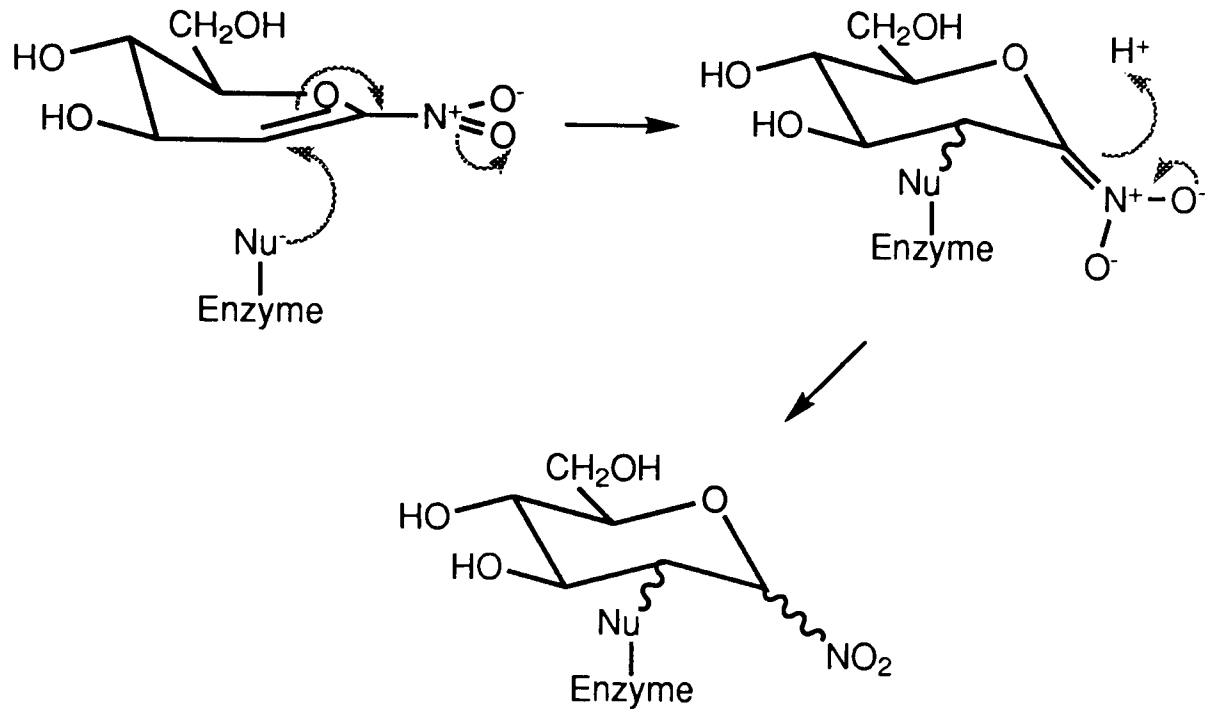

Figure 6.1. *Scheme showing a possible mechanism of enzyme inactivation by Michael addition to nitroglucal at the C-2 carbon.*

6.1.2 Nitroglucal

In the search for a more specific reagent the compound nitroglucal has been studied. There are two aspects that make 1-nitro-D-glucal (nitroglucal) a compound of interest. Firstly a nucleophilic carbon atom at C-2 and secondly a conformation and electronic character not dissimiliar to the oxocarbonium ion proposed as an intermediate for the phosphorylase catalytic mechanism (Chapter 2).

(i) Inactivation of Phosphorylase. Nitroglucal has been shown to inactivate glycogen phosphorylase in a time dependent manner under conditions promoting the T state or R state enzyme (Stirtan, 1993). In both the action was demonstrated to be irreversible since enzyme activity was not restored after excess nitroglucal was removed by dialysis. The inactivation is likely to be via conjugate Michael type addition to the activated C-2 position (Figure 6.1) by which process nitroglucal has already been shown to inactivate β-glucosidase (Stirtan, 1993).

This kinetic work also showed nitroglucal to have a longer inactivation process with R state phosphorylase (k_i=0.006min^{-1}) than with the T state enzyme (k_i=0.021min^{-1}). Interestingly the R state (K_m=4.1mM) has a 4-fold greater affinity for the compound than the T state (K_m=15.9mM).

Further inactivation tests in the presence of compounds known to bind at or to block the phosphorylase active site showed that glucose afforded 20% protection and caffeine 50% protection against the inactivation. These observations are consistent with the idea that the inactivation process occurs primarily at the active site, although nitroglucal may react at other enzyme sites. The inactivation of phosphorylase by nitroglucal was also shown to be pH dependent, with the K_i decreasing as the pH increased (the range of pH studied was 5.9-9.0). The rate constant k_i was observed to increase at the upper and lower end of the pH range. These observations are consistent with an inactivation process enhanced by acid and base catalysis. Nitroglucal does not change ionisation state over this pH range and it must be the enzyme changing its ionisation state. Thus it would seem that as the deprotonation of active site residues increases, with higher pH, the interaction between enzyme and nitroglucal must also increase.

(ii) Nitroglucal as a Transition State Analogue. In addition to possessing a reactive carbon atom, nitroglucal is forced to adopt a half chair conformation because of the double bond between C-1 and C-2. The nitro group at C-1 can inductively withdraw electron density from the pyranose ring oxygen. The double bond between C-1 and C-2 can mesomerically withdraw electrons from the same oxygen and both of these effects together lead to charge separation (Figure 6.2). Nitroglucal, with its electronic and steric effects, is similar to the proposed oxocarbonium ion intermediate of the phosphorylase mechanism. However, the hydroxy group at C-2 is missing. This group has been shown to be important in the catalytic mechanism (Street, Rupitz &Withers, 1989) and in Chapter 2 is was suggested that the contact between O-

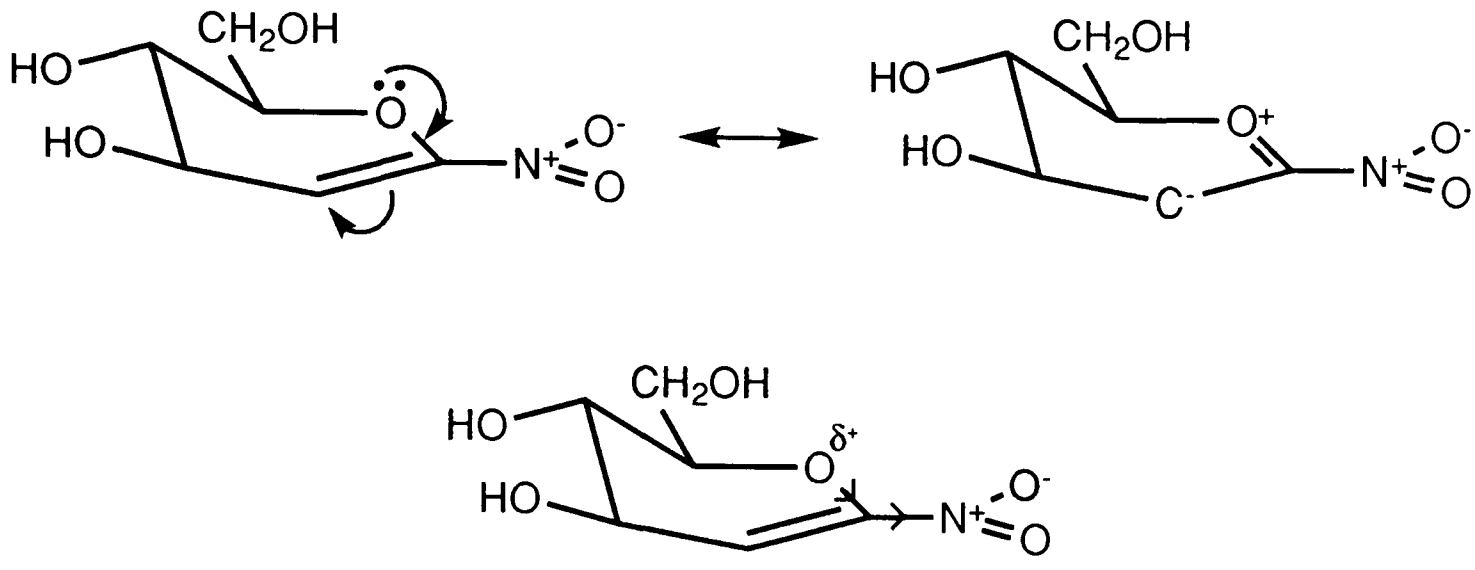

Figure 6.2. *The similarity of nitroglucal to an oxocarbonium ion. The top scheme illustrates the double bond mesomerically withdrawing electrons from the pyranose oxygen and the lower figure inductive electron withdrawal by the strongly electropositive nitro group.*

2 and the phosphate was important in orientating the phosphate group for catalysis. It would thus be interesting to see if phosphate can still bind at the T state active site in the presence of an oxocarbonium ion like compound but with the C-2 hydroxy group absent.

In conjunction with this comparison between nitroglucal and nojirimycin tetrazole, which has the O-2 oxygen and proven synergism with phosphate, it should also be possible to examine further the importance of electronic effects on phosphate binding. The compound glucal is missing the electron withdrawing nitro group of nitroglucal but still contains a double bond between C-1 and C-2 (Figure 6.3) and so the positive electronic character of O-1, the pyranose ring oxygen, is thus be reduced.

The studies on nojirimycon tetrazole, nitroglucal, glucal and glucose complexes with GPb and phosphate would give a set of results on a series of compounds each with different steric and electronic properties. This would allow a comparison of the relative importance of each effect.

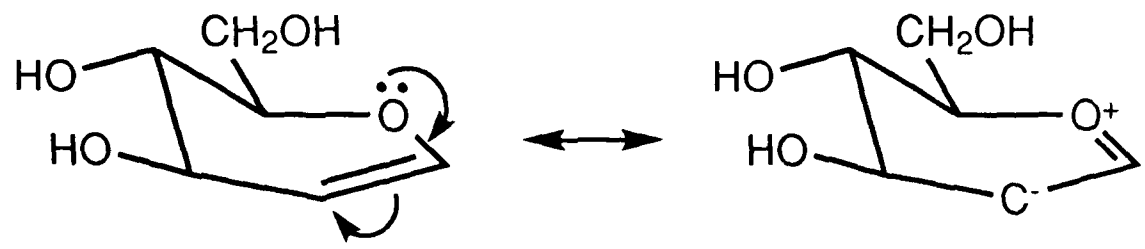

Figure 6.3. *Glucal with the mesomerically electron withdrawing double bond between C-1 and C-2.*

This chapter describes the X-ray crystallographic analysis of the binding of 1-nitro-D-glucal (nitroglucal) to T and R state glycogen phosphorylase. In the T state, additional experiments on the binding of nitroglucal and glucal in the presence of phosphate were carried out. Rather surprisingly, the results show that nitroglucal can synergistically bind phosphate at the active site of glycogen phosphorylase. Covalent binding of nitroglucal was observed in the experiments, but not at the active site.

6.2 EXPERIMENTAL METHODS

6.2.1 General

Purified rabbit skeletal muscle glycogen phosphorylase was prepared by the method of Fischer and Krebs (1962) with minor modification. Chemicals were purchased from Sigma Chemical Company. Nitroglucal was prepared by Dr Andrea Vasella and his group in Switzerland (Beer *et al.*, 1986).

A model of nitroglucal was generated using the program SYBYL (Tripos Associates) and the Powell method of minimisation contained within the program. The individual atomic charges were calculated using the AM1 method (Dewar, Zoebisch, Healy & Stuart, 1985).

6.2.2 T State Data Collection

Crystallisation of the T state GPb enzyme was carried out by Dr Nikos Oikonomakos and his group at the National Hellenic Foundation in Greece. T state enzyme was crystallised from solutions containing 20-40mg/ml glycogen phosphorylase b, 1mM IMP, 1mM spermine, 10mM BES, 0.1mM EDTA and 0.02% sodium azide (pH 6.7). Crystals grown under these conditions are tetragonal, space group $P4_32_12$, with unit cell a = b = 128.5Å and c = 116.3Å.

Binding studies using these crystals were carried out by diffusion of ligands into the enzyme crystal. Prior to data collection crystals of T state GPb were prepared by soaking native GPb crystals in a buffered solution (10mM BES, 0.5mM EDTA, 0.02% sodium azide, pH 6.7) containing nitroglucal plus/minus phosphate for between 2 hours to 4 days (Table 6.1). The half-life period of the reaction in solution, approximately 30 minutes, was used as a basis for the soak times. The experiment with a 2 hour soak in 100mM nitroglucal [1] gave identical

	Ligand concentration in the soak solution (mM)			Soak period
	Nitroglucal	Phosphate	Glucal	
(1)	100	0	0	2 hours
(2)	100	0	0	4 days
(3)[a]	100	0	0	24 hours
(4)	100	50	0	2 hours
(5)	100	10	0	2 hours
(6)	0	50	200	2 hours

[a]Experiment carried out at pH 8.0

Table 6.1. *Table of the complexes studied with composition of the soak solutions and soaking times.*

results to the 4 day soak. Since the crystal from the 4 day soak gave appreciably worse diffraction data, 2 hours was then used for the remaining experiments as the soak time. A supplementary experiment was carried out, soaking crystal in a buffer as above containing glucal and phosphate (Table 6.1). For collection of data the crystals were mounted in glass capillaries of diameter 2mm.

Data to 2.4Å resolution were collected on a Nicolet IPC multiwire detector (Howard *et al.*, 1987) using a Rigaku RU-200H rotating anode X-ray source with a graphite monochromator, producing CuK_α X-radiation of 1.54Å wavelength, operating at 50kV, 60mA and source size 0.3 x 0.3mm. The detector was placed 16cm away from the crystal and at a 2θ angle of 22° (2.2Å at the edge). Data frames of 0.2° oscillation were collected with exposure times of between 100 and 180 seconds for a total angular range of 90°. Each experiment was performed with a single crystal of phosphorylase. The data were subsequently processed with either the XENGEN (Howard *et al.*, 1987) package or with the XDS (Kabsch, 1993) package to produce scaled sets of intensities.

Crystal	Angular Range Collected (°)	Exposure Time (s)
(1)	21	160-240
(2)	15	200-320
(3)	30	200-240
(4)	15	240
(5)	21	240
(6)	20	240
(7)	30	240

Table 6.2. *Parameters for data collection from the R state crystals.*

6.2.3 R State Data Collection

R state phosphorylase was crystallised by Dr Nikos Oikonomakos and his group at the National Hellenic Foundation in Greece. R state enzyme crystals were obtained from solutions containing 1.2-1.4M ammonium sulphate and 6mM IMP at pH 7.5 (Leonidas, Oikonomakos, Papageorgiou & Sotiroudis, 1992) giving monoclinic crystals of space group $P2_1$ and of cell parameters a=119.0Å, b=190.0Å, c=88.2Å and β=109.35°.

The crystals were prepared for data collection by soaking in a buffered solution (10mM β-glycerophosphate, 0.5mM EDTA, 3mM DTT, 0.02% sodium azide, pH 7.0) of 1.2M sodium tartrate for at least 30 minutes. The crystals were then transferred to a solution of the same buffer containing 100mM nitroglucal for between 5.5 and 8 hours. These soak times were the longest possible to allow the nitroglucal to react and maintain crystal integrity. For data collection the crystals were mounted in thin quartz capillaries of diameter 1mm.

Data were collected from a total of 7 crystals on a MAR Research image plate system mounted on the wiggler beam line PX9.5 at the SRS Daresbury. The silicon monochromator was aligned for a wavelength of 0.95Å and a 0.3mm aperture collimator was positioned on the beam line.

The detector was placed 21.3cm away from the crystal to give a maximum resolution of 2.4Å at the edge of the detector. Data frames of 1.0° oscillation were collected from the crystals as detailed in Table 6.2. During the data collection the synchrotron was operated at an energy of 2.0GeV and the beam current varied between 221mA and 134mA.

Crystal orientations were determined using the autoindexing algorithm in DENZO (Otwinowski, 1993) and the data integrated also using DENZO. Inter-frame scaling, partial reflection summation, data reduction and post-refinement were performed by SCALEPACK (Otwinowski, 1993) to give a unique set of reflections.

6.3 RESULTS

6.3.1 Data Processing

The statistics for data collection from the T and R state GPb-nitroglucal and T state GPb-glucal complexes are shown in Table 6.3. All the T state crystals diffracted as expected, though a soak for 2 weeks resulted in a crystal that did not diffract. The R state crystals diffracted weakly and suffered radiation damage quickly in the X-ray beam. The data sets from the earlier R state GPb-tetrazole-phosphate complexes of Chapter 3 had been collected from just one crystal. The weakness of the diffraction from the GPb-nitroglucal R state crystals perhaps indicated that nitroglucal was reacting with the protein. Data were collected above 3.0Å resolution but the merging *R* factor increased rapidly beyond 3.0Å. The data are 62% complete to 3.0Å. The unit cell parameters for the R state data were found to be a=118.9Å, b=189.8Å, c=87.7Å and β=109.5°.

6.3.2 Fourier Difference Maps

For each experiment difference Fourier maps were calculated using $(F_o\text{-}F_c)$ coefficients, with F_o scaled to the native T state (Acharya, Stuart, Varvill & Johnson, 1990) GPb structure factors. For the R state a difference Fourier map was also calculated, but using structure factors and phases calculated from the native R state (Barford & Johnson, 1989). A difference map calculated using native R state observations was noisy and uninterpretable.

(i) T State GPb-Nitroglucal Complexes - [1], [2] and [3]. There were no significant differences at the active site between the three GPb-nitroglucal Fourier difference maps. Each contained well resolved density at the catalytic site for a nitroglucal molecule but, disappointingly, no covalent link from the C-2 carbon of nitroglucal to potential nucleophiles, such as OE1 Glu 672

Complex	Number of Reflections		Data Completeness (%)	$R_m(I)$ (%)	<I/σ>[a]	R_{iso}[b] (%)
	Unique	Measured				
T State						
(1)	31611	78318	81 (2.4Å)	7.3	21.5	9.5
(2)	33023	73410	84 (2.4Å)	9.5	14.6	15.1
(3)	31535	75309	81 (2.4Å)	6.6	15188	13.7
(4)	31432	74714	80 (2.4Å)	9.0	16852	13.7
(5)	30794	74835	79 (2.4Å)	8.7	17586	11.6
(6)	31283	75420	80 (2.4Å)	8.2	18028	11.6
R State						
GPb-nitro-glucal	45886	84347	62 (3.0Å)	8.3	34415	31.3

[a]<I/σ> given for XENGEN processed data and the number of reflections with I/σ > 3 for XDS processing. [b]Mean fractional isomorphous difference calculated for the T state with respect to native T state data (Acharya, Stuart, Varvill & Johnson, 1990) and the R state with respect to native R state native data from Chapter 3 of this thesis.

Table 6.3. *Crystallographic data collection and processing statistics for the T and R state complexes.*

(3.4Å away) and OH Tyr 573 (4.5Å away), was apparent (Figure 6.4a). In the Fourier map the nitro group at C-1 could be seen to be planar with the pyranose nitroglucal ring which was in the unreacted half-chair conformation. At the active site positive and negative density indicated movement of the ring of His 377 away from the O-6 of nitroglucal.

Near the side chain of His 73 situated in a gulley close to the enzyme surface, density in the Fourier maps did suggest covalent binding of nitroglucal to the histidine ring (Figure 6.5). This is the first time a ligand has been observed to bind, covalently or non-covalently, at this site. The density was not as well defined as that for nitroglucal at the active site and the conformation of the molecule, full or half chair, could not be interpreted from the map. However, the density was within covalent binding distance of NE2 of His 73, an atom that could potentially act as

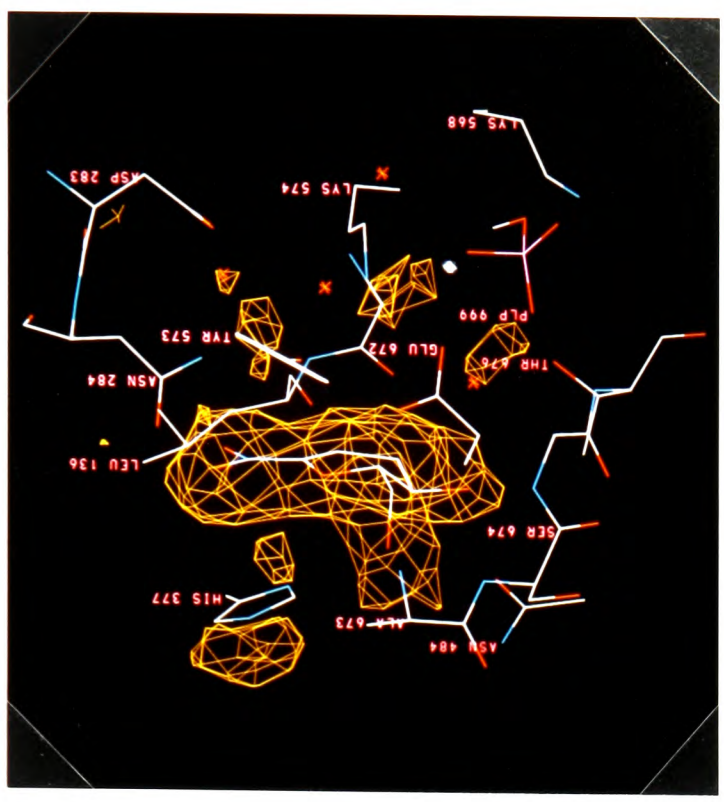

(a)

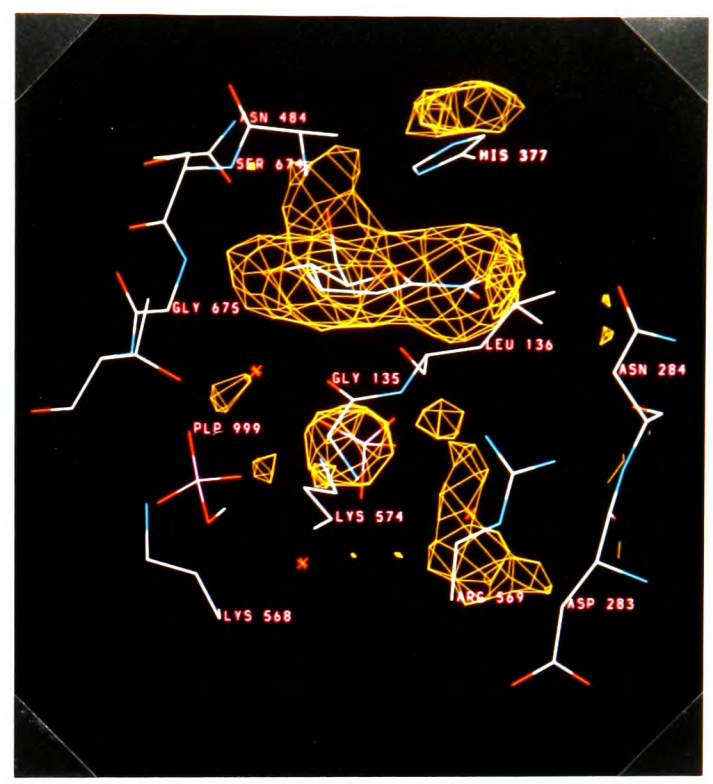

(b)

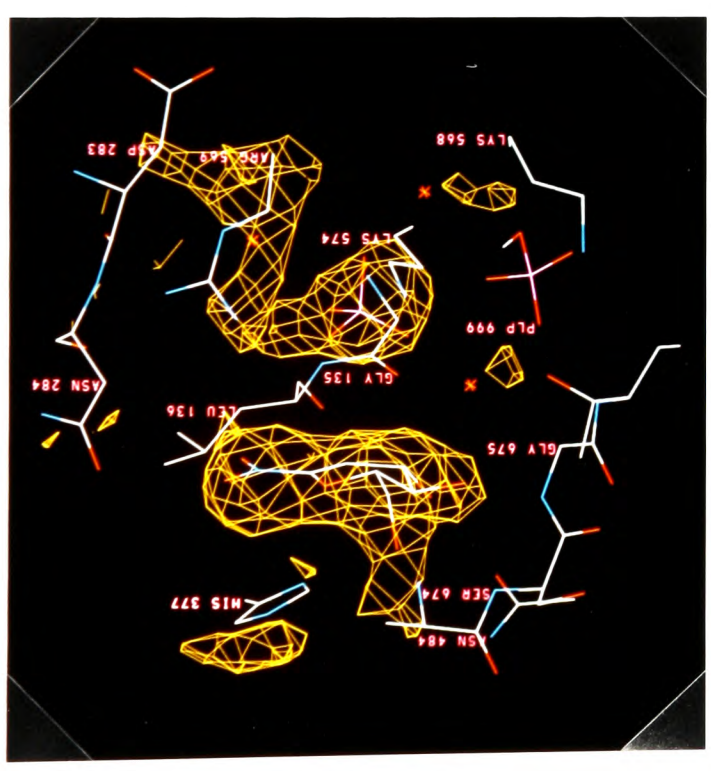

(c)

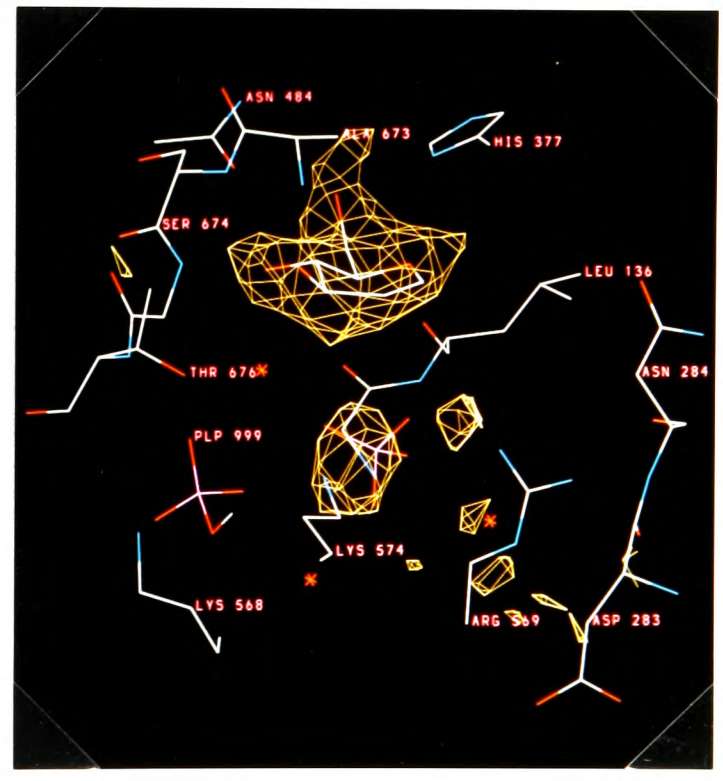

(d)

Figure 6.4a to 6.4d. *Comparison of the (F_o-F_c) Fourier difference maps from crystals soaked in: (a) 100mM nitroglucal alone (b) 100mM nitroglucal with 10mM phosphate (c) 100mM nitroglucal with 50mM phosphate and finally (d) 200mM glucal with 50mM phosphate.*

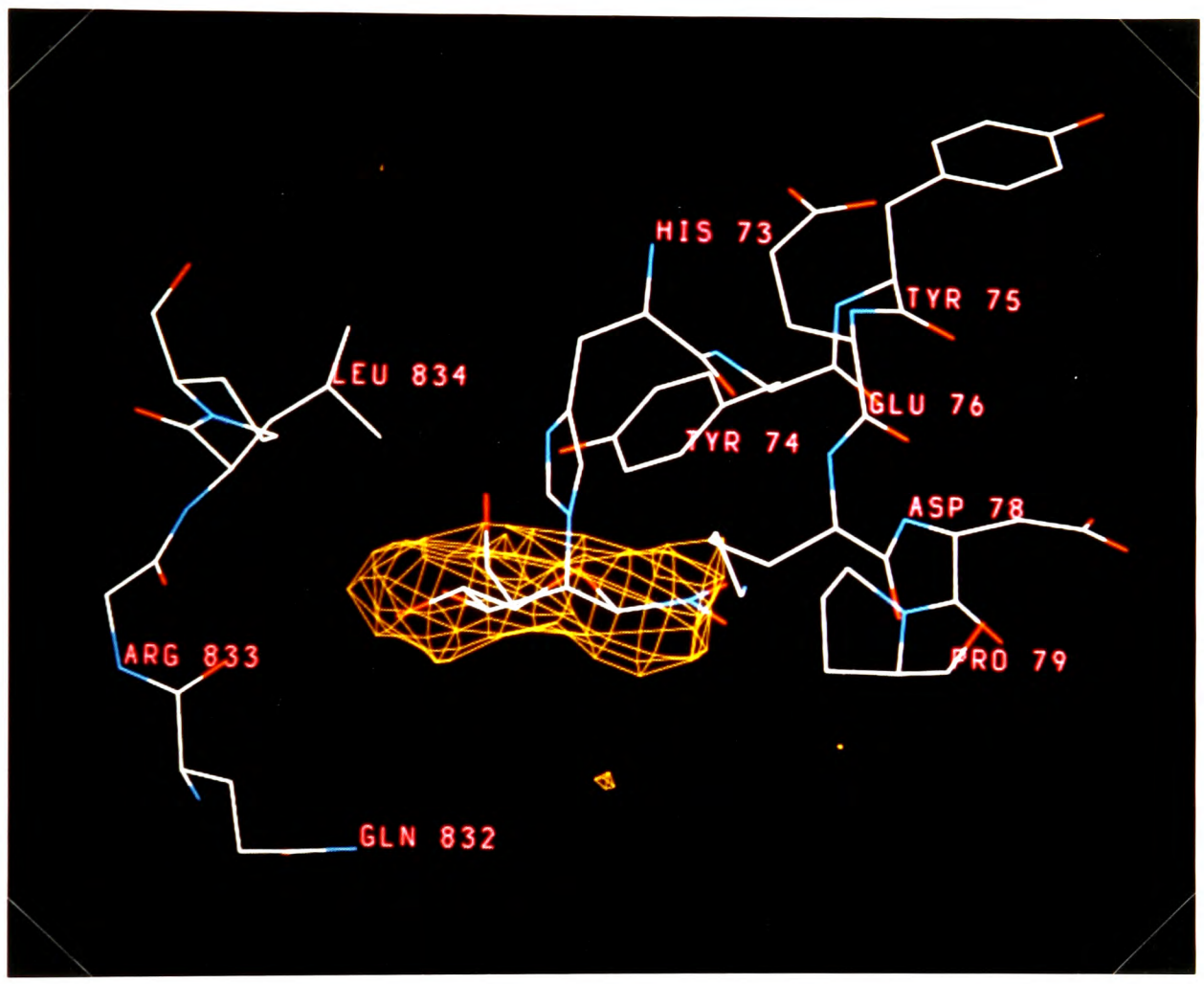

Figure 6.5. *The (F_o-F_c) Fourier density at the surface binding site for nitroglucal (His 73).*

a nucleophile. With a model of nitroglucal fitted to the density, NE2 was positioned axially above C-2. No other density at the His 73 surface site suggested any movement of that residue or indeed other residues to accommodate nitroglucal. The experiment for which a phosphorylase crystal was soaked for 2 days did show slightly improved density for nitroglucal at this site over the crystal soaked for 2 hours. It was surprising that the crystal soaked in buffer at pH 8.0 survived and diffracted well. No significant differences were observed between the difference map using data from this crystal and that from the other two crystals.

(ii) T State GPb-Nitroglucal-Phosphate Complexes - [4] and [5]. The Fourier difference map of the 100mM nitroglucal/50mM phosphate experiment clearly identified nitroglucal and phosphate bound at the active site, with movement of the His 377 side chain away from O-6 of nitroglucal (Figure 6.4c). The phosphate peak approximated to the same size as the peak observed for the GPb-tetrazole-phosphate (1mM tetrazole/50mM phosphate) complex, with the exception of the addition of a small lobe towards the 280s loop of residues. This may have been due to a water molecule bound close to the phosphate. Reorganisation of the active site to create the phosphate recognition pocket was evident from the Fourier difference map. The side chain of Arg 569 was covered in negative density and the new position coordinating the phosphate was clearly indicated with continuous positive density from the main chain of atoms. Negative density smothered the side and main chain atoms of Asp 283 and Asn 284, though little positive density suggested new locations.

A comparison of this difference map to those of the GPb-nojirimycin tetrazole-phosphate experiments reveals the nitroglucal-phosphate complex to contain more prominent indications of the active site conformational changes. The positive and negative density for Arg 569 and the 280s loop are more continuous, with further scattered negative density over Asn 282 and Phe 285 to Gly 288, suggesting movement in the 280s satellite residues. Additional indication of greater change of the active site towards the R state is given by negative density covering

His 571. In the tetrazole experiments this residue was not covered by negative density and was not observed significantly to change its conformation. The native R state structure shows the side chain of His 571 to swing out and open the active site channel to the surface.

The lower, 10mM, concentration of phosphate in these experiments resulted in the Fourier map features associated with phosphate binding at the active site being diminished: the phosphate peak and density for Arg 569 coordinating it became smaller, there was no negative density over the native side chain position of the arginine and negative density over the 280s loop was less extensive (Figure 6.4b). The relative heights of the phosphate peaks from the 100mM nitroglucal/50mM phopshate and 100mM nitroglucal/10mM phosphate Fourier maps were approximately 11 and 8 sigma respectively.

Binding of a phosphate ion at the allosteric site and movement of Arg 309 to coordinate was apparent in both experiments. Interestingly, the nitroglucal binding site at His 73 was poorly occupied in both cases, though slightly more in the lower phosphate experiment. The density for a molecule was very poor and this was perhaps due to acidification of the buffer by sodium dihydrogen phosphate rather than by conformational changes due to the presence of phosphate at the active or allosteric sites.

(iii) T State GPb-Glucal-Phosphate Complex - [6]. The Fourier difference map for this complex did indicate glucal and, surprisingly, some phosphate to bind at the active site (Figure 6.4d). The phosphate peak was lower than those observed for the GPb-nitroglucal-phosphate complexes, with a peak height of 7 sigma. Density suggesting movement of Arg 569 and the 280s residues to accommodate the phosphate was limited, consistent with a low occupancy by phosphate.

(iv) R State GPb-Nitroglucal Complex. Though this Fourier difference map was not noisy, it

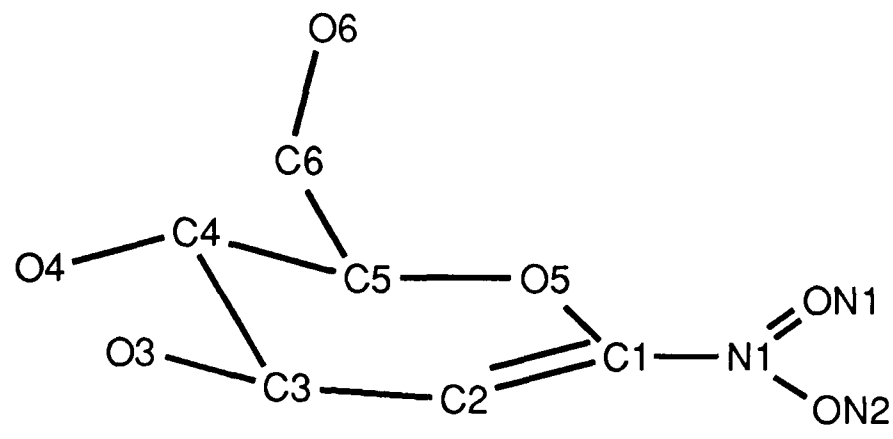

Figure 6.6. *The atom numbering scheme used for nitroglucal. The same phosphate atom numbers are used as shown in Figure 2.7 in Chapter 2.*

was difficult to interpret. Density was present at the active site but did not allow placing of nitroglucal and was not conclusive of any reaction of nitroglucal with the protein.

6.3.3 X-PLOR Refinement

Not all of the T state phosphorylase complexes were refined. The GPb-nitroglucal complex which had been soaked for 2 hours [1] was selected for refinement since the crystallographic data from this complex were the best of the three complexes. Both of the GPb-nitroglucal-phosphate complexes ([4] and [5]) were refined, but not the GPb-glucal-phosphate complex [6]. In an attempt to improve the quality of the R state GPb-nitroglucal difference map, some refinement of this complex was undertaken.

(i) The T State GPb Complexes. Similar refinement protocols to those previously used in this work for the nojirimycin tetrazole complexes described in Chapter 2 were selected for the T state nitroglucal complexes. The GPb-nitroglucal complex was refined using a conventional route and those complexes containing phosphate, and thus considerable adjustment of the active site, were refined using simulated annealing as well as conventional refinement.

The starting model for refinement was the refined structure of the GPb-glucose complex including residues 12 to 841 (Martin, Johnson & Withers, 1990) with the torsion angles of Arg 309 at the allosteric site adjusted. For the GPb-nitroglucal-phosphate complex the conformations of the 280s loop and Arg 569 were adjusted as described in Chapter 2 for the GPb-tetrazole-phosphate complexes. Models of nitroglucal, in the unreacted half-chair conformation, and phosphate were fitted to density at the active and allosteric sites. A model of reacted nitroglucal, with the nitro group equatorial and the NE2 atom of His 73 axial to C-2, was fitted at the His 73 surface site for the GPb-nitroglucal complex. Several active and allosteric site water molecules were removed from the files were they had been displaced by ligands.

The X-PLOR topology and parameter files for PLP and phosphate were included as previously detailed in Chapter 2 (Section 2.3.3). An AM-1 calculation was used to estimate the partial charges for the half-chair and full-chair nitroglucal molecules. The charges on the pyranose ring were similar to those used by W. Weiss in X-PLOR. The AM-1 calculation showed the charges on important atoms to be as follows: C-1 0.040; O-5 -0.265; N-1 0.438; ON-1 -0.306; ON-2 -0.306; C-2 -0.050. Refinement of the complexes was performed using X-PLOR (Brünger, 1988; Brünger, 1989; Brünger *et al.*, 1989).

The simulated annealing and conventional refinement protocols of Chapter 2 (Section 2.3.3) were again used here for the refinement of the T state complexes.

(ii) The R state GPb Complex. The starting model for the R state complex was the refined native structure (Barford & Johnson 1989) comprising residues 10 to 837. No nitroglucal molecule was modelled at the active site. The refinement commenced, using reflections from 8.0Å to 4.0Å resolution, by treating the subunits as individual rigid bodies (60 cycles) followed by similar rigid body refinement but this time on the domains of each subunit (35 cycles). The initial *R* factor was 28.3% and after rigid body refinement the *R* factor had dropped to 26.8%.

Subsequent refinement, using reflections between 8.0 and 3.0Å resolution, made use of ncs restraints of 200 (150 cycles) and 100kcal mol^{-1} (200 cycles) upon residues whose C-α positions differed by less than 1.0Å between the subunits. A final round of individual *B* factor refinement (70 cycles), using target standard deviations of 1.5 and 2.0$Å^2$ for bonded atoms and atoms bound to the same atom respectively, gave the final model with an *R* factor of 20.4% (initial *R* factor 32.9%).

The refined coordinates of the complexes, T and R state, were used to generate Fourier difference maps with SIGMAA ($2F_o$-F_c) coefficients. An (F_o-F_c) map was also generated for the R state complex. The maps were inspected for a satisfactory fit of the refined model to the electron density.

6.3.4 X-PLOR Refined Structures

In all of the complexes refined, the final ($2F_o$-F_c) Fourier maps agreed well with the refined model (Figure 6.7). The statistics for the refinements are shown in Table 6.4. The actual standard deviations of *B* factors for the complexes were approximately 3.3$Å^2$ and 5.1$Å^2$ for bonded atoms and atoms bound to the same atom respectively. After refinement no new density linking the nucleophilic nitroglucal C-2 to protein atoms was apparent at the active site. As observed previously in the experiments with nojirimycin tetrazole (Chapter 2), the complexes containing phosphate exhibited the greatest conformational changes, centred mainly upon the active site.

(i) T State GPb-Nitroglucal Complex [1]. The location of nitroglucal at the active site is well defined in the ($2F_o$-F_c) difference maps. The contacts from the pyranose ring oxygens (O-3, O-4 and O-6) are very similar to those made by glucose (Martin, Johnson & Withers, 1990). One hydrogen bond is made by the polar nitro group to Asn 284, but to no other protein atoms.

Figure 6.7. *An example of the ($2F_o$-F_c) Fourier difference map for the 100mM nitroglucal/50mM phosphate structure.*

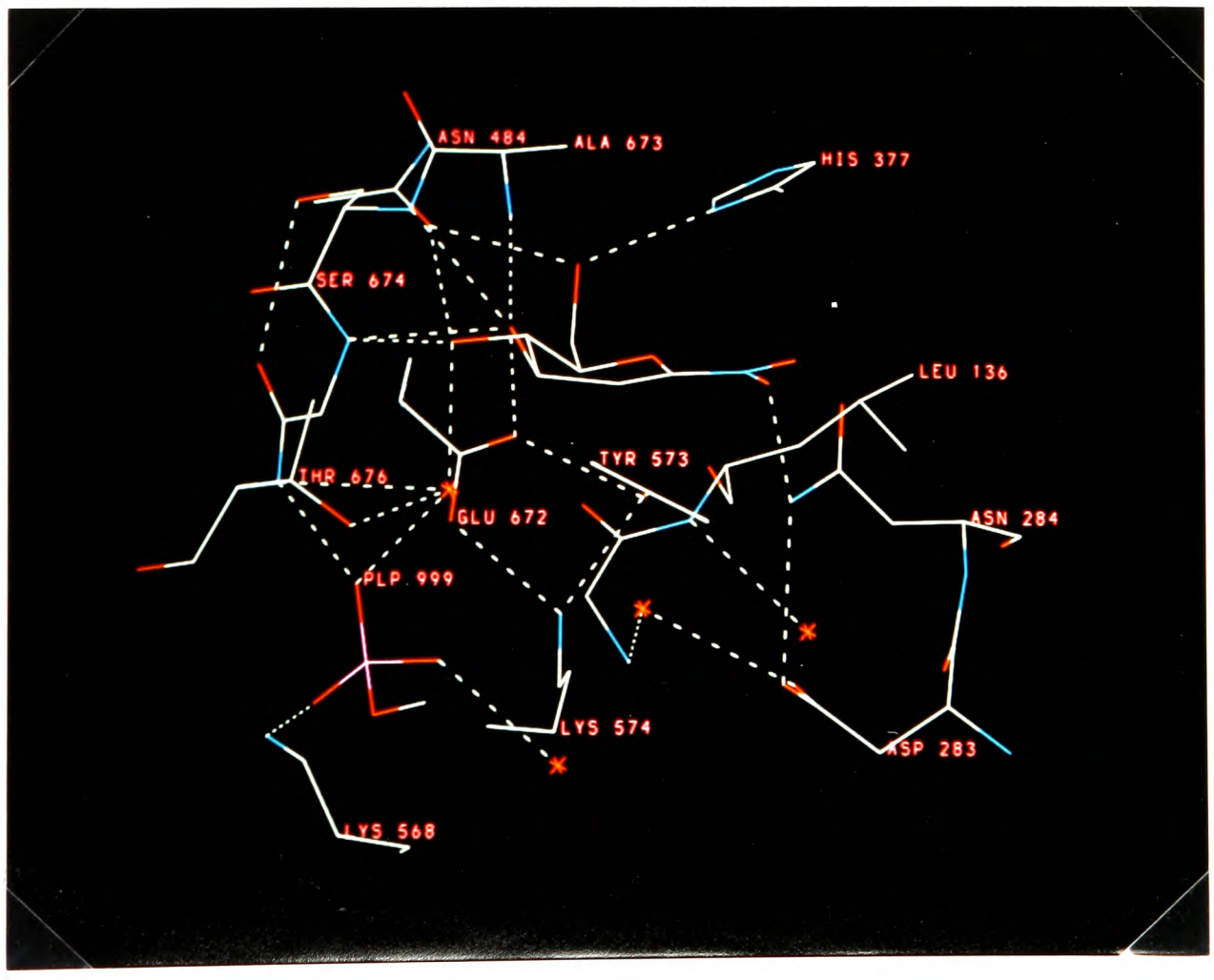

Figure 6.8. *Hydrogen bonds made by nitroglucal to the phosphorylase active site in the GPb-nitroglucal complex.*

		Complex		
		[1]	[4]	R state GPb-Nitro-glucal
Number of Atoms	Protein	6774	6780	26828
	Ligands	26	23	0
Number of Waters		576	575	0
Number of Reflections (8.0-2.4Å, I>0)		33008	30690	43366
R Factor	Starting (%)	24.4	24.5	32.9
	Final (%)	19.9	17.0	20.4
RMS Deviation	Bond Lengths (Å)	0.019	0.017	0.026
	Bond Angles (°)	3.5	3.3	4.3

Table 6.4. *The refinement statistics for the GPb-nitroglucal complexes.*

The details of the hydrogen bonds made by nitroglucal are shown in Table 6.5 and Figure 6.8.

The unreactive nature of nitroglucal at the active site is confirmed in the refined structures and the final map. The half-chair conformation is retained and there is no movement of side chains moving to within covalent bonding distance of C-2. The potential electrophilic atoms of OH Tyr 573 and OE2 Glu 672 remained 3.4Å and 4.1Å distant from C-2.

At the surface site, His 73, the refined structure returned density consistent with partial occupancy of the site by nitroglucal. At low map contour levels the density was defined and continuous from the histidine ring to C-2. The surface pocket at this site is very open and nitroglucal makes only one hydrogen bond to the protein, O-6 to OH Tyr 74 (3.0Å). The surface of nitroglucal away from His 73 is open and makes no Van der Waals contacts. The opposite

Ligand Atom	T State GPb Protein Atom	Hydrogen Bond Contact (Å)	
		[1]	[4]
Nitroglucal			
O-3	OE1 Glu 672	2.6	2.8
	N Ala 673	3.3	3.3
	N Ser 674	3.0	2.9
	N Gly 675	3.1	3.1
O-4	OD1 Asn 484	(3.4)	3.2
	N Gly 675	2.9	2.7
	WAT 897	2.6	2.7
O-6	ND1 His 377	2.7	2.7
	OD1 Asn 484	2.8	2.9
ON-1	ND2 Asn 284	2.9	-
ON-2	ND2 Asn 284	-	2.6
Phosphate			
OP-1	N Gly 135	NP	3.2
	N Leu 136	NP	2.8
OP-2	NH2 Arg 569	NP	2.9
	NZ Lys 574	NP	2.9
OP-3	NZ Lys 574	NP	3.3
	OP2 PLP 999	NP	2.8
	WAT 897	NP	2.7
OP-4	N Gly 135	NP	2.9
	WAT 879	NP	2.6
	WAT 887	NP	3.0

Table 6.5. *Hydrogen bond contacts made by nitroglucal and phosphate to phosphorylase. A dash indicates no contact and brackets imply a weak interaction. NP indicates no phosphate was included in the soak solution.*

side of the pyranose ring, however, contacts 8 different residues with a close contact of the nitro group to Pro 79. It is perhaps partly this unfavourable contact that leads to the less than 100% occupancy of nitroglucal at this site. The pocket is located 12Å away from the allosteric AMP binding site but there is no obvious link between nitroglucal binding to His 73 and a possible enzyme deactivation mechanism. This is thus, with the protection afforded by caffeine and glucose-1-phosphate, still consistent with the main deactivation mechanism being nitroglucal reacting at the active site and not at a surface site. However the reaction of nitroglucal with His 73 does illustrate that the compound is reactive in the enzyme crystal.

(ii) T State GPb-Nitroglucal-Phosphate Complex [4]. In the presence of phosphate, the binding position of nitroglucal and overall topology of the active site is maintained from the GPb-nitroglucal complex, with the exception of residues involved in the phosphate site creation. As observed before for the GPb-tetrazole-phosphate complexes, the side chain of Arg 569 swings into the active site to coordinate the phosphate ion. The 280s loop of residues shifts, allowing acidic Asp 283 to move out of the active site towards the native location of the Arg 569 guanadinium group (Figure 6.9). The residue Asn 284 also moves considerably and the movement of this residue and Asp 283 are echoed further down the protein chain in smaller conformational adjustments. A comparison between the GPb-nitroglucal-phosphate complex and the GPb-tetrazole-phosphate complexes, considered in more detail later, reveals the nitroglucal and phosphate to bind in the same positions as those of tetrazole and phosphate. Indeed, the surrounding protein frame of positive electrostatic groups, Lys 568, Arg 569 and Lys 574, for the phosphate is similar in both complexes. The phosphate ion contacts Gly 135, Leu 136, the PLP phosphate and the surrounding conserved water shell, but has of course lost the phosphate OP-2 to pyranose O-2 hydrogen bond (nitroglucal having a double bond between C-1 and C-2). A single contact to Arg 569 is made and the closest contact from phosphate to O-5 of nitroglucal is 3.9Å. These contacts are summarised in Table 6.5 and shown in Figure 6.10.

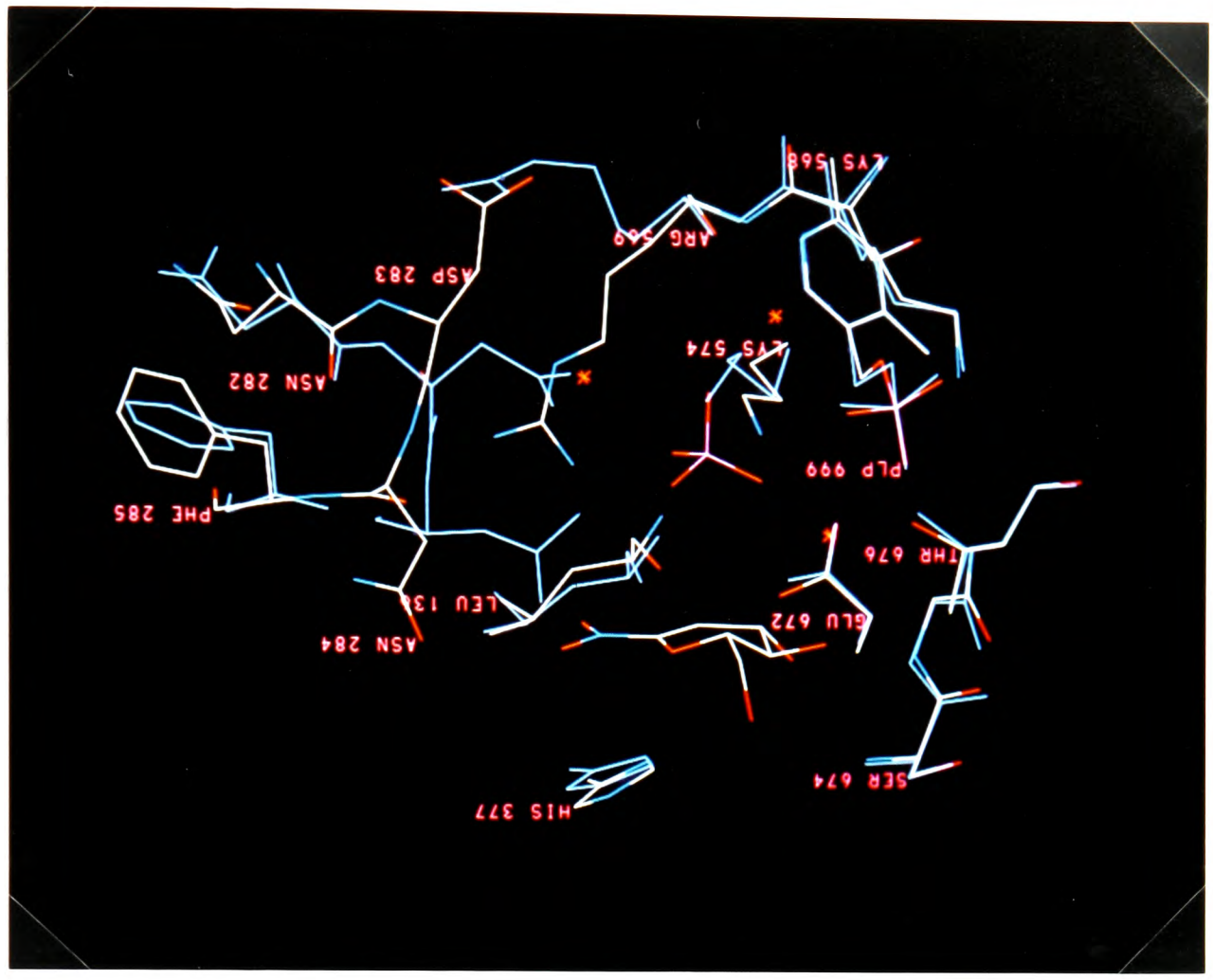

Figure 6.9. *The refined structure of the GPb-nitroglucal-phosphate complex with the native structure of GPb in the background (blue).*

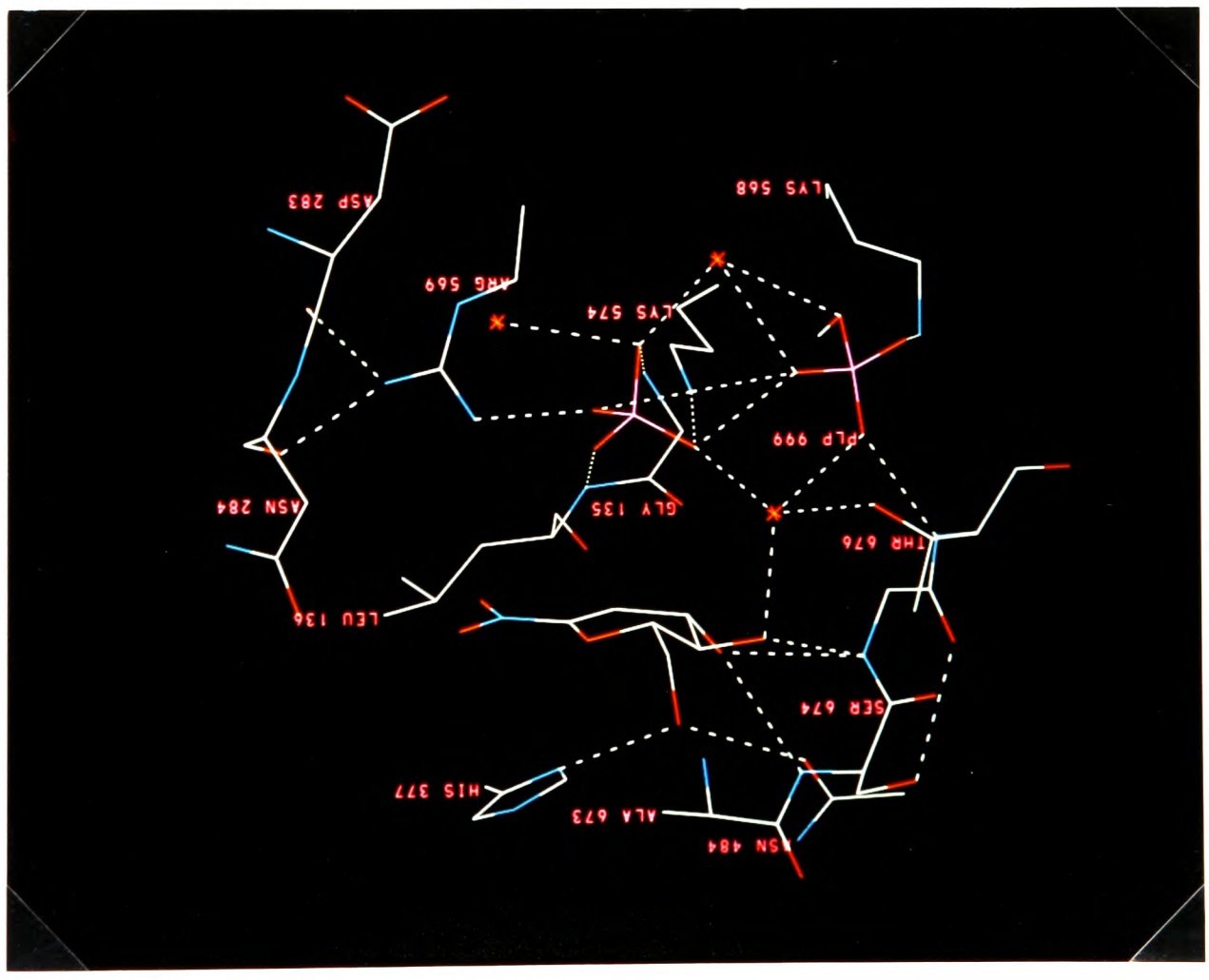

Figure 6.10. *Hydrogen bond contacts at the active site in the complex of phosphorylase with nitroglucal and phosphate.*

The Fourier difference map of the GPb-nitroglucal-phosphate complex does contain more conclusive density for the Arg 569 side chain and 280s loop residues than the nojirimycin tetrazole equivalent, perhaps suggesting a fuller transition towards the R state active site conformation.

(iii) R State GPb-Nitroglucal Complex. The refinement of the R state complex, with no ligands in the model, did give some improvement to the Fourier difference map, but still the density remained unresolved. Nitroglucal as a half-chair or full-chair could not be completely fitted, with the nitro group and O-5 out of density. At best, the map suggested reaction of nitroglucal with a sulphate ion of crystallisation. Such a reaction, though, would not explain the irreversible nature of the phosphorylase inactivation, since the product could diffuse out of the enzyme. Another possible explanation is that both nitrolgucal and a sulphate ion are bound but unreacted. In this work nitroglucal has been observed to bind phosphate at the T state active site and may also allow sulphate to bind in a similar manner in the R state. At this stage the data set was abandoned. Future work could perhaps concentrate on collecting data from a single frozen crystal of R state phosphorylase to give better quality data to higher resolution.

(iv) The Tower and Cap Regions. These regions of phosphorylase are involved in the subunit-subunit contacts and alter conformation on activation of the enzyme from the T to R state. These residues were not observed to change conformation in the GPb-tetrazole-phosphate complexes and the refined model of the GPb-nitroglucal-phosphate structure also shows no significant deviation from the native T state structure. The residues 252 to 261 are mobile in all the complexes studied and not surprisingly are poorly represented in the Fourier density. Dominating lattice contacts, which include the subunit-subunit contacts of the T state dimer, are likely to be responsible for the lack of movement of the tower and cap residues towards their R state conformations when nitroglucal and phosphate are both bound.

6.4 DISCUSSION

6.4.1 Comparison with the GPb-Tetrazole-Phosphate Structure

Though the general topology of the active site in both the tetrazole-phosphate and nitroglucal-phosphate GPb complexes are similar, there are subtle differences between them.

Phosphate and its surrounding entourage of coordinating ligands remain in similar positions (the rms deviation in position for active site C-α atoms between the GPb-tetrazole-phosphate and the nitroglucal equivalent is 0.26Å and 0.47Å between the nitroglucal complex and the native structure). However, the phosphate itself has undergone a change in orientation, rotating approximately about the phosphorus atom position (Figure 6.11). The ion has lost the contact of OP-2 to O-2 of the pyranose ring which was observed in the tetrazole complexes. Consequently to optimise contacts, the phosphate ion rotates but maintains the contact to the PLP 5'-phosphate. The result is an ion with three of the oxygens planar to the nitroglucal half-chair conformation and two new contacts of OP-1 to the main chain nitrogen atoms of Gly 135 and Leu 136. The electrostatic contact between the sugar ligand and phosphate is lengthened to 3.9A, for the tetrazole-phosphate complex this was 3.0Å. The increase in length of this contact is a combination of small alterations in the positions of the phosphate and nitroglucal with respect to nojirimycin tetrazole and its phosphate ion. A hydrogen bond from the nitro group to ND2 of Asn 284 may also help peg the nitroglucal further from the phosphate ion. This refined model from X-PLOR appears plausible in terms of the above argument and is supported by electron density in the $(2F_o\text{-}F_c)$ Fourier map. However, the precise orientation of the phosphate oxygens at 2.4Å resolution is not entirely secure. This problem has been addressed in Chapter 5 with the analysis of 1.7Å resolution data from the GPb-tetrazole-phosphate complex. In that case the X-PLOR refinement of the 2.4Å data from the complex (Chapter 2) was proved to be correct.

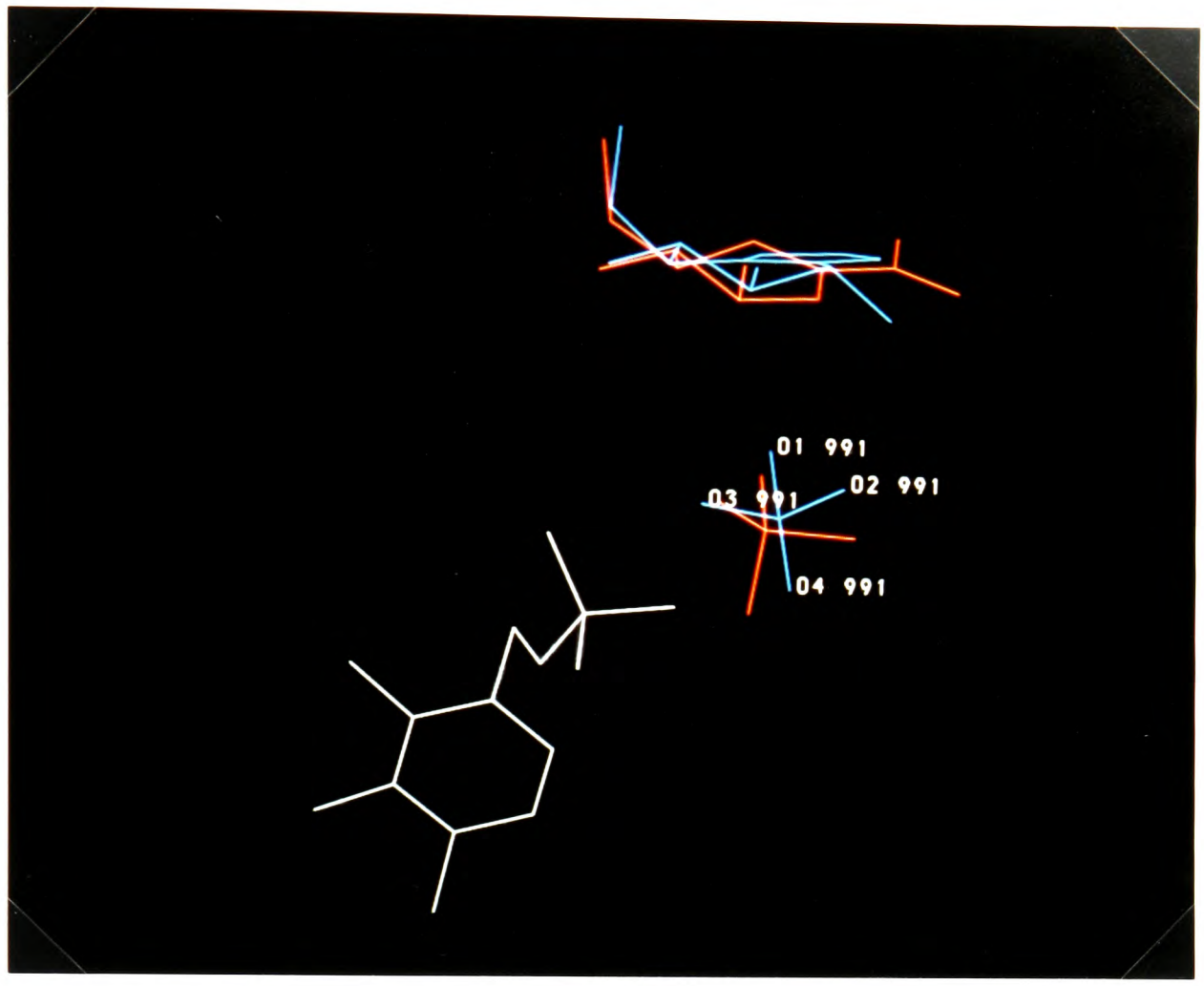

Figure 6.11. *Comparison of the orientation of the phosphate ion in the GPb-tetrazole-phosphate complex (blue) and in the GPb-nitroglucal-phosphate complex (orange).*

It was noted that for the GPb-tetrazole-phosphate complex His 571 remained very much in the native T state conformation. For the nitroglucal-phosphate complex His 571 changed conformation, as it did in the complex with heptulose-2-phosphate (Johnson, Acharya, Jordan & McLaughlin, 1990), to be more R state like. The torsion angle about Cα-Cβ changes from -91° (native) to -156° (complex). The histidine ring moves away from the incoming side chain of Arg 569 and towards Tyr 613, opening the active site channel. Many of the features of activation at the catalytic site, i.e. going from the T to R state conformation, are depicted as more enhanced in the Fourier maps of the GPb-nitroglucal-phosphate complex compared to the GPb-tetrazole-phosphate complexes. This is perhaps due to the lack of binding of the nitroglucal at the inhibitor site (Phe 285, Tyr 613).

Ligand	Relative Electrostatic Potential on Atom[a]		
	(O-5)	(C-1)	(O-5) - (C-1)
Nojirimycin Tetrazole	-0.076	0.241	0.316
Nitroglucal	-0.053	0.207	0.260
Glucal	-0.092	-0.175	0.084
Glucose	-0.152	0.007	-0.157

[a]ESP calculated using MOPAC (Dewar, Zoebisch, Healy & Stewart, 1985).

Table 6.6. *The relative electrostatic potentials at the atoms O-5 and C-1 for the ligands considered.*

6.4.2 The Catalytic Mechanism

In Chapter 2 (Section 2.4.6) the importance of O-2 from the glycosidic substrate for orientating the substrate phosphate was discussed. This study with nitroglucal, in which the O-2 atom is absent, is consistent with the vital role of O-2 in orientating the phosphate ion. With nitroglucal as the glycosidic analogue, phosphate adopts a different orientation to that observed with nojirimycin tetrazole. Simple modelling of the active site with oligosaccharide in place of the tetrazole (Chapter 2) suggested that the orientation observed in the GPb-tetrazole-phosphate complexes is suitable for catalysis and for donation of a proton to the glycosidic bond. The alternative orientation with nitroglucal, though only a small change, is perhaps not as ideal for catalysis. Donation of a proton by the phosphate to the glycosidic bond thus becomes more difficult and V_{max} decreases. Kinetic studies upon compounds missing O-2 or with fluorine (unable to donate a hydrogen bond *to* phosphate) in place of O-2 oxygen do exhibit a reduced V_{max} over the native substrate (Street, Rupitz & Withers, 1989).

6.4.3 Binding of Phosphate

The series of compounds resembling the proposed oxocarbonium ion phosphorylase transition state, nojirimycin tetrazole, nitroglucal and glucal, show a trend in their ability to bind phosphate at the GP active site. Tetrazole and nitrolgucal are both good, glucal is poor and glucose, a non-transition state analogue, does not bind phosphate to a significant extent. This trend can be linked with the relative electrostatic potential of the atom equivalent to the pyranose ring oxygen (N-1 of tetrazole and O-5 of nitroglucal, glucal and glucose). Referring to Table 6.6 it can be seen that the potential becomes increasingly less positive as the ability to form a complex with phosphate and phosphorylase decreases. This trend is highlighted in the difference in potentials between 'O-5' and C-1. As well as the high negative potential shown by glucose, the preferred conformation of glucose is a full-chair. Nitroglucal, nojirimycin tetrazole and glucal all adopt the half-chair conformation. This allows them to form canonical structures thereby making the electrostatic potential on 'O-5' more positive (Figures 6.2, 6.3 and 2.2).

6.3.4 Covalent Binding of Nitroglucal

A possible explanation for the difference between the kinetic and crystallographic results could be that a reaction requires a protein that is not conformationally restricted. Lattice constraints imposed on the enzyme in the crystal may prevent the protein from achieving a conformation suitable for reaction. Evidence that over the long term a reaction does proceed in the crystals is offered by the observation that crystals soaked for two weeks gave no diffraction. Normally phosphorylase crystals would survive such a soak. It is possible that in reacting with nitroglucal the T and R state crystals become disordered.

6.5 SUMMARY

Although kinetic studies with nitroglucal and chemical modification studies with carbodiimide have pointed towards an important nucleophilic residue at the active site (possibly a carboxylate group), these crystallographic studies have not been able to provide definite confirmation of this group or to establish its identity. Nitroglucal did, however, covalently bind to His 73 at the protein surface but this could not be structurally linked to a deactivation mechanism.

The similarity of nitroglucal to the oxocarbonium ion transition state, despite the lack of a hydroxy group at C-2, proved to be sufficient to bind a phosphate at the GP active site. Glucal was not as good as nitroglucal in creating the phosphate recognition site and from these experiments and those with tetrazole (Chapter 2), it has been shown that the phosphate site becomes increasingly untenable as the electrostatic potential of 'O-5' becomes less positive along the series tetrazole, nitroglucal and glucal.

7 SUMMARY

This work has presented an extensive study of the binding of phosphate at the active site of T and R state phosphorylase. The results have confirmed the findings of previous time resolved studies (Hajdu *et al.*, 1987; Duke, Wakatsuki, Hadfield & Johnson, 1994) and provided new detail of the phosphate binding mode. Unfortunately no clear distinction can be made between the two proposed catalytic mechanisms, the general acid-base and electrophilic, and it is unlikely that they can be distinguished on the basis of crystallographic studies alone. The general acid-base mechanism is, however, enzymatically and chemically aesthetic.

The cryo-crystallographic studies on phosphorylase have extended the resolution of native T state enzyme from 1.9Å to 1.5Å and the model is currently refined to an *R* factor of 22.8%. This is the first time such high resolution data has been collected from an enzyme of this size (94kDA per subunit). From the experimental observations from frozen T state crystals it is clear that it would be possible to collect 1.2Å resolution data. The low resolution, 2.4Å, room temperature study of the GPb-tetrazole-phosphate complex provided conclusive evidence for the location of the phosphate binding site and the high resolution, 1.7Å, low temperature structure has given direct evidence of the phosphate orientation leading to an unprecedentedly detailed view of the active site.

Kinetic work, by Steven Withers and his group in Canada, showed that nitroglucal was a permanent inactivator of phosphorylase. The subsequent crystallographic study failed to locate a covalent bond between nitroglucal and the phosphorylase active site, but did find a surface site where the ligand was covalently linked to His 73. The similarity of nitroglucal (and glucal) to the oxocarbonium ion intermediate of the phosphorylase reaction gave an opportunity to further elucidate the relationship between structure, charge and phosphate binding at the active site. A comparison between the complexes of nojirimycin tetrazole, nitroglucal and

glucal with phosphorylase and phosphate revealed a trend of increasing charge separation between the pyranose ring oxygen and the anomeric carbon with increased ability to bind phosphate. A half-chair conformation was also found to be necessary; glucose itself is unable to bind phosphate.

A subsidiary part of this thesis has been involvement with the ongoing diabetes phosphorylase inhibitor project. The results of two of the GPb-inhibitor complexes are presented in Appendix B. Both of these hydantoin based inhibitors were modelled, on two separate occasions, and both models suggested Inhibitor A to be potentially a good inhibitor. Following the organic synthesis, the kinetic analysis proved it to be the best inhibitor to date (K_i=3μM). A rationalistion of these observations, in terms of hydrogen bond contacts, followed with the structural analysis. Using these structural results a new improved inhibitor is currently being prepared and is awaited with interest.

Part of the cryo-crystallographic work has been recently published (Mitchell & Garman, 1994), papers on the nojirimycin tetrazole and nitroglucal results are in preparation and a paper on the two inhibitors of phosphorylase described in Appendix B has been submitted (Tetrahedron Letters).

SYMBOLS AND ABBREVIATIONS

AMP	Adenosine 5'-monophosphate
AMPS	Adenosine 5'-*O*-thiomonophosphate
ATP	Adenosine 5'-triphosphate
B	Temperature factor
BES	*N*,*N*-Bis[2-hydroxyethyl]-2-aminoethanesulphonic acid
d	Doublet
DAST	Diethylaminosulphur trifluoride
dd	Double doublet
ddd	Double double doublet
dt	Double triplet
DTT	Dithiothreitol
EDTA	Ethylenediaminetetraacetic acid
F_c	Calculated structure factor
F_o	Observed structure factor
Glc	Glucose
GPa and GPb	Glycogen phosphorylase a and b
G5	Maltopentaose
H2P	Heptulose-2-phosphate
IMP	Inosine 5'-monophosphate
J	Coupling constant
k_{cat}	Catalytic rate constant
k_i	Inactivation rate constant
K_i	Inhibition constant
K_m	Michaelis-Menten constant
m	Multiplet
NAD and NADH	Nicotinamide adenine dinucleotide and its reduced form

ncs	Non-crystallographic symmetry
nmr	Nuclear magnetic resonance
nojirimycin tetrazole	(5R,6R,7S,8R)-5,6,7,8-Tetrahydro-5-(hydroxymethyl)pyrido-[1,2-d]tetrazole-6,7,8-triol
PEG	Polyethylene glycol
Ph	Phenyl
P_i	Intracellular phosphate
PLP	Pyridoxal 5'-phosphate
PLPP	Pyridoxal 5'-pyrophosphate
PLPPGlc	Pyridoxal 5'-pyrophosphate glucose
ppm	Parts per million
PUG	D-Gluconhydroximo-1,5-lactone-*N*-phenylurethane
R	Crystallographic R factor: $\Sigma\|\|F_o\|-\|F_c\|\|/\Sigma\|F_o\|$
R_{free}	Free R factor, as above but using percentage of reflections set aside and not used in refinement.
R_{iso}	Mean fractional isomorphous difference of the structure factor amplitudes of the ligand protein complex (F_L) with respect to the native structure factor amplitudes (F_P): $\Sigma_h[\|\|F_L\|-\|F_P\|\|]/\Sigma_h[\|F_P\|]$.
R_m	Merging R factor for symmetry related reflections: $\Sigma_i\Sigma_h[\|I(h)-I_i(h)\|]/\Sigma_i\Sigma_h[I_i(h)]$ where $I_i(h)$ is the ith intensity measurement of reflection h and $I(h)$ is the mean intensity for that reflection.
rms	Root mean square
s	Singlet
SA	Simulated annealing
t	Triplet
tetrazole	(5R,6R,7S,8R)-5,6,7,8-Tetrahydro-5-(hydroxymethyl)pyrido-[1,2-d]tetrazole-6,7,8-triol
UDP	Uridine 5'-diphospho
V_{max}	Maximal velocity of enzymatic reaction

APPENDIX B

B.1 Introduction

As part of an on-going project to find a good inhibitor of glycogen phosphorylase (Martin *et al.*, 1991; Watson *et al.*, 1994) crystallographic studies of two glucose analogues were carried out. This work formed a subsidiary part of the thesis presented here.

The ultimate aim of the phosphorylase inhibitor project is to design a compound with a low K_i, at least three orders of magnitude better than α-D-glucose, which weakly inhibits phosphorylase with a K_i=1.7mM. Such a compound has potential use as a therapeutic agent for regulating glycogen metabolism in *diabetes mellitus* - adult type II diabetes (Watson *et al.*, 1994). Previous work has resulted in the synthesis and analysis, both kinetic and structural, of over fifty compounds based upon glucose. Structural analysis of these GPb-inhibitor complexes has given insight into the interactions favourable for strong binding, and thus strong inhibition. This has led to the best compound to date, which has a beta substituent on the anomeric carbon (C-1) of -NHCOMe (K_i=32μM). The high affinity of phosphorylase for this compound was attributed mainly to one strong hydrogen bond from the NH to O His 377. A water molecule was also displaced from the active site.

Structural analysis of the complex of the β-NHCOMe compound (Watson *et al.*, 1995), and also of the α-CONHMe inhibitor (K_i of 0.16mM, Watson *et al.*, 1994) led to the proposal of an inhibitor combining both anomeric groups: the hydantoin structure (Figure B.1) compounds were modelled and found to fit satisfactorily into the active site. Kinetic studies on the two compounds, inhibitor A and B, by Dr Nikos Oikonomakos and Spyros Zographos (National Hellenic Research Foundation, Greece) found them to have K_i values of 3.1μM and 28μM respectively. The crystallographic analyses of these inhibitors bound to GPb presented here

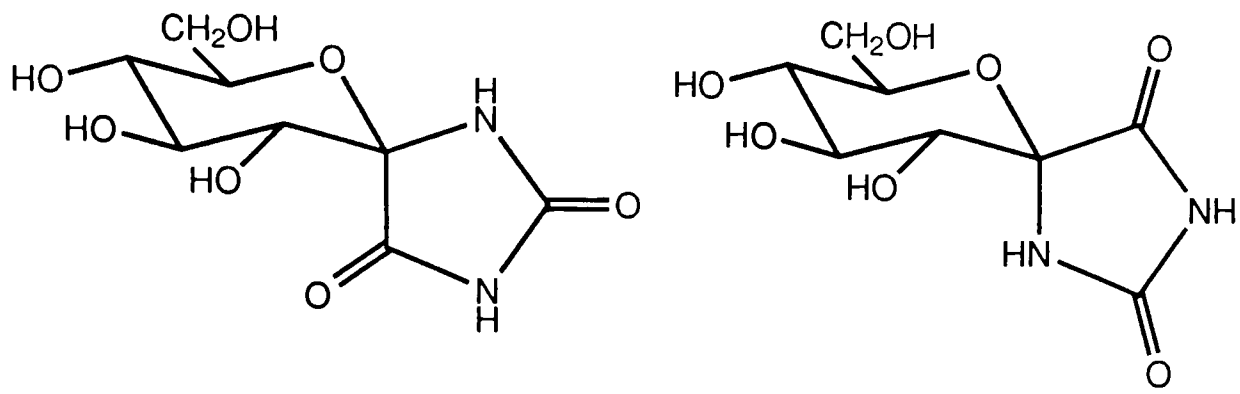

Inhibitor 'A' *Inhibitor 'B'*

Figure B.1. *The two analogues of glucose studied as inhibitors of GPb.*

rationalises the strong inhibitory nature of the compounds.

B.2 Experimental Methods

Crystals of T state phosphorylase b were prepared by Dr Nikos Oikonomakos and his group at the National Hellenic Foundation in Greece. The two inhibitors, (2*R*, 3*S*, 4*S*, 5*R*, 6*S*)-3,4,5-trihydroxy-2-(hydroxymethyl)-7,9-diaza-1-oxaspiro[5,4]decane-8,10-dione (inhibitor A) and (2*R*, 3*S*, 4*S*, 5*R*, 6*R*)-3,4,5-trihydroxy-2-(hydroxymethyl)-7,9-diaza-1-oxaspiro[5,4]decane-8,10-dione (inhibitor B) shown in Figure B.1, were prepared by Claire Bichard and Dr George Fleet of the Dyson Perrins Laboratory in Oxford (Bichard, 1994).

The T state crystals were prepared for data collection by soaking for 2 hours in a BES buffer containing 100mM concentration of the inhibitor (10mM BES, 0.1mM EDTA, 0.02% sodium azide, pH 6.7). Data from the crystals, which were mounted in thin glass capillaries, were collected using the in-house system as described in Chapter 2, Section 2.2.2. Data processing to produce unique sets of reflections was performed using the program XDS (Kabsch, 1993).

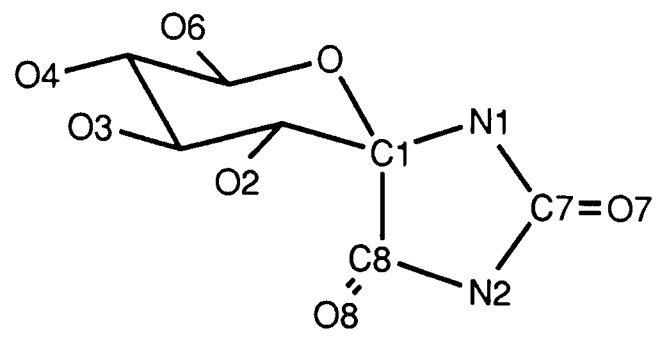

Figure B.2. Atom numbering scheme used for Inhibitor A.

B.3 Results and Discussion

(i) Data Processing and Refinement. The statistics for data collection and refinement of the two models are shown in Table B.1. Difference Fourier maps, using (F_o-F_c) coefficients where F_c and phases were taken from the native T state structure (Acharya, Stuart, Varvill & Johnson, 1991), were calculated. Both maps indicated inhibitor binding at the active site (Figure C.2). The Fourier maps also indicated movement of the side chain of His 377 and suggested some main chain changes of the residue, in particular of the main chain oxygen atom. A conformation change of Asn 284 was also indicated, with movement of the side chain away from the inhibitors. The Fourier map of the GPb-inhibitor B complex was poorly defined at the catalytic binding site. Evidence in the map suggested that perhaps a mixture of inhibitor A and B was bound. Nonetheless, refinement of both complexes continued with the appropriate inhibitor model, generated using the program SYBYL (Tripos Associates), fitted to the Fourier map density at the active site.

Refinement of the models, with the initial protein model taken from the refined coordinates of the GPb-glucose complex (Martin, Johnson & Withers, 1990) containing ligand and water molecules, proceeded using the protocol outlined below. Firstly, least squares positional refinement (200 cycles, tolerance 0.05Å) was followed by individual *B* factor refinement (40 cycles, target standard deviations of 1.5 and 2.0Å^2 for bonded atoms and atoms bound to the

		Inhibitor Complex	
		'A'	'B'
Data Collection			
Number of Reflections	Unique	31588	29616
	Measured	73869	74699
Completeness of Data (2.4Å) (%)		80	76
R_m (%)		7.4	10.5
Number of Reflections I/σ > 3		15141	13949
R_{iso} [a] (%)		11.7	17.2
Structural Refinement			
Number of Atoms	Protein	6774	6774
	Ligand	17	15
Number of Waters		575	575
Number of Reflections (8.0-2.3Å) I>0		30696	29228
R Factor	Initial (%)	23.6	29.5
	Final (%)	17.7	17.9
RMS Deviation	Bond Lengths (Å)	0.007	0.007
	Bond Angles (°)	1.4	1.4

[a] R_{iso} calculated with respect to the native T state data (Acharya, Stuart, Varvill & Johnson, 1991).

Table B.1. *The statistics of data collection, processing and refinement for the two T state GPb inhibitor complexes.*

same atom respectively). These models were then subjected to simulated annealing where each structure was heated to 2000K and then allowed to cool to 300K with a timestep of 2.5fs. Finally the protocol finished with another round of positional (100 cycles) and individual *B* factor (40 cycles) refinement. Fourier difference maps, using SIGMAA weighted ($2F_o$-F_c) coefficients (Read, 1986), were calculated using the refined structures and inspected for fit of the model to electron density.

(ii) X-PLOR Refined Stuctures. The statistics for refinement of the two structures are shown in Table B.2. The actual standard deviations of *B* factors for the complexes were approximately 3.3Å^2 and 5.1Å^2 for bonded atoms and atoms bound to the same atom respectively. The refinement of the complexes went well and the model of the GPb-inhibitor A complex correlated well with the ($2F_o$-F_c) Fourier difference map. The map from the GPb-inhibitor B complex was not of such good quality though. The inconsistency observed in the initial difference Fourier map was still apparent in the final Fourier map. This was traced to poor chromatographic separation of the two inhibitors during chemical synthesis leading to contamination of one inhibitor in the sample of the other. With a ten fold smaller K_i, inhibitor A was not affected by contamination by inhibitor B. However, inhibitor B with a higher K_i and up to 20% contaminant (nmr analysis) was affected and the results of the kinetic and crystallographic analyses were biased by inhibitor A. Thus the K_i of inhibitor B could in reality be far higher than the 28μM observed and the inconsistency of the difference Fourier maps does arise from a mixture of the two inhibitors being bound at the active site. A pure sample of inhibitor B for kinetic and structural analysis is currently being prepared.

The results of the structural study on the GPb-inhibitor A complex do explain the higher affinity of phosphorylase for the hydantoin inhibitor. The hydrogen bond formed by the β-NHCOME compound (Watson *et al.*, 1995) from N-H to O His 377 is also made by inhibitor A (Table C.2). Additionally, hydrogen bonds are made from O-7 to WAT 847 (2.8Å) and from

Ligand Atom	Protein Atom	Length of Hydrogen Bond Contact (Å)	
		Inhibitor A	β-NHCOMe
N-1	O His 377	2.9	2.9
O-7	WAT 847	2.8	-
O-8	WAT 872	2.8	-

Table B.2. *The hydrogen bonds made by the anomeric substituents of inhibitor A and the previous best compound.*

O-8 to WAT 897 (2.8Å, Figure B.3a and b). Water 897 goes onto contact Asp 283 and thus may help in stabilising the T state form of the enzyme. This is significant for any potential use of the inhibitors as diabetic drugs (Watson *et al.*, 1994). Only N-2 does not make any hydrogen bonds, but is located in a favourable electrostatic environment, being just 4Å away from the acidic side chain of Asp 283.

The water structure of the active site was, on the whole, maintained. The exceptions to this being water molecules close to the hydantoin ring: WAT 847, which for the β-NHCOMe inhibitor was displaced, is retained and waters 890 and 887 are less tightly bound in the complex than the native structure. A further change in structure is the position of Asn 284. The side chain of this residue shifts by almost 1Å away from the bulk of C7, O7 and N2 of the inhibitor. This alteration is echoed in smaller shifts of the remaining residues of the 280s loop.

In summary the additional two hydrogen bonds formed by O-7 and O-8 with the favourable electrostatic interaction of N-2 with Asp 283, though slightly offset by the retainment of WAT 847, leads to the ten fold decrease observed in the K_i value of inhibitor A over the β-NHCOMe compound.

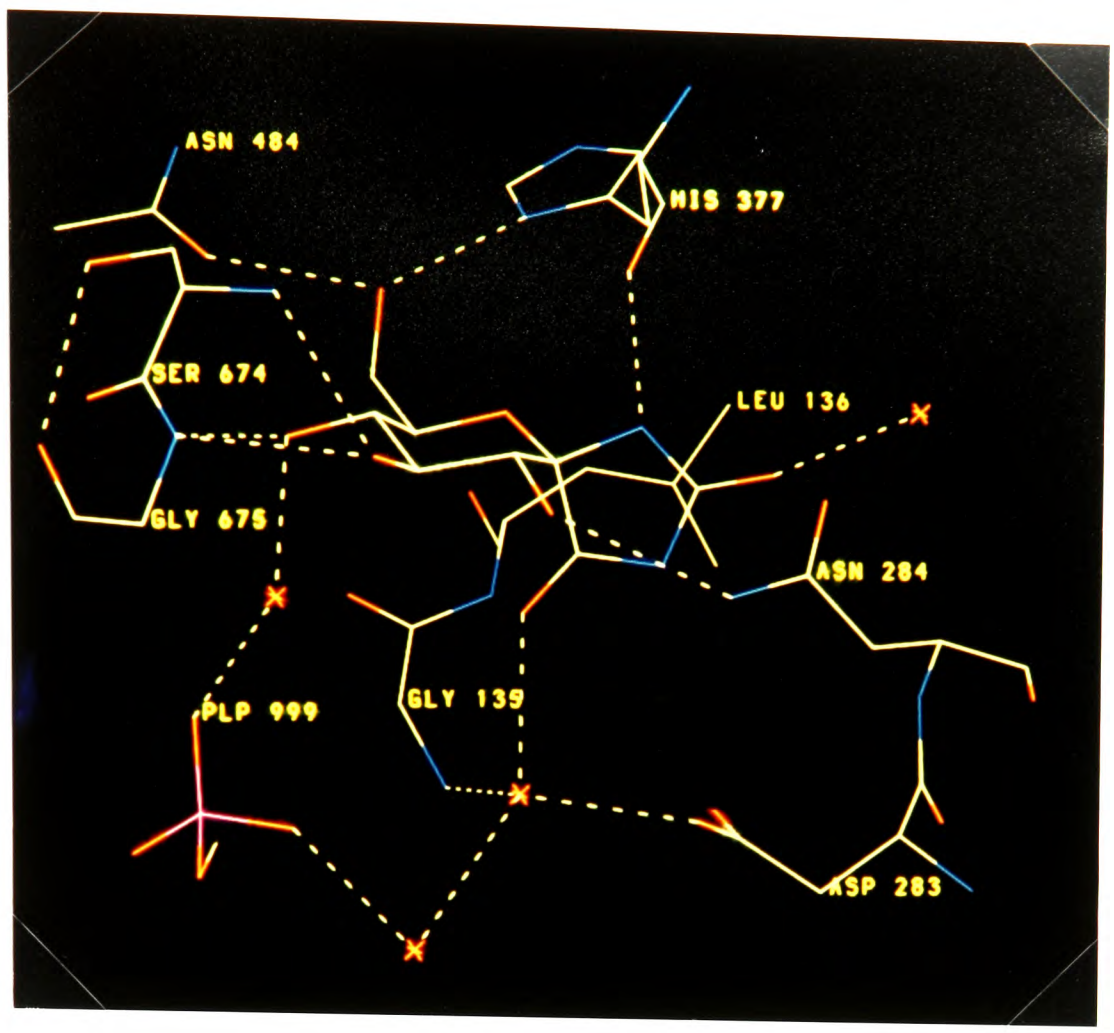

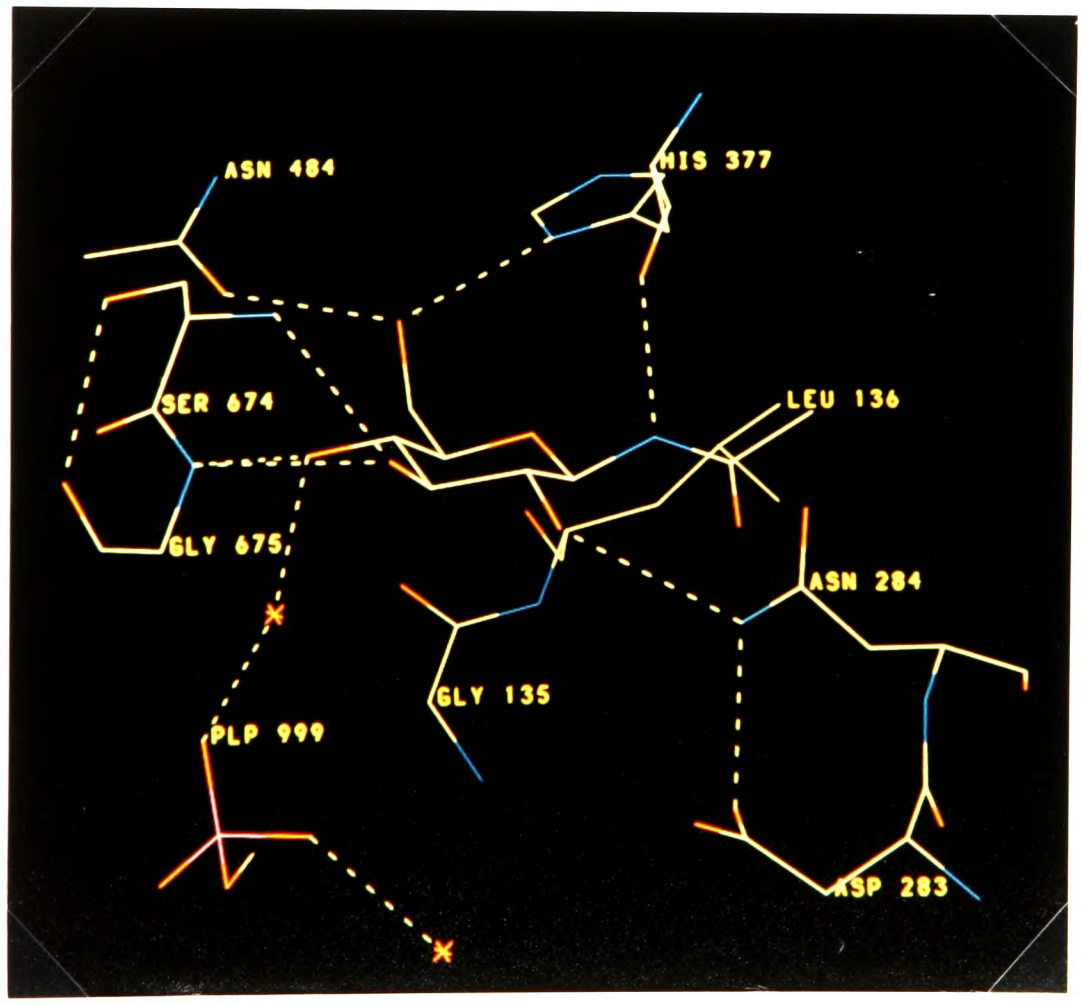

Figure B.3a and B.3b. *The refined structures of GPb complexed with inhibitor A (top) and with the previous best inhibitor, the β-NHCOMe compound (bottom).*

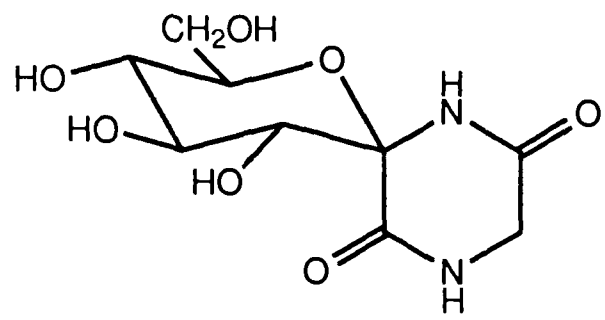

Figure B.4. *Diagram of the proposed new inhibitor C.*

Modelling work based upon the results from the GPb-inhibitor A complex suggests a design for a new inhibitor, inhibitor C (Figure B.4). All four polar groups of this inhibitor could form hydrogen bonds to the enzyme. The additional methylene group in the hydantoin ring allows N-2, previously not able to make a contact, to contact WAT 872 and also be placed closer to Asp 283 (3.5Å). The atom O-8 could make two hydrogen bonds, both to water molecules, whilst the hydrogen bonds from N-1 and O-7 can be maintained. The total number of contacts would be five, with N-2 in closer contact with Asp 283. The only drawback could be a poor contact of the methylene group to the side chain of Asn 284. However, as has been observed with inhibitor A this side chain is flexible and could move away to accommodate the new inhibitor.

The synthesis of the new proposed inhibitor is currently in progress. It is hoped the new compound will have a significantly lower K_i than the best inhibitor to date, inhibitor A.

APPENDIX C

C.1 Experimental procedures for the synthesis of 4-fluoro-4-deoxy-D-glucose (3)

The purity of all compounds was determined by nmr spectroscopy. Methyl α-D-galactopyranoside was obtained from the Sigma Chemical Company. The methods are taken from Reist, Spencer, Calkins, Baker & Goodman (1965), protection of methyl α-D-galactopyranoside, and from Withers, MacLennan & Street (1986) for the remaining compounds.

(i) Methyl 2,3,6-tri-O-benzoyl-α-D-galactopyranoside (1)

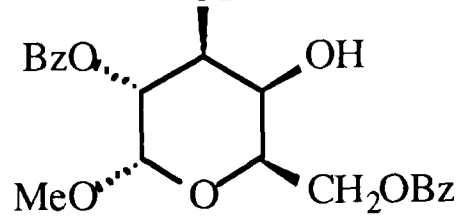

A solution of methyl α-D-galactopyranoside (9.75g, 0.05 mol) in dry pyridine (100ml) was cooled to 0°C, then benzoyl chloride (20ml) was added dropwise with stirring. The mixture was left at room temperature, with stirring, for 3 days. The excess benzoyl chloride was then destroyed by dropwise addition of the reaction mixture to ice-cold saturated aqueous sodium bicarbonate (500ml) with stirring. The aqueous mixture was extracted with chloroform (300ml) and the chloroform layer washed with 1M sulphuric acid (2 x 300ml), followed with water (2 x 150ml), dried, then evaporated *in vacuo* to give (**1**) as a crude white solid. Recrystallisation from methanol gave 15.9g (63%) of (**1**).

^{1}H n.m.r. data (500MHz, $CDCl_3$): δ 8.06 - 7.98 (6H, m, Ph), 7.59 - 7.35 (9H, m, Ph), 5.77 (1H, dd, $J_{2,3}$ 10.7 $J_{3,4}$ 3.1 Hz, H-3), 5.71 (1H, dd, $J_{2,3}$ 10.7 $J_{1,2}$ 3.6 Hz, H-2), 5.23 (1H, d, $J_{1,2}$ 3.6 Hz,

H-1), 4.69 (1H, dd, $J_{6,6'}$ 11.5 $J_{5,6}$ 5.8 Hz, H-6), 4.59 (1H, dd, $J_{6,6'}$ 11.5 $J_{5,6'}$ 6.9 Hz, H-6'), 4.43 (1H, dd, $J_{4,5}$ 6.3 $J_{3,4}$ 3.1 Hz, H-4), 4.38 - 4.36 (1H, m, H-5), 3.46 (3H, s, OMe).

(ii) Methyl 2,3,6-tri-O-benzoyl-4-deoxy-4-fluoro-α-D-glucopyranoside (2)

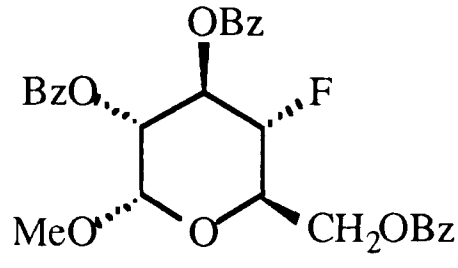

Methyl 2,3,6-tri-O-benzoyl-α-D-galactopyranoside (**1**) (2g, 0.4mmol) and 4-(dimethyl-amino)pyridine (0.98g, 0.8mmol) were dissolved in anhydrous dichloromethane (30ml) cooled to -20°C, and DAST, diethylamino sulphur trifluoride, (1.28ml, 0.6mmol) was slowly added during 15 minutes to the stirred solution under a nitrogen atmosphere. The mixture was slowly warmed to room temperature and after 24 hours cooled to 0°C and methanol (10ml) added to decompose the excess or reagents. The solution was evaporated *in vacuo*, and the resulting yellow oil purified by column chromatography on silica gel, using 19:1 dichloromethane-ethyl acetate. Recrystallisation from ethanol yielded (**2**) (0.90g, 45%). ^{1}H n.m.r. data (500MHz, $CDCl_3$): δ 7.98 - 8.12 (6H, m, Ph), 7.37 - 7.63 (9H, m, Ph), 6.14 (1H, dt, $J_{3,F}$ 14.0 $J_{2,3}$ 9.5 $J_{3,4}$ 9.5 Hz, H-3), 5.21 (1H, dd, $J_{2,3}$ 9.5 $J_{1,2}$ 3.5 Hz, H-2), 5.18 (1H, t, $J_{1,F}$ 3.5 $J_{1,2}$ 3.5 Hz, H-1), 4.77 (1H, dt, $J_{4,F}$ 50.9 $J_{3,4}$ 9.5 $J_{4,5}$ 9.5 Hz, H-4), 4.73 (1H, dt, $J_{6,6'}$ 12.3 $J_{5,6}$ 2.0 J 2.0 Hz, H-6'), 4.63 (1H, dd, $J_{6,6'}$ 12.3 $J_{5,6}$ 4.5 Hz, H-6), 4.31 - 4.36 (1H, m, H-5) p.p.m. ^{19}F n.m.r. data (400MHz, $CDCl_3$): δ 200.4 (dd, $J_{F,4}$ 50.9 $J_{F,3}$ 14.0 Hz) p.p.m.

(iii) 4-Deoxy-4-fluoro-D-glucopyranoside (3)

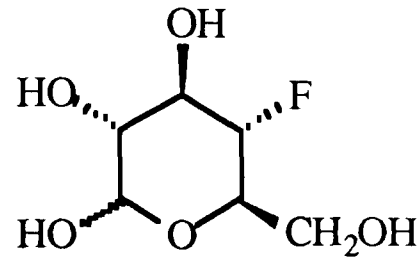

To a suspension of methyl 2,3,6-tri-O-benzoyl-4-deoxy-4-fluoro-α-D-glucopyranoside (**2**) (4.0g) in absolute methanol (16ml) was added M NaOMe in methanol (1.8ml), and the mixture was stirred for 18 hours at room temperature. The base was neutralised with Dowex 50W-X8 (H^+) resin, the suspension filtered, the filtrate concentrated *in vacuo* and the concentrate eluted from a column of silica gel using 9:1 ethyl acetate-acetone, recrystallisation from 1:1 ethyl acetate-acetone then yielded methyl 4-deoxy-4-fluoro-α-D-glucopyranoside (**3**) (1.16g, 75%).

Final deprotection to (**3**) was performed with a solution of methyl 4-deoxy-4-fluoro-α-D-glucopyranoside (0.40g, 0.2mmol) in water (40ml) containing Dowex 50W-X8 (H^+) ion-exchange resin (20ml). This mixture was heated at reflux, with stirring, for 25 hours. After cooling, filtering, and evaporating, the resultant gum crystallised, to yield impure (**9**) (0.35g, 90%).

C.2 Purification of (3) obtained in (iii) above

In order to purify the 4-fluro-4-deoxy-glucose obtained above, two additional synthetic steps were included as below.

(i) 1,2,3,6-Aceto-4-fluoro-4-deoxy-D-glucopyranoside (4)

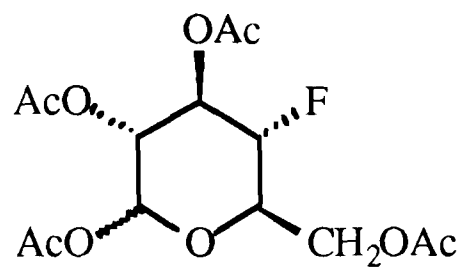

A mixture of crude 4-deoxy-4-fluoro-D-glucopyranoside (**3**) (0.580g, 3.2mmol) and acetic anhydride (12ml, 10 fold excess) were stirred at room temperature in dry pyridine (30ml) for 24 hours. The reaction was quenched with ice-cold methanol (10ml). The resulting mixture was evaporated *in vacuo*, redisssolved in chloroform (20ml) and partitioned against 2M HCl. The organic layer was washed with brine, dried and the solvent removed *in vacuo*. The resulting solid was purified by column chromatography (silica gel) using 1:1 ethyl acetate-petrol ether to give the protected product (0.407g).

^{1}H n.m.r.data (500MHz, $CDCl_3$): δ 5.71 (1H, d, $J_{1,2}$ 8.3 Hz, H-1), 5.35 (1H, dt, $J_{3,F}$ 14.9 $J_{2,3}$ 9.0 $J_{3,4}$ 9.0 Hz, H-3), 5.05 (1H, t, $J_{1,2}$ 9.0 $J_{2,3}$ 9.0 Hz, H-2), 4.49 (1H, dt, $J_{4,F}$ 50.5 $J_{3,4}$ 9.0 $J_{4,5}$ 9.0, H-4), 4.36 (1H, dt, $J_{6,6'}$ 12.4 J' 2.0 Hz, H-6), 4.22 (1H, ddd, $J_{6,6'}$ 12.4 J' 4.8 J'' 1.5 Hz, H-6'), 3.87 (1H, m, H-5), 2.07 (3H, s, OMe), 2.06 (3H, s, OMe), 2.05 (3H, s, OMe), 2.00 (3H, s, OMe) p.p.m.

(ii) 4-Deoxy-4-fluoro-D-glucopyranoside (3)

A suspension of 1,2,3,6-aceto-4-fluoro-4-deoxy-D-glucopyranoside (**4**) (0.300g) in absolute methanol (10ml) and NaOMe (as a solution in methanol, 0.12ml of 120mg Na in 15ml dry methanol) added. The mixture was stirred at room temperature under a nitrogen atmosphere for 3 hours. Dowex 50W-X8 (H^+) resin was added to bring the pH to 7.0 (indicator paper) and the mixture filtered. Evaporation of the solvent *in vacuo* gave (**3**) as a crude white solid. Purification by column chromatography (silica gel, 7:2:1 ethyl acetate-ethanol-water) and

recrystallisation (MeOH) gave the final pure product (**3**) as a white crystalline solid (0.150g, 96%).

α- Anomer. ^{1}H n.m.r. data (500MHz, D_2O): δ 5.26 (1H, t, $J_{1,2}$ 3.5 $J_{1,F}$ 3.5 Hz, H-1), 4.36 (1H, dt, $J_{4,F}$ 50.9 $J_{3,4}$ 9.3 $J_{4,5}$ 9.3 Hz, H-4), 3.70 - 4.07 (4H, m, H-3, H-5, H-6, H-6'), 3.60 (1H, dd, $J_{1,2}$ 3.5 $J_{2,3}$ 10.0 Hz, H-2) p.p.m. ^{19}F n.m.r. data (400MHz, D_2O): δ 200.3 (dd, $J_{F,4}$ 50.9 $J'_{F,3}$ 16.0) p.p.m.

β-Anomer. ^{1}H n.m.r. data (500MHz, D_2O): 4.72 (1H, dd, $J_{1,2}$ 8.0 $J_{1,F}$ 0.9, H1), 4.36 (1H, dt, $J_{4,F}$ 50.9 $J_{3,4}$ 9.3 $J_{4,5}$ 9.3 Hz, H-4), 3.70 - 4.07 (4H, m, H-3, H-5, H-6, H-6'), 3.32 (1H, t, $J_{1,2}$ 8.0 $J_{2,3}$ 8.0, H-2) p.p.m. ^{19}F n.m.r. data (400MHz, D_2O): δ 202.3 (dd, $J_{F,4}$ 50.9 $J_{F,3}$ 15.0) p.p.m.

APPENDIX D

Fundamentals of Protein Crystallography

Protein crystallography is concerned with the determination of the macromolecular structure by making use of the interaction of X-ray radiation with a crystal of the macromolecule.

A crystal is made up from an array of a single repeating unit arranged on a regular, ordered three-dimensional grid of points termed the lattice. The repeating unit, the unit cell, has dimensions of a, b and c and angles of α, β and γ. The unit cell contains one or more copies of the macromolecule and one or more copies of the asymmetric unit (the smallest repeating unit).

The interaction of X-rays with the crystal can be understood in terms of the radiation being reflected from planes passing through the crystal lattice. Bragg's Law predicts the angle of diffraction from the lattice planes:

$$n\lambda = 2d\sin\theta$$

where: n is an integer indicating the order of the reflection

λ is the X-ray wavelength

d is the inter-plane spacing

θ is the angle of diffraction from the plane.

The Bragg equation does not predict the intensity of a given reflection, which is proportional to the structure factor of the reflection $\mathbf{F}(h,k,l)$.

$$\mathbf{F}(h,k,l) = \sum_j f_j \exp\{2\pi i(hx_j + ky_j + lz_j)\}$$

where: f_j is the atomic scattering factor of the j^{th} atom

(x_j, y_j, z_j) are the coordinates of the jth atom expressed as fractions of the unit cell.

In practice crystals are not perfect, the atoms are subject to thermal motion, and the atomic scattering factors, which do assume the atoms to be at rest, must be adjusted by an exponential factor termed the *B* factor or temperature factor:

$$\exp\left(\frac{-B\sin^2\theta}{\lambda^2}\right)$$

where: $B = \frac{8}{3}\pi^2 u^2$

u^2 is the mean square displacement of the atom from its equilibrium position.

The Fourier transform of the structure factor equation, **F**(h,k,l), is the electron density ρ(x,y,z):

$$\rho(x,y,z) = \frac{1}{V}\sum_h\sum_k\sum_l \mathbf{F}(h,k,l)\exp\alpha(h,k,l)\exp\{-2\pi i(hx+ky+lz)\}$$

Knowing the amplitude and phase α for all reflections (h,k,l) allows the electron density ρ to be calculated for all points in the unit cell (x,y,z) and thus the structure can be determined. The summation is usually truncated over a finite number of terms since it is impossible to collect data for all reflections.

APPENDIX E

1070

FAST COMMUNICATIONS

Contributions intended for this section should be submitted to any of the Co-editors of Journal of Applied Crystallography. *In the letter accompanying the submission, authors should state why rapid publication is essential. The paper should not exceed two printed pages (about* 2000 *words or eight pages of double-spaced typescript including tables and figures) and figures should be clearly lettered. If the paper is available on 5.25″ IBM PC compatible or 3.5″ Apple/Macintosh diskettes, it would be helpful if these could be sent with the manuscript together with details of the word-processing package used. Papers not judged suitable for this section will be considered for publication in the appropriate section of* Journal of Applied Crystallography.

J. Appl. Cryst. (1994). **27**, 1070–1074

Flash freezing of protein crystals: investigation of mosaic spread and diffraction limit with variation of cryoprotectant concentration

BY EDWARD P. MITCHELL AND ELSPETH F. GARMAN

Laboratory of Molecular Biophysics, The Rex Richards Building, South Parks Road, Oxford OX1 3QU, England

(*Received* 23 *June* 1994; *accepted* 22 *July* 1994)

Abstract. The effect of a cryoprotectant (glycerol) upon the mosaicity of flash-frozen T-state glycogen phosphorylase b crystals has been investigated. Glycerol concentration in a buffered solution was varied between 0 and 70% *v/v*. The results show that there is a well defined optimum in glycerol concentration giving lowest mosaicity, maximum resolution and no ice formation. The results also demonstrate how flash-freezing conditions can be systematically determined in-house using a minimum number of crystals and before using synchrotron time.

Introduction. Flash-frozen crystals are increasingly being used to collect X-ray diffraction data from macromolecules. The technique prolongs the useful crystal lifetime in the X-ray beam so that a complete data set can be collected from a single crystal. This is a great advantage, since it is then unnecessary to merge data from different crystals, obviating scaling problems and resulting in better-quality data. The method involves transfer of the crystal to, or cocrystallization of the protein in, a cryoprotectant (Petsko, 1975). The crystal is then suspended in a small (less than 1 mm diameter) loop of fibre (Teng, 1990), where it is supported by a liquid film of cryoprotected buffer and flash frozen in a stream of cold (80–120 K) nitrogen gas. The cryoprotectant film freezes as an amorphous glass with no ordered water present.

The choice of cryoprotectant is dependent on the protein and its crystallization conditions. Typical cryoprotectants recommended are glycerol, ethylene glycol and PEG (polyethylene glycol) (Petsko, 1975; Hope *et al.*, 1989; Gamblin & Rodgers, 1993). In a brief survey of recently published structures where cryoprotectants were used, it was found that glycerol (Guo *et al.*, 1992; Lee *et al.*, 1994) and ethylene glycol (Freymann *et al.*, 1990; Rini, Schulze-Gahmen & Wilson, 1992) were both used twice, PEG (Ellenberger, Brandl, Struhl & Harrison, 1992) was used once and a glycerol/PEG mixture (Nikolov *et al.*, 1992) was used once.

Data from protein crystals are increasingly collected at synchrotron X-ray sources where time is limited. It is therefore important to determine the best cryoprotectant concentration and crystal soaking time beforehand. These should be chosen to optimize the diffraction limit and to give as low a mosaicity as possible. For data collection on an image plate, a high mosaic spread necessitates the use of a smaller oscillation angle to avoid overlapping spots, which results in a higher proportion of partially measured reflections and implies poorer data.

This paper describes the effect of a cryoprotectant, in this case glycerol, upon the mosaicity and diffraction limit of T-state glycogen phosphorylase b (GPb) crystals, and shows that there is a well defined optimum glycerol concentration for flash freezing these crystals. The results of this systematic study may be useful in determining flash-freezing conditions for other protein crystals.

Experimental. T-state GPb crystals ($P4_32_12$, $a = b = 128.5$, $c = 116.3$ Å) were grown as described previously (Oikonomakos, Melpidou & Johnson, 1985; Johnson, Madsen, Mosley & Wilson, 1974) from a buffer solution of 1.1×10^{-3} *M* IMP (inosine-5′-phosphate), 1.1×10^{-3} *M* spermine, 10^{-2} *M* *N*,*N*-bis(2-hydroxyethyl)-2-aminoethanesulfonic acid (BES), 2.9×10^{-3} *M* dithiothreitol and 10^{-4} *M* ethylenediaminetetraacetic acid (EDTA) at pH 6.7. Prior to data collection, crystals (between 0.2 and 0.3 mm in the largest dimension) were soaked for 5 min in a BES buffer solution containing glycerol concentrations from 0 to 70% *v/v* (10^{-2} *M* BES, 10^{-4} *M* EDTA, 0.02% sodium azide, pH 6.7). Previous tests with other possible

cryoprotectants had shown glycerol to be the most suitable candidate. At glycerol concentrations of 60 and 70%, the cryoprotected buffer was gently stirred after the crystal had been placed in to soak. For comparison, the following additional soaks were also carried out: 20 min and 2.5 h in 50% glycerol, sequential soaking for a total of 5 min in 10, 30 and 50% glycerol, 60% glycerol with no stirring and 60% glycerol for 20 min.

After the soaking, an Oxford Cryostream cooling device operating with nitrogen gas at 100 K was used to flash freeze the crystals and maintain this state during data collection. Transfer time from cryoprotected buffer to flash freezing was as short as possible and always less than 2 s. Precentring of the cryostream, before mounting the crystals, was vital to ensure the crystal was positioned in the coldest region of the nitrogen stream and not inadvertantly moved into a warmer part when it was already frozen and being centred at the beam position. Since the whole technique can fail if the stream is inaccurately centred, a special attachment, shown in Fig. 1, was designed to ensure foolproof centring. Centring of the Cryostream, using the attachment, was aided by mounting the coldhead on a system of screw adjusters allowing fine movements. It is also important to minimize air turbulence in the radiation housing and a plastic sheeting enclosure around the whole experiment is effective to this end. The Oxford Cryostream cooling device provides a dry (dew point 213 K) room-temperature air stream coaxially with the cold nitrogen stream. The flow rate of dry air is matched to that of the cold nitrogen gas. This cuts down turbulence between them, thus preventing the ingress of warm moist air, which could cause ice build up around the crystal. The thin-film loop method of mounting crystals developed by Teng (1990) was used. The loop, also precentred, was made out of a single strand of angora wool, used for its very high strength/weight ratio. It was mounted in a metal pin fixed to a steel button, held by a magnet on to the goniometer head. The metal pin provides a thermally conducting path across the cold nitrogen/warm dry air boundary, and this significantly reduces frost build up as compared with use of a nonconducting pin material.

Data were collected on a Siemens area detector mounted on a monochromatized Rigaku RU-200H rotating-anode X-ray source, operating between powers of 50 kV and 50 mA and 60 kV and 70 mA. The detector was placed 16 cm away from the crystal and at a swing angle of either 0° (maximum resolution 4.9 Å) or 22° (maximum resolution 2.3 Å). For each crystal, at least 15 data frames of 0.2° oscillation width each were collected, with exposure times of between 120 and 240 s. In the optimum cryoprotectant conditions (a glycerol concentration of 50%), data sets from two crystals were collected and subsequently processed [using the *XDS* package (Kabsch, 1993)] in order to check the unit-cell size and data quality.

Full widths at half-maxima of the reflection rocking curves as a function of oscillation angle were extracted using the program *OSCIL* (W. Minor, private communication). Reflections for these measurements were chosen so that the entire profile was contained within the total angular range over which data had been collected.

Results and discussion. By the above experimental technique, the mosaicities of three different crystals were measured for each glycerol concentration investigated. The results are summarized in Figure 2.

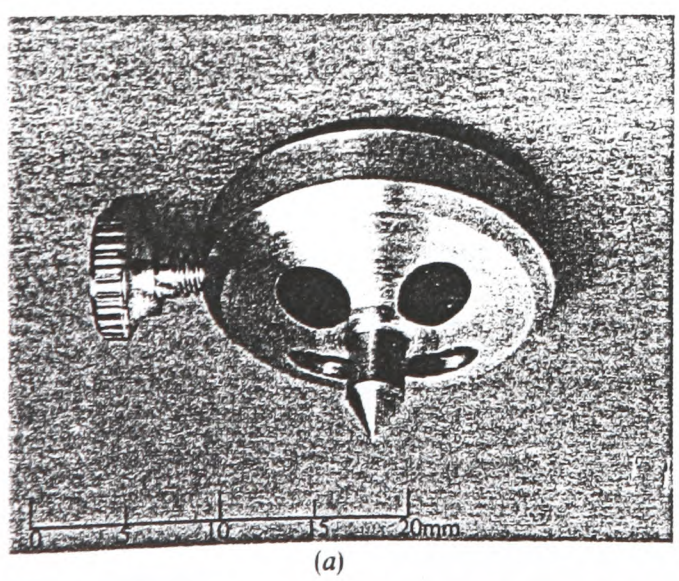

(*a*)

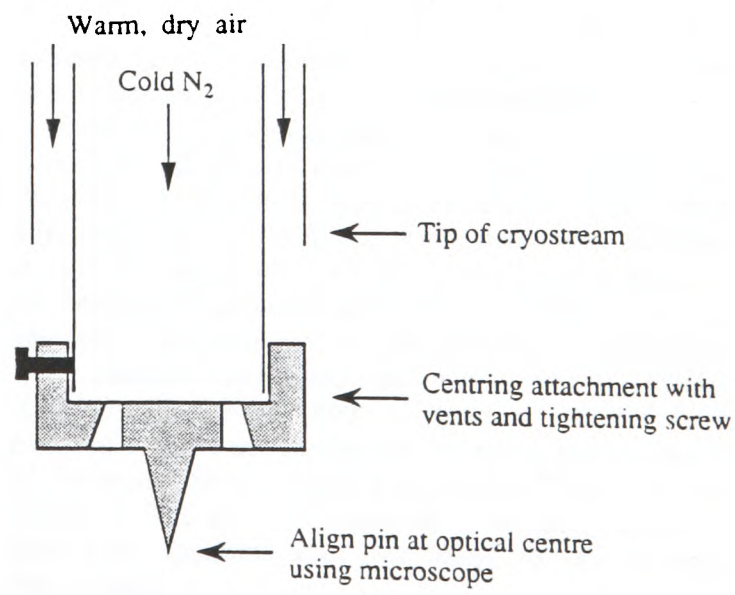

(*b*)

Fig. 1. (*a*) Photograph and (*b*) schematic diagram of the centring attachment. It consists of a collar that is held onto the cold nitrogen nozzle by a tightening screw. A pin below the centre of the collar allows centring, before crystals are mounted, of the cryostream with the X-ray beam position, using a microscope. Slots were drilled around the pin to enable cold nitrogen gas to escape and avoid back pressure on the cold stream during alignment. A stainless-steel metal with a low thermal-expansion coefficient was chosen since the prototype, made of brass, contracted too much when on the nozzle.

There are two parameters to consider in optimizing X-ray data quality from flash-frozen crystals: the diffraction limit of the crystals and their mosaic spread. In the present work, the maximum resolution obtained improved as the glycerol concentration was increased to 50% and then unexpectedly worsened at 60 and 70%. At 50% glycerol, the resolution of 2.9 Å was lower than the 2.3 Å normally observed in room-temperature data collection from large GPb crystals. This difference was due to the smaller crystals and low counting times used for the comparative freezing experiments, shown in Fig. 2. With a longer exposure, 2.3 Å diffraction was observed at 50% glycerol concentration. The mosaicity followed the same general trend as the resolution, dropping as the percentage of glycerol was increased, reaching a minimum at 50% glycerol and then rising as the glycerol concentration in the soak buffer was raised further (Fig. 2). The lowest mosaicity attained was 0.25°, which compares well with the 0.25–0.30° observed for T-state GPb crystals at room temperature (measured using the same X-ray optics). At 60 and 70% glycerol, the cryoprotected buffer became viscous and consequently was gently stirred to ensure good mixing of the crystal with the cryoprotectant. However, a trial with 60% glycerol where the crystal was soaked in buffer without stirring showed the mosaicity to be similar to that with the stirred buffer. Another trial of a 20 min soak in 60% glycerol with stirring showed no improvement over the 60% glycerol 5 min soak. As the concentration of glycerol is increased, bulk mother liquor is replaced by cryoprotectant, which better tolerates the flash freezing. Perhaps, as the concentration is raised above 50%, the viscosity of the buffer becomes so high that glycerol cannot diffuse into the crystal within a reasonable time, and upon flash freezing unreplaced water freezes as crystals, thus causing high mosaicity. Sequential soaks for an overall time of 5 min in 10, 30 and 50% glycerol gave indistinguishable results to the 50%-alone soak but, since they involved more crystal handling, were not pursued. A soak of 20 min in 50% glycerol gave results similar to the 5 min soak, whereas a 2.5 h soak made both the resolution and mosaicity worse. These tests showed that longer soaking times would not improve our optimum conditions.

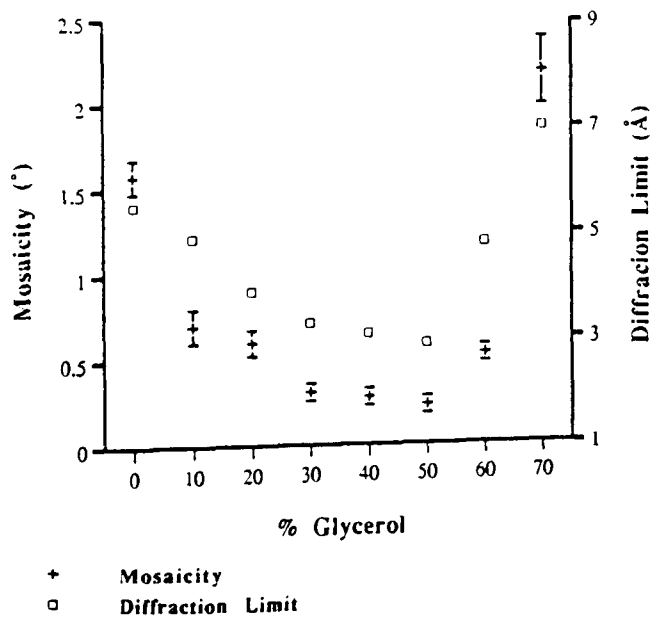

Fig. 2. Variation of mosaicity and diffraction limit of GPb crystals with percentage of glycerol in the buffer. The error bars represent statistical counting errors only.

At low glycerol concentrations (0 and 10%), the buffer solution did not freeze as a glass but instead produced an opaque solid containing ice. Strong ice diffraction rings were observed on the images (Fig. 3*a*). At 30% glycerol, the ice diffraction became less apparent, and it was not detectable at all at 40% glycerol and above (Fig. 3*b*). In order to ensure efficient data collection from a flash-frozen crystal at a synchrotron source, it is vital to determine the conditions as well as possible beforehand. From in-house resources, a suitable starting cryoprotectant for a particular protein buffer can be found without waste of any crystals. A poor cryoprotectant mixture will freeze to an opaque solid and give strong ice diffraction, whereas a potential cryoprotectant mixture will freeze to a clear glass and give no ice diffraction. However, satisfying this condition will not necessarily give an ideal cryoprotectant: experiments using crystals are required to fine tune the concentration of cryoprotectant and soaking times to give the lowest mosaicity and highest resolution.

From these results, a 5 min soak in 50% glycerol was the obvious choice for the cryoprotectant conditions, since both mosaicity and diffraction limit were optimized. The unit cell of frozen GPb crystals, soaked in 50% glycerol, was found to be $a = b = 126.7$ Å and $c = 115.6$ Å. This corresponds to approximate shrinkages of 1.4% on a and b and 0.6% on c and an overall volume decrease of 3.4% compared with native crystals from which data were collected at room temperature.

Under these optimum flash-freezing conditions, a T-state GPb data set was collected on station PX9.6 at the Daresbury Synchrotron Radiation Source. The crystal diffracted well to 1.8 Å and some data were collected at 1.65 Å. During the 5.5 h the crystal was exposed to the beam, no significant deterioration in diffraction was apparent. The statistics on the processed data, which were indexed, integrated and scaled using *DENZO* (Otwinowski, 1993), show a significant improvement over the original native data set (Acharya, Stuart, Varvill & Johnson, 1991) collected at station PX9.6 on film (Table 1). The unit cell measured using the synchrotron data was consistent with that found for the in-house frozen data.

Concluding remarks. The freezing experiments with glycerol cryoprotectant on GPb crystals show that as the glycerol concentration is increased there is a well defined minimum in the mosaic spread and maximum

Table 1. *Comparison of synchrotron-data statistics from GPb crystals: a 50%-glycerol-soaked flash-frozen crystal and the original native set collected from many crystals.*

Merging R factor for symmetry-related reflections, $R_m = \sum_i \sum_h |I(h) - I_i(h)| / \sum_i \sum_h I_i(h)$, where $I_i(h)$ is the ith intensity measurement of reflection h and $I(h)$ is the mean intensity for that reflection.

		Resolution limit (Å)	R_m (%) including partially measured reflections	Number of reflections		Unit-cell parameters (Å)
				Measured	Unique	
Flash-frozen data	2σ cutoff	1.65	4.6	422649	80096	$a = b = 126.7$, $c = 115.6$
	All data	1.65	6.6	600946	111275	
Original native data	All data	1.9	9.2	109416	71492	$a = b = 128.5$, $c = 116.3$

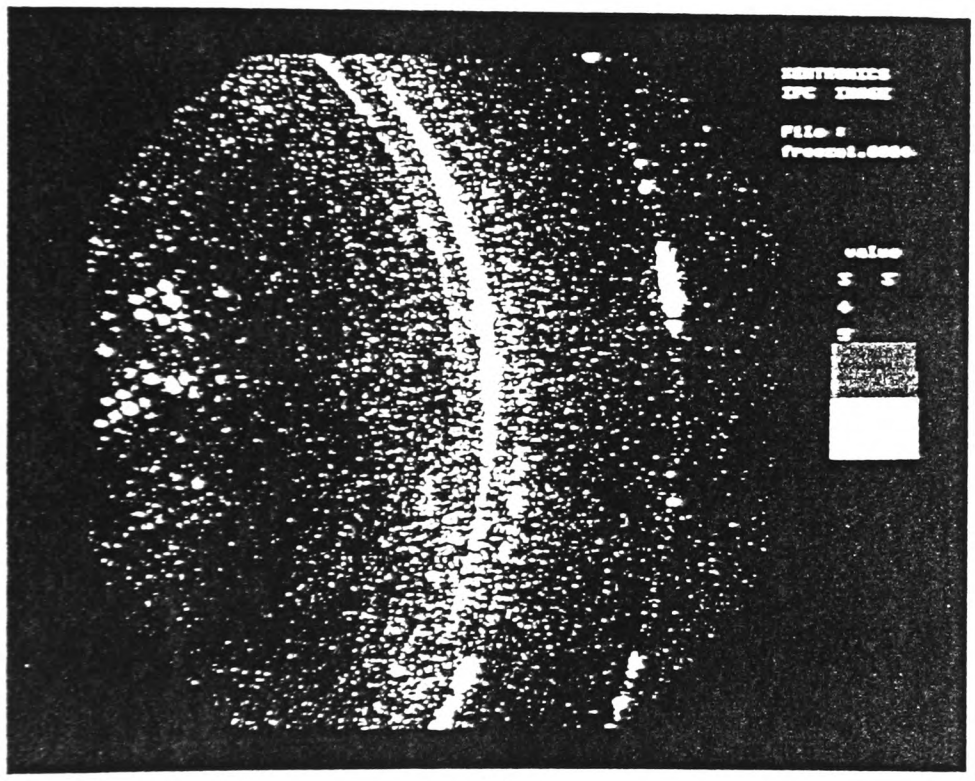

(*a*)

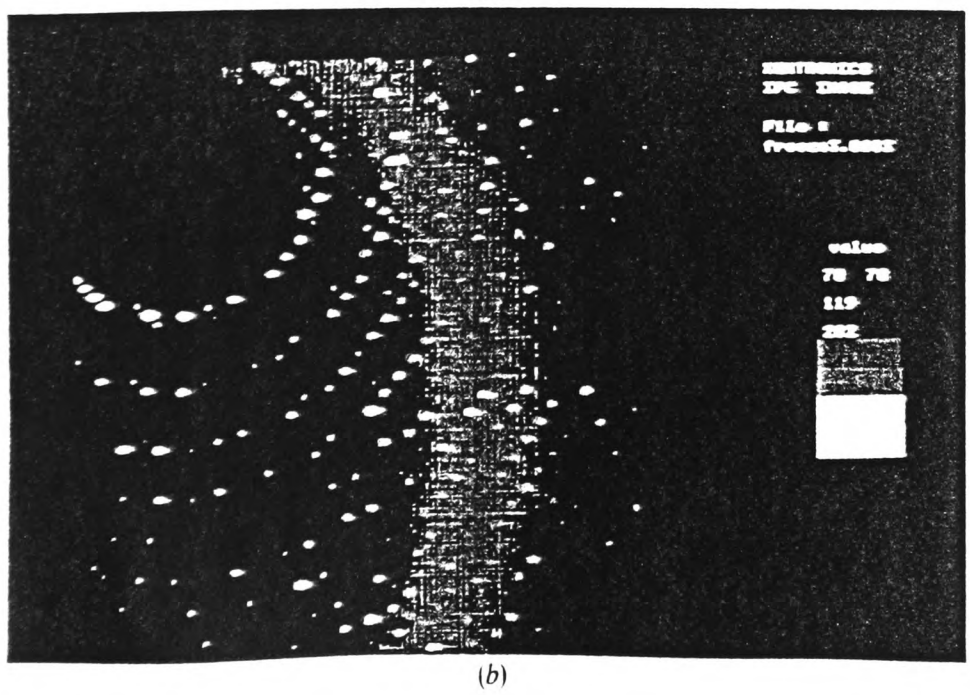

(*b*)

Fig. 3. Comparison of X-ray diffraction from GPb crystals soaked in (*a*) 10% and (*b*) 50% glycerol cryoprotectant mixtures. (*a*) depicts strong powder diffraction rings, showing as white at approximately 4.2 and 3.3 Å resolution, caused by ice formation in the buffer. (*b*) shows superior diffraction from the GPb crystal and diffuse scattering from disordered water molecules in the cryoprotected buffer but no diffraction from ice.

in the diffraction limit. Beyond this concentration, both the mosaicity and the diffraction limit worsen again. These results are relevant to the search for cryoprotectant conditions for freezing any protein crystals, in that they show the importance of a systematic approach to ensure the best possible data quality. The results demonstrate that, by observing how a buffer with cryoprotectant freezes, opaque or clear, a starting point for cryoprotectant conditions can be determined before any crystals are used. It is also clear from the comparison of room temperature and frozen data presented here that the technique of freezing protein crystals in a thin film can offer a significant improvement in data quality and thus in the accuracy with which three-dimensional crystal structures can be determined.

We thank Dr N. Oikonomakos for providing the crystals for this study, Dr R. Esnouf for practical assistance and Professor L. N. Jonson for useful discussions.

References

ACHARYA, K. R., STUART, D. I., VARVILL, K. M. & JOHNSON, L. N. (1991). *Glycogen Phosphorylase b: Description of the Protein Structure*. London: World Scientific.

ELLENBERGER, T. E., BRANDL, C. J., STRUHL, K. & HARRISON, S. C. (1992). *Cell*, **71**, 1223–1237.

FREYMANN, D., DOWN, J., CARRINGTON, M., RODITI, I., TURNER, M. & WILEY, D. (1990). *J. Mol. Biol.* **216**, 141–160.

GAMBLIN, S. J. & RODGERS, D. W. (1993). *Data Collection and Processing*, edited by L. SAWYER, N. ISAACS & S. BAILEY, pp. 28–33. Report DL/SCI/R34, SERC Daresbury Laboratory, Warrington, England.

GUO, H.-C., JARDENTZKY, T. S., GARRETT, T. P. J., LANE, W. S., STROMINGER, J. L. & WILEY, D. C. (1992). *Nature (London)*, **360**, 364–366.

HOPE, H., FROLOW, F., VON BÖHLEN, K., MAKOWSKI, I., KRATKY, C., HALFON, Y., DANZ, H., WEBSTER, P., BARTELS, K. S., WITTMANN, H. G. & YONATH, A. (1989). *Acta Cryst.* B**45**, 190–199.

JOHNSON, L. N., MADSEN, N. B., MOSLEY, J. & WILSON, K. S. (1974). *J. Mol. Biol.* **90**, 703–717.

KABSCH, W. (1993). *J. Appl. Cryst.* **26**, 795–800.

LEE, C.-H., KOMINOS, D., JACQUES, S., MARGOLIS, B., SCHLESSINGER, J., SHOELSON, S. E. & KURIYAN, J. (1994). *Structure*, **2**, 423–438.

NIKOLOV, D. B., HU, S.-H., LIN, J., GASCH, A., HOFFMANN, A., HORIKOSHI, M., CHUA, N.-H., ROEDER, R. G. & BURLEY, S. K. (1992). *Nature (London)*, **360**, 40–46.

OIKONOMAKOS, N. G., MELPIDOU, A. E. & JOHNSON, L. N. (1985). *Biochim. Biophys. Acta*, **832**, 248–256.

OTWINOWSKI, Z. (1993). *Data Collection and Processing*, edited by G. SAWYER, L. ISAACS & S. BAILEY, pp. 56–62. Report DL/SC1/R34, SERC Daresbury Laboratory, Warrington, England.

PETSKO, G. A. (1975). *J. Mol. Biol.* **96**, 381–392.

RINI, J. M., SCHULZE-GAHMEN, U. & WILSON, I. A. (1992). *Science*, **255**, 959–965.

TENG, T-Y. (1990). *J. Appl. Cryst.* **23**, 387–391.

REFERENCES

Acharya, K. R., Stuart, D. I., Varvill, K. M. & Johnson, L. N. (1991). *Glycogen Phosphorylase b: Description of the Protein Structure*. London: World Scientific Publishing Co.

Ariki, M. & Fukui, T. (1977). *J. Biochem. 81*, 1017-1024.

Ashwell, P. (1957). *Meth. Enzym. 5*, 190-211.

Avramovic-Zkic, O., Breidenbach, W. C. & Madsen, N. B. (1974). *Can. J. Biochem. 52*, 146-148.

Baranowski, T., Illingworth, B., Brown, D. H. & Cori, C. F. (1957). *Biochim. Biophys. Acta 25*, 16-21.

Barford, D., Schwabe, J. W. R., Oikonomakos, N. G., Acharya, K. R., Hajdu, J., Papageorgiou, A. C., Martin, J., Knott, J. C. A., Vasella, A. & Johnson, L. N. (1988). *Biochemistry 27*, 6733-6741.

Barford, D. & Johnson, L. N. (1989). *Nature 340*, 609-616.

Barford, D., Hu, S.-H. & Johnson, L. N. (1991). *J. Mol. Biol. 218*, 233-260.

Becker, S., Palm, D. & Schinzel, R. (1994). *J. Biol. Chem. 269*, 2485-2490.

Beer, D., Bieri, J. H., Macher, I., Prewo, R. & Vasella, A. (1986). *Helv. Chim. Acta 69*, 1172-1190.

Blake, C. C. F., Pulford, W. C. A. & Artymiuk, P. J. (1983). *J. Mol. Biol. 167*, 693-723.

Brünger, A. T. (1988). *J. Mol. Biol. 203*, 803-816.

Brünger, A. T. (1989). *Acta Crystallogr. A45*, 42-50.

Brünger, A. T., Karplus, M. & Petsko, G. A. (1989). *Acta Crystallogr. A45*, 50-61.

Brünger, A. T. (1992). *Nature 355*, 472-475.

Buc, H. (1967). *Biochem. and Biophys. Res. Commun. 28*, 59-64.

Buc, M. H. & Buc, H. (1968). *4th Fed. European Biochem. Soc., Symp. Regulaton of Enzyme Activity and Allosteric Interactions*, Oslo, Norway, 1967, p.109. Academic Press, New York.

CCP4 (1979). *The SERC (UK) Collaborative Computing Project No 4: A Suite of Programs for Protein Crystallography.* Daresbury Laboratory, Warrington, UK.

Chang, Y. C., McAlmont, T. & Graves, D. J. (1983). *Biochemistry 22*, 4987-4993.

Chang, Y. C. & Graves, D. J. (1985). *J. Biol. Chem. 260*, 2709-2714.

Chang, Y. C., Scott, R. D. & Graves, D. J. (1987). *Biochemistry 26*, 360-367.

Cohn, M (1949). *J. Biol. Chem. 180*, 771-781.

Copley, R. J. & Barton, G. J. (1994). *J. Mol. Biol. 242*, 321-329.

Cori, G. T. & Cori, C. F. (1940). *J. Biol. Chem. 135*, 733-756.

Cori, C., Cori, G. & Green, A. (1943). *J. Biol. Chem. 151*, 39-55.

Cosier, J. & Glazer, A. M. (1986). *J. Appl. Cryst. 19*, 105-107.

Dewar, M. J. S., Zoebisch, E. G., Healy, E. F. & Stewart, J. J. P. (1985). *J. Am. Chem. Soc. 107*, 3902-3909.

Douzou, P. & Petsko, G. A. (1984). *Adv. Protein Chem. 36*, 245-361.

Dreyfus, M., Vandenburger, B. & Buc, H. (1980). *Biochemistry 19*, 3634-3642.

Dreyfuss, M., Vandenburger, B. & Buc, H. (1980). *Biochemistry 20*, 1748-1756.

Duke, E. M. H., Wakatsuki, S., Hadfield, A. & Johnson, L. N. (1994). *Protein Science 3*, 1178-1196.

Ellenberger, T. E., Brandl, C. J., Struhl, K. & Harrison, S. C. (1992). *Cell 71*, 1223-1237.

Engers, H. D., Bridger, W. A. & Madsen, N. B. (1969). *J. Biol. Chem. 244*, 5936-5942.

Engers, H. D., Shechosky, S. & Madsen, N. B. (1970). *Can. J. Biochem. 48*, 746-754.

Engh, R. A. & Huber, R. (1991). *Acta Crystallogr. A47*, 392-400.

Ermert, Ph. & Vasella, A. (1991). *Helv. Chim. Acta. 74*, 2043-2053.

Ermert, Ph., Vasella, A., Weber, M., Rupitz, K. & Withers, S. G. (1993). *Carbohydr. Res. 250*, 113-128.

Feldmann, K. & Hull, W. E. (1977). *Proc. Natl. Acad. Sci. (USA) 74*, 856-860.

Fersht, A. (1985). *Enzyme Structure and Mechanism, 2nd edition.* New York: Freeman. pp 97-122.

Finer-Moore, J. S., Kossiakoff, A. A., Hurley, J. H., Earnest, T. & Stroud, R. M. (1992). *Proteins Struct. Funct. Genet. 12*, 203-222.

Firsov, L. M., Bogacheva, T. L. & Bressler, S. E. (1974). *Eur. J. Biochem. 42*, 605-609.

Fischer, E. M. & Krebs, E. G. (1962). *Methods Enzymol. 5*, 369-372.

Freymann, D., Down, J., Carrington, M., Roditi, I., Turner, M. & Wiley, D. (1990). *J. Mol. Biol. 216*, 141-160.

Gamblin, S. J. & Rodgers, D. W. (1993). *Data Collection and Processing*, edited by L. Sawyer, N. Isaacs and S. Bailey, pp. 28-33. SERC Daresbury Laboratory: DL/SCI/R34.

Gold, A. M., Johnson, R. M. & Tseng, J. K. (1970). *J. Biol. Chem. 245*, 2564-2572.

Gold, A. M., Legrand, E. & Sánchez, G. R. (1971). *J. Biol. Chem. 246*, 5700-5706.

Goldsmith, E. J., Sprang, S. R., Hamlin, R., Xuong, N.-H. & Fletterick, R. J. (1989). *Science 245*, 528-532.

Graves, D. J. & Wang, J. H. (1972). *The Enzymes, 3rd edition*, edited by P Boyer, pp 435-482. New York: Academic Press.

Gray, W. R. (1962). *Methods in Enzymology Vol. 2*, ed. S P Colowick and N O Kaplan, p 649. New York: Academic Press.

Guo, H.-C., Jardentzky, T. S., Garrett, T. P. J., Lane, W. S., Strominger, J. L. & Wiley, D. C. (1992). *Nature 360*, 364-366.

Haas, D. J. (1968). *Acta Cryst. B24*, 604-605.

Haas, D. J. & Rossmann, M. G. (1970). *Acta Cryst. B26,* 998-1004.

Hajdu, J., Acharya, K. R., Stuart, D. I., McLaughlin, P. J., Barford, D., Oikonomakos, N. G., Klein, H. & Johnson, L. N. (1987). *EMBO J. 6*, 539-546.

Hanozet, G., Pircher, H.-P., Vanni, P., Oesch, B. & Semenza, G. (1981). *J. Biol. Chem. 256*, 3703-3711.

Hedrick, J. L., Shaltiel, S. & Fischer, E. H. (1966). *Biochemistry 5*, 2117-2124.

Henderson, R. (1990). *Proc. R. Soc. Lond. B 241*, 6-8.

Hope, H. (1988). *Acta Cryst. B44*, 22-26.

Hope, H., Frolow, F., von Böhlen, K., Makowski, I., Kratky, C., Halfon, Y., Danz, H., Webster, P., Bartels, K. S., Wittmann, H. G. & Yonath, A. (1989). *Acta Cryst. B45*, 190-199.

Howard, A. J., Gilliland, G. L., Finzel, B. C., Poulos, T. L., Oklendorf, D. H. & Salemme, F. R. (1987). *J. Appl. Crystallogr. 20*, 383-387.

Hu, H.-Y. & Gold, A. M. (1978). *Biochim. Biophys. Acta 525*, 55-60.

Hu, S.-H. (1991). DPhil Thesis, Oxford.

Illingworth, B., Jansz, H. S., Brown, D. H. & Cori, C. F. (1958). *Proc. Natl. Acad. Sci. (USA) 44*, 1180-1191.

Jenkins, J. A., Johnson, L. N., Stuart, D. I., Stura, E. A., Wilson, K. S. & Zanotti, G. (1981). *Philos. Trans. R. Soc. London B293*, 23-41.

Johnson, L. N., Madsen, N. B., Mosley, J. & Wilson, K. S. (1974). *J. Mol. Biol. 90*, 703-717.

Johnson, L. N., Stura, E. A., Sansom, M. S. P. & Babu, Y. (1983). *Biochem. Soc. Trans. 11*, 142-144.

Johnson, L. N., Cheetham, J. C., McLaughlin, P. J., Acharya, K. R., Barford, D. & Phillips, D. C. (1988). *Curr. Top. Microbiol. Immunol. 139*, 81-134.

Johnson, L. N., Acharya, K. R., Jordan, M. D. & McLaughlin, P. J. (1990). *J. Mol. Biol. 211*, 611-645.

Johnson, L. N. & Barford, D. (1993). *Annu. Rev. Biophys. Biomol. Struct. 22*, 199-232.

Kabsch, W. (1993). *J. Appl. Crystallogr. 26*, 795-800.

Kastenschmidt, L. L., Kastenschmidt, J. & Helmreich, E. J. M. (1968). *Biochemistry 7*, 4543-4556.

Kasvinsky, P. J. & Madsen, N. B. (1976). *J. Biol. Chem. 251*, 6852-6859.

Kasvinsky, P. J., Madsen, N. B., Fletterick, R. J. & Sygusch, J. (1978a). *J. Biol. Chem. 252*, 1290-1296.

Kasvinsky, P. J., Madsen, N. B., Sygusch, J. & Fletterick, R. J. (1978b). *J. Biol. Chem. 253*, 3343-3351.

Klein, H. W., Palm, D. & Helmreich, E. J. M. (1982). *Biochemistry 21*, 6675-6684.

Klein, H. W., Im, M. J., Palm, D. & Helmreich, E. J. M. (1984). *Biochemistry 23*, 5853-5861.

Klein, H. W. & Helmreich, E. J. M. (1985). *Curr. Top. Cell. Regul. 26*, 281-294.

Klein, H. W., Im, M. J. & Palm, D. (1986). *Eur. J. Biochem. 157*, 107-114.

Koshland Jr, D., Némethy, G. & Filmer, D. (1966). *Biochemistry 5*, 365-385.

Laskowski, R. A., MacArthur, M. W., Moss, D. S. & Thornton, J. M. (1993). *J. Appl. Cryst. 26*, 283-291.

Leatherbarrow, R. J. (1990). *Analyt. Bioch. 184*, 274-278.

Lee, C.-H., Kominos, D., Jacques, S., Margolis, B., Schlessinger, J., Shoelson, S. E. & Kuriyan, J. (1994). *Structure 2*, 423-438.

Legler, G. (1990). *Adv. Carb. Chem. Biochem. 48*, 319-384.

Leonidas, D. D., Oikonomakos, N. G., Papageorgiou, A. C. & Sotiroudis, T. G. (1992). *Protein Science 1*, 1123-1132.

Low, B. W., Chen, C. C. H., Berger, J. E., Singman, L. & Pletcher, J. F. (1966). *Proc. Natl. Acad. Sci. USA 56*, 1746-1750.

Madsen, N. B. (1986). *The Enzymes: Enzyme Control by Phosphorylation 17*, edited by P. Boyer and E. Krebs. New York: Academic Press.

Madsen, N. B. & Withers, S. G. (1986). *Glycogen Phosphorylase in Coenzymes and Cofactors, Vol. 1 Vitamin B_6 Pyridoxal Phosphate*, edited by D. Dolphin, R Poulson and Avramovic. New York: John Wiley & Sons.

Martin, J. L., Johnson, L. N. & Withers, S. G. (1990). *Biochemistry 29*, 10745-10757.

Martin, J. L., Velurajah, K., Ross, K., Johnson, L. N., Fleet, G. W. J., Ramsden, N. G., Bruce, I., Orchard, M. G., Oikonomakos, N. G., Papageorgiou, A. C., Leonidas, D. D. & Tsitoura, H. S. (1991). *Biochemistry 30*, 10101-10116.

McLaughlin, P. J., Stuart, D. I., Klein, H. W., Oikonomakos, N. G. & Johnson, L. N. (1984). *Biochemistry 23*, 5862-5873.

McLaughlin, P. J. (1985). DPhil Thesis, Oxford University, UK.

Mitchell, E. P. & Garman, E. F. (1994). *J. Appl. Cryst. 27*, 1070-1074.

Monod, J., Wyman, J. & Changeux, J. (1965). *J. Mol. Biol. 12*, 88-118.

Newgard, C. B., Hwang, P. K. & Fletterick R. J. (1989). *Crit. Rev. Biochem. and Mol. Biol. 24*, 69-99.

Nikolov, D. B., Hu, S.-H., Lin, J., Gasch, A., Hoffmann, A., Horikoshi, M., Chua, N.-H., Roeder, R. G. & Burley, S. K. (1992). *Nature 360*, 40-46.

Oikonomakos, N. G., Melpidou, A. E. & Johnson, L. N. (1985). *Biochim. Biophys. Acta 832*, 248-256.

Oikonomakos, N. G., Johnson, L. N., Acharya, K. R., Stuart, D. I., Barford, D., Hajdu, J., Varvill, K. M., Melpidou, A. E., Papageorgiou, A. C., Graves, D. J. and Palm, D. (1987). *Biochemistry 26*, 8381-8389.

Oikonomakos, N. G., Acharya, K. R., Stuart, D. I., Melpidou, A. E., McLaughlin, P. J. & Johnson, L. N. (1988). *Eur. J. Biochem. 173*, 569-578.

Otwinowski, Z. (1993). *Oscillation data reduction program in 'Data Collection and Processing'*, ed. G. Sawyer, L. Isaacs and S. Bailey, pp 56 -62. SERC Daresbury Laboratory DL/SC1/R34.

Papageorgiou, A. C., Oikonomakos, N. G. & Leonidas, D. D. (1989). *Arch. Biochem. Biophys. 271*, 376-385.

Papageorgiou, A. C., Oikonomakos, N. G., Leonidas, D. D., Bernet, B., Beer, D. & Vasella, A. (1991). *Biochem. J. 274*, 329-338.

Parrish, R. F., Uhing, R. J. & Graves, D. J. (1977). *Biochemistry 16*, 4824-4831.

Petsko, G. A. (1975). *J. Mol. Biol. 96*, 381-392.

Pfeuffer, T., Ehrlich, J. & Helmreich, E. (1972). *Biochemistry 11*, 2125-2145.

Quiocho, F. A. & Richards, F. M. (1964). *Proc. Natl. Acad. Sci. USA 52*, 833-839.

Ray, W. J. Jr. & Koshland, D. E. Jr. (1962). *J. Biol. Chem. 237*, 2493-2505.

Read, R. J. (1986). *Acta Cryst. A42*, 140-149.

Reist, E. J., Spencer, R. R., Calkins, D. F., Baker, B. R. & Goodman, L. (1965). *J. Org. Chem. 30*, 2312-2317.

Rini, J. M., Schulze-Gahmen, U. & Wilson, I. A. (1992). *Science 255*, 959-965.

Shaltiel, S., Hedrick, J. L., Pocker, A. & Fischer, E. H. (1969). *Biochemistry 8*, 5189-5196.

Sinnott, M. L. (1990). *Chem. Rev. 90*, 1171-1202.

Sprang, S. R., Goldsmith, E. J., Fletterick, R. J., Withers, S. G. & Madsen, N. B. (1982). *Biochemistry 21*, 5364-5371.

Sprang, S. R., Goldsmith, E. J. & Fletterick, R. J. (1987). *Science 237*, 1012-1019.

Sprang, S. R., Acharya, K. R., Goldsmith, E. J., Stuart, D. I., Varvill, K., Fletterick, R. J., Madsen, N. B. & Johnson, L. N. (1988). *Nature 336*, 215-221.

Sprang, S. R., Withers, S. G., Goldsmith, E. J., Fletterick, R. J. & Madsen, N. B. (1991). *Science 254*, 1367-1371.

Stirtan, W. (1993). DPhil Thesis, University of British Columbia, Canada.

Street, I. P., Rupitz, K. & Withers, S. G. (1989). *Biochemistry 28*, 1581-1587.

Takagi, M., Fukui, T. & Shimomura, S. (1982). *Proc. Natl. Acad. Sci. (USA) 79*, 3716-3719.

Teng, T-Y. (1990). *J. Appl. Crystallogr. 23*, 387-391.

Thomanek, V. F., Parak, F., Mossbauer, R. L., Formanek, H., Schwanger, P. & Hope, W. (1973). *Acta Cryst. A29*, 263-265.

Tripos Associates Inc., 1699 S. Hanley Road, Suite 303, St. Louis, Missouri 63144-2813, USA.

Tu, J. I., Jacobson, G. R. & Graves, D. J. (1971). *Biochemistry 10*, 1229-1236.

Vandenburger, B. & Buc, H. (1983). *Eur. J. Biochem. 133*, 509-513.

Verlinde, C. L. M. J., Noble, M. E. M., Kalk, K. H., Groendijk, H., Wierenga, R. K. & Hol, W. G. J. (1991). *Eur. J. Biochem. 198*, 53-57.

Watson, K. A., Mitchell, E. P., Johnson, L. N., Son, J. C., Bichard, C. J. F., Orchard, M. G., Fleet, G. W. J., Oikonomakos, N. G., Leonidas, D. D., Kontou, M. & Papageorgiou, A. (1994). *Biochemistry 33*, 5745-5758.

Watson, K. A., Mitchell, E. P., Johnson, L. N., Cruciani, G., Son, J. C., Bichard, C. J. F., Fleet, G. W. J., Oikonomakos, N. G., Leonidas, D. D., Kontou, M. (1995). *Acta Cryst D*, paper

in print.

Weber, I. T., Johnson, L. N., Wilson, K. S., Yeates, D. G. R., Wild, D. & Jenkins, J. A. (1978). *Nature 274*, 433-437.

Withers, S. G. & Madsen, N. B. (1980). Biochem. Biophys. Res. Commun. 97, 513-519.

Withers, S. G., Madsen, N. B., Sykes, B. D., Takagi, M., Shimomura, S. & Fukui, T. (1981a). *J. Biol. Chem. 256*, 10759-10762.

Withers, S. G., Madsen, N. B. & Sykes, B. D. (1981b). *Biochemistry 20*, 1748-1756.

Withers, S. G., Madsen, N. B., Sprang, S. R. & Fletterick, R. J. (1982). *Biochemistry 21*, 5372-5382.

Withers, S. G., MacLennan, D. J. & Street, I. P. (1986). *Carbohydrate Research 154*, 127-144.

Zhang, X.-J. & Matthews, B. W. (1994). *Protein Science 3*, 1031-1039.